



Kuntz, Elodie Marie (2017) *An investigation of metabolic vulnerabilities in chronic myeloid leukaemic stem cells*. PhD thesis.

<http://theses.gla.ac.uk/8615/>

Copyright and moral rights for this work are retained by the author

A copy can be downloaded for personal non-commercial research or study, without prior permission or charge

This work cannot be reproduced or quoted extensively from without first obtaining permission in writing from the author

The content must not be changed in any way or sold commercially in any format or medium without the formal permission of the author

When referring to this work, full bibliographic details including the author, title, awarding institution and date of the thesis must be given

Enlighten:Theses
<http://theses.gla.ac.uk/>
theses@gla.ac.uk

An Investigation of Metabolic Vulnerabilities in Chronic Myeloid Leukaemic Stem Cells

Elodie Marie Kuntz

Thesis submitted to the University of Glasgow in accordance with the
requirements for the degree of Doctor of Philosophy

Institute of Cancer Science
College of Medical, Veterinary and Life Sciences
University of Glasgow
October 2017

CRUK Beatson Institute
Garscube Estate
Switchback Road
Bearsden, Glasgow



University
of Glasgow



CANCER
RESEARCH
UK

BEATSON
INSTITUTE

Abstract

Chronic myeloid leukaemia (CML) is a myeloproliferative disorder that originates at the haematopoietic stem cell (HSC) level. CML is driven by BCR-ABL, a fusion oncoprotein with a constitutive tyrosine kinase activity. The discovery of imatinib, a c-Abl specific tyrosine kinase inhibitor (TKI), revolutionised the treatment of CML by inducing cytogenetic and molecular responses in the majority of CML patients in chronic phase. However, imatinib and second/third generation TKIs do not eradicate leukaemic stem cells (LSCs), leading to disease persistence with associated risk of toxicity, drug resistance and relapse. This suggests that effective eradication of CML LSCs requires identification of novel target(s) that can be exploited therapeutically in combination with TKI treatment.

In recent years, a plethora of studies have demonstrated that cancer cells rewire their metabolism to fuel their high energy demands and targeting these metabolic alterations can be of therapeutic benefit. Thus far, investigation of CML LSCs metabolism has been restricted by technical limitations. In this study, we aimed to identify and target the metabolic dependencies in CML LSCs using stem cell enriched (CD34⁺) primary cells isolated from CML patients and healthy donors.

We initially investigated the metabolism of differentiated CD34⁻ and primitive CD34⁺ cells and demonstrated that glucose and fatty acid oxidation was elevated in CD34⁺ CML cells. We as well demonstrated that CML CD34⁺ cells displayed an increase in their mitochondrial oxygen consumption rate (OCR). Next, we compared the metabolism of CD34⁺ and CD34⁺CD38⁻ CML cells to their respective normal counterparts, which revealed that stem cell-enriched CML cells possess increased mitochondrial functions in comparison to normal cells.

Of clinical significance, we show that the antibiotic tigecycline, an inhibitor of mitochondrial translation, reduced this aberrant oxidative metabolism. The combination of imatinib and tigecycline targeted primitive CML cells at a clinically achievable concentration while having minimal effect on colony formation potential of CD34⁺ cells derived from healthy donors. To validate these findings *in vivo*, human CML CD34⁺ cells were injected into irradiated immune-deficient mice. Remarkably, four-week combination treatment with tigecycline and imatinib *in vivo* eliminated the majority of CML LSCs, targeting 95% of the cells. Moreover,

mice maintained low levels of CML LSCs upon discontinuation of the combination treatment whereas imatinib-treated mice showed signs of relapse.

These results indicate that oxidative phosphorylation is crucial for the survival of CML LSCs and inhibition of mitochondrial metabolism with tigecycline, in combination with imatinib treatment, might be a suitable therapeutic strategy to selectively target these cells and improve cure rates.

Contents

Abstract	2
Author's declaration.....	9
Acknowledgments	10
Abbreviations.....	12
Introduction.....	17
1.1 Haematopoiesis and haematopoietic stem cells (HSCs)	17
1.1.1 Ontogeny of haematopoiesis	17
1.1.2 Hematopoietic cells hierarchy	17
1.1.3 Regulation of HSCs	18
1.1.4 Identification and isolation of HSCs	20
1.2 The cancer stem cell (CSC) model	21
1.2.1 Introduction	21
1.2.2 Historical overview	21
1.2.3 Others characteristics of CSCs.....	22
1.2.4 Cell of origin	22
1.2.5 Controversies of the CSC model	23
1.3 CML	24
1.3.1 Introduction	24
1.3.2 Epidemiology	25
1.3.3 Disease progression	25
1.3.4 Molecular pathophysiology of CML.....	26
1.3.5 CML diagnosis and monitoring	27
1.3.6 BCR-ABL signalling pathway	28
1.3.7 CML Treatment.....	29
1.3.8 CML LSCs persistence	35
1.4 Metabolism and HSC fate	38
1.4.1 Metabolism at a glance	38
1.4.2 Use of stable isotopes as tracers.....	40
1.4.3 Metabolic regulation of HSCs	40
1.5 Cancer Metabolism	42
1.5.1 Metabolic reprogramming of cancer cells	42
1.5.2 The Warburg effect and glycolysis in cancer	43
1.5.3 Mitochondrial metabolism in cancer.....	44
1.5.4 Targeting metabolic vulnerabilities of cancer cells.....	46
1.6 Aims	50

Chapter 2	Material and Methods	51
2.1	Material	51
2.1.1	General reagents	51
2.1.2	Flow cytometry reagents.....	53
2.1.3	Western blot antibodies	54
2.1.4	Primers	54
2.1.5	Primary cells	54
2.1.6	Cell lines	55
2.1.7	Equipment.....	55
2.1.8	Composition of tissue culture media, solutions and buffers.....	55
2.2	Methods	59
2.2.1	Primary samples	59
2.2.2	Tissue Culture.....	60
2.2.3	Cell proliferation assay.....	61
2.2.4	Flow cytometry.....	62
2.2.5	Quantitative PCR	65
2.2.6	Western blotting.....	66
2.2.7	Immunolabelling.....	68
2.2.8	Hematopoietic stem and progenitors cells functional assays	68
2.2.9	Metabolomics.....	70
2.2.10	Seahorse	71
2.2.11	Double transgenic mice experiments.....	73
2.2.12	NSG mouse engraftment	75
2.2.13	Statistical analyses	77
Chapter 3	Investigation of metabolic vulnerabilities in CML LSCs	78
3.1	Introduction	78
3.2	Results	79
3.2.1	Imatinib does not target CML LSCs.....	79
3.2.2	Increased oxidative metabolism in primitive CML cells compared to differentiated cells	81
3.2.3	CML LSCs cells have elevated mitochondrial oxidative metabolism compared to normal counterparts	88
3.3	Discussion.....	98
3.4	In summary	101
Chapter 4	Using phenformin to target CML LSCs.....	102
4.1	Introduction	102
4.2	Results	104

4.2.1	Phenformin is a more potent inhibitor of mitochondrial respiration than metformin	104
4.2.2	Inhibition of mitochondrial metabolism with phenformin targets K562 cells	107
4.2.3	Phenformin preferentially targets BCR-ABL expressing cells.....	111
4.2.4	Inhibition of aberrant oxidative metabolism with phenformin targets CML LSCs <i>in vitro</i>	113
4.2.5	Modelling CML disease <i>in vivo</i> using a transgenic BCR-ABL mouse model	115
4.2.6	Phenformin and imatinib combination does not target LSCs <i>in vivo</i>	116
4.3	Discussion.....	122
4.4	In summary	125
Chapter 5 Using tigecycline to target CML LSCs		127
5.1	Introduction	127
5.2	Results	128
5.2.1	Tigecycline mediated inhibition of mitochondrial oxidative metabolism targets CML cell lines.....	128
5.2.2	Tigecycline preferentially inhibits cell proliferation of BCR-ABL expressing cells.....	132
5.2.3	Tigecycline inhibits oxidative metabolism in primary CD34 ⁺ CML cells	133
5.2.4	Tigecycline in combination with imatinib targets CD34 ⁺ CML cells <i>in vitro</i>	137
5.2.5	Tigecycline in combination with imatinib targets CML LSCs <i>in vitro</i>	141
5.2.6	Tigecycline-mediated inhibition of oxidative metabolism targets LSCs <i>in vivo</i> when used in combination with imatinib	144
5.2.7	The combination of tigecycline and imatinib marginally affects normal HSCs <i>in vivo</i>	151
5.2.8	The combination of tigecycline and imatinib prevents CML relapse	153
5.3	Discussion.....	155
5.4	In summary	159
Chapter 6 Conclusion and future directions		161
6.1	Oxidative metabolism in LSCs	161
6.2	Metabolism of CML LSCs following TKI treatment.....	163
6.3	Inhibiting oxidative metabolism targets CML cells in combination with TKI	165
6.4	Tigecycline efficacy against TKI resistant cells.....	165
6.5	Clinical applicability for tigecycline use	169
6.6	Others inhibitors of oxidative metabolism	170
6.7	Additional remarks	171

List of Figures

Figure 1. 1 Haematopoiesis	19
Figure 1. 2 BCR-ABL signalling pathway	29
Figure 1. 3 Persistence of CML LSCs following imatinib treatment.....	37
Figure 1. 4 Overview of cellular metabolism.....	39
Figure 2. 1 Procedure summary for haematopoietic LTC-IC assay.	69
Figure 3. 1 Imatinib fails to eliminate CML LSCs.....	80
Figure 3. 2 Primitive CML cells show an increase in oxidative metabolism compared to differentiated counterparts.	83
Figure 3. 3 Primitive CML cells show an increase in mitochondrial respiration compared to differentiated counterparts.	86
Figure 3. 4 Primitive CML cells have an increased glucose oxidation compared to differentiated counterparts.	87
Figure 3. 5 Enhanced fatty acid oxidation in primitive CML cells compared to normal undifferentiated haemopoietic cells.....	91
Figure 3. 6 Enhanced glucose oxidation and anaplerosis in primitive CML cells compared to normal counterparts.	94
Figure 3. 7 CD34 ⁺ CML cells display increased mitochondrial respiration compared to normal counterparts.	95
Figure 3. 8 CML LSCs have increased mitochondrial functions compared to normal HSCs.	96
Figure 3. 9 Oxidative metabolism is similar between CML LSCs and CML progenitor cells.	97
Figure 3. 10 CD34 ⁺ CML cells display increased glucose oxidation compared to normal counterparts.	100
Figure 4. 1 Mechanism of action of metformin on a cellular level.....	103
Figure 4. 2 Phenformin is a more potent inhibitor of oxidative metabolism than metformin.	106
Figure 4. 3 Phenformin synergises with imatinib to target K562 cells.	109
Figure 4. 4 Phenformin targets K562 cells by inhibiting mitochondrial respiration.	110
Figure 4. 5 Phenformin in combination with imatinib targets selectively BCR-ABL expressing cells.....	112
Figure 4. 6 Inhibition of aberrant oxidative metabolism with phenformin targets CML LSCs <i>in vitro</i>	114
Figure 4. 7 Experimental outline using a DTG model to study <i>in vivo</i> drug/combination efficacy against CML cells.....	119
Figure 4. 8 The addition of phenformin does not potentiate the effect of imatinib against differentiated leukaemic cells.	120
Figure 4. 9 Phenformin and imatinib combination does not target LSCs <i>in vivo</i>	121
Figure 5. 1 Tigecycline inhibits mitochondrial respiration in CML cell lines.....	130
Figure 5. 2 Tigecycline in combination with imatinib targets CML cell lines <i>in vitro</i>	131
Figure 5. 3 Tigecycline preferentially targets BCR-ABL-expressing cells.	132
Figure 5. 4 Tigecycline inhibits oxidative metabolism in CD34 ⁺ CML cells through inhibition of mitochondrial protein expression.	135

Figure 5. 5 Tigecycline inhibits glutamine oxidation and FAO in CD34 ⁺ CML cells.....	136
Figure 5. 6 Tigecycline is a potent inhibitor of CD34 ⁺ CML cells proliferation.	139
Figure 5. 7 Tigecycline combined to imatinib selectively targets CD34 ⁺ CML cells <i>in vitro</i>	140
Figure 5. 8 Tigecycline in combination with imatinib targets LSCs <i>in vitro</i>	143
Figure 5. 9 Tigecycline affects the TET-OFF gene expression system.....	147
Figure 5. 10 Tigecycline alone or when combined to imatinib is not toxic towards normal cells.	148
Figure 5. 11 Tigecycline in combination with imatinib targets human LSCs <i>in vivo</i>	149
Figure 5. 12 Tigecycline inhibits the expression of mitochondrial-encoded proteins of CD34 ⁺ CML cells <i>in vivo</i>	150
Figure 5. 13 The combination of imatinib and tigecycline marginally affects normal HSCs <i>in vivo</i>	152
Figure 5. 14 Tigecycline in combination with imatinib prevents CML relapse.	154
Figure 5. 15 Tigecycline impairs glycolysis in CD34 ⁺ CML cells <i>in vitro</i>	156
Figure 6. 1 Tigecycline impairs the proliferation of KCL22 ^{PonRes} cells.....	167
Figure 6. 2 Tigecycline targets KCL22 ^{PonRes} cells <i>in vitro</i>	168

List of Tables

Table 1: Comparative steady-state metabolomics analysis of patient-matched CD34 ⁺ and CD34 ⁻ CML cells measured by LC-MS.....	84-85
Table 2: Comparative steady-state metabolomics analysis of CD34 ⁺ CML and CD34 ⁺ normal cells measured by LC-MS.....	92-93

Author's declaration

I hereby testify that all the work presented in this thesis is my own, unless otherwise stated. I confirm that this work has not been previously submitted for consideration of any other degree.

Elodie Marie Kuntz

Acknowledgments

I would like first to thank my two supervisors Professor Eyal Gottlieb and Dr. Guðmundur Vignir Helgason. Eyal, I will be always indebted to you for offering me the opportunity to do a PhD in your laboratory. You have been a charismatic and inspirational mentor who allowed me to pursue my own ideas, while guiding and providing me with support throughout this journey. Vignir, I will never be able to repay you for all the help, support and guidance you have given me. Thanks to you, I was able to grow as a scientist and professionally. This thesis would not have been feasible without your help.

I would like to give a huge thank you to Dr. Pablo Baquero. I really enjoyed working alongside such an amazing person for the past four years. You never lost patience and were always willing to share your experience with me! I will always remember the great times we had working together.

I would like to give as well a special thank you to my office mate, Elaine MacKenzie. I could always count on you to teach me your extremely valuable years of experience in the lab and will never forget the extensive support you have given for more than four years. I could not have wished to share my office with another person Elaine! You always had my back and were such a great listener, which helped me in more ways than you can imagine!

I would like to thank as well all the previous and current R12 and Vignir's lab members: Leon, Nadja, Zach, Johan, Saverio, Jiska, Henry, Simone, Rebecca, Amy, Kevin, Angela, Lucie for all the helpful scientific discussions and great moments shared together. I am as well extremely grateful for all the technical support in mass spectrometry provided by Gillian, Niels and David. I would like to mention as well Tim Harvey and Tom Gilbey for the great technical support in flow cytometry they have given me for the past four years. All the hours spent in front of the FACS with them will definitely be an experience I will not forget!

I would like to thank all the people from the Paul O' Gorman Leukaemia Research Centre, particularly Tessa Holyoake, Karen Dunn, Alan Hair and Alison Michie. Tessa, your charisma was an inspiration to me and I am extremely grateful to have received your support. Karen, I truly enjoyed working with you and I thank you for

all the technical help you have providing me with the *in vivo* work. Thanks Alan for all the numerous patient samples you have selected for me!

I would like to acknowledge Cancer Research UK, the Beatson Institute, the University of Glasgow, the NHS Biorepository Research Department and all the patients who have accepted to donate samples and made this work possible.

I want to thank as well all the great friends I made throughout the years who made this journey possible. Nicola, Brunella, Alvaro and Arantxa, you have been amazing friends to meet! Thank you for the Icelandic trip we did all together; I hope we will be able to repeat it soon! A big thank you to Barbara Vale Vale, Valentin, Florian, Sergi, Evangelos for the numerous laughs that helped me to deal with the stress!

Un énorme merci également à Papa, Maman, Guillaume pour votre aide tout au long de ces dernières années. Au travers de tous vos sacrifices, vous m'avez offert l'incroyable opportunité de poursuivre mes études et m'avez toujours soutenu pour faire une thèse malgré l'éloignement.

Finalmente, no quisiera terminar sin dedicar unas palabras a mi novio Pablo. Esta tesis no podría haber sido posible sin tu ayuda, amor y apoyo durante estos cuatro años!!!. Has sido la 'roca' donde sostenerme durante tiempos difíciles y estoy segura de que mi próximo camino va a ser increíble contigo de mi lado. Te quiero mucho.

Abbreviations

2-DG	2-Deoxy-glucose
2-DG-P	2-Deoxy-glucose phosphate
2-HG	2-Hydroxyglutarate
ABC	ATP-binding cassette
ABL	Abelson murine leukaemia viral oncogene homolog
ALL	Acute lymphoblastic leukaemia
Allo-SCT	Allogeneic stem cell transplantation
AML	Acute myeloid leukaemia
ANOVA	Analysis of variance
AP-CML	Acute phase chronic myeloid leukaemia
APS	Ammonium Persulfate
ATP	Adenosine triphosphate
ATP5a	ATP synthase subunit alpha
BC	Blast crisis
BCR	Breakpoint cluster region
BIT	Bovine serum albumin, insulin and transferrin
BM	Bone marrow
BPTES	Bis-2-(5-phenylacetamido-1,2,4-thiadiazol-2-yl)ethyl sulphide
BSA	Bovine serum albumin
CCyR	Complete cytogenetic response
CFC	Colony forming-cell
CHR	Complete haematological response
CLP	Common lymphoid progenitor
CML	Chronic myeloid leukaemia
CML LSCs	Chronic myeloid leukaemia stem cells
CMP	Common myeloid progenitor
CoA	Coenzyme A
CP-CML	Chronic phase chronic myeloid leukaemia
CPT1	Carnitine palmitoyltransferase 1
CSC	Cancer stem cell
DAPI	4',6-diamidino-2-phenylindole
DLBCL	Diffuse large B-cell lymphoma

DMEM	Dulbecco's Modified Eagle Medium
DMSO	Dimethylsulfoxide
DNA	Deoxyribonucleic acid
DTG	Double transgenic
ECAR	Extracellular acidification rate
ETC	Electron transport chain
FACS	Fluorescence-activated cell sorting
FAO	Fatty acid oxidation
FBS	Foetal bovine serum
FDG-PET	¹⁸ F-deoxyglucose positron emission tomography
FH	Fumarate hydratase
FLT3L	FMS-like tyrosine kinase 3 ligand
Fru-2,6-BP	Fructose-2,6-biphosphate
Fru-6P	Fructose-6-phosphate
FSC	forward-angle light scatters
G6PDH	Glucose-6-phosphate dehydrogenase
G-CSF	Granulocyte colony-stimulating factor
Glc-6P	Glucose-6-phosphate
GLS	Glutaminase
GM-CSF	Granulocyte-macrophage colony-stimulating factor
GMP	Granulocyte-macrophage progenitor
h	Hour
HBSS	Hanks' Buffered Salt Solution
HIF-1 α	Hypoxia-inducible factor 1-alpha
HK	Hexokinase
HSC	Haematopoietic stem cell
HSP-90	Heat shock protein-90
HSPCs	Haematopoietic stem and progenitor cells
IDH	Isocitrate dehydrogenase
IFN- α	Interferon-alpha
IL-3	Interleukin-3
IL-6	Interleukin-6
IM	Imatinib
IMDM	Iscove's Modified Dulbecco's Medium

iPSC	Induced pluripotent stem cell
IRIS	International Randomized Study of Interferon and ST1571
LC-MS	Liquid chromatography-mass spectrometry
LDH	Lactate dehydrogenase
L-IC	Leukaemic-initiating cell
LIF	Leukaemic inhibitory factor
Lin	Lineage
LSC	Leukaemic stem cell
LTC-IC	Long-term culture-initiating cell
LT-HSC	Long-term haematopoietic stem cell
MAP	Mitogen-activated protein
MCT	Monocarboxylate transporters
MCyR	Major cytogenetic response
MEP	Megakaryocyte/erythroid progenitor
MIP-1 α	Macrophage inflammatory protein
MITF	Microphthalmia-associated transcription factor
MMR	Major molecular response
MPP	Multipotent progenitor
MT-CO1	Cytochrome c oxidase subunit 1
MT-CO2	Cytochrome c oxidase subunit 2
NF κ B	Nuclear factor- κ B
NSCLC	Non-small-cell lung carcinoma
OCR	Oxygen consumption rate
OCT1	Organic cation transporter 1
OXPPOS	Oxidative phosphorylation
PC	Pyruvate carboxylase
PDH	Pyruvate dehydrogenase
PDK	Pyruvate dehydrogenase kinase
PFK	Phosphofructokinase
PFKFB3	Phosphofructo-2-kinase/fructose-2,6-biphosphate 3
PGC1- α	Peroxisome proliferator-activated receptor gamma coactivator 1- alpha
PGI	Phosphoglucose isomerase
P-gp	P-glycoprotein

Ph	Philadelphia
PH	Phenformin
PHD	Prolyl hydroxylase domain
PI	Propidium iodide
PI3K	Phosphoinositide 3-kinase
PIP	phosphatidylinositol phosphates
PML	Promyelocytic leukaemia protein
PMS	Phenazine Methosulfate
PonRes	Ponatinib resistant
PPAR	Peroxisome proliferator-activated receptor
PPP	Pentose phosphate pathway
PTPMT1	Protein-tyrosine phosphatase mitochondrial
RNA	Ribonucleic acid
RPMI	Roswell Park Memorial Institute
S.D.	Standard deviation
S.E.M	Standard error of the mean
SCF	Stem-cell factor
SDH	Succinate dehydrogenase
SDS	Sodium dodecyl sulfate
Sec	Second
SMO	Smoothened
SSC	Side-angle light scatter
STAT5	Signal transducer of activation and transcription 5
STIM	Stop Imatinib
TCA	Tricarboxylic acid
TEMED	Tetramethylenediamine
TIG	Tigecycline
TIGAR	TP53-induced glycolysis and apoptosis regulator
TKI	Tyrosine kinase inhibitor
TMRM	Tetramethylrhodamine, methyl ester
TP53	Tumour protein 53
Trap-1	Tumour necrosis factor receptor-associated protein-1
TRE	Tetracycline-response element
tTA	Tetracycline transactivator protein

UCP2	Uncoupling protein 2
UQCRC2	Ubiquinol-cytochrome c reductase core protein II
WBC	White blood cell

Chapter 1 Introduction

1.1 Haematopoiesis and haematopoietic stem cells (HSCs)

1.1.1 Ontogeny of haematopoiesis

Haematopoiesis, or haemopoiesis, is a tightly regulated process that produces all the components of the blood system throughout the entire life of an individual. During human embryonic development, haematopoiesis takes place at first in the yolk sac and generates principally nucleated erythrocytes (reticulocytes) that are essential to support the high oxygen demand of the nascent embryo (1). The second wave of foetal haematopoiesis occurs within the embryo, in the aorta-gonad-mesonephros at first, and sequentially moves to the placenta, foetal liver and the spleen (2). Before birth, haematopoiesis finally establishes in the bone marrow (BM) where it will remain throughout the entire life.

1.1.2 Hematopoietic cells hierarchy

The existence of a cell able to regenerate all the cellular components of the haematopoietic system or “stem cell” was first demonstrated in 1963 by Till, McCulloch and colleagues. During their work on the reconstitution of the blood system, they observed the formation of splenic colonies following ten days post-transplantation of murine haematopoietic cells into recipient mice. They further demonstrated that these myelo-erythroid colonies in the spleen had for origin a single haematopoietic cell that had the capacity to self-renew and differentiate, a pioneer finding that laid out the fundamental properties of haematopoietic stem cells (HSCs) (3-5).

Accounting for less than 0.05% of BM cells, rare HSCs sit at the top of the haematopoietic hierarchy and have the ability of generating all the cellular components of the blood (6). More precisely, HSCs differentiate into multipotent progenitors cells (MPPs) that have no longer self-renewal activity. MPPs can then generate common lymphoid or myeloid progenitors (CLP, CMP) that can further differentiate into mature blood cells such as red blood cells, megakaryocytes, myeloid cells and lymphocytes (**Fig. 1.1**). These terminally differentiated cells are

short-lived and, therefore, need to be constantly replenished at an intensive rate of 1.5 million cells per second in adult humans (7). Concurrently to the production of mature cells, HSCs ensure their persistence throughout the entire lifetime by self-renewal. In order to maintain a constant number of HSCs at homeostasis while generating differentiated cells, HSCs can engage in two modes of divisions. They can either divide by symmetric division, that produces two daughter cells with the similar fate or engage in an asymmetric division, generating one HSC and one differentiated MPP cell (8). The choice between the type of cellular division is regulated by many factors and any alteration in this process can have dramatic consequences; a decrease in self-renewal potential or increase in the differentiation process can result in the exhaustion of HSCs (9, 10).

1.1.3 Regulation of HSCs

The BM niche plays a crucial role in regulating HSCs function and maintaining them in a quiescent state at homeostasis. HSCs have been shown to principally reside within the endosteal (osteoblastic) and the vascular niche of the BM. The specific localisation of HSCs within the BM can regulate their fate, such as differentiation, quiescence and self-renewal (11). For instance, studies have demonstrated that HSCs are maintained in a quiescent state in the endosteal region by interacting with osteoblasts while proliferating HSCs associate with the vascular niche (12). However, several reports have discussed that the osteoblastic and the vascular niche are not clearly dissociable anatomically and might very well overlap in their function and localization (13).

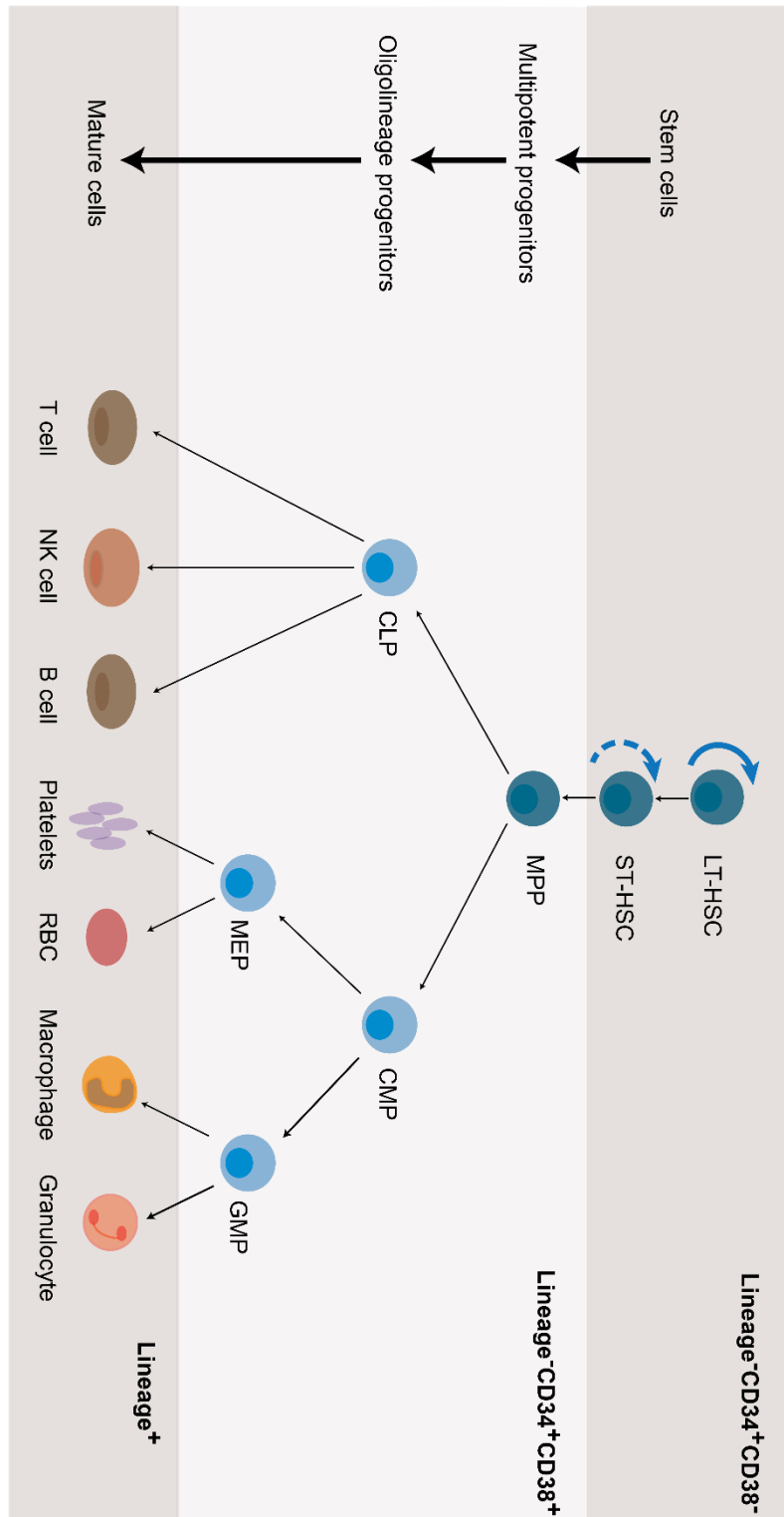


Figure 1. 1 Human haematopoiesis.

LT-HSC, long-term haematopoietic stem cell; ST-HSC, short-term haematopoietic stem cell; MPP, multipotent progenitor; CLP, common lymphoid progenitor; CMP, common myeloid progenitor; MEP, megakaryocyte/erythroid progenitor; GMP, granulocyte-macrophage progenitor.

1.1.4 Identification and isolation of HSCs

Many studies have focused their efforts in findings cell surface markers to isolate and purify rare HSCs. However, it is only the development of monoclonal antibodies and multi-colour flow cytometry sorting that allowed the purification of murine HSCs for the first time almost thirty years ago. These crucial technical advances allowed Sprangrude and colleagues to isolate a rare population of cells (1 in 2000) enriched for murine HSCs. This HSCs-enriched population, phenotypically characterised as Thy-1^{low}Lineage (Lin) negative (-) Sca positive (+), was able to regenerate the haematopoietic system in the long term, while Sca⁻ and Lin⁺ cells were not (14). Subsequent studies have allowed a more extensive characterisation of murine HSCs to the point of enabling single-cell transplantation. In 1996, one study on mouse haematopoietic cells demonstrated that one out of three cells harbouring the phenotypical markers CD34⁺Lin⁻Sca⁺ckit⁺ was able to regenerate the entire murine haematopoietic system (15).

Similar to mouse HSCs, studies based on the expression of cell surface markers were performed to purify human HSCs. However, although phenotypic markers are needed to enrich for HSCs, their expression can be modified in stressful conditions. Hence, studies conducted on HSCs always need to be coupled with functional assays. The colony forming potential of progenitors and HSCs can be assessed *in vitro* by colony-forming cell (CFC) and long-term culture-initiating cell (LTC-IC) assays respectively. The principal method for testing the stem cell potential of human cells remains the transplantation in immuno-deficient (SCID and NOD/SCID) mice and demonstration of their ability to reconstitute long-term haematopoiesis. Initially, the selection of cells enriched for stem cell activity was based on the high expression of the CD34 at the cell surface. *In vivo*, transplantation of CD34-expressing cells led to long-term reconstitution of haematopoiesis (16). However, the CD34⁺ cell population was shown to be a heterogeneous population and mainly constituted of progenitor cells. Baum, Weissman *et al.* later showed that the CD34⁺CD90⁺(Thy-1)⁻Lin⁻ cell population differentiated into myeloid and lymphoid cells when transplanted in SCID mice, while CD34⁺CD90⁻Lin⁻ were not able to generate both progenies, suggesting that the CD34⁺CD90⁺Lin⁻ subset contains pluripotent cells and is more enriched in HSCs (17). Subsequent studies demonstrated that a small subset of cells (1-10%) within the CD34-expressing

population that do not express CD38 (refer to as CD34⁺CD38⁻) can generate all haematopoietic lineages (18). Moreover, the CD34⁺CD38⁻ subset was shown to be highly enriched for cells with long-term culture-initiating potential and able to differentiate into multilineage progenies in either SCID or NOD/SCID mice (19). Since then, the most enriched HSC population has been identified as harbouring Lin⁻CD34⁺CD38⁻CD90⁺CD45RA⁻ phenotypic markers (20).

1.2 The cancer stem cell (CSC) model

1.2.1 Introduction

Similar to normal stem cells, cancer stem cells (CSCs) possess self-renewal and repopulating capacity that enable them to regenerate themselves and all cells from a given cancer. Representing a small subset of the tumour, CSCs constitute a reservoir for tumour maintenance. Many studies have shown that CSCs are quiescent which promotes their resistance to current therapies that mainly target highly proliferating cells. It is therefore believed that targeting CSCs will lead to enhanced cure rates and fewer relapses.

1.2.2 Historical overview

The CSC concept initially emerged from research in blood malignancies. In 1994, a study on acute myeloid leukaemia (AML) cell subsets demonstrated that leukaemic cells harbouring the CD34⁺CD38⁻ cell-surface phenotype were able to initiate leukaemia in SCID mice, while CD34⁺ or CD34⁺CD38⁺-expressing cells were not. Moreover, limiting dilution assays revealed that leukaemic-initiating cells (L-ICs) constituted a small fraction of the bulk of the malignancy, representing 1 in 250,000 leukaemic cells approximately (21). A few years later, Bonnet and Dick, by performing transplantation experiments of additional AML patients in severely immuno-deficient NOD-SCID mice, reached a similar conclusion (22). Given that L-ICs and normal HSCs display similar cell-surface markers (CD34⁺CD38⁻), these studies suggested that primitive stem cells are the target of transformation in AML.

Plethora of investigations have since then aimed to identify CSCs in other malignancies, including in solid tumours. Al-Hajj *et al.* performed the initial

characterisation of CSCs in breast cancer in 2003. They demonstrated that the serial transplantation of CD44⁺CD24⁻ breast cancer cells leads to tumour formation in immuno-compromised mice that resembles the parental malignancy (23).

Put together, these studies demonstrated for the first time the existence of a rare population of cancer cells that has a remarkable ability to self-renew and regenerate the tumour entirely.

1.2.3 Others characteristics of CSCs

CSCs share the proliferation traits of normal stem cells, alternating between quiescence, slow-cycles, and active growth. For instance, quiescent CSCs can be identified in human colon adenocarcinoma cell line as well as in ovarian cancer patient samples (24, 25). Moreover, in a mouse model of AML, leukemic stem cells (LSCs) have been shown to reside within the endosteal region of the BM in a quiescent state (26, 27). Interestingly, these LSCs displayed enhanced resistance to the chemotherapeutic agent cytarabine. This is line with other studies that have shown that CSCs are markedly resistant to standard therapies. Of note, part of this resistance is conferred by their slow-cycling/quiescent status as conventional chemotherapy principally target fast-dividing cells (28). Accordingly, many studies have demonstrated that LSCs in chronic myeloid leukaemia (CML) patients are inherently resistant to the first line therapy imatinib whereas the drug effectively eliminates the bulk of the leukaemic population (29). Of note, these studies will be discussed in more details in a subsequent paragraph (1.3.8).

1.2.4 Cell of origin

It is important to note that the cell of origin in cancer, defined as the cell that acquires the first oncogenic transformation, has to be differentiated from the CSC that propagates the tumour. In other words, the cell of origin does not necessarily have CSC traits at first but rather can acquire stemness properties following additional mutational hits (30). While there is compelling evidence that CSCs derive from normal stem cells in some malignancies, CSCs have been shown to originate as well from progenitor cells that have gained self-renewal ability by second hits (9). Interestingly, several studies demonstrated that the generation of

induced pluripotent stem cells (iPSCs) from adult human dermal fibroblasts only requires the combination of four transcription factors, indicating that the acquisition of stem cell traits by more differentiated cells is a possibility (31, 32). Having said this, the cell of origin can be as well distinct from the CSC. For instance, the cell of origin could be derived from a normal stem cell that has acquired oncogenic mutations, while the propagating CSCs is a more differentiated progenitor cell. This scenario has been shown to occur in the final blast crisis (BC) stage of CML and in some AML subtypes. In CML, the initial oncogenic transformation occurs initially at the stem-cell level (in other words, the cell of origin is a HSC) and this cell is responsible for sustaining the disease in the early stage of the disease. However, during BC, the LSC pool that propagates leukaemia has been shown to share granulocyte/macrophage progenitor characteristics (33). Moreover, analysis of BM samples isolated from AML patients harbouring the AML-ETO fusion protein revealed that the disease originates in AML-ETO- expressing HSCs, however, the cells able to generate leukaemic blast *in vitro* were comprised within the Thy1⁻ progenitor cell fraction (34). Altogether, these studies indicate that, in some particular cases, the leukaemic transformation can start at the HSC level but the propagation of the disease occurs at a progenitor stage.

1.2.5 Controversies of the CSC model

Much scientific debate has evolved around the existence and the frequency of CSCs. The first confusion is in the origin of the CSC that is not necessarily derived from a normal stem cell. As mentioned previously, a CSC is defined as a cell that shares the functional properties of a normal stem cell, which does not entail that one derives from another (35, 36). The second misconception lies in the identification of CSC and in the stability of the CSC compartment. While the number of normal stem cells is relatively constant at homeostasis, studies have demonstrated that the frequency of LSCs varies dramatically between patients. Indeed, Bonnet and Dick evaluated that the number of LSCs ranged from 0.2 to 100 per million of mononuclear cells in seven AML patients tested (22). This could indicate that the pool of CSCs is not stable and might fluctuate as a function of the environment, treatment or disease progression. This alleged plasticity of CSCs would therefore prevent future therapy to effectively eradicate them.

Furthermore, the phenotypical markers of LSCs are highly variable among leukaemic patients, making their identification even more challenging (37). In addition, CSCs are often detected experimentally by their ability to reconstitute tumours in xenotransplantation mouse models. The fact that mice maintain some level of immunity and provide a different microenvironment than humans can result in the selection of a cell subset that is not necessarily able to generate tumours but has the ability to engraft in mice and in the underestimation of the frequency of tumorigenic cells (38). This has for instance been demonstrated in melanoma. Initially, melanoma was thought to be driven by CSCs, but when more immuno-compromised mice were used, researchers have realised that approximately 25% of the cells were able to generate tumours *in vivo*, suggesting that this cancer does not follow the CSC model (39, 40).

Despite the outlined controversies, the scenario is different for CML. While this will be discussed further in the next section, compelling evidence has shown that CML originates from a HSC and is driven by CML LSCs, making CML a suitable model for cancer stem cell studies.

1.3 CML

1.3.1 Introduction

As previously mentioned, CML is a myeloproliferative disorder that originates at the HSC level, making CML a highly suitable model for cancer stem cells studies. CML is driven by BCR-ABL, a fusion onco-protein with a constitutive tyrosine kinase activity. The discovery of imatinib, a c-Abl tyrosine kinase inhibitor (TKI), revolutionised the treatment of CML by inducing cytogenetic and molecular responses in the majority of CML patients in chronic phase. However imatinib and second/third generation TKIs only target dividing cells and do not eradicate CML stem cells (CML LSCs), leading to disease persistence with associated risk of toxicity, drug resistance and relapse. In the following sections, we will review in detail the pathophysiology and the treatments of CML, including the current strategies to target LSCs.

1.3.2 Epidemiology

CML accounts for 10-15% of all cases of leukaemia in Western countries. Reports have described that CML incidence ranges between 0.6 to 2.0 cases per 100,000 persons per year (41). In Scotland particularly, Harrison, Johnson and Holyoake reported a CML incidence of 0.64 per 100,000 persons between 1999 and 2000 (42). Since the introduction of new treatments that dramatically improved the survival of patients, the prevalence rates of CML have been increasing every year and is estimated to go from 70,000 cases in 2010 to reach a plateau of 181,000 cases in 2050 in the United States (43). At diagnosis, the median age of CML patients is 53 years and, with a male-to female ratio of 1.3-1.8, men are more frequently affected with CML than women (41).

There is no clear evidence of risk factors that could cause CML and, despite being caused by a genetic abnormality, CML is not a hereditary disease. However, studies have shown that certain environmental factors can increase the risk of developing CML. First, atomic bomb survivors in Japan and Chernobyl liquidators that were exposed to high dose of radiation display increased incidence rate of leukaemia in general, including CML (44). Similarly, people exposed to benzene or pesticides have a higher risk of developing CML (45).

1.3.3 Disease progression

CML presents in three distinct phases, starting with chronic phase CML (CP-CML) that sequentially evolves, if untreated, to acute phase CML (AP-CML) and BC (46, 47). The vast majority of patients (85%) are diagnosed at CP-CML and present subtle symptoms such as fatigue, weight loss, splenomegaly, discomfort, left upper quadrant pain and/or nights sweats. Because of this insidious onset, CP-CML is often diagnosed during a routine health check. Patients in CP-CML display elevated number of myeloid progenitor cells that retain their capability of differentiation, leading to a concomitant increase in the number of mature granulocytes as well as in basophils and eosinophils. Immature blast cells account for less than 2% of the WBCs (47). Additional mutations during CP-CML can drive evolution of the disease into AP-CML, characterised by an increased splenomegaly and in the number of leucocytes or white blood cells (WBCs). At this stage, the

differentiation is arrested and immature blast cells are present in a higher amount, accounting for 10-19% of total WBCs (48). Following AP-CML or directly after CP-CML, the disease can progress to the final BC stage that is associated with worsened symptoms and resistance to therapy (although already present at the AP-CML stage). The blasts represent more than 20% of WBCs in the BM at this phase (49).

1.3.4 Molecular pathophysiology of CML

In 1960, Nowel and Hungerford identified the presence of an abnormal shortened chromosome 22 in cells isolated from CML patients (50, 51). This chromosome was later designated “Philadelphia (Ph) chromosome”, eponym of the city in which it was initially discovered (52). Subsequent studies demonstrated that the Ph chromosome is a result of a reciprocal translocation between the long arms of chromosome 9 and 22 (refer to as t(9;22)) and is found in more than 90% of CML patients. Precisely, the genes involved in this translocation are the breakpoint cluster region (BCR) on chromosome 22 and the Abelson murine leukaemia viral oncogene homolog (ABL) on chromosome 9 that encodes for a tyrosine kinase (53). Consequently, the t(9;22) translocation forms two chimeric genes: BCR-ABL and ABL-BCR genes on chromosome 22 and 9 respectively. Of note, the ABL-BCR gene does not seem to be involved in CML, and no protein has been isolated so far. In contrast, the BCR-ABL gene encodes for a fusion BCR-ABL protein with a constitutively activated tyrosine kinase (54, 55). The breakpoint on the BCR gene can occur at different sites and three different BCR-ABL genes can be generated accordingly. However, the 210 kDa cytoplasmic BCR-ABL protein, also referred to as p210^{BCR/ABL}, is found in most patients (56). Importantly, the expression of the fusion protein was demonstrated to be necessary and sufficient to cause and maintain CML. Indeed, in transgenic mice models, expression of BCR-ABL in HSC was responsible for initiating and maintaining a leukaemic phenotype that resembles CP-CML in humans (57-59). In other words, one single hit that induces a chromosomal translocation and expression of the BCR-ABL protein (at the HSC level; see below) is sufficient for leukaemic transformation.

Evidence of the stem cell origin of CML came initially from the work of Fialkow and colleagues. They demonstrated that erythrocytes and myeloid cells in female

CML patients with heterozygous X-linked glucose-6-phosphate dehydrogenase (G6PDH) had the same single enzyme type for G6PDH while other cells in the body were heterogeneous (60). This suggested that both erythrocytes and granulocytes originated from the same stem cell, indicating that CML is a clonal disease with a stem cell origin. They as well demonstrated in subsequent studies that the leukaemic clone could give rise to B lymphocytes in CML patients, further indicating the HSC origin of CML (61, 62). Additional proof came from one recent study that analysed BCR-ABL mRNA levels in CML patients with major molecular response (MMR) following imatinib treatment. This study revealed that residual BCR-ABL-expressing cells could still be isolated from CML patients in MMR, and importantly, these leukaemic cells were almost entirely comprised within the HSC subset (63). This observation, together with the fact that the persistent CML cells have the ability to repopulate the disease in half of the patients with MMR upon imatinib discontinuation (discussed below **1.3.8**), was a conclusive evidence of the stem cell origin of CML.

1.3.5 CML diagnosis and monitoring

Given the presence of the Ph chromosome in more than 90% of CML patients, the diagnosis of the disease relies mainly on the detection of the abnormal chromosome by cytogenetic analysis of BM samples. Noteworthy, the Ph chromosome can be present in AML and acute lymphoblastic leukaemia (ALL). CML monitoring is commonly performed by blood counts tests, cytogenetic analysis of the BM and quantification of mRNA levels of BCR-ABL transcripts. Several terms are commonly used in the clinic to assess the response to treatments. Complete haematological response (CHR) is defined as the normalisation of the blood counts, the WBCs differential and the spleen at physical examination. A major cytogenetic response (MCyR) represents a decrease in the percentage of Ph⁺ cells in the BM, and a complete cytogenetic response (CCyR) by extension is achieved when no Ph⁺ cells can be detected. Finally, a major molecular response (MMR) is defined as a 3-log reduction in BCR-ABL transcripts compared to standardised baseline levels (64).

1.3.6 BCR-ABL signalling pathway

Tyrosine kinases catalyse the transfer of the ATP phosphate group to a tyrosine on a protein, thereby activating a number of downstream signalling pathways. In physiological conditions, the ABL protein shuttles between the cytoplasmic and nuclear compartment (65). However, the nuclear-cytoplasmic transport is impaired in the fused protein and BCR-ABL localises almost exclusively in the cytoplasm where it signals to downstream partners. Moreover, while ABL kinase activity is auto-inhibited in physiological conditions, BCR-ABL has a constitutive tyrosine kinase activity, which promotes protein folding into an active conformation and induces auto-phosphorylation. This will favour binding sites to the SH2 domains of downstream proteins including phosphoinositide 3-kinase (PI3K), mitogen-activated protein (MAP) kinase, nuclear factor- κ B (NF κ B), RAS, and signal transducer of activation and transcription 5 (STAT5; Fig. 1.2) (66-68). Precisely, BCR-ABL forms a complex with the GRB2 protein and Son of Seventhless (GRB2/GAB2/SOS) that activates the RAS downstream pathway (69, 70). Active RAS will then activate MAP kinases, which promotes cellular proliferation. Moreover, the GRB2/GAB2/SOS complex activates the PI3K/AKT pathway that acts on the apoptotic machinery to promote cell survival (71). In addition, constitutive activation of STAT5 confers growth factors independence to CML cells (72). MYC has as well been shown to be directly upregulated by BCR-ABL and seems to be involved in the progression of the disease (73).

In the end, all these pathways act concomitantly to promote cell survival, proliferation and leukaemogenesis.

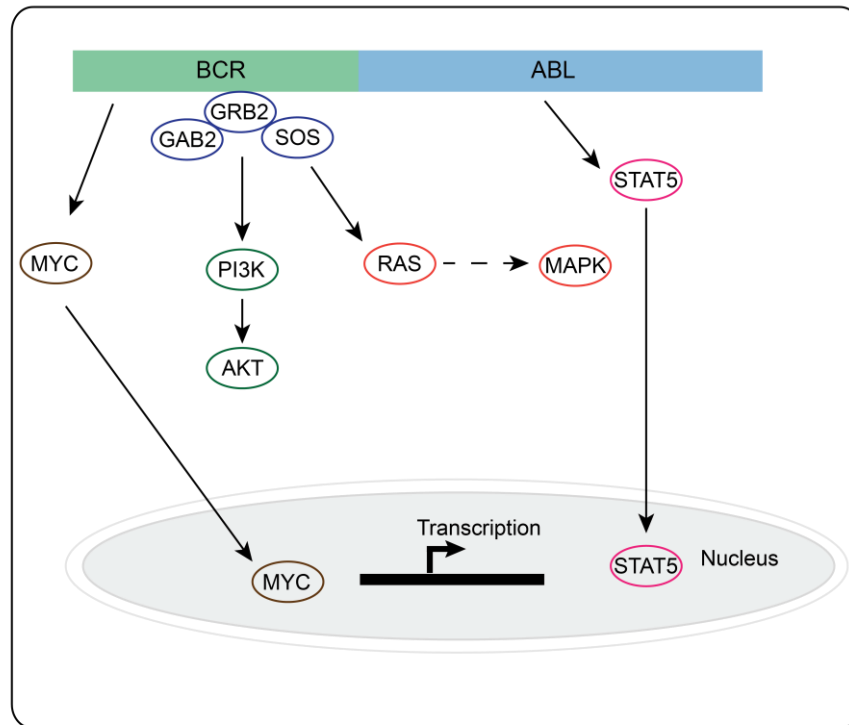


Figure 1. 2 BCR-ABL signalling pathway.

SOS, Son of Seventhless; STAT5, signal transducer of activation and transcription 5; PI3K, phosphoinositide 3-kinase; MAP, mitogen-activated protein.

1.3.7 CML Treatment

1.3.7.1 Historical Overview

In the end of the 19th century, treatment options for CML patients were very limited, with the only reported therapy being the use of arsenic. In the 20th century, CP-CML patients were treated with splenic radiotherapy at first and sequentially with two chemotherapeutic agents, busulfan and hydroxyurea. With fewer adverse events, hydroxyurea prolonged the duration of CP-CML and survival compared to busulfan (74, 75). However, neither busulfan nor hydroxyurea were able to control the disease and patients eventually progressed to BC within a few years, making CML a fatal and incurable disease at that time.

Allogeneic stem cell transplantation (allo-SCT) became the treatment of choice for CML in the mid-1970s. A three-year follow up study on 450 CP-CML patients who underwent BM transplantation reported relapse rates and an overall survival of 11.5% and 56% respectively (76). Despite improving survival rates, allo-SCT is

associated with substantial risk of death and complications, including host-graft reactions, infections, and rejection of the graft. Moreover, the strict criteria of eligibility prevented the vast majority of CML patients (>80%) from receiving the transplantation. For instance, allo-SCT was restricted to patients under sixty years old without any other comorbidities. Nowadays, allo-SCT remains the only proven curative treatment of CML (77).

Prior to being tested in CML, interferon-alpha (IFN- α) had demonstrable effect against other malignancies and was known to induce leukopenia in patients. This initial observation led Verma *et al.* to investigate the effect of IFN- α against CML cells (78). More than a decade later, a cooperative randomised clinical trial on over 1500 CML patients demonstrated that IFN- α significantly improved the five-year survival rate to 55% in comparison to 37% for patients treated with busulfan or hydroxyurea (79). Increased survival in patients treated with IFN- α in comparison to chemotherapeutic drugs was confirmed by several multi-centered trials (80-83). Moreover, 15% of CML patients treated with IFN- α achieved a CCyR that was sustained for six years in 10% of the patients following treatment discontinuation, an observation that had never been seen outside the allo-SCT option (84). Combination of IFN- α with low dose cytarabine was as well found to increase cytogenetic response rates compared to the single agent (85, 86). Nonetheless, one fifth of the patients had to discontinue IFN- α treatment due to severe adverse effects. The mechanisms of action of IFN- α are not fully understood, but it has been suggested that IFN- α acts as a cytostatic agent, restore the adhesion of leukaemic progenitor cells, or even target the immune system to enhance immune responses (87-89).

1.3.7.2 The imatinib era

In 1990s, the development of the first TKI against BCR-ABL, imatinib (STI571, Gleevec®, Glivec®, formerly CGP 57148B), by biochemist Nicholas Lyndon brought a revolution in the management of CML. Imatinib is an inhibitor of the tyrosine kinase activity of ABL, BCR-ABL, c-KIT and PDGFRA. Imatinib binds to the ATP binding-pocket of the Abl kinase domain and locks it in an inhibited conformation, therefore impairing the tyrosine kinase activity and preventing phosphorylation to key downstream substrates that promote CML. The idea that BCR-ABL, with its

constitutive tyrosine kinase activity, drives CML pathogenesis combined with promising pre-clinical results led Brian Druker to test imatinib treatment in CML patients (90). Impressive results were initially obtained during phase I and II clinical trials on patients who failed IFN- α therapy, with 95% of patients achieving CHR, 41% a CCyR and 89% of patients maintained in CP-CML after 18 months (91). Moreover, the oral bioavailability of imatinib and its inferior toxicity in comparison to previous treatments reduced the frequency of treatment interruptions. In 2000, the International Randomized Study of Interferon and ST1571 (IRIS) trial investigated the efficacy of imatinib (400 mg daily) in comparison to IFN- α in combination with low-dose cytarabine in 1106 newly diagnosed CP-CML patients. All outcomes were better in the imatinib treated arm; imatinib demonstrated increased tolerability, CHR, CCyR, progression-free survival compared to IFN- α and cytarabine. Precisely, CHR and CCyR was achieved in 95% and 74% of patients treated with imatinib versus 56% and 9% in the combination treatment arm. Moreover, after a median of 9 months, 90% of patients treated with IFN- α had switched to imatinib (92). Soon after this phase III study (in December 2001), the FDA approved imatinib as a first-line therapy for the treatment of Ph⁺ CP-CML patients. The six-year follow-up of the IRIS trial revealed that the estimated overall survival was 95% for CML patients treated with imatinib, when only CML-related death were taken into account (93).

1.3.7.3 Response to imatinib

The best outcomes with imatinib are seen for patients with CP-CML, and patients who presents with AP-CML or BC poorly respond to imatinib treatment. In 2013, the European LeukemiaNet (ELN) provided detailed recommendations for managing and monitoring the response to imatinib. Based on these suggestions, CHR is expected to be achieved in less than three months after treatment initiation, which is seen in 98% of the patients (94). Failure to obtain or maintain CHR is a sign of progression of CML and requires modification of the therapy. Ideally, CCyR and MMR should be achieved within six and twelve months of treatment.

1.3.7.4 Resistance to imatinib

CML represents the first success story of targeted therapy. However, despite its superiority in comparison to previous standard treatments, it soon became apparent that a subset of CML patients were failing therapy and showed signs of drug resistance. Primary resistance is defined as the failure of achieving CHR and MCyR at three and six months of treatment respectively. On the other hand, the term acquired resistance is used upon the loss of previous imatinib response, such as an increase in BCR-ABL mRNA levels by five to ten-fold compared to previous tests.

Several mechanisms of acquired resistance to imatinib have been identified, notably mutations in the ABL-kinase domain, amplification of BCR-ABL, overexpression of the multidrug-resistant P-glycoprotein (MDR-1), as well as the development of BCR-ABL-independent signalling pathways (95).

BCR-ABL dependent mechanism of resistance

Point mutations

The predominant cause of acquired resistance are point mutations in the ABL tyrosine kinase site; precisely in the drug-binding site, the phosphate-binding domain, the catalytic site and the activation loop - all preventing efficient drug binding (96-98). More than a hundred mutations have been reported so far, one of the most frequent being the substitution of threonine to isoleucine at position 315 (T315I) (99, 100) .

BCR-ABL amplification

Amplification of the BCR-ABL fusion protein has been reported in some patients in BC (99). Moreover, BCR-ABL amplification in CD34⁺ CML cells has been shown to confer resistance to imatinib and results in increased mutational rates (101). However, Hochhaus *et al.* reported in 2002 that this mechanism of resistance occurred in few CML patients and as such does not represent a major cause of drug resistance (102).

BCR-ABL independent pathways mechanism of resistance

Pharmacokinetics

The plasma concentration of imatinib has been shown to vary markedly among CML patients, with a low concentration associated with a suboptimal response and failure to achieve CHR. Inter-individual differences in cytochrome P450 and in plasma acute phase protein, α 1-acid glycoprotein that respectively metabolises and binds to imatinib have both been suggested to play a role in this primary resistance to imatinib (103, 104). Treatment compliance has as well been reported as being essential to achieve MMR. Indeed, patients with less than 90% treatment adherence have a significant decreased probability of achieving MMR (105).

Drug efflux

Proteins of the ATP-binding cassette (ABC) transporter family, such as the multidrug resistance gene product P-glycoprotein (P-gp; ABCB1) and the breast cancer resistance protein, have been implicated in the loss of drug response in many malignancies, including for imatinib and other TKIs in CML. ABC proteins family can actively export drugs from the intracellular compartment, leading to a decrease in the intracellular concentration of the drug. Noteworthy, the expression of P-gp has been reported to be particularly elevated in primitive haematopoietic cells and even more so in leukaemic cells from BC CML patients. Moreover, overexpression of P-gp has been associated with a lack of reaching a cytogenetic response with imatinib. In addition, low expression of organic cation transporter 1 (OCT1), responsible for imatinib uptake, can result in poor response to treatment (106).

Clonal evolution

Clonal evolution is known as the development of additional cytogenetic abnormalities, namely trisomy 8 and 19, aberration of chromosome 17q with loss of p53 or a second copy of the Ph chromosome. This mechanism of resistance is believed to be primordial, as 50% of patients that lost imatinib response harbour chromosomal abnormalities in CP-CML and AP-CML and up to 80% in BC (107).

1.3.7.5 Strategies to overcome resistance

Second and third generation of TKIs with increased affinity for BCR-ABL have been developed to overcome drug resistance.

Nilotinib -2nd generation

Nilotinib is structurally similar to imatinib and is characterised by a 30-50 times increased affinity for the unmutated BCR-ABL ATP-binding site. Moreover, it has been shown to target leukaemic cells harbouring point mutations, apart from the T315I mutation. The ENESTnd clinical trial compared nilotinib and imatinib safety and efficacy in newly diagnosed CP-CML. This study demonstrated that patients treated with nilotinib had significantly increased MMR rates in comparison to imatinib at twelve months. Similarly, 85% of the patients treated with nilotinib achieved CCyR versus 77% in the imatinib treated group (108). Moreover, the five-year follow-up revealed that 52% of the patients in the nilotinib arm achieved deep molecular response, defined as 4.5 log reduction in BCR-ABL transcripts on the international scale (MR(4.5)), while less than one-third (31%) of imatinib-treated patients achieved MR(4.5) (109). Due to this improved efficacy, nilotinib has been approved as a first-line therapy for Ph+ CP-CML patients (110).

Dasatinib-2nd generation

The second-generation TKI dasatinib (Sprycel®; Bristol Myers Squibb) is 325 times more potent inhibitor than imatinib against BCR-ABL and can as well target kinases from the c-KIT, SRC and PDGF-R family. Importantly, dasatinib can inhibit mutated BCR-ABL, with the exception of the T315I mutation, and target leukaemic cells that are resistant to imatinib. Similar to nilotinib, newly-diagnosed CP-CML patients treated with dasatinib displayed faster and increased rates of achieving CCyR and deep molecular responses in comparison to imatinib, which led to the approval of dasatinib as a first-line treatment for CP-CML patients (111, 112).

Bosutinib-2nd generation

Bosutinib is an inhibitor of BCR-ABL and SRC kinase and, in contrast to dasatinib, has no significant effect against c-KIT and PDGF-R. Bosutinib has been shown to target unmutated BCR-ABL in the nanomolar range as well as mutated BCR-ABL, with the exception of the T315I mutation. The bosutinib versus imatinib in newly diagnosed CP-CML BELA trial revealed that the rate of CCyR was similar between bosutinib (70%) and imatinib (68%) at twelve months. However, the MMR rate was superior in the bosutinib-treated group (41%) compared to imatinib (27%) (113). Importantly, a phase I/II study demonstrated that bosutinib induced MCyR in approximately 60% of CP-CML patients resistant or intolerant to imatinib. This

response was seen for all types of point mutations, apart from T315I (114). In 2012, bosutinib was approved as a second-line therapy for CP-CML patients with resistance or intolerance to previous TKI therapy (115).

Ponatinib- 3rd generation

The search for inhibitors that target the T315I mutation was finally successful with the development of the pan-BCR-ABL inhibitor ponatinib in 2012. *In vitro* studies demonstrated that ponatinib inhibited proliferation of leukaemic cells carrying native and mutated BCR-ABL with respective IC₅₀ values of 0.5 nM and 36 nM (116). However, phase II clinical trials demonstrated that ponatinib, while being effective in CP-CML patients carrying the T315I mutation, led to increased cardiovascular risk (117, 118). As a result, the planned phase III trial that aimed to compare imatinib to ponatinib was stopped and ponatinib is now only indicated for the treatment of CML patients with the T315I mutations or for those who failed to respond to other available TKIs (118, 119).

1.3.8 CML LSCs persistence

Despite the emergence of TKI-resistance, some patients reach CMR and have undetectable levels of BCR-ABL transcripts. The Stop Imatinib (STIM) trial investigated the effect of imatinib discontinuation in CML patients that were in CMR for a minimum two years under imatinib treatment. Strikingly, more than half of the patients (58%) relapsed with CML within six months of imatinib discontinuation. Of note, all relapsed patients responded to reintroduction of TKI therapy, indicating that the relapsed CML is similar to the initial disease (120). Similarly, the Australian TWISTER study that used similar selection criteria of entry to the STIM study showed that less than half of the patients (47.1%) were free of relapse at 24 months (121). In addition, subsequent studies demonstrated that CML LSCs could still be detected in CML patients with deep molecular response under TKI treatment (122).

While these studies showed that TKI therapy could be safely stopped in some cases, they as well demonstrated the persistence of CML LSCs that are at the origin of a molecular relapse in approximately half of the patients. This means that these patients will need to be treated with TKIs all their life to prevent CML relapse.

Importantly, these trials were performed in the best-TKI responders, indicating that the real percentage of CML patients requiring life-long therapy is far higher than the 50% observed in clinical studies.

Accordingly, many *in vitro* studies have demonstrated that CML LSCs are not addicted to BCR-ABL activity and therefore not eliminated by TKI therapy (Fig. 1.3) (123-127). Corbin *et al.* demonstrated initially that CML LSCs were able to survive TKI therapy despite equivalent inhibition of BCR-ABL activity in both differentiated and primitive cells (123). Moreover, quiescent primitive CML cells survive imatinib treatment at a concentration 10 times higher than the reported inhibitory concentration of differentiated cells (125). Additionally, Hamilton *et al.* showed that prolonged treatment with the potent ABL kinase inhibitor dasatinib, combined with absence of growth factors, is not sufficient to target primitive CML LSCs despite complete inhibition of BCR-ABL tyrosine kinase activity (126).

Put together, these studies demonstrated that CML LSCs are inherently resistant to TKIs and thus, new therapeutic strategies targeting BCR-ABL independent signalling pathways may be needed to effectively eliminate them.

Many studies have been investigating combinational approaches of TKIs with other agents targeting survival pathways of CML LSCs. For instance, Zhang B *et al.* demonstrated that imatinib in combination with histone deacetylases inhibitors can target quiescent CML cells *in vitro* and CML LSCs in a humanised mouse model (128). Another study showed that inhibition of ALOX5, an enzyme that catalysed the transformation of fatty acid into leukotrienes, was primordial for CML LSCs survival and prolonged survival of leukaemic mice (129). Perturbation of the Hedgehog pathway by loss of Smoothed (SMO) was as well demonstrated to eliminate CML LSCs (130). As a result, a phase I clinical trial was initiated to assess the safety and efficacy of imatinib with a SMO inhibitor in combination with dasatinib in CP-CML patients. However, the reported toxicity of the SMO inhibitor combined with its lack of clinical efficacy was not in support for further investigation and its use in CP-CML (131). Another study demonstrated that CML LSCs are sensitive to pioglitazone-mediated peroxisome proliferator-activated receptor alpha (PPAR- α) activation. Moreover, pioglitazone treatment in combination with imatinib led to sustained CMR in CML patients, albeit this was

performed in only three patients (132). Interestingly, in a cohort of twenty-four CP-CML patients treated with the combination of pioglitazone and imatinib, 56% achieved MR(4.5) while less than half (21%) were estimated to reach the same outcome with imatinib alone (133). More recently, Holyoake and colleagues showed that Tumour protein 53 (TP53) activation combined with MYC inhibition is able to eliminate CML LSCs (134). However, this combination of treatment does not include a TKI, the current standard care for CML management; therefore, this new approach might be disregarded in TKI-responders CP-CML patients.

While many *in vitro* and preclinical studies have uncovered new strategies to target CML LSCs, so far they were not translated to the clinic and patients are still in need of an effective strategy to eradicate CML LSCs.

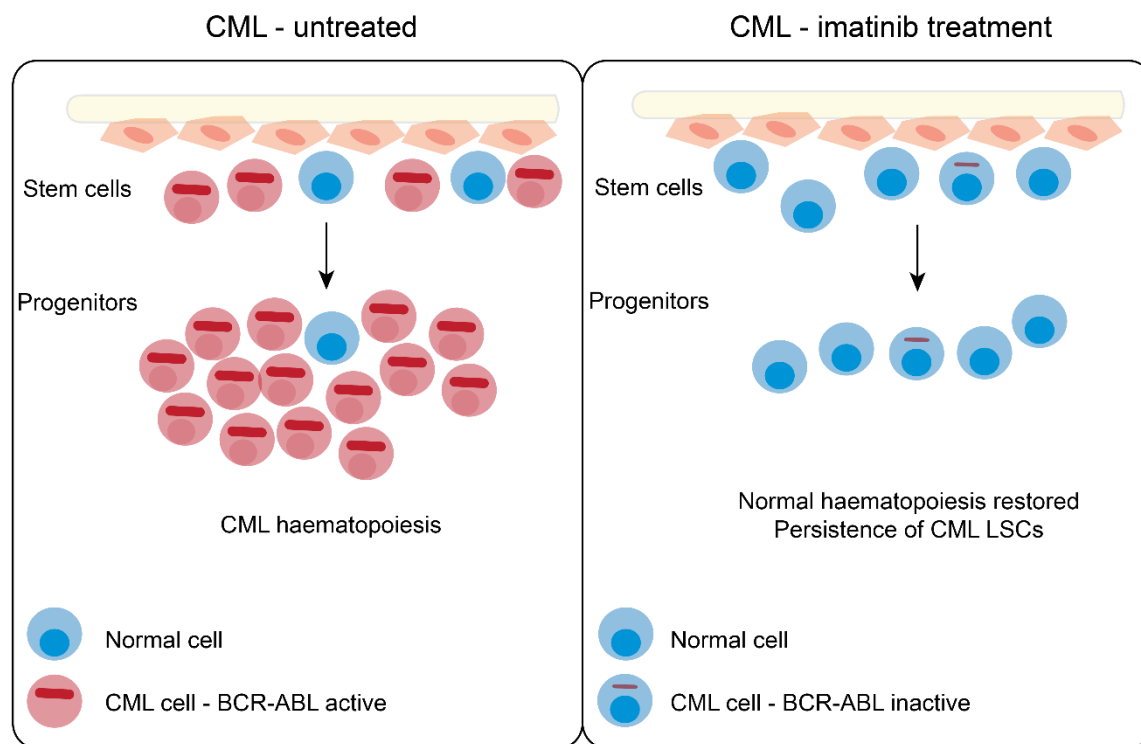


Figure 1. 3 Persistence of CML LSCs following imatinib treatment.

(Left) BCR-ABL promotes proliferation of CML cells. (Right) Upon imatinib treatment, normal haematopoiesis is restored but CML LSCs persist and are the origin of CML relapse upon treatment discontinuation.

Adapted from (111).

1.4 Metabolism and HSC fate

1.4.1 Metabolism at a glance

Glycolysis is a series of ten metabolic steps that converts one molecule of glucose into two molecules of pyruvate, generating two molecules of ATP and NADH. Glucose enters the cells by specific transporters from the GLUT family and once intracellular, glucose is rapidly phosphorylated into glucose-6-phosphate (Glc-6P) by the hexokinases (HKs, **Fig. 1.4**). Glc-6P can either enter the pentose phosphate pathway (PPP) to generate reducing equivalents and precursors for nucleotides biosynthesis or be isomerised into fructose-6-phosphate (Fru-6P) by phosphoglucose isomerase (PGI). The last step of glycolysis is the formation of pyruvate by pyruvate kinase.

Pyruvate can have two distinct fates: it is either reduced to lactate by lactate dehydrogenase (LDH) or enters the mitochondria where it will be oxidised to acetyl coenzyme A (coA) by pyruvate dehydrogenase (PDH) to fuel the tricarboxylic acid (TCA) cycle (**Fig. 1.4**). The TCA cycle is a hub for metabolism and integrates fatty acid, carbohydrate and amino acid metabolism. For instance, fatty acid oxidation (FAO) generates acetyl coA that can be oxidised in the TCA cycle. Moreover, the TCA cycle is central to energy production and a source of biosynthetic precursors; it is therefore crucial to control the concentrations of TCA cycle metabolites. This is achieved by anaplerotic reactions that maintain homeostasis and replenish TCA cycle metabolites. For instance, reactions catalysed by pyruvate carboxylase (PC) and glutamate dehydrogenase ensure the replenishment of oxaloacetate and α -ketoglutarate respectively. Importantly, the TCA cycle generates reduced NADH and FADH₂ that will be used by the electron transport chain (ETC). The ETC consists of proteins localised in the inner membrane of the mitochondria that are organised as four large complexes (I, II, III and IV). Together with ATP synthase or complex V, they form the oxidative phosphorylation (OXPHOS) machinery. NADH and FADH₂ produced during the TCA cycle are then oxidised and transfer their electrons to complex I and II respectively. The electrons are subsequently transferred from one complex to another by a series of oxidative-reduction reactions which releases energy that is

used to pump proton from the matrix to the intermembrane space. The resulting proton gradient is used by ATP synthase to generate ATP (135).

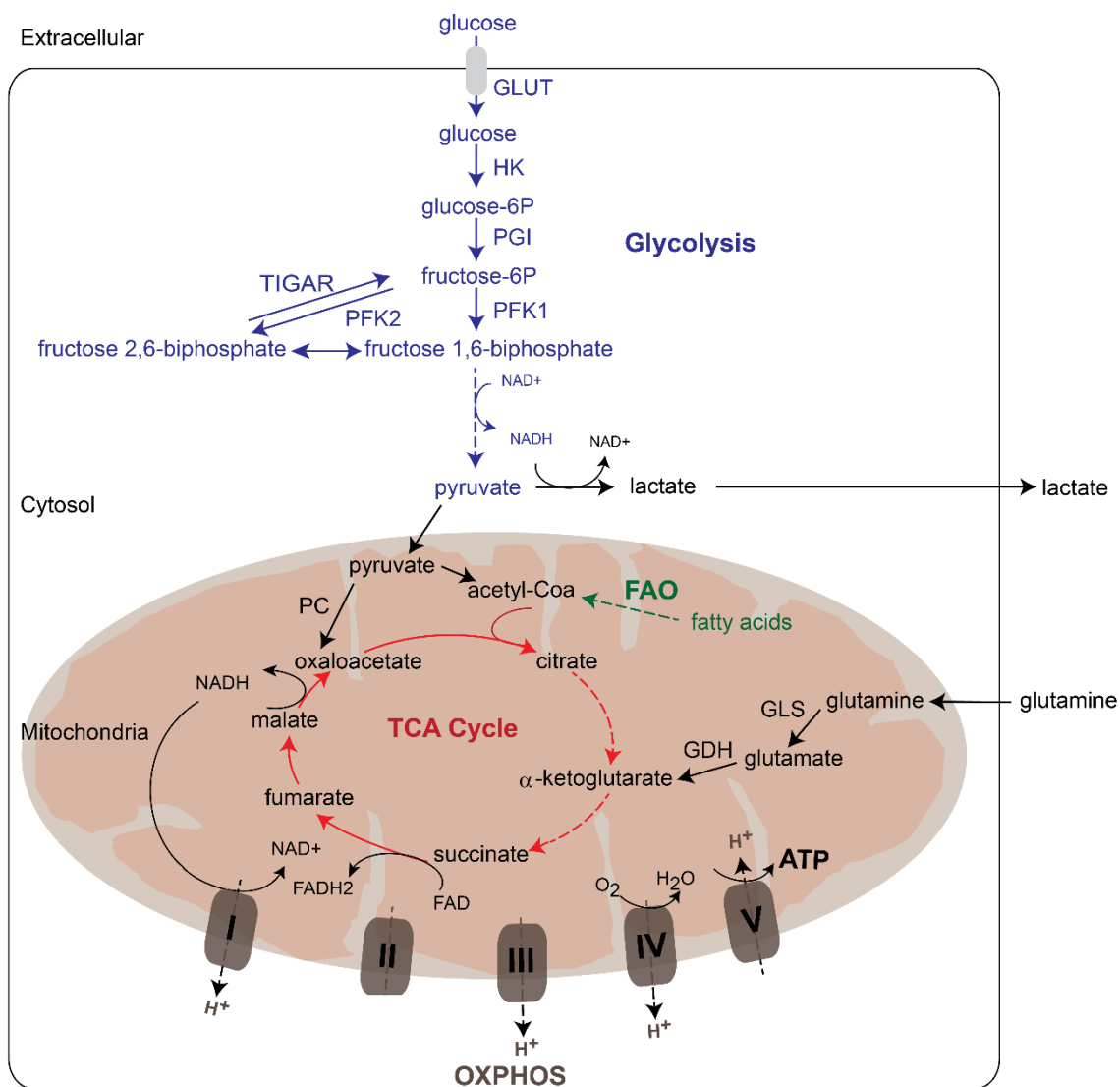


Figure 1. 4 Overview of cellular metabolism.

HK, hexokinase; PGI, phosphoglucose isomerase; PFK1/2, phosphofructokinase 1 and 2; TIGAR, TP53-inducible glycolysis and apoptosis regulator; PC, pyruvate carboxylase; FAO, fatty acid oxidation; GLS, glutaminase; GDH, glutamate dehydrogenase; OXPHOS, oxidative phosphorylation.

1.4.2 Use of stable isotopes as tracers

Metabolomics is ‘the quantitative measurement of the dynamic multiparametric response of living systems to pathophysiological stimuli or genetic modification’ or in other words, the study that aims to identify and quantify metabolites within a given system (cells, fluids, tissue) (136). Metabolic profiling is performed by two major approaches: nuclear magnetic resonance (NMR) and mass spectrometry (MS) in combination with a chromatographic separation method. As such, the use of liquid chromatography (LC) enables the separation of metabolites based on their physical properties.

Metabolomics often uses stable isotopes as tracers as it allows the exploration of the dynamic nature of metabolism in a robust manner. By definition, isotopes only differ in their number of neutrons and can therefore be distinguished by their atomic mass. Many isotopic tracers have been used in metabolic studies, including fully labelled glucose ($^{13}\text{C}_6$ -glucose), fully labelled palmitate ($^{13}\text{C}_{16}$ -palmitate) and fully labelled glutamine ($^{13}\text{C}_5$ -glutamine) in which the natural occurring ^{12}C carbon atoms have been replaced with ^{13}C atoms. This brings a mass shift of one Dalton per ^{13}C carbon atom that is detectable by mass-spectrometry and allows tracing the fate of a given metabolite into various metabolic pathways and assessment of metabolic fluxes.

1.4.3 Metabolic regulation of HSCs

One long lasting model states that quiescent HSCs reside within hypoxic regions of the BM and rely principally on glycolysis for energy production (137-140). Moreover, the low oxygen tension found in the BM niche is believed to be crucial for HSC quiescence (137, 138). Indeed, *in vitro* culture of cord blood HSCs under hypoxic condition has been shown to sustain their quiescence and stem-cell potential in comparison to normoxia (141). Moreover, several studies have shown that HSCs and progenitor cells (HSPCs) retained high level of the hypoxic probe pimonidazole *in situ* (142, 143). In contrast, recent advances in imaging techniques have suggested that HSPCs are principally found in heterogeneous perivascular regions (sinusoidal or periarterial) and that quiescent HSPCs face

higher oxygen levels than cycling counterparts, suggesting that hypoxia is not the only determinant for their proliferative status (144, 145).

Despite these controversies, the current consensus is that HSCs display a hypoxic profile that dictates their glycolytic phenotype. Accordingly, murine HSCs exhibit elevated levels of glycolytic intermediates, notably fructose-1,6-bisphosphate and pyruvate, and increased pyruvate kinase activity compared to differentiated progenitor cells (139, 146). Moreover, several studies have indicated that low mitochondrial metabolism, by limiting oxidative stress, acts as a gatekeeper of HSCs quiescence (146, 147). For instance, Takubo *et al.* demonstrated that pharmacological inhibition of pyruvate oxidation, resulting in inhibition of mitochondrial metabolism, maintained the stem cell potential of HSCs even after four weeks of *in vitro* culture (146).

Despite the glycolytic phenotype of HSCs at steady-state, several studies highlighted the importance of mitochondrial metabolism, particularly upon HSCs differentiation. Indeed, impairment of mitochondrial metabolism by deletion of the mitochondrial tyrosine phosphatase PTPMT1 in haematopoietic cells resulted in a block of differentiation, haematopoietic failure and accumulation of HSCs by 40-fold. The decrease in mitochondrial metabolism was shown to be mediated by high substrate levels of phosphatidylinositol phosphates (PIPs) that directly activated mitochondrial uncoupling protein 2 (UCP2) and prevented pyruvate entry into the TCA cycle (148). Interestingly, a recent study investigating the fate of old and new mitochondria upon division of HSCs revealed that daughter cells that kept stem cell traits received more newly-formed and less old mitochondria compared to cells that lost their stem cell potential, suggesting the importance of maintaining healthy mitochondria in HSCs (149).

The role of FAO in controlling HSC maintenance and fate has as well been put in the limelight in recent years. It was first shown that deletion of the tumour suppressor gene and promyelocytic leukaemia protein (PML) results in HSCs exhaustion by loss of quiescence. Moreover, PML was found to be essential for CML LSCs survival in humanised mouse models (150). A couple of years later, Ito *et al.* demonstrated that PML regulated HSC cell fate by acting on PPAR- δ and FAO. As such, deletion of PML or PPAR- δ , as well as pharmacological inhibition of FAO, resulted in the symmetric division of HSCs (giving rise to two committed daughter

cells) while activation of PPAR- δ promoted asymmetric division, generating one committed and one self-renewing HSC (151).

It can be puzzling to reconcile the idea that HSCs need to sustain low levels of mitochondrial metabolism with their parallel requirements for FAO, as FAO feeds the TCA cycle with acetyl coA. It has been suggested that the FAO-derived acetyl coA and oxaloacetate are used to generate citrate. Once exported in the cytoplasm, citrate can be converted into malate in two enzymatic steps, which then produces NADPH, by malic enzyme. Some have speculated that the reducing agent NADPH, by preventing oxidative stress, could be essential for stem cell maintenance. However, FAO is not anaplerotic and as such, it does not support a net production of oxaloacetate or citrate. Moreover, the prediction is that it would be far more effective to utilise glucose at the PPP rather than letting FAO support malic enzyme activity to generate NADPH. It is therefore unlikely or unclear how FAO contributes to NADPH production through the proposed mechanisms. A more plausible idea is that elevated levels of acetyl coA produced from FAO can regulate HSC fate through epigenetic mechanism and modification of histone acetylation. Nonetheless, the aforementioned points remain speculative and further investigations are required to determine the precise mechanisms between FAO and HSC regulation.

Altogether, these studies demonstrate that metabolic regulation of HSC is primordial for their maintenance and suggest that targeting selective metabolic pathways can reprogram HSC fate.

1.5 Cancer Metabolism

1.5.1 Metabolic reprogramming of cancer cells

Quiescent cells such as HSCs require energy at homeostasis to maintain housekeeping functions such as securing cell membrane potentials and protein synthesis. However, the demand in energy and nutrients increases significantly upon cellular division. In order to proliferate, cells need to double their biomass and replicate their genome, processes that not only require energy but as well nucleotides, proteins and lipids. One example of metabolic remodelling that occurs during proliferation is the activation of T cells. While quiescent T cells

display low rate of energy metabolism, activated/proliferating T cells rewire their metabolism and engage in anaerobic glycolysis (152-154). Similarly, cancer cells need to adapt their metabolism, notably by increasing nutrients uptake and metabolism, to sustain their uncontrolled proliferation (155). In fact, the metabolism of cancer cells is not only an indirect consequence of proliferation as it can be as well directly reprogrammed by oncogenic signalling (156, 157). For instance, activation of the PI3K/AKT pathway, commonly observed in cancer, stimulates aerobic glycolysis by increasing the expression GLUT transporters and activating HK (158-160). Similarly, the frequently dysregulated oncogene MYC has been shown to regulate glutamine as well as glucose metabolism and induce mitochondrial biogenesis (161-163). However, the molecular and biochemical mechanisms leading to the altered metabolism of cancer cells are often complex and involve multiple pathways (164).

1.5.2 The Warburg effect and glycolysis in cancer

In the 1920s, Otto Warburg described that cancer cells preferentially metabolise glucose into lactate even in presence of oxygen, a process commonly refer to as ‘aerobic glycolysis’ or the ‘Warburg effect’ (165). It was initially proposed that dysfunctional mitochondria in cancer cells were the reasons for this glycolytic phenotype and even the cause of cancer; however, mitochondria were since then shown to be active in the majority of tumour types (166, 167). The increased glycolytic phenotype has been utilised in the clinic with ^{18}F -deoxyglucose positron emission tomography (FDG-PET), a tracer that enables *in vivo* imaging of solid tumours (168).

In line with Warburg’s initial observation, dysregulation in the expression and/or activity of glycolytic enzymes have since then been reported in many experimental models of cancer. For instance, the transcription factor hypoxia-inducible factor 1-alpha (HIF-1 α), induced by hypoxia and found increased in solid tumours, transactivates genes encoding for glycolytic enzymes such as phosphofruktokinase (PFK1) and HK (169-172). Moreover, it induces the expression of 6-phosphofruktose-2-kinase/fructose-2,6-biphosphate 3 (PFKFB3), that converts Fru-6P into the allosteric PFK1 activator fructose-2,6-biphosphate (Fru-2,6-BP, **Fig. 1.4**) (173). This regulation was suggested to play a significant role in the glycolytic phenotype

of cancer cells (174). TP53 has as well been shown to control glycolysis by lowering the intracellular levels of Fru-2,6-BP via TP53-induced glycolysis and apoptosis regulator (TIGAR) (175). Consequently, loss of TP53 function can indirectly promote glycolysis. Another example of the glycolytic upregulation in cancer cells is the increased expression of LDH-A observed in many types of solid tumours, which is essential to maintain elevated glycolytic flux as it replenishes the NAD⁺ pool (176-178).

1.5.3 Mitochondrial metabolism in cancer

As mentioned before, Warburg and others postulated that defects in mitochondrial functions were the cause of aerobic glycolysis. However, a plethora of studies have since then demonstrated that most cancer cells not only exhibit proper functioning mitochondria but as well require mitochondrial ATP production for their growth and survival (179-181).

In addition to glucose, oxidation of fatty acids and amino acids sustain mitochondrial metabolism in cancer cells by providing precursors to the TCA cycle. Indeed, glutamine, the most abundant amino acid in the blood, is essential for TCA anaplerosis as well as nitrogen supply for nucleotide and amino acid biosynthesis. Interestingly, increased glutamine consumption has been reported in various cancer models. For instance, Wise *et al.* and Gao *et al.* showed that MYC expression induced a transcriptional program that promoted glutamine metabolism and uptake (163, 182). They further demonstrated that glutamine was vital for sustaining the pool of TCA cycle intermediates and MYC-expressing cells essentially became addicted to glutamine. Similarly, some oncogenes have been shown to drive mitochondrial biogenesis and metabolism. For instance, a study by Vazquez *et al.* demonstrated that the melanoma oncogene microphthalmia-associated transcription factor (MITF) induced peroxisome proliferator-activated receptor gamma coactivator 1-alpha (PGC1- α) expression, promoting mitochondrial biogenesis and OXPHOS in a subset of melanoma cells (183).

The importance of FAO for cancer cell function and survival has as well been demonstrated in recent studies. In the cytoplasm, fatty acids are conjugated to carnitine by the rate-limiting enzyme carnitine palmitoyltransferase 1 (CPT1),

which allows their transport across the mitochondrial membrane. Once in the mitochondria, the catabolism of fatty acids generates acetyl coA that can enter the TCA cycle to generate NADH and FADH₂ for mitochondrial ATP production. Interestingly, CPT1 is overexpressed in numerous cancer and has been shown to confer protection to cancer cells against metabolic stress, such as glucose and oxygen restriction (184, 185).

Importantly, the increase in OXPHOS observed in some cancer cells has been associated with a dependency to this pathway, rendering cancer cells particularly sensitive to mitochondrial inhibition. This has been shown in models of AML, pancreatic cancer, chemo-resistant prostate cancer as well as diffuse large B-cell lymphoma (DLBCL) (186-190). Indeed, N. Danial and colleagues demonstrated in a recent study that a subset of DLBCL, resistant to B-cell receptor inhibition, displayed a transcriptional signature of OXPHOS genes and targeting this pathway was selectively toxic for cancer cells (191, 192).

In contrast to the aforementioned points, some hereditary forms of cancer are associated with a loss in mitochondrial function. Indeed, mutations and loss of function of the TCA cycle enzymes succinate dehydrogenase (SDH) and fumarate hydratase (FH) are associated respectively with paraganglioma and renal cell cancer (193-196). Loss of function of these enzymes leads to a truncated TCA cycle, mitochondrial dysfunction and a build-up of their respective enzymatic substrate: succinate for SDH loss and fumarate for FH loss. Consequently, prolyl hydroxylase domain (PHD) enzymes are inhibited and oncogenic HIF-1 is stabilised, leading to a pseudo-hypoxic and hypermethylated phenotype (197-199). Additionally, mutation in isocitrate dehydrogenase (IDH), observed in subsets of glioma and AML, results in gain of enzymatic function and generates 2-hydroxyglutarate (2HG) from α -ketoglutarate whereas the unmutated IDH catalyses the conversion of isocitrate to α -ketoglutarate. The resulting accumulation of the oncometabolite 2HG has been suggested to contribute to tumourigenesis, albeit the mechanisms have not been fully uncovered yet (200). Interestingly, two clinical trials demonstrated that IDH inhibition with enasidenib (Idhifa) resulted in the complete remission, defined as less than 5% of blasts in the BM and no evidence of disease, in 19% of patients with relapsed/refractory AML and IDH mutation (201). In August 2017, the FDA approved Idhifa for the

treatment of patients with relapsed/refractory AML who harbour the IDH mutation (202).

1.5.4 Targeting metabolic vulnerabilities of cancer cells

Given that cancer cells harbour a dysregulated metabolism, targeting metabolic vulnerabilities became an appealing strategy for anticancer therapy. Several anti-metabolic agents have actually been used for the past decades in cancer treatment. For instance, the class of anti-metabolites analogues of nucleosides, that includes 5-fluorouracil, gemcitabine and fludarabine, impair DNA synthesis and have been proven effective in a variety of cancer.

Because normal cells share similar metabolic pathways with cancer cells for ATP production, it has long been presumed that targeting the metabolism of cancer cells would have significant side effects. Indeed, the use of the chemotherapeutic agents described above often have significant adverse effects as they target the same metabolic pathways/enzymes in normal cells. Nonetheless, cancer cells have been shown to become addicted to certain metabolic pathways and their inhibition could offer a therapeutic window. Similarly, the identification of metabolic pathways that are redundant in normal cells and not in cancer cells could prevent unwanted toxicity. One successful example of this is the use of L-asparaginase in the clinic to selectively target ALL cells. This selectivity stems from the fact that ALL cells are auxotroph for asparagine and thus particularly sensitive to L-asparaginase (which breaks down asparagine in the blood), whereas normal cells can synthesise asparagine *de novo* from aspartic acid and glutamine by asparagine synthetase (203, 204). Finally, finding complementary, and potentially synergistic drug combination, might be a strategy to reduce the dose of each single agent and prevent undesirable side effects.

1.5.4.1 Targeting glycolysis and lactate metabolism

The observations that cancer cells display high rates of glycolysis, particularly in a hypoxic environment, led to the hypothesis that cancer cells are dependent on this pathway for ATP production. As such, most glycolytic enzymes have been regarded as potential therapeutic targets for cancer treatment.

2-deoxy-glucose (2-DG) is a synthetic structural analogue of glucose that acts as a glucose competitor at the HK level. Intracellularly, 2-DG is phosphorylated into 2-DG-P by HK. However, lack of the hydroxyl group prevents 2-DG-P to be further metabolised which results in its accumulation inside the cell and a decrease in glycolysis and consequently a drop in ATP levels. Many experimental models of cancer displayed sensitivity to 2-DG *in vitro*, particularly in hypoxic condition (205). *In vivo*, 2-DG did not seem to affect tumour growth as a single agent but sensitised pancreatic, osteosarcoma and non-small-cell lung-derived tumours to chemo- and radiotherapy (206).

Given that LDH-A catalyses a reaction essential to maintain elevated glycolysis, many studies have investigated the anticancer potential of LDH-A inhibition. *In vitro*, the proliferation of human hepatocellular carcinoma cells and colony-forming potential of MYC transformed cells is significantly impaired by targeting LDH-A (207). Similarly, pharmacological and/or genetic inhibition of LDH-A reduced tumourigenicity in many xenograft models, including human hepatocellular carcinoma, non-small-cell lung carcinoma (NSCLC), esophageal squamous cell carcinoma and breast cancer (208-211). However, no LDH-A inhibitors have been developed so far for human use.

In addition to glycolytic inhibitors, preventing the export of the glycolytic-derived lactate has been considered as a therapeutic approach in cancer. Highly glycolytic cells produce large amounts of lactate that need to be excreted outside the cells by monocarboxylate transporters (MCTs). Four MCTs proton-linked isoforms (MCT1-4) transporting lactate across the plasma membrane have been identified. Interestingly, while most tissue express MCT-1 at low levels, several solid tumours display high expression of MCT-1, suggesting a potential therapeutic window for targeting this transporter. Moreover, MCT-1 inhibition impaired tumour growth in preclinical cancer models (212, 213). Currently, a phase I study is recruiting patients with advanced solid tumours and DLBCL to test the toxicity, and later the effect, of pharmacological inhibition of MCT-1 with AZD3965 (214). However, MCT-1 has limited efficacy against some tumours, potentially because of the compensatory expression of MCT-4 in hypoxia or the ability of some cancer to engage in oxidative metabolism (212, 213).

1.5.4.2 Targeting mitochondrial metabolism

The failure of glycolytic inhibitors to significantly impair tumour cell growth *in vivo* has been associated with the ability of cancer cells to switch from a glycolytic phenotype to OXPHOS for ATP production. Moreover, some cancers display high rates of mitochondrial metabolism at steady-state, suggesting that inhibition of oxidative metabolism could be a therapeutic strategy in these tumours. Similar to glycolysis, normal cells use OXPHOS to generate ATP, and it is important to consider that a complete inhibition of this pathway could be detrimental towards normal cells. However, the fact that metformin and the antibiotic tigecycline are currently used in the clinic together with their reported ability to inhibit mitochondrial ATP production *in vitro* and in preclinical models (see below) indicates that inhibition of mitochondrial metabolism can be achieved without causing major toxicity in normal cells.

Epidemiological studies have shown that diabetic patients treated with metformin have a lower risk of developing cancer compared to patients treated with other antidiabetic agents (215). *In vitro* and *in vivo* studies have confirmed the anticancer activity of metformin and demonstrated that part of this effect is mediated by inhibition of mitochondrial complex I activity (216-218). Currently, there are numerous clinical studies investigating whether metformin can sensitise cancer cells to standard treatment across multiple tumour types (219). Similarly, a more potent analogue of metformin, phenformin, has proven effective in targeting cancer cells, notably KRAS-driven NSCLC with loss of LKB1 and in combination with BRAF inhibitors in melanoma harbouring the BRAF^{V600E} mutation (220, 221). However, phenformin is more toxic than metformin and has therefore been withdrawn from the market. Future studies will need to assess whether the greater potential antitumoural activity of phenformin counterweights for its increased toxicity in comparison to metformin.

Importantly, Škrtić *et al.* presented an innovative approach to target AML cells by inhibiting mitochondrial metabolism with an FDA-approved antibiotic. In this study, they initially performed a drug screening and found that the antibiotic tigecycline impaired the survival of AML cells lines and patient-derived cells *in vitro* and in a human xenograft mouse model. They further demonstrated that tigecycline acted by inhibiting the translation of mitochondrial encoded proteins,

which resulted in a decrease in mitochondrial function. Furthermore, they showed that AML cells were dependent on mitochondrial metabolism and consequently particularly sensitive to tigecycline treatment (187). This study was a robust example of how targeting mitochondrial metabolism can be a potential strategy exploited for cancer treatment.

Another approach to target mitochondrial oxidative metabolism is to inhibit glutamine catabolism. As mentioned previously, glutamine is a major anaplerotic source to maintain the levels of TCA cycle metabolites and support their use for biosynthetic purposes. Inside the cell, glutamine is converted into glutamate by glutaminase (GLS), followed by the conversion of glutamate into the TCA cycle intermediate α -ketoglutarate by glutamate dehydrogenase or aminotransferases. Several *in vitro* studies have demonstrated that glutamine is vital for MYC and KRAS-driven cancer cells, and thus, inhibition of glutamine catabolism has been proposed as a new approach for cancer treatment (181, 182, 222, 223). Accordingly, the two small inhibitors of GLS, compound 968 and bis-2-(5-phenylacetamido-1,2,4-thiadiazol-2-yl) ethyl sulphide (BPTES) have proven effective in reducing tumour growth in pre-clinical cancer models (224).

Finally, recent studies have demonstrated that targeting FAO to reduce mitochondrial metabolism can be of therapeutic interest. Indeed, pharmacological inhibition of FAO with the CPT1 inhibitor etomoxir markedly impaired growth of MYC-expressing triple-negative breast tumours in mice (225). Etomoxir was as well found to sensitise primary AML cells to apoptosis induction with the anti-apoptotic inhibitor ABT-737 and potentiated the effect of cisplatin in an *in vitro* model of colon cancer (226, 227). Noteworthy, one clinical trial assessing the effect of FAO inhibition in patients with congestive heart failure revealed that etomoxir was hepatotoxic in some patients (228). It would therefore be interesting to test the efficacy of safer FAO inhibitors in the future, such as the CPT1 inhibitor perhexiline that is approved for human use in Australia.

1.6 Aims

In this study, we first aimed to uncover metabolic alterations specific to CML LSCs by performing metabolomic analysis of patient-derived CML LSCs in comparison to normal counterparts and patient-matched differentiated leukaemic cells.

The second aim of this project was to pharmacologically target dysregulated metabolic pathway(s) and assess drug efficacy and selectivity against CML LSCs.

Chapter 2 Material and Methods

2.1 Material

2.1.1 General reagents

¹³ C ₁₆ -labelled palmitate	Cambridge Isotope Laboratories	408-35-5
¹³ C ₅ -labelled glutamine	Cambridge Isotope Laboratories	56-85-9
¹³ C ₆ -labelled glucose	Cambridge Isotope Laboratories	50-99-7
Ammonium acetate	Sigma	A1542
Ammonium persulfate	Sigma	248614
Antimycin A	Sigma	A8674
Bis-acrylamide 30%	Severn Biotech Ltd	20-2100-10
BIT 9500 Serum Substitute	Stem Cell Technologies	9500
Bovine Serum Albumine (BSA)		
Fatty Acid Free	Sigma	A8806
CD34 MicroBead Kit, human	Miltenyi Biotec	130-046-702
Cell Tak	Thermo Fisher Scientific	10317081
CellTrace Violet	Life technologies	C34557
Citrate Solution	Sigma	S5770
Collagen I, Coated Plate, 24 well	Thermo Fisher Scientific	A1142802
DAPI	Sigma	D9542
Dimethyl Sulfoxide (DMSO)	Fisher Scientific	D/4121/PB08
DMEM	Life technologies	21969035
DNase I Solution (1 mg/mL)	Stem Cell Technologies	7900
ECL full range		
Rainbow molecular weight marker	GE Healthcare LS	RPN800E
ECL Western Blotting substrate	Fisher Scientific	10005943
Empty Gel Cassette Combs		
1.5 mm, 10 well	Life technologies	NC3510
Empty Gel Cassettes, mini, 1.5 mm	Life technologies	NC2015
Ethanol	Chemical Stores	L/278/01
Ethylenediaminetetraacetic acid (EDTA)	Sigma	EDS
Fast SYBR® Green Master Mix	Applied Biosystems	4385612
FCCP	Sigma	C2920
FCCP	Sigma	C2759
Foetal bovine serum (FBS)	GIBCO	10270
Galactose	Sigma	G5388
Glycine	Sigma	G8898
HBSS- W/O PHENOL RED	Life technologies	14025100
HCL	Sigma	258148
Human Flt3-Ligand	PeprTech	300-19
Human GM-SCF	PeprTech	300-03
Human IL-3	PeprTech	200-03
Human IL-6	PeprTech	200-06
Human LIF	PeprTech	300-05

Human MIP-1 α	PeproTech	300-08
Human SCF	PeproTech	300-07
Human Serum Albumin	National Blood Transfusion Service	N/A
Hydrocortisone	Sigma	H0888
Hydroxychloroquine sulfate	Abcam	ab120827
Imatinib	LC Laboratories	I-5508
Imatinib Mesylate	LC Laboratories	I-5508
IMDM	Life technologies	21980
Isopropanol	Chemical Stores	L/585
L-Glutamine 100x (200 mM)	Gibco	25030
Magnesium Chloride	Sigma	208337
Magnesium Chloride powder	Sigma	208337
Metformin hydrochloride	Sigma	M0605000
Methanol	Chemical Stores	L/425/IE
Methanol (HPLC grade)	Fisher Scientific	67-56-1
MethoCult™ H4034	Stem Cell Technologies	4034
MicroAmp® Fast Reaction Tubes	Thermo Fischer Scientific	4358297
MitoTracker Green FM	Life technologies	M-7514
Monoclonal anti-actin ANTIBODY	Sigma	A4700
Mouse IL-3	Biologend	575504
Mouse IL-3	Biologend	575504
Mouse IL-6	Biologend	575704
Mouse IL-6	Biologend	575704
Mouse SCF	Biologend	579704
Myelocult H5100	Stem Cell Technologies	5150
Nitrocellulose membrane	Sigma	GERPN303D
NuPAGE™ LDS Sample Buffer	Thermo Fischer Scientific	NP0007
Oligomycin	Sigma	O4876
PBS	Homemade	N/A
PE	Homemade	N/A
Penicillin-Streptomycin	GIBCO	15140
Phenazine methosulfate (PMS)	Sigma	P9625
Phenformin hydrochloride	Sigma	P7045
PicoPure™ RNA Isolation Ki	Thermo Fisher Scientific	KIT0204
Pierce™ BCA Protein Assay Kit	Thermo Fischer Scientific	23225
Pierce™ Bovine Serum Albumin		
Standard Ampules, 2 mg/mL	Thermo Fischer Scientific	23209
Ponceau	Sigma	P7170
Potassium bicarbonate	Sigma	60339
Pre-Separation Filters (30 μ m)	Miltenyi Biotec	130-041-407
Protease inhibitors cocktail	Sigma	P8340
Protein assay kit, BCA	Fisher Scientific	13276818
RNeasy Mini Kit	Qiagen	74106
Rotenone	Sigma	R8875
RPMI 1640 Medium, no glutamine	Life technologies	3187005
SCF CARRIER FREE	Biologend	579704
Seahorse Base Medium	Agilent Technologies	102353
Separation columns	Miltenyi Biotec	130-042-401
Sodium Azide	Sigma	13412

Sodium bicarbonate (NaHCO ₃)	Sigma	S5761
Sodium chloride (NaCl)	Sigma	S5886
Sodium dodecyl sulfate (SDS)	Sigma	L5750
Sodium hydroxide (NaOH)	Sigma	S0899
Sodium pyruvate	Gibco	11360070
Streptavidin, Pacific Blue	Life technologies	S-11222
SuperScript™ VILO™ Master Mix	Thermo Fisher Scientific	11755050
Tetramethylethylenediamine (TEMED)	Sigma	T9281
Tigecycline	LKT Laboratories	T3324
TMRM	Life technologies	T-668
Tris	Sigma	T1378
Triton X-100	Sigma	T9284
Trypsin 2.5% 10X	Gibco	15090
Tween-20	Sigma	P2287
Western Strip Buffer	Thermo Fischer Scientific	46430
XF Calibrant	Seahorse Bioscience	
XTT	Sigma	X4626
β-mercaptoethanol	Sigma	M3148

2.1.2 Flow cytometry reagents

4',6-diamidino-2-phenylindole (DAPI)	D9542	Sigma
7-AAD staining solution	559925	BD Biosciences
Annexin V (APC)	550475	BD Biosciences
Annexin V (FITC)	640906	BD Biosciences
APC anti-mouse CD45	559864	BD Biosciences
APC anti-human CD34	555824	BD Biosciences
APC anti-mouse CD150	115910	Biologend
APC anti-mouse c-kit	135107	Biologend
APC anti-mouse Gr-1	108412	Biologend
Biotin Rat anti-mouse B220	553086	BD Biosciences
Biotin Rat anti-mouse CD4	553649	BD Biosciences
Biotin Rat anti-mouse CD5	553019	BD Biosciences
Biotin Rat anti-mouse CD8a	553029	BD Biosciences
Biotin Rat anti-mouse GR-1	553125	BD Biosciences
Biotin Rat anti-mouse Mac-1	553309	BD Biosciences
Biotin Rat anti-mouse TER119	553672	BD Biosciences
Celltrace Violet	C34557	Life Technologies
FC block	553142	BD Pharmigen
FITC anti-human CD45	555842	BD Biosciences
FITC anti-mouse CD45.1	110706	Biologend
FITC anti-mouse TER-119	116206	Biologend
Mitotracker green (MTG)	M-7514	Life Technologies
Pacific Blue™ anti-mouse CD45.2	109820	Biologend
PE anti-human CD133	372803	Biologend
PE anti-mouse CD48	103406	Biologend
PE/Cy7 anti-mouse Sca	122514	Biologend
PE/Cy7 anti-mouse/human CD11b (Mac-1)	101216	Biologend

PerCP anti-human CD38	303520	Biolegend
PerCP/Cy5.5 anti-mouse CD45.2	109827	Biolegend
Propidium Iodide	P4170	Sigma
Streptavidin, Pacific Blue	S-11222	Life technologies
Tetramethylrhodamine, methyl ester	T-668	Life Technologies

2.1.3 Western blot antibodies

OXPHOS cocktail	Abcam	ab110413
MT-CO2	Thermo Fisher Scientific	A-6404
Anti-mouse HRP-linked	Santa Cruz	sc-516102

2.1.4 Primers

<i>MT-CO1_F</i>	CTTTTCACCGTAGGTGGCCT
<i>MT-CO1_R</i>	AGTGGAAGTGGGCTACAACG
<i>MT-CO2_F</i>	CCGTCTGAACTATCCTGCCC
<i>MT-CO2_R</i>	GAGGGATCGTTGACCTCGTC
<i>18S_F</i>	GTAACCCGTTGAACCCATT
<i>18S_R</i>	CCATCCAATCGGTAGTAGCG

2.1.5 Primary cells

Patient sample: age/gender/disease and state/BCR-ABL status

CML 1: 63/M/CML Chronic Phase (CP)/BCR-ABL positive

CML 2: 55/M/CML-CP/BCR-ABL positive

CML 3: 61/F/CML-CP/BCR-ABL positive

CML 4: 56/M/CML-CP/BCR-ABL positive

CML 5: 56/F/CML-CP/BCR-ABL positive

CML 6: 48/F/CML-CP/BCR-ABL positive

CML 7: 58/M/CML-CP/BCR-ABL positive

CML 8: 46/M/CML-CP/BCR-ABL positive

CML 9: 30/M/CML-CP/BCR-ABL positive

CML 10: 33/M/CML-CP/BCR-ABL positive

CML 11: 28/F/CML-CP/BCR-ABL positive

CML 12: 62/M/CML-CP/BCR-ABL positive

CML 13: 50/M/CML-CP/BCR-ABL positive

CML 14: 43/M/CML-CP/BCR-ABL positive

CML 15: 69/M/CML-CP/BCR-ABL positive

Non-CML 020: 60/M/mantle cell lymphoma/BCR-ABL negative

Non-CML 026: 69/M/mantle cell lymphoma/BCR-ABL negative

Non-CML 029: 66/M/Diffuse Large B-Cell lymphoma/BCR-ABL negative

2.1.6 Cell lines

K562 and KCL22 cell lines were available in 'house'. The murine IL-3 dependent pro-B cell line Ba/F3 and Ba/F3 p210, stably expressing the native p210 isoform of BCR-ABL, were a kind gift from Professor Junia Melo. M2-10B4 and S1/S1 stromal cells lines were a kind gift from the Terry Fox Laboratory (Vancouver, BC, Canada). All cell lines were tested for mycoplasma contamination.

2.1.7 Equipment

7500 Fast Real-Time PCR System	Applied Biosystems
Mastercycler™ PCR machine	Eppendorf UK Ltd
FACSAria™ Fusion sorter	BD Biosciences
FACSVerse™	BD Biosciences
FACSCalibur™ Z6003	BD Biosciences
Seahorse flux analyser XF96	Agilent Seahorse Technologies
Q Exactive Orbitrap Mass Spectrometer	Thermo Fisher Scientific
NanoDrop™ 2000 Spectrophotometer	Thermo Fisher Scientific
NanoDrop™ 2000 Spectrophotometer	Thermo Fisher Scientific
CASY cell counter and analyser	Roche Applied Science
SpectraMax Plus 384	Molecular Devices
Absorbance Microplate Reader	
UltiMate 3000 HPLC system	Thermo Fisher Scientific

2.1.8 Composition of tissue culture media, solutions and buffers

RPMI⁺

RPMI 1640	500ml
FBS Heat inactivated	10%

RPMI-Galactose

RPMI no glucose	500ml
FBS Heat inactivated	10%
Galactose (1M)	11.1 mM

DMEM⁺

DMEM	500ml
FBS Heat inactivated	10%
L-Glutamine	2 mM

DMEM*1 for M2-10B4

DMEM	500ml
------	-------

FBS Heat inactivated	10%
L-Glutamine (200mM)	2 mM
Hygromycin	62.5 µg/mL
Geneticin G418	400 µg/mL

DMEM*2 for S1/S1

DMEM	500ml
FBS Heat inactivated	10%
L-Glutamine (200mM)	2 mM
Hygromycin	125 µg/mL
Geneticin G418	800 µg/mL

DAMP

DNase I (2500U/ml)	2 ml
Magnesium chloride (400X, 1.0M)	1.25 ml
Trisodium citrate (0.155M)	53 ml
Human Serum Albumin (20%, Scottish National Blood Transfusion Service)	25 ml
PBS	419ml

Serum free medium (SFM)

BIT	25 ml
Penicillin/Streptomycin (both 10,000U/ml)	1.25 ml
2-mercaptoethanol (50 mM)	250 µl
IMDM	97.25 ml

SFM supplemented with physiological growth factors (SFM+φGFs)

SFM	10 ml
LIF (0.1 µg/ml)	5 µl
SCF (0.5 µg/ml)	4 µl
G-CSF (2 µg/ml)	5 µl
GM-CSF (0.1 µg/ml)	20 µl
IL6 (5 µg/ml)	2 µl
MIP-α (0.1 µg/ml)	20 µl

XF Assay Media⁺ for primary cells

XF Base Media	24.1 ml
LIF (0.1 µg/ml)	12.5 µl
SCF (0.5 µg/ml)	10 µl
G-CSF (2 µg/ml)	12.5 µl
GM-CSF (0.1 µg/ml)	50 µl
IL6 (5 µg/ml)	5 µl
MIP-α (0.1 µg/ml)	50 µl
Glucose (1.66 M)	377 µl
L-Glutamine (200 mM)	250 µl
Pyruvate (100 mM)	250 µl

XF Assay Media⁺⁺ for cell lines

XF Base Media	24.3 ml
Glucose (1.66 M)	167 μ l
L-Glutamine (200 mM)	250 μ l
Pyruvate (100 mM)	250 μ l

PBS (pH 7.4)

NaCl	137 mM
KCl	2.7 mM
Na ₂ HPO ₄	10 mM
KH ₂ PO ₄	2 mM

Trypsin*

PE (PBS, 0.01% EDTA)	90%
10X Trypsin	10%

RIPA (pH 8.0)

Tris-HCl	50 mM
NaCl	150 mM
Triton x100	1%
NP-40	1%
SDS	0.1%
Protease inhibitors cocktail	1%

Running gel

H ₂ O	5.5 ml
30% Bis-acrylamide	6 ml
1 M Tris (pH8.8)	7.5 ml
10% SDS	200 μ l
10% APS	100 μ l
TEMED	100 μ l

Stacking gel

H ₂ O	10.8 ml
30% Bis-acrylamide	2 ml
1 M Tris (pH 6.8)	1.9 ml
10% SDS	150 μ l
10% APS	100 μ l
TEMED	100 μ l

Running Buffer (pH 8.3)

Tris	25 mM
Glycine	192 mM
SDS	0.01%

Blotting Buffer (pH 8.3)

Tris	25 mM
Glycine	192 mM

SDS	0.01%
Methanol	20%
Fc block*	
Fc block	1 μ l
PBS, 2% FBS (v/v)	49 μ l
Lin cocktail	
Biotin anti-mouse CD4	3.2 μ l
Biotin anti-mouse CD5	6.4 μ l
Biotin anti-mouse CD8a	6.4 μ l
Biotin anti-mouse Mac-1	24.8 μ l
Biotin anti-mouse B220	24.8 μ l
Biotin anti-mouse TER119	100 μ l
Biotin anti-mouse GR-1	50 μ l
PBS	284.4 μ l
Murine ST/LT HSC mix	
Pacific Blue Lin cocktail	22 μ l
Sca anti-mouse PeCy7	1 μ l
cKit anti-mouse APC/780	1 μ l
CD48 anti-mouse PE	3.2 μ l
CD150 anti-mouse APC	1 μ l
FITC anti-mouse CD45.1	1 μ l
PerCP/Cy5.5 anti-mouse CD45.2	3 μ l
PBS	17.8 μ l
Murine myeloid mix	
FITC anti-mouse CD45.1	0.5 μ l
PerCP/Cy5.5 anti-mouse CD45.2	1.5 μ l
APC anti-mouse GR-1	1 μ l
PeCy7 anti-mouse Mac-1	0.5 μ l
FITC anti-mouse TER119	1 μ l
Streptavidin*	
Streptavidin	1 μ l
PBS, 2% FBS (v/v)	100 μ l
Myelocult*	
Myelocult™	100 ml
Hydrocortisone hemisuccinate (1×10^{-4} M)	1 ml
Human HSC/LSC staining	
APC anti-human CD34	3 μ l
PerCP anti-human CD38	3 μ l
FITC anti-human CD45	10 μ l
PBS	84 μ l

Human CD45 staining

APC anti-mouse CD45	3 μ l
FITC anti-human CD45	10 μ l
PBS	87 μ l

Red blood cell lysis

Ammonium acetate	8.02 g
KHCO ₃ potassium bicarbonate	1 g
EDTA	0.02g
H ₂ O	to 1 L

2.2 Methods

Most of the methods described above were taken or adapted from our Letter entitled '*Targeting mitochondrial oxidative phosphorylation eradicates therapy-resistant chronic myeloid leukemic stem cells*' (accepted for publication in Nature Medicine, August 2017).

2.2.1 Primary samples

2.2.1.1 Primary samples origin

Ethical approval has been given to the research tissue bank (REC 15/WS/0077) and for using surplus human tissue in research (REC 10/S0704/60). CML samples were leukapheresis products from patients in CP-CML at the time of diagnosis, with informed consent in accordance with the Declaration of Helsinki and approval of the National Health Service Greater Glasgow Institutional Review Board. Normal samples were; i) BM products from healthy donors, ii) surplus cells collected from femoral head BM, surgically removed from patients undergoing hip replacement (with written patient consent and approval from the NHS Greater Glasgow and Clyde Biorepository), or iii) leukapheresis products from patients with non-myeloid Ph-negative haematological disorders. The presence of Philadelphia chromosome in CML samples was confirmed by cytogenetic analysis.

2.2.1.2 Selection of CD34⁺ and CD34⁺CD38⁻ cells from primary samples

CD34⁺ cells were isolated using CD34 Microbeads Kit or CliniMACS; the flow through consisting of CD34⁻ cells. For positive selection of human CD34 cells with

Microbeads, 100×10^6 cells were centrifuged at $400 \times g$ for 10 min and suspended in a mixture of 300 μ l PBS, 100 μ l FcR blocking reagent and 100 μ l of CD34 Microbeads for 30 min at 4°C . The cells were then washed in PBS, suspended in 500 μ l of PBS and added to the magnetic column for separation. After three washes, the magnetically labelled cells were collected by pushing the plunger into the column. For isolation of the $\text{CD34}^+\text{CD38}^-$ population, CD34^+ samples were co-stained with anti-human CD34 (APC) and anti-human CD38 antibodies and FACS-sorted.

2.2.2 Tissue Culture

2.2.2.1 Maintenance of primary cells and cell lines in culture

K562 and KCL22 CML cell lines as well as Ba/F3 p210 cells were cultured in RPMI⁺ (2.1.8). Cells were passaged every 2-3 days and sub-cultured at a concentration of 2×10^5 cells/ml. The murine IL-3 dependent Ba/F3 pro-B cell line was grown in RPMI⁺ supplemented with IL-3 (10 ng/ml). M2-10B4 and S1/S1 murine fibroblast cell lines were cultured every alternative week in DMEM⁺ and in a puromycin and hygromycin supplemented media: DMEM^{*1} for M2-10B4 and DMEM^{*2} for S1/S1 (2.1.8) to avoid proliferation of untransformed cells. Primary cells were cultured in SFM+ ϕ GFs (2.1.8) in non-adherent tissue culture flasks. Primary cells were seeded at concentration of 1.0×10^6 cells/ml for overnight recovery after thawing. For experimental procedures, primary cells were seeded at $2.5\text{-}5 \times 10^5$ cells/ml. Primary cells and cell lines were all maintained in an incubator at 37°C with 5% CO_2 .

2.2.2.2 Cryopreservation of mammalian cells lines and primary cells

Primary CML and normal samples were cryopreserved in a freezing solution consisting of 50% (v/v) IMDM, 10% dimethylsulfoxide (DMSO, v/v) and 40% (v/v) FBS. For cell lines, the freezing media consisted of 90% (v/v) FBS and 10% (v/v) DMSO. Cells were suspended in the corresponding freezing media at an approximate concentration of 5×10^6 cells/ml and 1 ml of this solution was aliquoted into individual cryovials. The cryovials were rapidly transferred into the CoolCell to allow a steady decrease in temperature, and placed into a -80°C freezer for 24 hours (h) before transfer into liquid nitrogen containers.

2.2.2.3 Thawing of human primary cells

Frozen human primary cells were defrosted in a 37°C water bath until removal of the ice crystals. The cell suspension was then transferred to a 50 ml falcon tube. DAMP solution was added drop by drop (10 ml DAMP was added over 20 min) while gently shaking. The cells were then centrifuged for 10 min at 450 x g and washed with DAMP. This procedure was repeated twice. The cells were then suspended in SFM+ ϕ GFs at a concentration of 1.0×10^6 cells/ml and plated into a 25cm³ non-adherent tissue culture flask to let them recover overnight.

2.2.2.4 Thawing of cell lines

Cryovials were placed into in a 37°C water bath for approximately one minute. The cell suspension was then transferred into a 15mL tube containing 10 ml of pre-warmed complete growth media. Cells were centrifuged and then suspended in complete growth media at a concentration of 2.5×10^5 cells/ml.

2.2.2.5 Drug treatment and preparation

Imatinib was dissolved in sterile distilled water at a concentration of 1 mM and this stock solution was stored at 4°C for a maximum of three months. Solutions of tigecycline were freshly prepared the day of the assay at a concentration of 5 mM in DMSO the day of the experiment. Stock solution of phenformin and metformin were prepared at the time of the assay in water. *In vitro* drug treatments were performed at a concentration of 2 μ M for imatinib, 2.5 μ M for tigecycline, 20 μ M for phenformin, unless stated otherwise.

2.2.3 Cell proliferation assay

2.2.3.1 Cell count

Cell counts were performed with the automated CASY® cell counter or manually with a haemocytometer. Suspension cell lines and primary cells were suspended in their media and 50-200 μ l of the cell suspension subjected to the CASY® cell counter. When the cell number or the volume of the cell suspension was limiting, cells were counted manually with a haemocytometer.

2.2.3.2 XTT assay

Background: XTT is a colorimetric assay that assesses cell proliferation and viability. Oxidoreductase enzymes reduce XTT into the coloured derivative formazan that absorbs between 450-500 nanometer. The absorbance intensity is function of the enzymes and the cell number. As XTT does not enter the cell, the addition of the electron acceptor phenazine methosulfate (PMS) greatly potentiates the reaction.

Method: At day 0, 8-10 different drug concentrations were prepared by serial 1:2 dilution of the stock solution (the concentration of the stock solution was pre-optimised for each of the drug used in the assay). Each drug concentration was seeded into a minimum of four wells of a 96-well plate (technical replicates). A vehicle control was as well included for each drug. Cells were suspended in RPMI⁺ at a concentration of 2×10^5 cells/ml. 50 μ l of the cell suspension (i.e. 10,000 cells) were seeded into each well the 96-well plate containing various concentration of the drugs. After 72 h, 3 mg of XTT salt was added in 3 ml of RPMI⁺ and placed in water bath at 37°C for 20 minutes. After dissolution of the salt, 15 μ l of phenazine methosulfate (PMS) stock solution (7 mg of PMS in 5 ml of PBS; aliquots kept at -20°C in the dark) were added to the XTT solution. 25 μ l of the resulting solution was added to each well. Absorbance was read between 2 and 4 h depending on the cell line at 492 nm.

2.2.4 Flow cytometry

Flow cytometry enables the detection of physical and phenotypic parameters of single cells or particles. Briefly, a flow cytometer is composed of lasers that can excite antibodies conjugated with fluorescent dyes. The fluorescence emitted by the cells can be detected and measured by the flow cytometer detectors. Fluorochrome-labelled antibodies are commonly used in the field of haematology to resolve the expression of cellular markers. Flow cytometry can as well distinguish different cell types by their physical properties such as the size and the granularity of the cells reflected respectively by the forward-angle light scatters (FSC) and the side-angle light scatter (SSC). Fluorescence-activated cell sorting (FACS) is a particular type of flow cytometer that is used to collect the

cells of interest. Data collected by flow cytometry were analysed with the FlowJo software.

2.2.4.1 CellTrace Violet staining

Background: CellTrace Violet is a fluorescent dye that binds covalently intracellular amino acids residues. Due to this covalent link, the dye can be retained for long periods and is not transferred during cellular division. Therefore, every time a population of cells divide, there will be a loss of the dye, and hence fluorescence, that can be monitored by flow cytometry.

Method: CD34⁺ CML cells were stained at day 0 with 1 μM of the CellTrace Violet dye for 30 min at 37°C. The reaction was quenched by adding cell culture media containing 10% FBS. Cells were then washed and suspended in SFM+ ϕ GFs. The fluorescence was analysed by flow cytometry at 3 and 6 days.

2.2.4.2 Annexin V staining

Background: During apoptosis, cells undergo morphological changes such as cell shrinkage, membrane blebbing, chromatin condensation (i.e. pyknosis) and nuclear fragmentation. Apoptosis is associated as well with the translocation of the membrane phospholipid phosphatidylserine (PS) from the inner plasma membrane to the cell surface. Annexin V can bind PS with high affinity in a calcium dependent manner. As such, detection of Annexin V positive cells by flow cytometry (with fluorochrome-labelled Annexin V) is linked to the presence of PS on the outer leaflet of the plasmatic membrane and allows the measurement of apoptotic and dead cells.

Method: $0.5\text{-}2.5 \times 10^5$ cells were washed once with HBSS and incubated with 2.5 μl Annexin-V (APC) in 50 μl HBSS for 15 min in the dark at room temperature. For analysis of cell death in the CD34 and CD133 population, $0.5\text{-}2.5 \times 10^5$ cells were washed once with HBSS and incubated with 2.5 μl Annexin-V (FITC), 2.5 μl CD133 (Pe) and 1 μl of CD34 (APC) in 50 μl HBSS for 15 min in the dark at room temperature. After the incubation period, 300 μl of HBSS was added to the cell suspension and flow cytometry analysis was performed within the hour.

2.2.4.3 Propidium Iodide (PI) exclusion

Background: PI is a fluorescent dye that is impermeable to live cells but can penetrate membranes of dying or dead cells. When bound to DNA, PI fluorescence increases by 20 to 30 fold. The percentage of cells with high PI fluorescence is therefore a read-out for dead cells.

Method: $1-5 \times 10^5$ cells were washed once with PBS and suspended in 300 μ l of PI solution (1 μ g/ml) for 30 min in the dark at room temperature. After this, 300 μ l of PBS was added and fluorescence intensity was measured by flow cytometry.

2.2.4.4 Mitochondrial content

Background: Mitotracker Green is a fluorescent dye that accumulates selectively in mitochondria. Its fluorescence can be measured by flow cytometry and directly correlates to the mitochondrial content of the cells.

Method: To assess mitochondrial mass in stem cells, CD34⁺ CML and normal cells were co-stained with 100 nM Mitotracker Green with 1 μ l anti-human CD34 (APC) and 2.5 μ l anti-human CD38 (PerCP) antibodies for 30 min at room temperature in the dark. Cells were then washed twice to ensure removal of the fluorescent probes and suspended in 300 μ l of PBS. The cell suspension was then immediately subjected to flow cytometry analysis.

2.2.4.5 Mitochondrial membrane potential

Background: The electron transport chain in the mitochondria creates a potential between the mitochondria inner membrane by pumping protons from the inner membrane to the intermembrane space. Tetramethylrhodamine, methyl ester (TMRM) is a cationic fluorescent dye that accumulates in the negatively charged mitochondrial matrix, leading to a shift in its absorption and fluorescence emission spectra. In live cells, TMRM fluorescence intensity is directly proportional to the mitochondrial membrane potential and can therefore be used as a readout for mitochondrial activity.

Method: For mitochondrial membrane potential assessments, cells were stained with 100 nM TMRM, 1 μ l anti-human CD34 (APC) and 2.5 μ l anti-human CD38 (PerCP) antibodies for 30 min at room temperature in the dark. Cells were then

washed twice and suspended in 300 µl of PBS for fluorescence analysis by flow cytometry.

2.2.5 Quantitative PCR

2.2.5.1 Primers design

The cDNA sequence was first identified from [Ensembl genome browser 87](#) and the primers designed and verified with NCBI/Primer-Blast. The sequence of each primer is listed in 2.1.4.

2.2.5.2 RNA extraction

The RNeasy Mini Kit and, when the number of cells was limited, the PicoPure® RNA Isolation Kit were used according to the manufacturer's instructions. The quality and concentration of the RNA were measured with NanoDrop 2000 Spectrophotometer and the RNA stored at -80°C until further use.

2.2.5.3 Reverse transcription

The cDNA was synthesized from RNA with the cDNA Reverse Transcription Kit according to manufacturer's instructions. Briefly, 0.25-1 µg of RNA and 4 µl of SuperScript™ VILO™ Master Mix were mixed and placed in MicroAmp® Fast Reaction tubes. The total volume was adjusted to 20 µl with H₂O and the reverse transcription performed using a Mastercycler™ PCR machine.

2.2.5.4 Quantitative PCR

cDNAs and the Fast SYBR® Green Master Mix were mixed with each primer (0.25 µM). The total volume was adjusted to 20 µl with water. The PCR was performed with the following steps: 20 s at 95°C - 40 cycles of 3s at 95° - 30 s at 60°C. The relative quantitation of mRNA was performed by the comparative $\Delta\Delta C_t$ method using *18S* for normalization.

2.2.6 Western blotting

2.2.6.1 Protein lysis with RIPA buffer

The cells from different conditions were counted and collected in falcon tubes. The cells were then washed once with PBS and then transferred to a 1.5 ml Eppendorf tube for a second PBS wash. The resulting cell pellet was then thoroughly suspended in RIPA lysis buffer supplemented with a cocktail of protease inhibitors to get a concentration of lysed cells of $2.5\text{-}5 \times 10^6$ cells/ml. The Eppendorf tubes were kept on ice for a minimum of 15 min to ensure proper lysis of the cells, after which the cell lysates were centrifuged at $16,000 \times g$ for 10 min and the supernatant collected and stored at -20°C until further use.

2.2.6.2 Protein quantification

Background: Bicinchoninic acid (BCA) assay was used for the detection and quantification of proteins. This protein assay binds to copper ions and peptides binds to form a coloured end product that absorbs at 562 nm. More precisely, a complex between Cu^{2+} and the proteins will be formed at first, which, in an alkaline environment, is followed by the reduction of copper (II) ion, Cu^{2+} , into the copper (I) ion Cu^+ . This reduction is associated with the presence of the amino acids cysteine, cystine, tryptophan and tyrosine and is therefore proportional to the quantity of protein present in each sample.

Method: Multiple protein standards (i.e. samples for which the protein concentration is known and spread across the working range of the BCA assay) are assayed in parallel to the unknown samples. As a result, the protein concentration of unknown samples can be determined by interpolation of the graphed standard curve. Protein standards were prepared by serial 1:2 dilutions of a $2000 \mu\text{g}/\mu\text{l}$ BSA stock to obtain the following concentrations: 2000 - 1000 - 500 - 250 - 125 - 62.5 - 31.75 - 0 $\mu\text{g}/\mu\text{l}$. These standards were kept at -20°C . The day of the assay, 10 μl of each standard and unknown samples were added in duplicate in a 96-well plate. For protein quantification, the Pierce™ BCA Protein Assay Kit was used according to manufacturer's instructions. Briefly, 98% (v/v) Reagent A was mixed with 2% (v/v) Reagent B and 200 μl of this solution distributed in a 96-well plate. The plate was placed at 37°C for 30 min and the absorbance at 562 nm was measured with a spectrophotometer plate reader. The concentration of unknown samples was

determined by interpolating their absorbance values with the standard curve. Equal amounts of proteins (5-20 µg depending on the experiment) were loaded for western blot analysis.

2.2.6.3 Sodium dodecyl sulfate polyacrylamide gel electrophoresis

Background: Sodium dodecyl sulfate polyacrylamide gel electrophoresis (SDS-PAGE) is a method that separates proteins based on their molecular mass. The separation of proteins based on their size is possible by using SDS that forces proteins to unfold from a tertiary to a negatively charged linear structure. The negatively charged proteins will move towards the positive electrode upon application of an electric field.

Method: Equal amounts of proteins were taken from each condition, 4X Laemmli buffer was added and the final volume was normalized by adjusting it with RIPA lysis buffer. The samples were then placed for 5 min at 100°C for their reduction and denaturation. In the meantime, the running and stacking gels were made in 50 ml falcon tubes as described before (2.1.8) and, importantly, APS and TEMED were added right before pouring the gel to not induce polymerisation in the tube. The solution was immediately transferred to a 5 mm cassette. After a short centrifugation, the denatured protein samples were loaded onto a gel. To estimate the molecular weight of the proteins detected, 4-6 µl of protein ladder were loaded in the first and last lane. Gels were run with 1X running buffer (2.1.8) at 120V for 1 h 30 min or until desired separation was achieved in a mini-cell electrophoresis system.

2.2.6.4 Transfer to nitrocellulose membrane

Following the SDS-PAGE, the proteins were transferred to a nitrocellulose membrane enclosed in a western blot « sandwich » made as follows: 2 sponges - 3 paper Whatman - Nitrocellulose membrane - 3 paper Whatman - 2 sponges. All components were soaked in transfer buffer (2.1.8) before assembly of the « sandwich ». The proteins were then transferred for 1 h at 400 mA and the presence of proteins on the nitrocellulose verified by incubating the membrane for five minutes with Ponceau red.

2.2.7 Immunolabelling

The membrane was incubated for 1 h with blocking buffer consisting of 5% (m/v) BSA in TBST (2.1.8) followed by an overnight incubation with primary antibodies diluted in blocking buffer and 0.01% sodium azide. The next day, the membrane was washed for 4x5 min with TBST and incubated for 1 h with the appropriate HRP-linked secondary antibody (1:3000 dilution). The membrane was washed again 4x5 min with TBST and revealed by chemiluminescence. Precisely, the membrane was incubated for 1 min with a working solution made of equal part of luminol-enhancer and peroxide solution (Pierce™ ECL Western Blotting Substrate). Of note, in presence of hydrogen peroxide and an enhancer, the reaction catalysed by HRP (i.e. the conversion of luminol to its product 3-aminophthalate) is accompanied with light emission light.

2.2.8 Hematopoietic stem and progenitors cells functional assays

2.2.8.1 CFC assay

Background: Colony-forming cell (CFC) assay is a common method used in the field of haematology to test the ability of progenitor cells to differentiate into colonies in a semi-solid medium. The number of colonies at end-point reflects the number of viable progenitors.

Method: Primary cells were plated SFM+ ϕ GFs in the presence of indicated drugs at a concentration of $2.5-5 \times 10^5$ cells/ml in duplicate. After 3 days, cells from each condition were counted and 3,000 cells transferred in 1.5 ml of methylcellulose-based medium (Methocult H4034 Optimum) and vortexed for 5 sec. The methylcellulose mixture was transferred to a 35 mm dish and incubated for 12-14 days at 37°C, 5% CO₂. Colonies were then scored manually.

2.2.8.2 Long-term culture-initiating cell (LTC-IC) assay

The genetically modified stromal cells lines M2-10B4 (expressing G-CSF and IL-3) and S1/S1 (expressing SCF and IL-3) were irradiated at 80 Gy to block cellular proliferation during the time course of the assay. Vials of 5×10^6 irradiated cells were frozen in 90% (v/v) FBS, 10% (v/v) DMSO for long-term storage. The day prior to the assay, M2-10B4 cells and S1/S1 were defrosted and mixed in a 1:1 ratio to

get a final concentration of 2×10^5 cells/ml in media for long-term culture of haematopoietic cells supplemented with hydrocortisone (Methocult*, 2.1.8). 1 ml of this suspension was distributed in 24-well collagen-coated plates and then transferred at 37°C, 5% CO₂ to let the cells adhere overnight (Fig. 2.1). The next day, 500 µl of Methocult* was removed and 5×10^4 CD34⁺ CML cells suspended in 500 µl of Methocult* were plated onto the irradiated stromal layers in the presence of indicated drugs. Cells were kept for a minimum of 5 weeks at 37°C, 5% CO₂ with weekly half-media change. After 5-6 weeks, the cells were harvested and the number of viable progenitors was assessed by CFC assay. Precisely, the supernatant from each LTC-IC well was collected in a 15 ml falcon tube. The remaining adherent cells were dissociated with trypsin* (2.1.8) and collected in the corresponding falcon tube. The cells were centrifuged for 10 min at 400 x g. After removal of the supernatant, the cell pellet was suspended in 50 µl methylcellulose media and the entire cell suspension transferred in 3 ml of methylcellulose for CFC assay (2.2.8.1). Colonies were scored manually after 12-14 days.

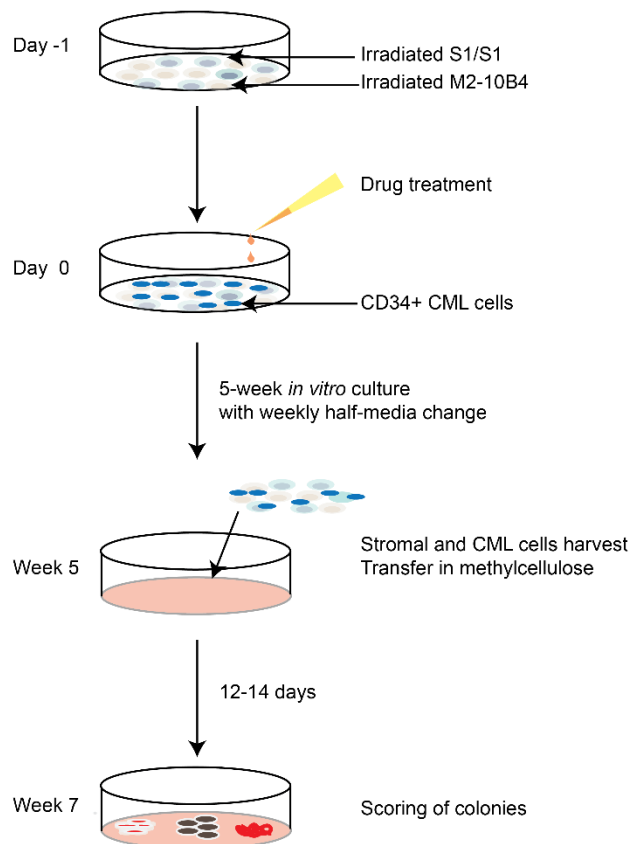


Figure 2. 1 Procedure summary for haematopoietic LTC-IC assay.

2.2.9 Metabolomics

2.2.9.1 Stable isotopes tracing

Primary cells were plated in presence of $^{13}\text{C}_6$ -labelled glucose, $^{13}\text{C}_5$ -labelled glutamine, $^{13}\text{C}_{16}$ -labelled palmitate for 24 h at a concentration of 0.5×10^6 cells/ml in PlasMax, a custom-made media formulation containing nutrient concentrations comparable to human serum.

2.2.9.2 Intracellular metabolites extraction

After 24 h, cells were washed twice with ice-cold PBS and intracellular metabolites extracted with a cold solution of methanol, acetonitrile, and water (5:3:2). The cell extracts were centrifuged at $16,000 \times g$ for 10 min at 4°C and the supernatants were subjected to LC-MS analysis.

2.2.9.3 LC-MS analysis

As described previously, a Q-Exactive Orbitrap mass spectrometer (Thermo Scientific) was used together with a Thermo Scientific Accela HPLC system (229, 230). The HPLC setup consisted of a ZIC-pHILIC column (SeQuant, 150×2.1 mm, $5 \mu\text{m}$, Merck KGaA), with a ZIC-pHILIC guard column (SeQuant, 20×2.1 mm) and an initial mobile phase of 20% 20 mM ammonium carbonate, pH 9.4, and 80% acetonitrile. Cell extracts ($5 \mu\text{l}$) were injected and metabolites were separated over a 15 min mobile phase gradient, decreasing the acetonitrile content to 20%, at a flow rate of $200 \mu\text{l}/\text{min}$ and a column temperature of 45°C . The total analysis time was 22.2 min. All metabolites were detected across a mass range of 75-1000 m/z using the Q-Exactive mass spectrometer at a resolution of 35,000 (at 200m/z), with electrospray ionization and polarity switching to enable both positive and negative ions to be determined in the same run. Lock masses were used and the mass accuracy obtained for all metabolites was below 5 ppm. Data were acquired with Thermo Xcalibur software. The peak areas of different metabolites were determined using Thermo LCquan software where metabolites were identified by the exact mass of the singly charged ion and by known retention time on the HPLC column. Commercial standards of all metabolites detected had been analysed previously on this LC-MS system with the pHILIC column. The ^{13}C labelling patterns

were determined by measuring peak areas for the accurate mass of each isotopologue of metabolites. Intracellular metabolites were normalized to cell number and volume.

2.2.10 Seahorse

The Seahorse XF96 Analyser is a system that enables repeated measurements of molecular OCR in real time at steady-state. It can as well assess the functionality of the mitochondria by assessing mitochondrial respiration following pharmacological stimuli.

2.2.10.1 Day 1

Preparation of coated plates

Background: For non-adherent cells, the coating agent Cell-tak was used to immobilize the cells onto Seahorse XF96 Cell Culture Microplates and allow accurate readings of OCR. Cell-tak is a polyphenolic protein solution isolated from mussels. To ensure optimal performance of Corning Cell-tak, the adsorption method was used as a coating method. Basically, Corning Cell-tak spontaneously adsorbs to the surface it is placed on at neutral pH.

Method: 38 µl of Corning Cell-Tak was added to 2.5 ml sodium bicarbonate (0.1M, pH 8) and the pH adjusted to 6.5-8 with 1N NaOH. This coating solution was immediately dispensed into each well of a Seahorse 96 cell culture plate (30 µl/well) and left to adsorb for 30 min at room temperature. The coating solution was then aspirated and the cell culture plate was washed twice with distilled water and placed at 4°C for next day use.

Hydration of the probes

The XF96 Sensor cartridges were hydrated overnight by adding 200 µl Seahorse Bioscience XF96 Calibrant solution pH 7.6 to each well of a Seahorse-96 utility plate. The sensor cartridge was then placed on the top of the utility plate, sealed with paraffin film to prevent evaporation overnight, and stored in a CO₂-free incubator overnight at 37°C.

2.2.10.2 Day 2

Media preparation

XF Assay Media⁺ and XF Assay Media⁺⁺ (2.1.8) were prepared the day of the assay and used for primary cells and cell lines respectively. The media was then warmed at 37°C and the pH adjusted to 7.4±0.1.

Drugs preparation for Mito Stress Test

Background: Inhibitors/modulators that target specific components of the electron transport chain (ETC) are used in the Mito Stress Test to complement basal mitochondrial measurements and to give a more comprehensive view of the mitochondrial function. The changes in oxygen consumption following the sequential injections of oligomycin, carbonyl cyanide-4-(trifluoromethoxy) phenylhydrazone (FCCP), and a mix of antimycin A and rotenone, measure respectively the respiration coupled to ATP synthesis, maximal respiration, and non-mitochondrial respiration. More precisely, the injection of the ATP synthase inhibitor oligomycin induces a decrease in OCR. The difference in OCR between baseline and post-oligomycin treatment is known as the respiration coupled to ATP synthesis. FCCP uncouples mitochondrial respiration from ATP synthesis by disrupting the mitochondrial membrane potential. The flow of electron is therefore no longer limited by ATP production and oxygen consumption reaches its maximum level. The last injection consists of rotenone and antimycin A, an inhibitor of complex I and III respectively. As a result, mitochondrial respiration stops and OCR drops dramatically. The remaining OCR following the injection of antimycin A and rotenone reflects the non-mitochondrial respiration.

Method: Stock solution of oligomycin (5 mM in ethanol), FCCP, antimycin A and rotenone (all in 10 mM in DMSO) were aliquoted and kept at -20°C. Of note, the concentrations of oligomycin and FCCP were optimised for each cell type used in the Seahorse assay. The day of the assay, working solutions of oligomycin (1 µM), FCCP (1.5 µM), and the mix antimycin A and rotenone (both 1 µM) were prepared in XF Assay Media⁺ (2.1.8) for primary cells. For cells lines, these solutions were prepared in XF Assay Media⁺⁺ (2.1.8) and the concentrations of both oligomycin and the mix antimycin A and rotenone were similar the ones used for primary cells. FCCP was however prepared at a concentration of 0.6 µM and 0.4 µM for

K562 and KCL22 cells lines respectively. All solutions were vortexed before loading in the XF sensor cartridge.

Loading the XF sensor cartridge with drugs

Using the loading guides provided, 25 µl of oligomycin, FCCP and the mix antimycin A and rotenone were loaded respectively in port A, B and C of the sensor cartridge. The cartridge was placed back a CO₂-free incubator at 37°C for 10 min, then inserted in the Seahorse XF96 Analyser for calibration.

Seeding of the cells

While the Seahorse was calibrating, the cells were counted and washed once in PBS. The cells were then suspended in the corresponding XF Assay Media at a concentration of 2.9x10⁶ cells/ml for primary cells and 1.7x10⁶ cells/ml for cell lines and 35 µl of the cell suspension was dispensed into each well of a Seahorse XF96 cell culture microplate. The cells were then centrifuged at 40 x g for 10 seconds with a centrifuge set at zero braking. After the first spin, the microplate was turned by 180° and the cells were centrifuged again at 60 x g for 10 seconds. The microplate was then transferred in CO₂-free incubator 37°C for 30 min to ensure complete cell attachment. After visual confirmation of cell adhesion to the plate, 140 µl of XF Assay Media was gently added to each well. Special care to not disturb the cells was taken for primary cells as they loosely attach to the plate. The microplate was then transferred for 10 min a CO₂-free incubator at 37°C then inserted in the Seahorse XF96 Analyser.

2.2.11 Double transgenic (DTG) mice experiments

Outline of the *in vivo* experiment

Femurs, tibiae and hips from CD45.2 SCLtTA/BCR-ABL (DTG) were crushed in 2x10 ml of PBS to isolate BM cells. Cells were counted with the CASY® cell counter and suspended at a concentration of 5x10⁶ cells/ml in PBS. 200 µl of the cell suspension was transplanted into the tail vein of CD45.1 wild type (WT) B6 (B6.SJL-*Ptprc*^a *Pepc*^b/BoyJ) mice sub-lethally irradiated the previous day. Transplanted mice were kept for a period of 4 weeks on tetracycline to ensure proper recovery from the irradiation before induction of the disease. After this period, tetracycline was removed from the drinking water. 10 days post tetracycline removal, tail vein blood was taken to analyse the expression of CD45.1 and CD45.2 in haematopoietic

cells by flow cytometry and confirm the engraftment of donor CD45.2 cells in recipient mice. Precisely, 20 µl of blood from each mouse was transferred in a polypropylene tube and 1 ml of red blood cell lysis was added. The solution was vortexed for 5 sec and after 10 min incubation at room temperature, the reaction was quenched with 2 ml of PBS. The cells were then centrifuged for 10 min at 400 x g and suspended with a mixture of 0.5 µl anti-mouse CD45.1 (FITC), 0.5 µl CD45.2 (Pacific Blue), 0.5 µl GR-1 (APC) and 0.5 µl Mac-1 (Pe/Cy7) for 20 min at room temperature. The cells were then washed with 2 ml of PBS and suspended in 300 µl of PBS for immediate flow cytometry analysis.

After 18 days post-tetracycline removal, mice were treated with imatinib (100 mg.kg⁻¹, oral gavage, twice daily) and phenformin (100 mg.kg⁻¹, oral gavage, once daily) for 4 weeks. Mice were then sacrificed and femurs, tibiae, hips, spleen and blood were collected for subsequent analysis.

Isolation of cells of interest

To isolate BM cells, cleaned bones were placed in a large mortar containing 10 ml PBS supplemented with 2% (v/v) FBS and crushed with a pestle. The collected BM was then filtered through a 40 µm cell strainer to remove debris. These steps were repeated once more (i.e. re-adding 10 ml of FBS-PBS and crushing the bones) to ensure complete isolation of BM cells. The splenic cells were harvested by pushing the spleen through a 40 µm cell strainer with the rubber end of a 5 ml syringe. The cell suspension was flushed twice with 10 ml PBS supplemented with 2% (v/v) FBS.

Flow cytometry analysis of murine cells

1 ml of the BM cell suspension from each mouse was transferred into a polypropylene tube and centrifuged at 400 x g for 10 min. Cell pellet was suspended in 50 µl of Fc block* (2.1.8) and kept on ice for 5 min. BM cells were then stained for 20 min with an ST/LT HSC antibody mix (2.1.8) to identify murine LT-HSCs by flow cytometry. Cells were then washed with 2 ml of PBS and stained with 100 µl of Streptavidin* (2.1.8) for 30 min. The cells were washed again with 2 ml of PBS and suspended in 500 µl of PBS. In separate polypropylene tubes, 200 µl of cell suspension from the BM and spleen were stained with the myeloid mix (2.1.8) for 15 min at room temperature. Cells were then washed with 2 ml of PBS

and suspended in 300 µl of PBS. Of note, appropriate controls (unstained, fluorescence minus one and single colour) were prepared in parallel. The samples were immediately analysed by flow cytometry.

2.2.12 NSG mouse engraftment

2.2.12.1 Survival of CML LSCs following *in vivo* drug treatment

Outline of the *in vivo* experiment

To study the *in vivo* engraftment of CD34⁺ CML cells, 1.5x10⁶ CD34⁺ cells from CML samples were transplanted via tail vein into 8 week-old sub-lethally irradiated (2.5Gy) female NOD.Cg-PrkdcscidIl2rgtm1Wjl/SzJ NSG mice (The Jackson Laboratory). 6 weeks post-transplant, human engraftment levels were analysed in each mouse. Briefly, 20 µl of tail vein blood was added in polypropylene tubes and red blood cells were lysed as described previously (2.2.11). The cells were then stained with 1.5 µl anti-mouse CD45 (APC) and 10 µl anti-human CD45 (FITC) for 20 min at room temperature. The cells were then washed with 2 ml of PBS and suspended in 300 µl of PBS for immediate flow cytometry analysis. Mice were then split into 4 different arms according to their human engraftment levels and drug treatment was started with imatinib (100 mg.kg⁻¹; oral gavage twice daily) and tigecycline for 4 weeks (week 1: 25 mg.kg⁻¹, week 2: 50 mg.kg⁻¹, weeks 3-4: 100.mg kg⁻¹; intraperitoneal once daily). At the end of the 4-week treatment, mice were euthanized and femurs, tibiae and spleens were harvested.

Isolation of the cells of interest

See 2.2.11

Flow cytometry analysis of human cells

1 ml of BM and 0.5 ml of spleen suspension cells were distributed into polypropylene tubes. The cells were centrifuged at 400 x g for 5 min and 5 µl of Fc block* solution was added to the cell suspension. After 5 min of incubation, 100 µl of human HSC/LSC staining (2.1.8) and human CD45 staining (2.1.8) was added to BM and spleen cells respectively. The single colours and fluorescence minus one (FMO) mix antibodies were prepared in parallel for colour compensation in the flow cytometer. After 30 min incubation at room temperature in the dark, cells were washed and suspended in 500 µl of PBS for immediate flow cytometry

analysis. To quantify the frequency of Ph⁺ cells within the engrafted human CD45⁺ cells, dual-fusion D-FISH was performed by Dr. Pablo Baquero as previously described (231).

2.2.12.2 Long-term recovery of CML stem cells *in vivo* - drug discontinuation

Outline of the *in vivo* experiment

As described before (2.2.12.1), CD34⁺ cells from CML samples were transplanted via tail vein into 8-10 week-old sub-lethally irradiated female NSG mice. Two independent experiments were performed and mice were split according to their engraftment levels (2.2.12.1). In experiment 1, the drug treatment was started 7 weeks post-transplant with imatinib (100 mg.kg⁻¹; oral gavage twice daily) and tigecycline for 3 weeks (week 1: 25 mg.kg⁻¹, week 2: 50 mg.kg⁻¹, weeks 3: 100 mg.kg⁻¹; intraperitoneal once daily). At the end of the 3-week treatment, mice were kept for an additional 3 weeks to analyse the long-term effect of the drug treatment on CML stem cells. In experiment 2, the drug treatment was started 8 weeks post-transplant with imatinib (100 mg.kg⁻¹; oral gavage twice daily) and tigecycline (week 1: 25 mg.kg⁻¹, week 2: 50 mg.kg⁻¹, weeks 3-4: 100 mg.kg⁻¹; intraperitoneal once daily) for 4 weeks. Drug treatment was then stopped and the mice were kept for an additional 2 weeks before analysis of LSCs survival.

Isolation of cells of interest and flow cytometry analysis of human cells

See section 2.2.11.1

2.2.12.3 Survival of normal stem cells following *in vivo* drug treatment

Outline of the *in vivo* experiment

To study the *in vivo* engraftment of normal CD34⁺ cells, 0.7x10⁵ CD34⁺ cells from one cord blood sample were transplanted via tail vein into 8 week-old sub-lethally irradiated (2.5 Gy) female NSG mice. Before starting drug treatment, mice were split according to their engraftment levels (2.2.12.1). 7 weeks post-transplant, drug treatment was initiated with imatinib (100 mg.kg⁻¹; oral gavage twice daily) and tigecycline for 4 weeks (week 1: 25 mg.kg⁻¹, week 2: 50 mg.kg⁻¹, weeks 3-4: 100 mg.kg⁻¹; intraperitoneal once daily). At the end of the 4-week treatment, mice were euthanized and femurs, tibiae and spleens were harvested.

Isolation of cells of interest and flow cytometry analysis of human cells

See 2.2.11.1

2.2.13 Statistical analyses

We did not use any statistical method to predetermine sample size. For in vitro experiments, a minimum of three patient samples were chosen as a sample size to ensure adequate power, unless stated otherwise. Data obtained from each patient sample represents an independent experiment. We were not blinded to mice allocation during in vivo experiments and mice were allocated based on their pre-treatment engraftment levels. No method of randomization was used. All mice were cared for equally in an unbiased fashion by animal technicians and investigators. No animal was excluded from the analysis.

P values were calculated by two-tailed paired or unpaired Student's t-test using GraphPad Prism software (GraphPad Software 5.0) as indicated in the figures legends. Where indicated, variables were transformed using the natural logarithms before t-tests were performed to meet the assumption of equal variances.

Chapter 3 Investigation of metabolic vulnerabilities in CML LSCs

3.1 Introduction

Targeting metabolic vulnerabilities for cancer therapy has been the subject of numerous studies in solid tumours and in some blood malignancies such as AML; however, much less effort has been made to apply this concept to CML. Indeed, to our best knowledge, no study has yet investigated the metabolism of primitive CML LSCs in detail. Although it has been reported that targeting metabolic pathways in CML cells can be of therapeutic interest, these studies were performed in CML cell lines and failed to demonstrate its applicability in patient-derived CML LSCs.

Investigation of metabolism in rare cancer stem cells has so far been restricted by technical limitations in measuring metabolic changes using low numbers of cells. We therefore developed improved protocols for metabolic flux assays which allowed us to profile the metabolism of stem-cell enriched CML and normal cells as well as differentiated CML cells, aiming to unveil selective new targets against CML LSCs. In this chapter, we describe the use of labelled carbon tracer to detect different isotopologues of many intracellular metabolites over time, using a state-of-the-art liquid chromatography-mass spectrometry (LC-MS) system. Moreover, we optimised techniques to measure mitochondrial respiration (by OCR), in rare primitive non-adherent haematopoietic cells.

The data provided in this chapter delivers the first metabolic analysis of primitive haematopoietic cells isolated from CML patients compared with primitive Ph negative cells. Of note, the majority of the results described in this chapter were accepted for publication in *Nature Medicine* in August 2017 as a Letter entitled “*Targeting mitochondrial oxidative phosphorylation eradicates therapy-resistant chronic myeloid leukemic stem cells.*”

3.2 Results

3.2.1 Imatinib does not target CML LSCs

Many studies have demonstrated that imatinib and second-third generation TKIs fail to eradicate LSCs (123-127). To assess the effect of imatinib in our experimental conditions, patient-derived cells were enriched for stem cells by positive selection of the CD34 surface expression (CD34⁺ CML cells). CD34⁺ CML cells were treated with 2 μ M imatinib, a concentration achievable in patients, and the expression on the CD34 cell surface marker assessed by flow cytometry. This revealed that upon *in vitro* culture, proliferating CD34⁺ CML cells differentiate and lose their CD34 expression over time (**Fig. 3.1a**). However, imatinib treatment led to an enrichment of more primitive CD34⁺ CML cells by inducing apoptosis in differentiated CD34⁻ CML cells (**Fig. 3.1a,b**). Indeed, after six days of *in vitro* culture, the percentage of viable CD34⁻ cells was higher in untreated condition compared to imatinib-treated cells (24% versus 13% respectively). On the contrary, imatinib induced an increase in the percentage of CD34⁻ cells targeted for apoptosis in compared to untreated condition (36% versus 22% respectively, **Fig. 3.1b**). Moreover, imatinib reduced the number of viable CML progenitors, as demonstrated by the reduction of colonies in a short-term CFC assay (**Fig. 3.1c**). However, imatinib failed to reduce the number of CML stem cells in long-term culture-initiating cell (LTC-IC) assays (**Fig. 3.1d**).

In line with previously published data, these results demonstrated that imatinib is able to target differentiated cells, including progenitor cells, but fails to eliminate primitive CML LSCs, highlighting the need to identify novel therapeutic targets for their eradication.

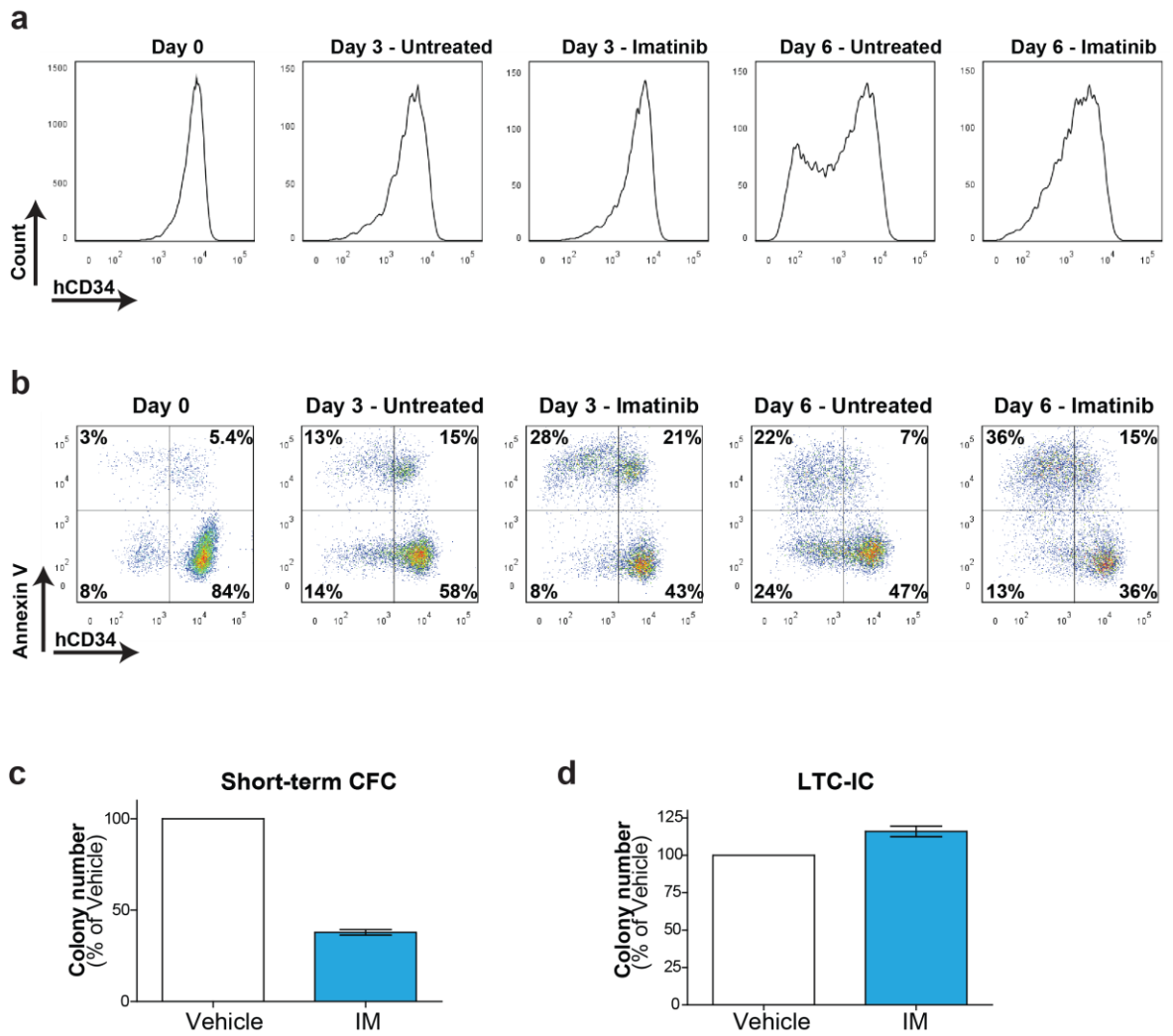


Figure 3. 1 Imatinib fails to eliminate CML LSCs.

(a) CD34 expression following *in vitro* culture of CD34⁺ CML cells with imatinib (2 μ M). (b) CD34 expression and cell death following *in vitro* culture of CD34⁺ CML cells with imatinib (2 μ M). (c) Number of colonies measured by CFC assay following a 72 hours (h) drug treatment of CD34⁺ CML cells with imatinib (2 μ M). Mean \pm S.E.M. n=4 patient samples. (d) Number of colonies measured by LTC-IC assay following single drug treatment of CD34⁺ CML cells with imatinib (2 μ M). Mean \pm S.E.M. n=3 patient samples.

3.2.2 Increased oxidative metabolism in primitive CML cells compared to differentiated cells

To investigate whether LSCs exhibit a different metabolic profile compared to differentiated CML cells, the metabolism of stem cell-enriched CD34⁺ and differentiated CD34⁻ CML cells derived from four patients was analysed by recording the steady-state levels of 70 metabolites. This revealed that stem cell-enriched cells displayed increased levels of carnitine, acylcarnitine derivatives and glycerol-3-phosphate, as well as a decrease in oleic and stearic free fatty acids, reflecting a potential increase in lipolysis and FAO (Fig. 3.2a, Table 1).

In order to validate and further substantiate these findings, CD34⁺ and CD34⁻ CML cells were cultured for 24 h in medium containing uniformly ¹³C₁₆-labelled palmitate, and ¹³C isotopic enrichment of intracellular metabolites was analysed by LC-MS. In stem cell-enriched CD34⁺ CML cells, TCA cycle metabolites contained a significantly larger fraction of isotopologues with 2 or more ¹³C atoms compared to those in differentiated CD34⁻ cells from the same patient (Fig. 3.2b). Moreover, TCA cycle metabolites and TCA cycle-derived amino acids steady-state levels were increased in CD34⁺ CML cells, while the steady-state levels of lactate were decreased. Of note, the steady-state level of the TCA cycle-derived amino acid aspartate has been identified as genuine indicator of mitochondrial oxidative metabolism (232-234). In line with this, CD34⁺ CML cells isolated from four patients displayed a 3.0-fold increase in mitochondrial OCR on average compared to CD34⁻ CML cells (Fig. 3.3a,b). Nevertheless, the increased levels of acetyl coA derived from FAO cannot support a net production of TCA cycle metabolites, which requires anaplerotic oxidizable sources, such as glucose and/or glutamine. Therefore, the increase in the steady-state levels of TCA cycle metabolites could not be entirely explained by an elevated FAO.

We next assessed anaplerosis and oxidative metabolism by tracing the fate of glucose-derived carbons in CD34⁺ CML and patient-matched CD34⁻ cells cultured for 24 h in presence of uniformly ¹³C₆-labelled glucose. The analysis of the ¹³C isotopic enrichment indicated a significant enhancement in glucose-derived carbons in the TCA cycle metabolites and derived amino acids in CD34⁺ CML cells in comparison to patient-matched differentiated CD34⁻ cells (Fig. 3.4a). Moreover, glutamate and aspartate contained larger fractions of isotopologues

with 2 or more ^{13}C atoms, in line with an elevated anaplerosis and oxidative metabolism in CD34^+ CML cells. In contrast, glucose-derived lactate ($^{13}\text{C}_3$ -lactate) was reduced in CD34^+ CML cells, reflecting that pyruvate is preferentially diverted toward oxidation through the TCA cycle.

PC catalyses the decarboxylation of pyruvate to oxaloacetate, an anaplerotic reaction that plays an important role in replenishing oxaloacetate into the TCA cycle (**Fig. 3.4a**). Moreover, acetyl coA is a positive allosteric activator of PC (235). Therefore, increased acetyl coA levels produced from fatty acid catabolism are expected to stimulate PC activity but decrease PDH activity. To link the activity of both enzymes with the FAO trait described previously, the relative activity of PC and PDH was evaluated by measuring the relative levels of the nearest detected labelled enzymatic product in $^{13}\text{C}_6$ -glucose-labelled CD34^+ and CD34^- CML cells. As such, the relative levels of $^{13}\text{C}_3$ -aspartate and $^{13}\text{C}_2$ -citrate were used to assess the relative activity of PC and PDH respectively (**Fig. 3.4a**). While there was no change in $^{13}\text{C}_2$ -citrate, the significant increase in the percentage of $^{13}\text{C}_3$ -aspartate confirmed that CD34^+ CML cells have increased levels of PC activity and anaplerosis in comparison to differentiated CD34^- CML cells (**Fig 3.4a,b**).

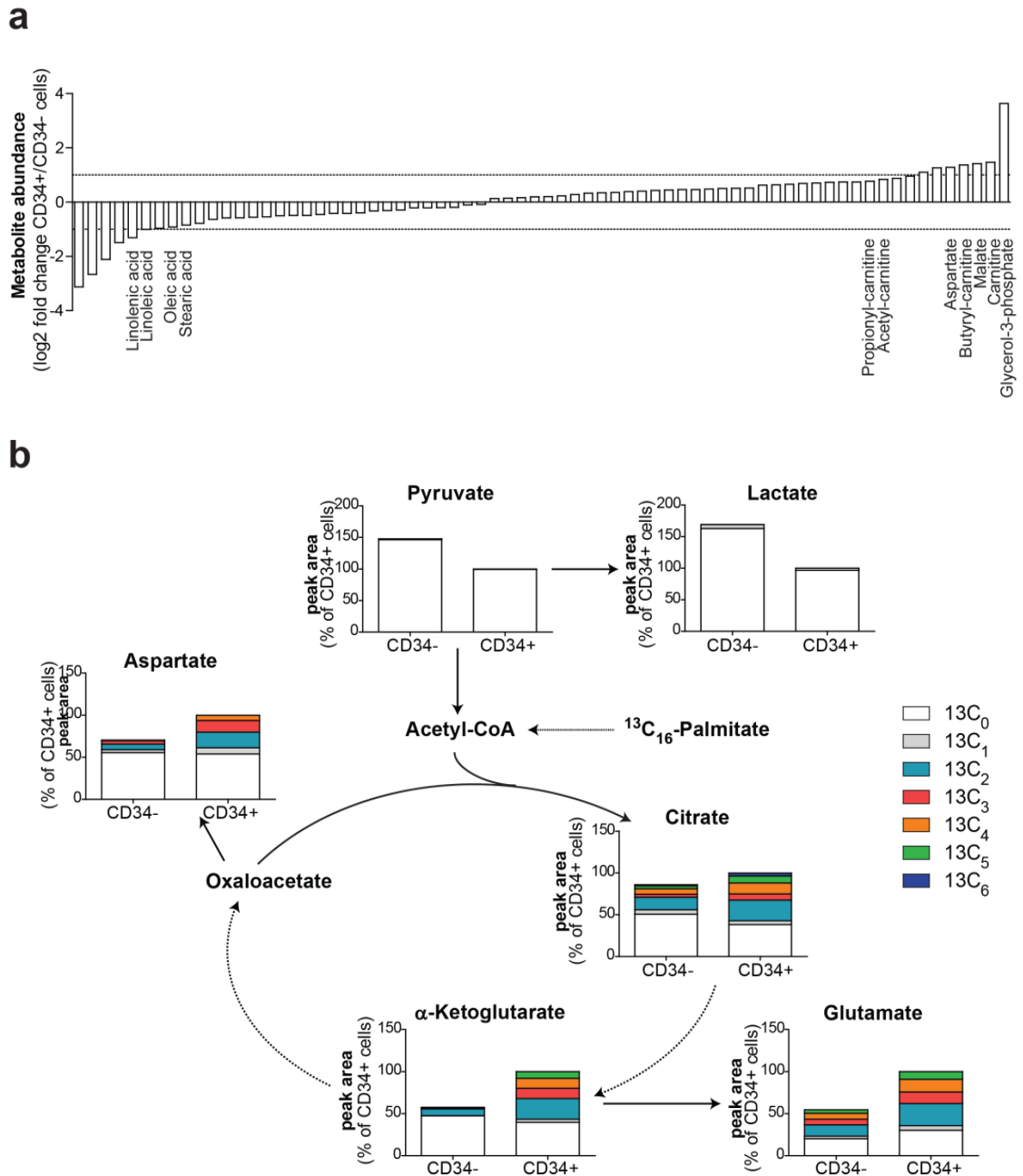


Figure 3. 2 Primitive CML cells show an increase in oxidative metabolism compared to differentiated counterparts.

(a) Comparative steady-state metabolomics analysis of patient-matched CD34⁻ and CD34⁺ CML cells measured by LC-MS. Mean ± S.E.M. n=4 patient samples. (b) Relative isotopologue distribution of intracellular metabolites in CD34⁻ and CD34⁺ CML cells measured by LC-MS following 24 h incubation with ¹³C₁₆-labelled palmitate. n=1 patient sample.

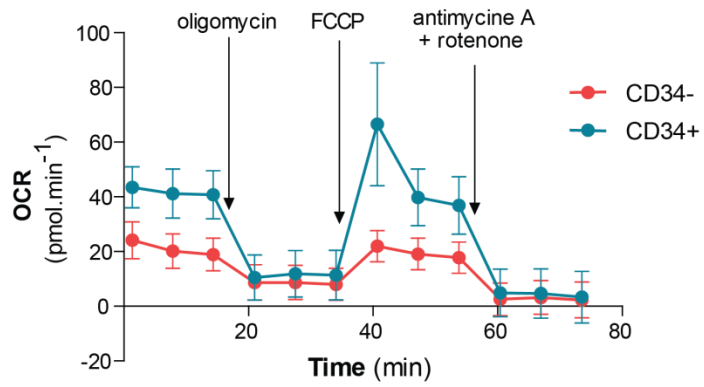
Metabolites	FC CD34+/ CD34- CML1	FC CD34+/ CD34- CML2	FC CD34+/ CD34- CML3	FC CD34+/ CD34- CML4	Average FC	Paired T test
Glycerol 3-phosphate	5.78	30.29	8.87	4.72	12.42	0.06
Carnitine	1.37	5.59	2.79	1.35	2.77	0.08
Malate	1.40	5.35	2.57	1.36	2.67	0.07
Butyryl-carnitine	1.49	6.42	1.67	0.77	2.59	0.77
Aspartate	1.56	2.21	4.39	1.59	2.44	0.07
UDP	0.67	5.47	0.77	2.69	2.40	0.65
Proline	1.22	3.36	2.62	1.38	2.14	0.07
PEP	1.79	1.05	2.19	2.73	1.94	0.08
ADP	1.53	2.54	1.34	1.94	1.84	0.05
Acetyl-carnitine	1.55	2.00	1.59	1.99	1.78	0.00
Propionyl-carnitine	0.98	4.13	1.21	0.49	1.70	0.42
AMP	1.17	2.40	0.93	2.20	1.67	0.20
Asparagine	1.49	2.18	1.54	1.48	1.67	0.05
Citrulline	1.82	2.46	0.95	1.39	1.66	0.09
Threonine	1.13	2.69	1.54	1.13	1.63	0.15
Thiamine	1.31	2.15	1.48	1.52	1.62	0.01
Tryptophan	1.58	2.61	1.14	0.97	1.58	0.12
CTP	0.68	2.23	0.85	2.46	1.56	0.66
Isoleucine	1.48	2.75	0.82	1.11	1.54	0.22
UTP	0.62	2.78	0.81	1.52	1.43	0.99
Phenylalanine	1.15	2.10	1.19	1.25	1.42	0.08
Dihydroxyacetone phosphate	0.62	1.08	1.24	2.72	1.42	0.48
α -Ketoglutaric acid	0.94	2.78	1.58	0.29	1.40	0.87
Leucine	1.18	1.95	0.95	1.44	1.38	0.25
Methionine	1.61	1.84	1.05	1.03	1.38	0.19
Cis-Aconitic acid	0.79	2.52	1.62	0.55	1.37	0.39
Glutamine	0.91	2.26	1.10	1.13	1.35	0.35
Lysine	1.15	1.54	1.57	1.03	1.32	0.05
ATP	0.98	1.81	1.14	1.32	1.31	0.16
Alanine	0.83	2.28	1.05	0.97	1.28	0.53
Valine	1.19	1.78	0.86	1.25	1.27	0.29
Glutamate	0.74	1.16	1.55	1.57	1.26	0.55
Glycine	1.03	1.28	1.12	1.45	1.22	0.08
Succinyl-GSH	0.70	2.55	0.93	0.51	1.17	0.78
Ornithine	1.36	1.06	1.37	0.81	1.15	0.58
Eicosapentaenoic acid	1.27	0.73	1.12	1.47	1.15	0.44
Cytidine	0.27	1.24	0.16	2.81	1.12	0.67
Betaine	0.63	2.06	0.97	0.76	1.11	0.83
Ethanolamine phosphate	1.19	0.57	0.84	1.78	1.09	0.93
GSH	0.56	1.33	0.59	1.30	0.94	0.31
Citric acid	0.74	1.06	1.15	0.77	0.93	0.70
Arachidonic acid	1.46	0.70	0.39	0.95	0.88	0.22
Pyruvate	0.66	0.58	0.76	1.49	0.87	0.69

Taurine	0.83	1.24	0.73	0.67	0.87	0.38
GDP	0.75	0.52	0.64	1.55	0.86	0.57
Creatine	0.90	1.15	0.42	0.80	0.82	0.35
Arginine	0.69	0.80	0.64	1.09	0.81	0.17
Urate	0.65	0.62	0.64	1.29	0.80	0.16
Nicotinamide	0.61	0.70	0.64	1.08	0.76	0.19
UDP-N-acetyl-D-glucosamine	0.60	0.20	0.78	1.42	0.75	0.98
Serine	0.68	0.65	0.64	1.03	0.75	0.09
Guanine	0.50	1.35	0.55	0.53	0.73	0.19
Adenine	0.46	0.75	0.85	0.79	0.71	0.16
Palmitoleic Acid	0.95	0.23	0.30	1.37	0.71	0.25
Octanoic Acid	0.54	0.53	0.48	1.27	0.71	0.21
Hexanoic Acid	0.58	0.49	0.50	1.18	0.69	0.23
Lactate	0.54	0.52	0.65	1.00	0.68	0.07
Succinate	0.59	0.65	0.68	0.77	0.67	0.07
Dodecanoic acid	0.67	0.43	0.34	1.24	0.67	0.20
Myristic Acid	0.73	0.35	0.40	1.09	0.64	0.24
GTP	0.42	0.62	0.38	0.89	0.58	0.11
Stearic Acid	0.47	0.27	0.24	1.25	0.56	0.21
Oleic Acid	0.54	0.23	0.31	1.04	0.53	0.18
Cystine	0.95	0.05	0.15	0.90	0.51	0.24
Linoleic Acid	0.47	0.24	0.27	1.01	0.50	0.19
Linolenic Acid	0.47	0.10	0.13	0.92	0.40	0.13
Adenosine	0.31	0.15	0.26	0.70	0.36	0.11
Uridine diphosphate						
glucose	0.34	0.25	0.10	0.24	0.23	0.18
NAD+	0.17	0.26	0.09	0.10	0.16	0.14
Hypoxanthine	0.11	0.07	0.02	0.26	0.11	0.03

Table 1: Comparative steady-state metabolomics analysis of patient-matched CD34⁺ and CD34⁻ CML cells measured by LC-MS.

FC, fold change of metabolites levels at steady-state in CD34⁺ CML cells relative to CD34⁻ CML cells. n=4 patient samples. Significant differences in metabolite levels between the two cell types are highlighted in red.

a



b

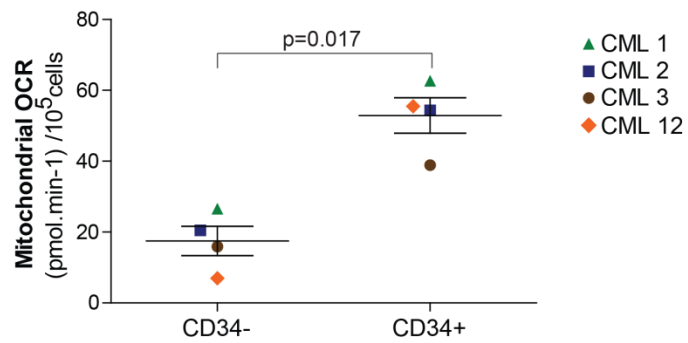


Figure 3. 3 Primitive CML cells show an increase in mitochondrial respiration compared to differentiated counterparts.

(a) Representative respirometry output in CD34⁻ and CD34⁺ CML cells. n=1 patient sample. Mean \pm S.D. (b) Basal mitochondrial OCR of CD34⁻ and CD34⁺ CML cells. n=9 patient samples and n=4 normal samples. Mean \pm S.E.M. P values were calculated by paired Student's t-test.

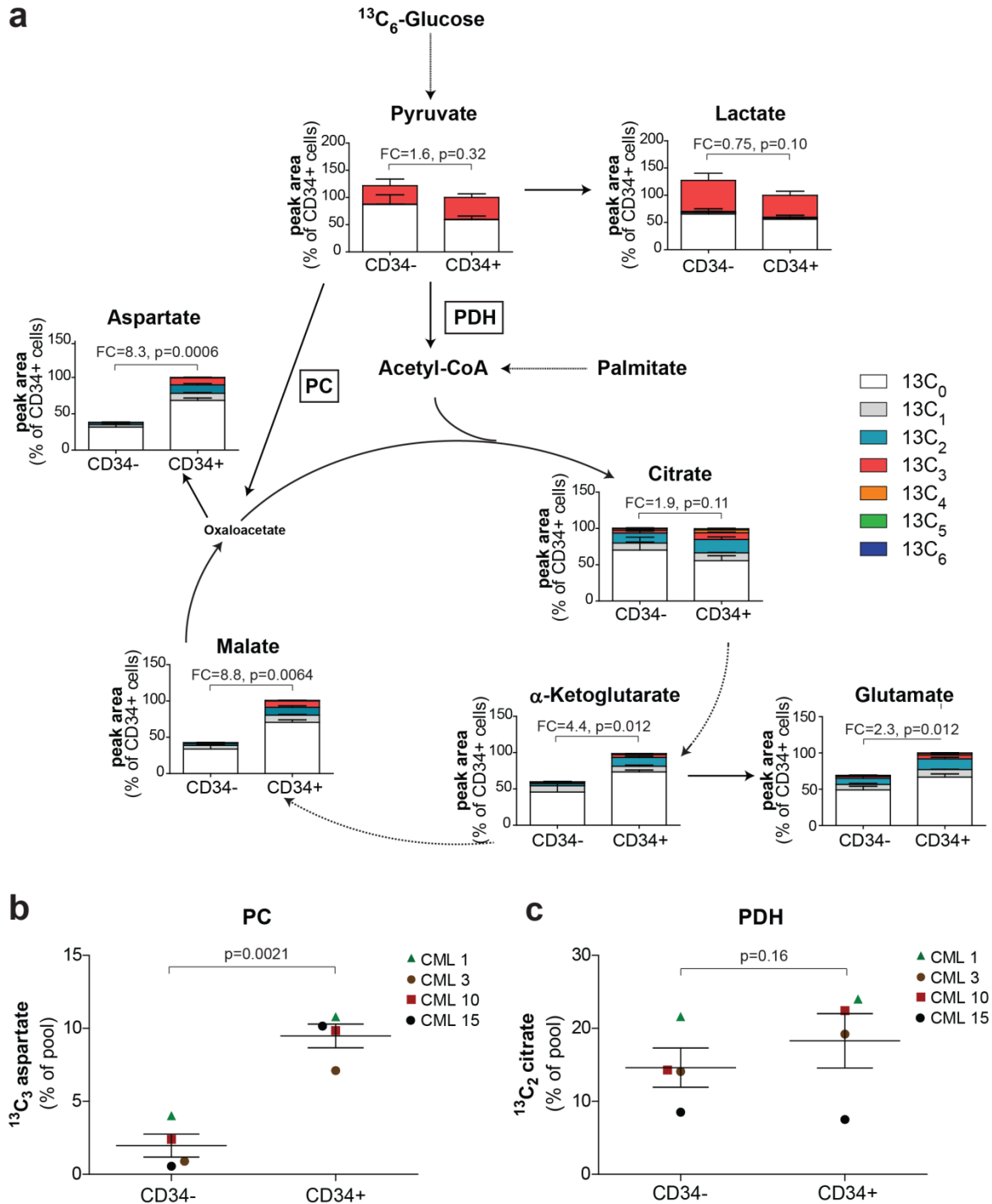


Figure 3. 4 Primitive CML cells have an increased glucose oxidation compared to differentiated counterparts.

(a) Relative isotopologue distribution of intracellular metabolites in CD34⁺ and CD34⁻ CML cells measured by LC-MS following 24 h incubation with ¹³C₆-labelled glucose. Mean ± S.E.M. n=4 patient samples. FC, fold change of glucose-derived (¹³C ≥ 2) metabolite abundance relative to CD34⁻ CML cells. (b-c) Relative abundance of (b) ¹³C₃-aspartate and (c) ¹³C₂-Citrate in CD34⁻ and CD34⁺ CML cells measured by LC-MS following 24 h incubation with ¹³C₆-labelled glucose. Mean ± S.E.M. n=4 patient samples. P-values were calculated by paired Student's t-test.

3.2.3 CML LSCs cells have elevated mitochondrial oxidative metabolism compared to normal counterparts

To investigate whether the oxidative phenotype observed in CD34⁺ CML cells is unique to primitive CML cells and not a common feature shared by CD34⁺ normal and CML cells, we next profiled intracellular metabolites at steady-state in CD34⁺ cells from four CML patients and four normal haematopoietic CD34⁺ cells donors. This indicated that FAO was increased in CD34⁺ CML cells. Indeed, carnitine and acyl-carnitines derivatives were elevated in CD34⁺ CML cells, while free fatty acids, such as linolenic and oleic acid, were reduced (**Fig. 3.5a, Table 2**). We next assessed the fate of the fatty acid palmitate by culturing CD34⁺ CML and normal cells for 24 h in presence of ¹³C₁₆-labelled palmitate and analysed the ¹³C isotopologues distribution by LC-MS (**Fig. 3.5b**). In line with an enhanced FAO, the absolute ¹³C enrichment of citrate, glutamate and aspartate from ¹³C₁₆-labelled palmitate was significantly higher in CD34⁺ CML cells compared to normal haematopoietic counterparts.

To gain a better understanding of anaplerosis and oxidative metabolism, CD34⁺ CML and normal cells were cultured for 24 h with ¹³C₆-glucose and the enrichment of glucose-derived ¹³C isotopes analysed by LC-MS. In CD34⁺ CML cells, the TCA cycle metabolite citrate and the TCA cycle-derived amino acids glutamate and aspartate contained a significant increase in ¹³C isotopologues from ¹³C₆-glucose compared to CD34⁺ normal cells, demonstrating a selective increase in glucose oxidation and anaplerosis in the leukaemic cells (**Fig. 3.6a-c**). Accordingly, the relative activity of both the anaplerotic enzyme PC and the oxidative enzyme PDH were significantly increased in CD34⁺ CML compared to normal counterparts (**Fig. 3.6d,e**). Moreover, as represented in **Figure 3.7a**, both the ATP-linked and mitochondrial respiration was increased in CD34⁺ CML cells compared to normal counterparts. Indeed, the mitochondrial respiration of leukaemic CD34⁺ samples from nine CML patients was on average 3.7-fold higher than that of CD34⁺ normal cells from four donors (**Fig. 3.7b**).

Altogether, these results demonstrated that anaplerosis and oxidative metabolism is significantly increased in CD34⁺ CML cells in comparison to CD34⁺ normal cells. Thus far, our experiments on primitive cells were performed in CD34⁺ cells that consist of a pool of progenitor and stem cells; therefore, we complemented our

studies in a subset of cells further enriched for stem cell activity. A rare quiescent population of cells enriched in CML LSCs and HSCs can be isolated within the CD34⁺ population. These cells represent about 5-10% of the bulk of CD34⁺ cells and are characterised by the lack of the human CD38 surface expression. CD34⁺CD38⁻ cells are enriched for cells with LTC-IC capacity compared to CD34⁺CD38⁺ cells and are able to repopulate immuno-deficient mice (19, 236).

To verify our findings in this stem cell-enriched population, CD34⁺ cells isolated from CML patients and healthy donors were stained with an anti-human CD38 antibody together with mitochondrial fluorescent probes for flow cytometric assessment of mitochondrial functions, namely the mitochondrial mass and the membrane potential, within CD34⁺CD38⁻ cells. As reflected by the representative histograms in **Figure 3.8 a and b**, the mitochondrial content and mitochondrial membrane potential of CD34⁺CD38⁻ CML cells was significantly increased compared to normal counterparts. This increase in mitochondrial mass and mitochondrial membrane potential was respectively 1.5 and 2.7 fold higher in CD34⁺CD38⁻ CML cells and indicated that CML LSCs possess increased mitochondrial oxidative functions compared to normal HSCs (**Fig. 3.8a,b**).

Finally, we performed a challenging experiment to investigate the metabolism of primitive haematopoietic cells. Briefly, FACS-sorted CD34⁺CD38⁻ cells from two CML patients and two normal cells donors were cultured in presence of ¹³C₆-glucose for 24 h and the ¹³C isotopic distribution of metabolites was analysed by LC-MS. This revealed that in CD34⁺CD38⁻ CML cells, citrate, glutamate and aspartate had higher levels of ¹³C isotopologues with 2 or more ¹³C atoms in comparison to CD34⁺CD38⁻ normal cells (**Fig. 3.8c-e**).

To understand whether subsets within the CD34⁺ cell population were metabolically different, we next analysed the metabolic profile of CD34⁺CD38⁺ cells following 24 h incubation with ¹³C₆-labelled Glucose in parallel to CD34⁺CD38⁻ cells. Precisely, we assessed the ratio between the oxidative and glycolytic pathway within each cell type. The contribution of glucose-derived carbons into the TCA cycle-derived amino acid glutamate (¹³C₂₋₂-Glutamate) and the glycolytic end-product lactate (¹³C₃-Lactate) were used as readout for oxidative metabolism and glycolysis respectively. This revealed that the ratio of glucose-derived glutamate over glucose-derived lactate was equivalent (or even increased in one

of the two patients) in CD34⁺CD38⁻ CML cells compared to CD34⁺CD38⁺ CML cells, suggesting that oxidative metabolism is similar between primitive and progenitor CML cells (**Fig 3.9**). In contrast, the ratio of oxidative to glycolytic metabolism was lower in CD34⁺CD38⁻ normal cells compared to CD34⁺CD38⁺ normal cells, suggesting that primitive haematopoietic cells are less oxidative than progenitor cells.

These results confirmed that primitive CD34⁺CD38⁻ CML cells have an increased oxidative metabolism in comparison to normal counterparts.

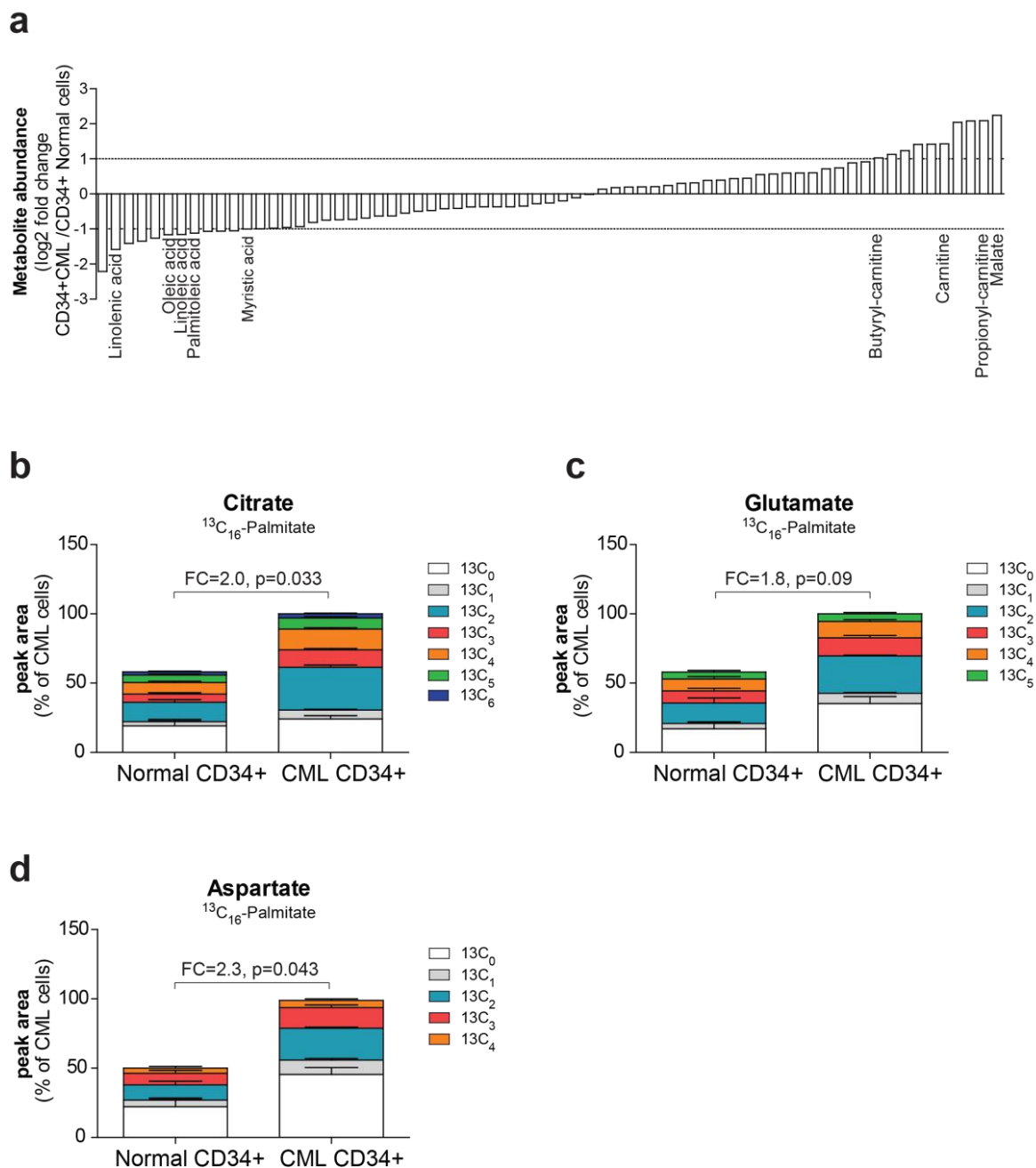


Figure 3. 5 Enhanced fatty acid oxidation in primitive CML cells compared to normal undifferentiated haematopoietic cells.

(a) Comparative steady-state metabolomics analysis of CD34⁺ CML and normal cells measured by LC-MS. Mean \pm S.E.M. n=4 patient and normal samples. (b-d) Relative isotopologue distribution of (b) citrate, (c) glutamate and (d) aspartate in CD34⁺ CML and normal cells measured by LC-MS following 24 h incubation with ¹³C₁₆-labelled palmitate. n=3 patient and normal sample. P values were calculated by unpaired Student's t-test. Mean \pm S.E.M

Metabolites	FC CD34+ CML/ CD34+ Normal1	FC CD34+ CML/ CD34+ Normal2	FC CD34+ CML/ CD34+ Normal3	FC CD34+ CML/ CD34+ Normal4	Average FC	Unpaired T test
Malate	5.50	2.82	6.32	4.28	4.73	0.01
Propionyl-carnitine	4.12	3.27	3.26	6.37	4.25	0.03
Dihydroxyacetone phosphate	1.84	2.10	11.48	1.56	4.24	0.28
Phosphoenolpyruvate	2.17	1.35	11.81	1.16	4.12	0.19
Carnitine	1.93	1.26	1.69	5.89	2.69	0.13
Proline	3.20	2.19	1.88	3.43	2.67	0.03
GSH	1.83	6.12	1.69	1.02	2.66	0.14
Cis-Aconitic acid	1.93	1.67	2.87	2.93	2.35	0.00
ADP	1.67	2.37	2.97	1.73	2.19	0.24
Butyryl-carnitine	2.01	3.29	1.33	1.53	2.04	0.02
Thiamine	1.84	1.78	1.05	2.88	1.89	0.08
α-Ketoglutaric acid	0.98	1.25	3.52	1.66	1.85	0.27
Aspartate	1.61	1.90	1.91	1.28	1.68	0.01
Glycerol 3-phosphate	2.08	1.45	1.94	1.10	1.64	0.38
ATP	1.29	1.39	2.16	1.24	1.52	0.27
Threonine	1.58	1.70	1.00	1.77	1.51	0.11
Alanine	1.67	1.77	1.12	1.48	1.51	0.15
Glutamine	1.58	2.36	1.04	0.94	1.48	0.35
NAD+	5.17	0.23	0.18	0.28	1.47	0.51
Glutamate	1.18	1.14	2.04	1.10	1.36	0.13
UTP	1.19	0.89	2.76	0.57	1.35	0.53
Citric acid	1.28	1.01	1.49	1.47	1.31	0.11
Asparagine	1.37	1.29	1.33	1.24	1.31	0.09
UDP-N-acetyl-D- glucosamine	3.57	1.08	0.19	0.15	1.25	0.34
AMP	1.08	0.83	1.43	1.60	1.24	0.56
Betaine	1.37	1.08	1.01	1.26	1.18	0.48
CTP	1.04	0.92	2.17	0.48	1.15	0.66
Tryptophan	1.37	1.21	0.62	1.41	1.15	0.80
UDP	1.17	0.84	2.26	0.31	1.15	0.69
Citrulline	1.42	1.09	0.67	1.36	1.13	0.73
Taurine	0.70	0.70	1.90	1.10	1.10	0.79
Glycine	1.24	0.80	1.07	0.86	0.99	0.87
Adenosine	1.66	0.47	0.56	1.02	0.93	0.93
Phenylalanine	1.07	0.96	0.40	1.05	0.87	0.53
Cytidine	2.42	0.46	0.27	0.21	0.84	0.40
Isoleucine	1.05	0.97	0.34	0.93	0.82	0.75
Guanine	2.38	0.27	0.30	0.20	0.79	0.46
Acetyl-carnitine	0.85	0.83	0.97	0.44	0.78	0.31
Valine	0.75	0.70	0.33	1.31	0.77	0.17
Leucine	0.98	0.99	0.38	0.75	0.77	0.80
Adenine	0.76	0.73	0.84	0.76	0.77	0.24
Lysine	0.80	0.72	0.35	1.14	0.75	0.29
Ornithine	0.81	0.65	0.38	1.14	0.75	0.53

Nicotinamide	0.64	0.64	0.39	1.21	0.72	0.36
Succinate	0.92	0.37	0.58	0.98	0.71	0.29
Serine	0.70	0.81	0.65	0.58	0.68	0.02
Arginine	0.96	0.68	0.27	0.68	0.65	0.04
Lactate	0.74	0.52	0.60	0.71	0.65	0.00
Arachidonic acid	1.63	0.58	0.19	0.08	0.62	0.31
Methionine	0.78	0.74	0.32	0.57	0.60	0.39
Cystine	0.56	0.83	0.07	0.94	0.60	0.19
Stearic Acid	0.71	0.49	0.54	0.64	0.59	0.44
Hexanoic Acid	0.71	0.42	0.60	0.54	0.57	0.34
Octanoic Acid	0.59	0.41	0.56	0.53	0.52	0.12
Urate	0.33	0.77	0.22	0.75	0.52	0.31
Eicosapentaenoic acid	0.62	0.47	0.62	0.32	0.51	0.39
Dodecanoic acid	0.58	0.42	0.63	0.38	0.50	0.05
Myristic Acid	0.60	0.46	0.52	0.42	0.50	0.01
GTP	0.52	0.27	0.82	0.32	0.48	0.10
Creatine	0.60	0.28	0.58	0.46	0.48	0.06
Pyruvate	0.46	0.49	0.44	0.51	0.48	0.01
Palmitoleic Acid	0.68	0.53	0.33	0.30	0.46	0.21
Linoleic Acid	0.66	0.51	0.38	0.24	0.45	0.22
Oleic Acid	0.69	0.46	0.36	0.28	0.45	0.15
GDP	0.65	0.16	0.68	0.18	0.42	0.20
Hypoxanthine	1.32	0.16	0.05	0.04	0.39	0.03
Ethanolamine phosphate	0.17	0.19	0.95	0.19	0.38	0.04
Linolenic Acid	0.88	0.32	0.08	0.06	0.33	0.11
Uridine diphosphate glucose	0.09	0.50	0.23	0.05	0.22	0.02

Table 2: Comparative steady-state metabolomics analysis of CD34⁺ CML and CD34⁺ normal cells measured by LC-MS.

FC, fold change of metabolites levels at steady-state in CD34⁺ CML cells relative to CD34⁺ normal cells. n=4 patient and normal samples. Significant differences in metabolite levels between the two cell types are highlighted in red.

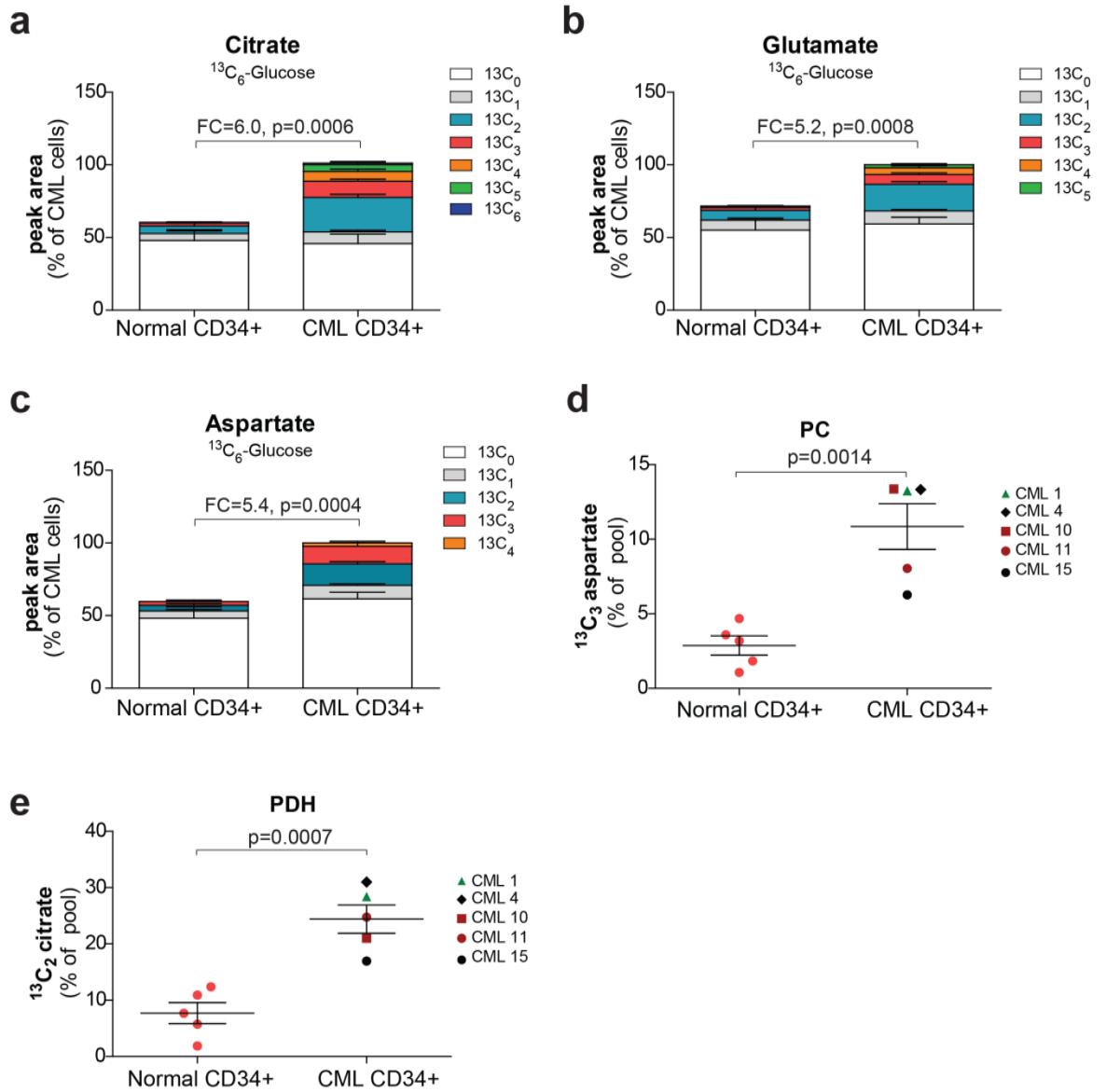
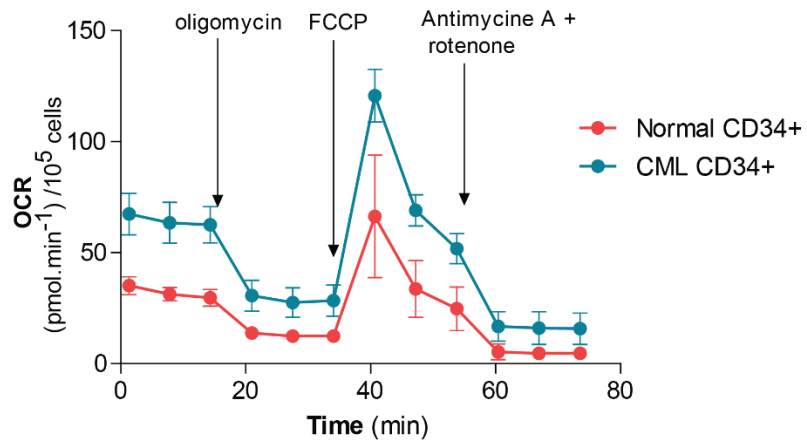


Figure 3. 6 Enhanced glucose oxidation and anaplerosis in primitive CML cells compared to normal counterparts.

(a-c) Relative isotopologue distribution of (a) citrate, (b) glutamate and (c) aspartate in CD34⁺ CML and normal cells measured by LC-MS following 24 h incubation with $^{13}\text{C}_6$ -labelled glucose. Mean \pm S.E.M. n=5 patient and normal samples. (d-e) Relative abundance of (d) $^{13}\text{C}_3$ aspartate and (e) $^{13}\text{C}_2$ Citrate in CD34⁺ CML and normal cells measured by LC-MS following 24 h incubation with $^{13}\text{C}_6$ -labelled glucose. Mean \pm S.E.M. n=5 patient and normal samples.

a



b

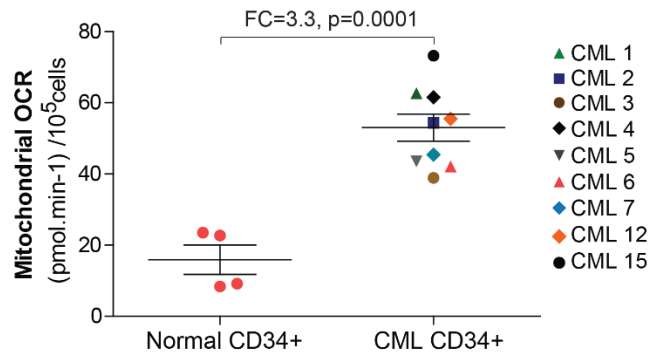


Figure 3. 7 CD34⁺ CML cells display increased mitochondrial respiration compared to normal counterparts.

(a) Representative respirometry output in CD34⁺ CML and CD34⁺ normal cells. Mean \pm S.D. (b) Basal mitochondrial OCR in CD34⁺ CML and CD34⁺ normal cells. Mean \pm S.E.M. n=9 patient samples and n=4 normal samples. P values were calculated by unpaired Student's t-test.

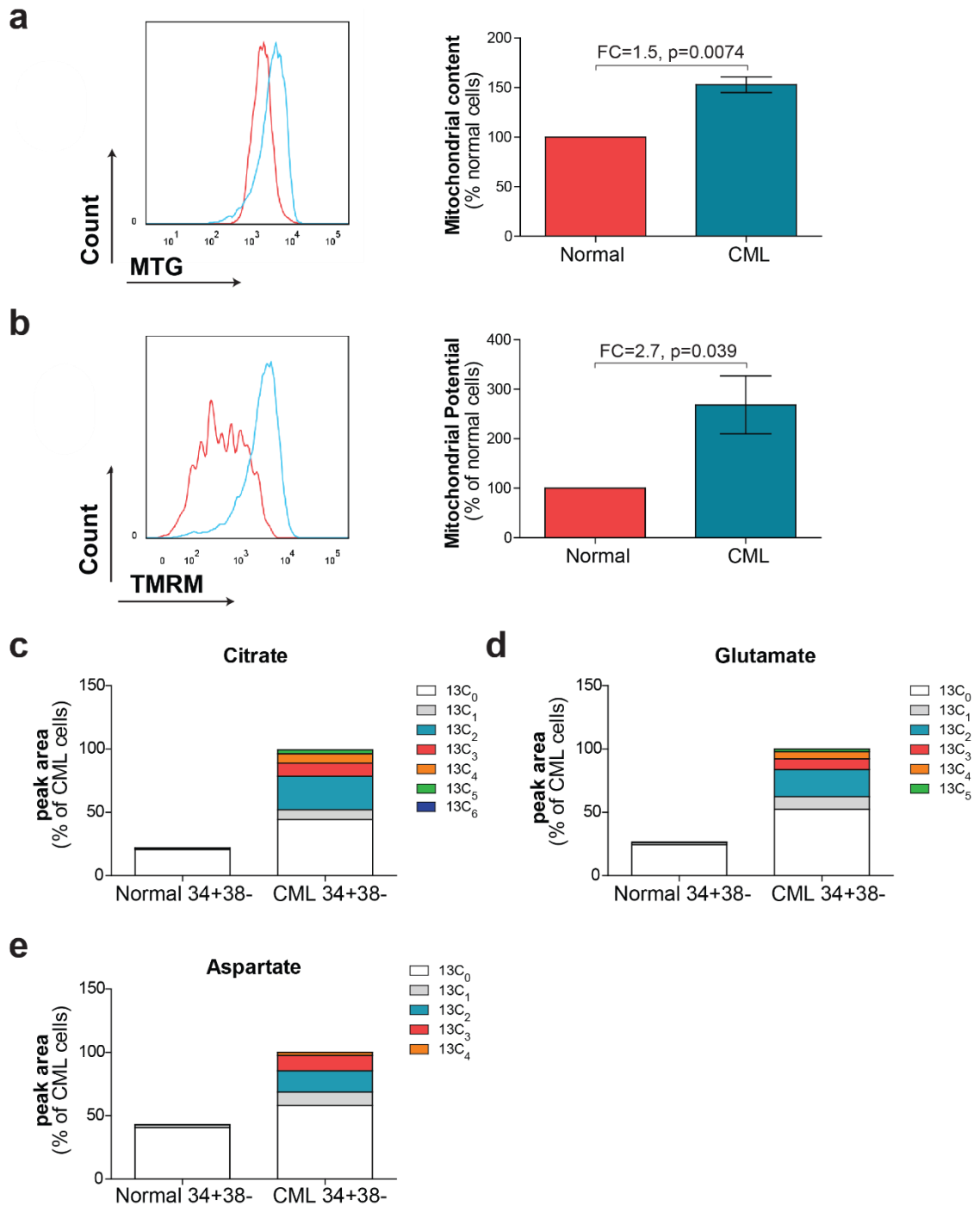
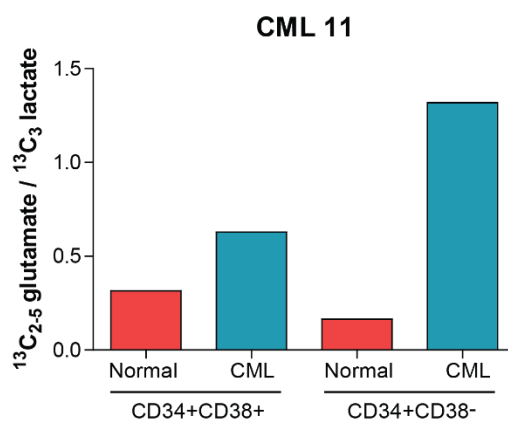


Figure 3. 8 CML LSCs have increased mitochondrial functions compared to normal HSCs.

(a) Representative histograms of Mitotracker Green-labelled CD34⁺CD38⁻ CML cells (blue) and CD34⁺CD38⁻ normal cells (red). The mitochondrial content was determined from the geometric mean of Mitotracker Green-labelled cells. Mean \pm S.E.M. n=3 patient and 3 normal samples. FC, fold change relative to CD34⁺CD38⁻ normal cells. P values were determined by one sample t-test. (b) Representative histograms of TMRM-labelled CD34⁺CD38⁻ CML (blue) and CD34⁺CD38⁻ normal (red) cells. The mitochondrial membrane potential cells was determined from the geometric mean of TMRM-labelled cells. Mean \pm S.E.M. n=3 patient and 3 normal samples. FC, fold change relative to CD34⁺CD38⁻ normal cells. P values were determined by one sample t-test. (c-d) Isotopologues labelling profile of (c) citrate, (d) glutamate, (e) aspartate in CD34⁺CD38⁻ CML and normal cells cultured for 24 h in presence of $^{13}C_6$ -labelled glucose. n=2 patient and normal samples.

a



b

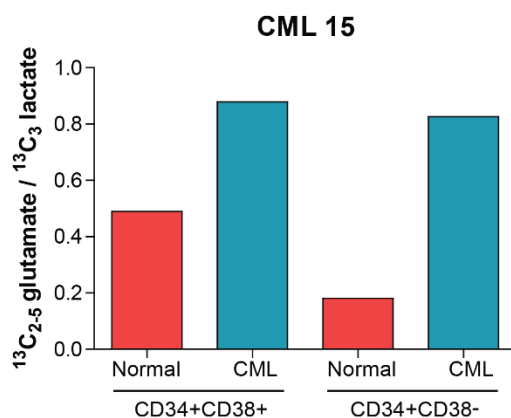


Figure 3. 9 Oxidative metabolism is similar between CML LSCs and CML progenitor cells.

(a-b) Ratio of glucose-derived glutamate ($^{13}\text{C}_{2.5}$ Glutamate) over glucose-derived lactate ($^{13}\text{C}_3$ lactate) in CD34⁺CD38⁺ and CD34⁺CD38⁻ CML and normal cells measured by LC-MS following 24 h incubation with $^{13}\text{C}_6$ -labelled glucose. Mean \pm S.E.M. n=2 patients and normal samples.

3.3 Discussion

In this chapter, we first showed that primitive CD34⁺ CML cells enhance FAO in comparison to CD34⁻ cells. Interestingly, FAO has been shown to play a crucial role in HSCs maintenance by producing cytosolic NADPH that prevents high ROS levels (151). Similarly, LSCs in AML have been suggested to rely on FAO for their survival (226). The selective increase in PC but not in PDH activity observed in CD34⁺ CML cells supported their FAO profile, as elevated acetyl coA levels from FAO are expected to increase PC activity. Moreover, we demonstrated that mitochondrial respiration and the levels of ¹³C-labelled isotopologues of TCA cycle metabolites from ¹³C₁₆-palmitate and ¹³C₆-glucose were significantly increased in CD34⁺ CML cells in comparison to CD34⁻ CML cells.

Altogether, these results have demonstrated that CD34⁺ CML cells display a significant increase in oxidative metabolism in comparison to CD34⁻ CML cells. Previous studies have shown that normal HSCs rely primarily on glycolysis for their energy production and possess low mitochondrial functions (140, 146). Therefore, it would have been interesting to compare the metabolism of CD34⁺ and CD34⁻ normal cells to see whether a similar metabolic difference is observed in normal haematopoietic cells. These experiments were however not performed due to lack of primary material. Moreover, the cellular composition of differentiated cells varies between normal and leukaemic haematopoiesis - the latter being characterised by an expansion of the myeloid cell lineage, which prevents a direct comparison between normal and leukaemic differentiated cells. One possibility would have been to sort for different cell types and analyse their metabolism individually. However, this study did not aim to assess the metabolic differences between HSC and progenitors at homeostasis and future investigations are necessary to address this point.

Our metabolic comparison of CD34⁺ cells from CML patients and normal cell donors revealed that FAO is elevated in CD34⁺ CML cells compared to CD34⁺ normal cells. Accordingly, CD34⁺ CML cells had a significant increase in palmitate-derived TCA cycle intermediates and derived amino acids, confirming that the aforementioned increase in FAO in primitive CML cells is selective to them. Moreover, we have demonstrated that mitochondrial respiration, glucose oxidation and anaplerosis

were significantly elevated in CD34⁺ leukaemic cells compared to normal counterparts. Noteworthy, a significant difference regarding the proliferation status of CD34⁺ CML and normal cells exists, with BCR-ABL driving the proliferation of CD34⁺ CML cells and CD34⁺ normal cells being mainly quiescent in our *in vitro* culture conditions. Therefore, proliferating CD34⁺ CML cells and quiescent CD34⁺ normal cells are expected to have distinct metabolic requirements and it could be argued that an increase in metabolic activity, such as the higher OXPHOS observed in CD34⁺ CML cells, was somewhat predicted. Conversely, studies have described that highly proliferative cancer cells tend to rely mainly on glycolysis for their energy production; albeit more recent studies have shown that mitochondrial oxidative metabolism is crucial for cancer progression and maintenance (1.5.3 and 1.5.4). To circumvent the proliferation bias, we assessed the ratio between the oxidative and glycolytic pathway in CD34⁺ CML and normal cells by measuring respectively the contribution of glucose-derived carbons into glutamate and lactate (Fig. 3.10). The ratio of glucose-derived glutamate (¹³C₂₂-Glutamate) over glucose-derived lactate (¹³C₃-Lactate) was significantly higher in CD34⁺ CML cells in comparison to CD34⁺ normal cells, confirming that oxidative metabolism is significantly elevated in primitive leukaemic cells despite normalising for the intrinsic characteristics of the cells.

These experiments were performed on CD34⁺ cells, consisting of a mixture of progenitors and stem cells. There are currently more rigorously-defined HSC and LSC populations and using these defined subsets of cells might have been more appropriate in this study. We therefore decided to recapitulate some of our key experiments in more stem cell-enriched subsets (CD34⁺CD38⁻). To our knowledge, this was the first time that targeted metabolomics in this rare and primitive haematopoietic cell population was performed from patient-derived material. Of note, these experiments were only done in two patients and two normal cell donors given the limitations of working with very small cell populations from primary material. Indeed, to isolate CD34⁺CD38⁻ cells, CML and normal haematopoietic cells are first selected for expression of the CD34 cell surface marker, which represents about 1% of total leukocytes. Then, 20 millions of CD34⁺ cells are subjected to a FACS for selection CD34⁺CD38⁻ cells, which yields about 0.5-1 million cells. We therefore optimised all our techniques to measure intracellular metabolites in a few number of suspension cells, and despite these

technical difficulties, we managed to perform targeted metabolomic analysis in CD34⁺CD38⁻ cells from two CML patients and two normal donors. The data obtained from the two independent experiments were very similar and in line with our previous results, confirming that primitive CML cells possess increase mitochondrial functions in comparison to normal counterparts. The comparison of the metabolic phenotype between CD34⁺CD38⁻ and CD34⁺CD38⁺ cells indicated an interesting difference between normal and CML cells. While in leukaemic cells, the oxidative metabolism was similar in CD34⁺CD38⁻ and CD34⁺CD38⁺ cell subsets, our results indicated that CD34⁺CD38⁻ normal cells were more glycolytic than CD34⁺CD38⁺ normal cells, in line with previous studies demonstrating that normal HSCs display low mitochondrial metabolism in comparison to progenitor cells. Of note, more primitive markers are available to further enrich for stem cells, but this was not possible given the number of cells required in our assays. As such, primitive HSCs are characterised phenotypically by being lineage (Lin) negative CD34⁺CD38⁻CD90⁺CD45RA⁻ (237). Future technological developments are required to investigate the metabolism of this rare population and address the metabolic difference between CD34⁺CD38⁻CD90⁺CD45RA⁻ normal and CML cells.

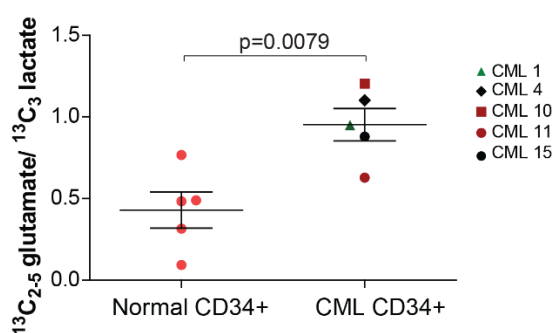


Figure 3. 10 CD34⁺ CML cells display increased glucose oxidation compared to normal counterparts.

Ration of glucose-derived glutamate (¹³C₂₋₅ Glutamate) over glucose-derived lactate (¹³C₃ lactate) in CD34⁺ CML and normal cells measured by LC-MS following 24 h incubation with ¹³C₆-labelled glucose. Mean ± S.E.M. n=5 patients and normal samples. P value was calculated by unpaired Student's t-test.

3.4 In summary

In this chapter, we analysed the metabolic profile of differentiated and stem cell-enriched cells from CML patients and normal cell-donors. For the first time, we profiled the steady-state levels of primitive CD34⁺ CML cells and more differentiated CD34⁻ cells and identified a FAO signature in stem-cell enriched CD34⁺ CML cells, that we later confirmed using ¹³C₁₆-labelled palmitate as a tracer. Moreover, we demonstrated increased mitochondrial metabolism, glucose oxidation and anaplerosis in CD34⁺ CML cells in comparison to differentiated patient-matched cells. We next showed that this mitochondrial oxidative profile was selective to CD34⁺ CML cells, as normal counterparts had reduced fatty acid and glucose oxidation in comparison. We as well traced the fate of glucose-derived carbons using ¹³C₁₆-labelled glucose in the rare population of CD34⁺CD38⁺ normal and CML cells and confirmed increased oxidative metabolism in primitive CML cells.

Put together, our results revealed a striking metabolic difference between primitive and differentiated leukaemic cells, with CD34⁺ CML cells being more oxidative than differentiated CD34⁻ CML cells. This was later proven to be selective to leukaemic cells, as CD34⁺ CML cells displayed a significant increase in mitochondrial oxidative metabolism in comparison to CD34⁺ normal cells. Finally, our results were strengthened by performing metabolic experiments on a rare population of primitive CD34⁺CD38⁻ cells, which confirmed an oxidative metabolic signature of primitive CML cells in comparison to normal counterparts.

Chapter 4 Using phenformin to target CML LSCs

4.1 Introduction

Our findings revealed that stem cell-enriched CD34⁺ CML cells have elevated levels of oxidative metabolism in comparison to normal counterparts and differentiated CD34⁻ CML cells. Importantly this metabolic trait was also confirmed by two different techniques in the more primitive CD34⁺CD38⁻ cell subset. We hypothesised that mitochondrial oxidative metabolism is crucial for energy and anabolic precursors production in CML LSCs and questioned whether inhibiting this pathway with inhibitors of mitochondrial metabolism would target CML LSCs.

Metformin, a biguanide derivative, is widely prescribed drug and the first line therapy to reduce hyperglycaemia in patients with type II diabetes. Metformin has been shown to reduce gluconeogenesis in the liver and potentiates the effect of insulin that favours cell glucose-uptake (238). While metformin does not usually induce hypoglycaemia and prevents weight gain, two common side effect of insulin and sulphonylureas treatment based regimens, it can induce lactic acidosis, a rare but potentially fatal condition (239). Interestingly, numerous epidemiologic have suggested that metformin possess anti-cancer properties. Reduction in the risk of cancer has for instance been observed in metformin-treated diabetic patients in comparison to patients treated with other anti-diabetic agents. Further studies assessing the potential therapeutic value of metformin use for cancer prevention and treatment in healthy/non diabetic patients are however necessary. Nonetheless, many *in vitro* studies have since then been performed and described metformin as a potential anti-cancer agent. On a cellular level, metformin affects the activity of mitochondrial complex I, leading to reduction in mitochondrial oxidative metabolism and consequently an increase in glycolysis and lactate production (240-242). The drop in ATP levels induces a metabolic stress which activates AMPK (**Fig. 4.1**) (243).

Phenformin is an analogue to metformin that was previously used to treat type II diabetes and has greater capacity to inhibit mitochondrial complex I compared to metformin. As such, the risk of lactic acidosis is increased upon phenformin

treatment (0.4-0.6 cases per 1000 patients), which eventually led to its withdrawal from the markets in the 1970s (244).

In this chapter, we compared the potency of metformin and phenformin to inhibit mitochondrial oxidative metabolism in CML lines and tested whether impairing this metabolic pathway can affect the survival of CML cell lines and patient-derived primitive CML LSCs.

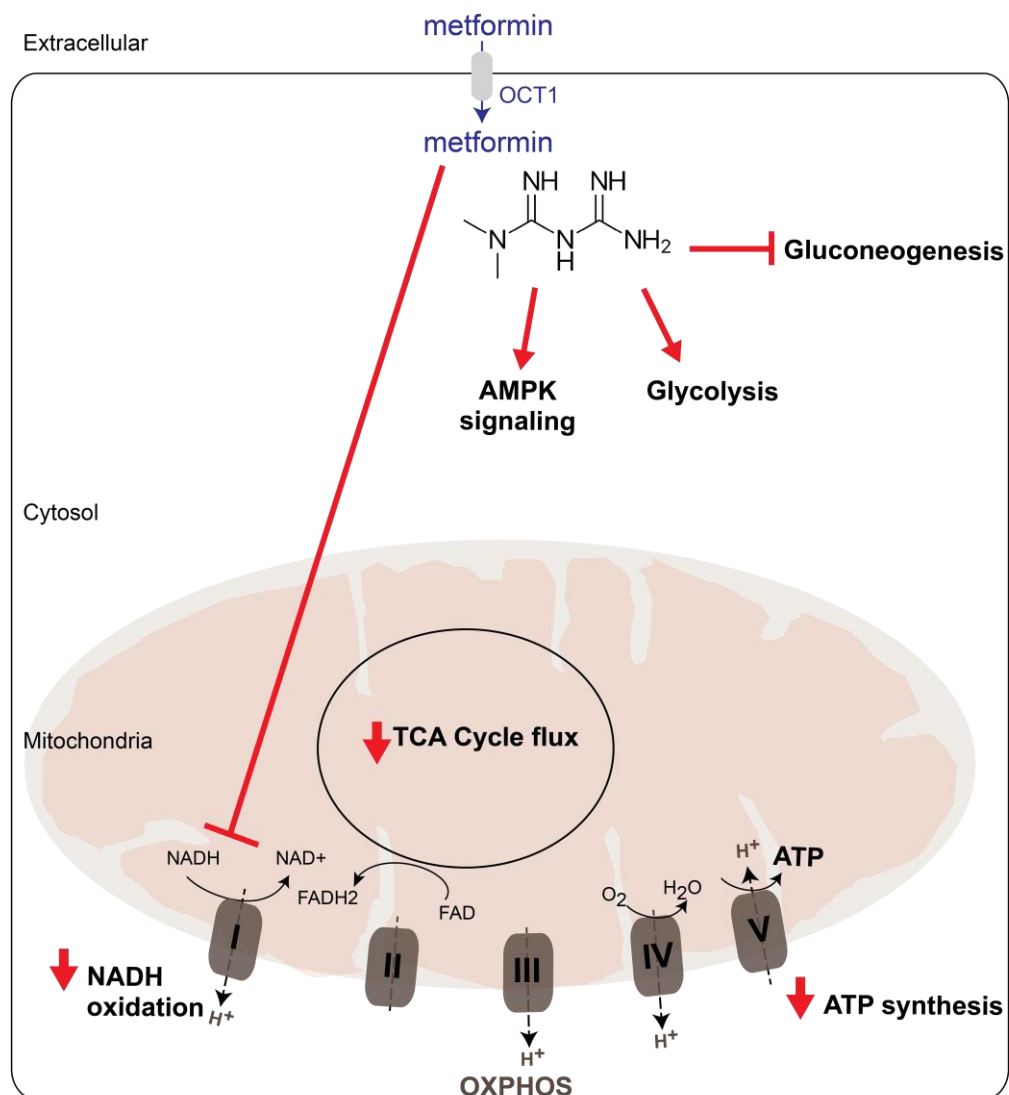


Figure 4. 1 Mechanism of action of metformin on a cellular level.

Adapted from (241).

4.2 Results

4.2.1 Phenformin is a more potent inhibitor of mitochondrial respiration than metformin

Given the unique increase of mitochondrial oxidative metabolism in CD34⁺ CML cells, restraining their mitochondrial function may have a therapeutic benefit. As previously mentioned, metformin is a widely used anti-diabetic drug that has been shown to inhibit complex I of the mitochondrial respiratory chain. To measure the anti-leukaemic effect of metformin and the relevant concentration of drug to use in our subsequent assays, the CML cell line of erythroblast crisis K562 was treated with a concentration range of metformin (from 39 μM to 10 mM) and the relative number of cells evaluated at 72 h by XTT assay. Metformin reduced cell growth by 51% at a concentration of 10 mM with an EC₅₀ value of 973 μM in K562 cells (**Fig. 4.2a**).

In healthy non-diabetic adults, the maximum plasma concentration of metformin has been evaluated to reach 12 ± 3 μM (245). However, the concentration that showed some effect in K562 cells was around 1 mM; more than 80 times higher than what is achieved in humans. This led us to test the activity of phenformin, an analogue of metformin that has been shown previously to be a more potent complex I inhibitor. Similar cell growth experiments were performed in K562 cells with various concentration of phenformin ranging from 0.3 μM to 100 μM . Phenformin inhibited K562 cell proliferation by 45% at a concentration of 37.5 μM and the relative EC₅₀ value was estimated to be 3.85 μM (**Fig. 4.2b**).

To confirm a reduction in oxidative metabolism, K562 cells were treated for 24 h with either phenformin (10 μM) or metformin (1 mM) and mitochondrial respiration was assessed. As expected, both drugs reduced mitochondrial respiration. However, despite using a concentration of phenformin 100 times lower, both drugs inhibited mitochondrial OCR to a similar extent; making phenformin approximately 100 times more potent inhibitor of mitochondrial oxidative metabolism than metformin (**Fig. 4.2c**).

Studies have shown that both metformin and phenformin increase glycolysis as a result of AMPK activation when oxidative phosphorylation is inhibited (246, 247).

Extracellular acidification rate (ECAR) consists of a measurement of pH changes over time and can be used to indirectly determine the rate of production of lactate from pyruvate, indicative of glycolysis. Other cellular processes such as CO₂ release from the TCA cycle can influence the pH of the media and therefore the measurement, however ECAR can be determined in parallel to mitochondrial respiration and the increase in glycolysis upon phenformin/metformin treatment has been widely described (217, 248). Therefore, to assess whether phenformin and metformin increase glycolysis, ECAR was measured following 72 h of treatment with phenformin (10 μM) or metformin (1 mM). Phenformin and metformin induced an increase in ECAR, suggesting that K562 cells upregulated glycolysis following 72 h of drug treatment with these complex I inhibitors (**Fig. 4.2d**). Noteworthy, the increase in ECAR was equivalent between the two inhibitors, mirroring the effect observed on mitochondrial respiration.

Finally, the effect of a range of concentrations of phenformin on oxidative metabolism was tested in K562 and KCL22 cells, a second CML cell line of erythroblast crisis. Following 24 h *in vitro* treatment, phenformin induced a decrease in mitochondrial respiration in a dose-dependent manner in both cell lines, with a near-to-complete inhibition of mitochondrial respiration seen at a concentration of 20 μM (**Fig 4.2e**).

Altogether, these results confirmed that phenformin has a greater potency than metformin to inhibit mitochondrial respiration. As we aimed to test the effect of inhibiting mitochondrial oxidative metabolism to target CML LSCs *in vivo*, the more potent inhibitor phenformin was selected for subsequent *in vitro* and animal work.

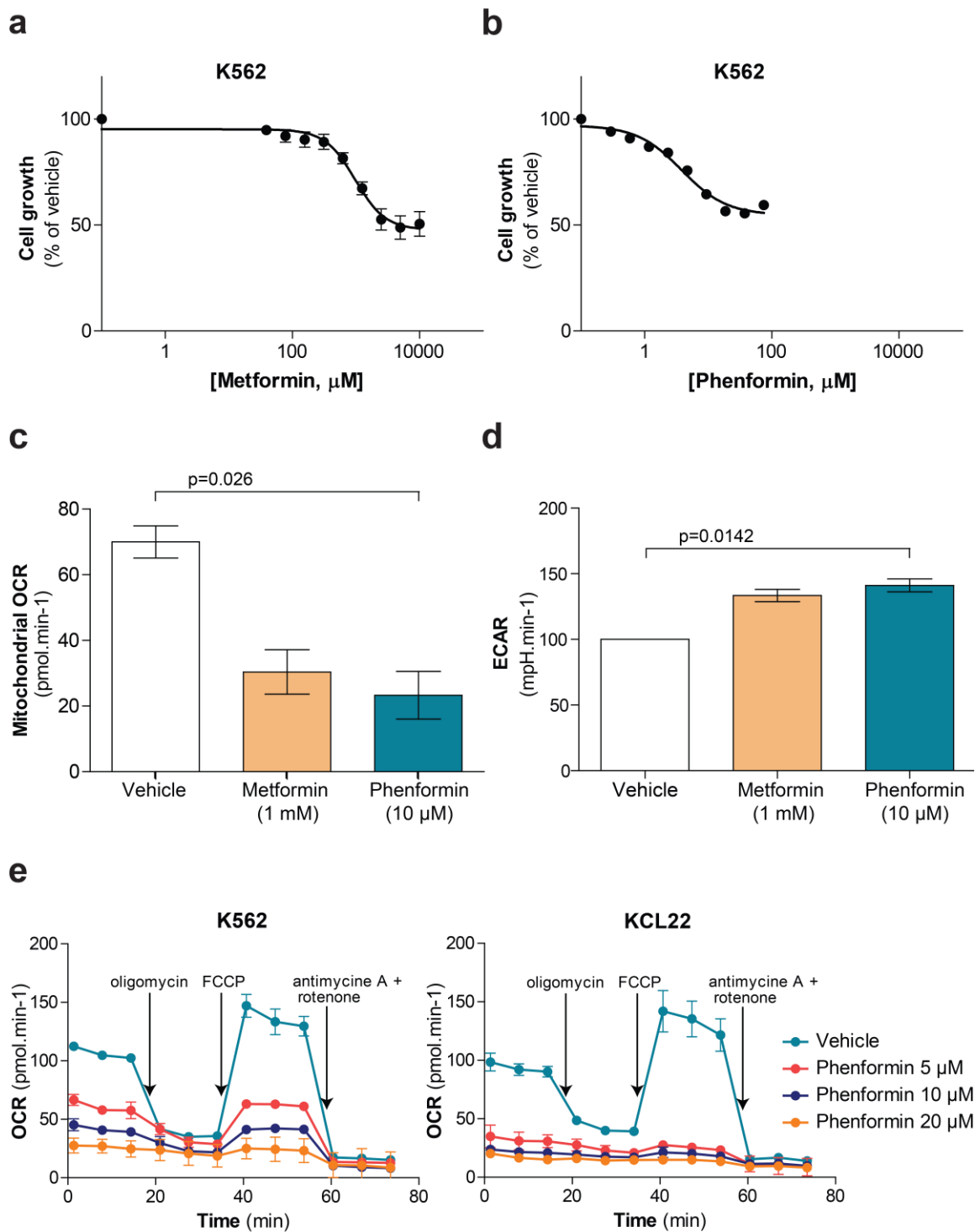


Figure 4. 2 Phenformin is a more potent inhibitor of oxidative metabolism than metformin.

(a-b) Proliferation of K562 cells upon exposure to various concentrations of (a) metformin or (b) phenformin. $n=3$ independent experiments. (c) Basal mitochondrial OCR in K562 cells upon 72 h treatment with metformin (1 mM) or phenformin (10 μM). P values were calculated by unpaired Student's t-test. $n=3$ independent experiments for phenformin treatment, $n=2$ independent experiments for metformin treatment (d) ECAR of K562 cells upon 72 h treatment with metformin (1 mM) or phenformin (10 μM). $n=3$ independent experiments for phenformin treatment, $n=2$ independent experiments for metformin treatment. P values were calculated by one sample Student's t-test. (e) Representative respirometer output of K562 (left) and KCL22 (right) cells following 24 h treatment with various concentrations of phenformin (5, 10 and 20 μM). Data are represented as Mean \pm S.E.M.

4.2.2 Inhibition of mitochondrial metabolism with phenformin targets K562 cells

The majority of CML patients in chronic phase will undergo treatment with TKIs, the first-line therapy for CML-CP. It is therefore important to determine the nature of a drug combination between a TKI and a new agent aimed to be used against CML stem cells (in our case phenformin). To this end, the combination index (CI) between phenformin and imatinib in CML cell lines was determined based on the equation of Chou-Talalay. K562 cells were treated for 72 h with a single concentration of phenformin (10 μM) in combination with a concentration range of imatinib (from 0.078125 μM to 2.5 μM) and cell proliferation was assessed by XTT assay. The percentage of inhibition of proliferation was then computed for each drug concentration in the CompuSyn software. The percentage of inhibition of proliferation was then computed in the CompuSyn software for each drug concentration, as a single agent or in combination. This program predicts the effect that should be observed for the combination based on the single agent dose-response curves and, by comparing it to the empirical values, evaluates the nature of the drug combination: synergism ($\text{CI} < 1$), additive ($\text{CI} = 1$) or antagonism ($\text{CI} > 1$). This revealed that the CIs were inferior to 1 for all 3 doses of imatinib tested in combination with phenformin (10 μM) (**Fig. 4.3a,b**).

Imatinib and other TKIs are potent anti-proliferative agents, particularly in CML cell lines. Indeed, K562 cells treated with a concentration of imatinib five times lower than the plasma concentration measured in patients induced a cell cycle arrest in the G1 phase (**Fig. 4.3c**). Given that imatinib and other TKIs are strong cytostatic agents, analysing the effect of the drug combination on the proliferation of CML cells might not be the optimal readout. For this reason, we next assessed cell viability in K562 cells following treatment with imatinib (500 nM), phenformin (10 μM) or the combination for 72 h by 7-AAD exclusion. While phenformin treatment alone did not significantly affect the viability of leukaemic cells compared to untreated conditions, the combination of imatinib and phenformin significantly reduced the number of viable cells by more than 15% compared to imatinib alone (**Fig. 4.3d,e**).

Contrary to glycolysis of glucose that produces two net ATP, the oxidation of galactose to pyruvate does not yield any net ATP. As a result, the cells adapt by

upregulating mitochondrial metabolism to compensate the lack of ATP produced from glycolysis. In line with this, replacing glucose in the culture media with galactose has been shown to induce mitochondrial metabolism and therefore render cells particularly sensitive to mitochondrial poisons.

To demonstrate that the decrease in cell viability observed in K562 cells treated with the combination phenformin and imatinib is mediated by its effect on mitochondrial respiration, K562 cells were grown in media containing galactose as a sole sugar or in complete medium (11 mM glucose). Following 24 h incubation in galactose-medium, K562 displayed a two-fold increase in mitochondrial respiration compared to cells plated in complete medium (**Fig. 4.4a**). Cell viability was next assessed by Propidium Iodide (PI)-exclusion following 72 h treatment with phenformin (10 μ M), imatinib (500 nM) and combination in either galactose or complete medium. The presence of galactose greatly potentiated the effect of phenformin, in combination with imatinib or as a single agent, compared to complete-medium (**Fig. 4.4b**). Indeed, while phenformin did not induce any significant cell death in complete medium, only 33% of K562 cells remained viable in the presence of galactose. Similarly, combining phenformin to imatinib reduced viability to 43% in complete medium, whereas less than 6% of cells were viable in galactose containing medium.

These results showed that cells relying solely on mitochondrial metabolism are highly sensitive to phenformin, and demonstrated that the cell death observed upon phenformin treatment is mediated by inhibition of respiration.

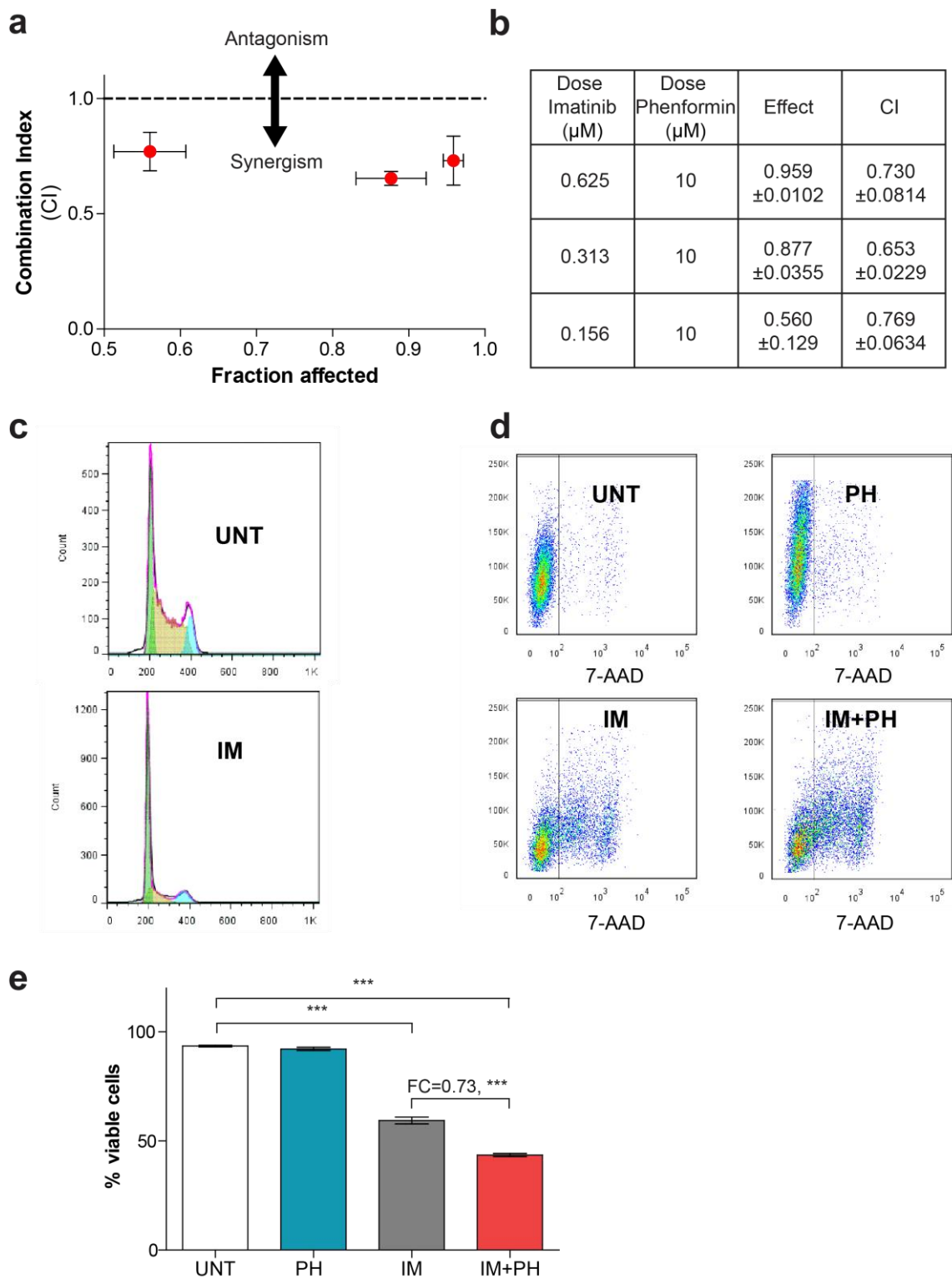


Figure 4. 3 Phenformin synergises with imatinib to target K562 cells.

(a) Proliferation of K562 following 72 h exposure to phenformin (10 μM) and various concentrations of imatinib (156, 313 and 625 nM). The determination of the combination index was carried out using Calcsyn software as described in Methods to determine synergy (defined as CI values < 1). n=3 independent experiments (b) Representative cell death measurement in K562 cells treated for 6 days with imatinib (500 nM), phenformin (10 μM) or combination. (c) Cell death in K562 cells treated for 6 days with imatinib (500 nM), phenformin (10 μM) or combination. n=3 independent experiments. Data are presented as Mean \pm S.E.M. ***P<0.001, evaluated by one-way analysis of variance (ANOVA) with post hoc Bonferroni analysis. FC, Fold change relative to IM-treated cells. Unt, untreated; PH, Phenformin; IM, imatinib.

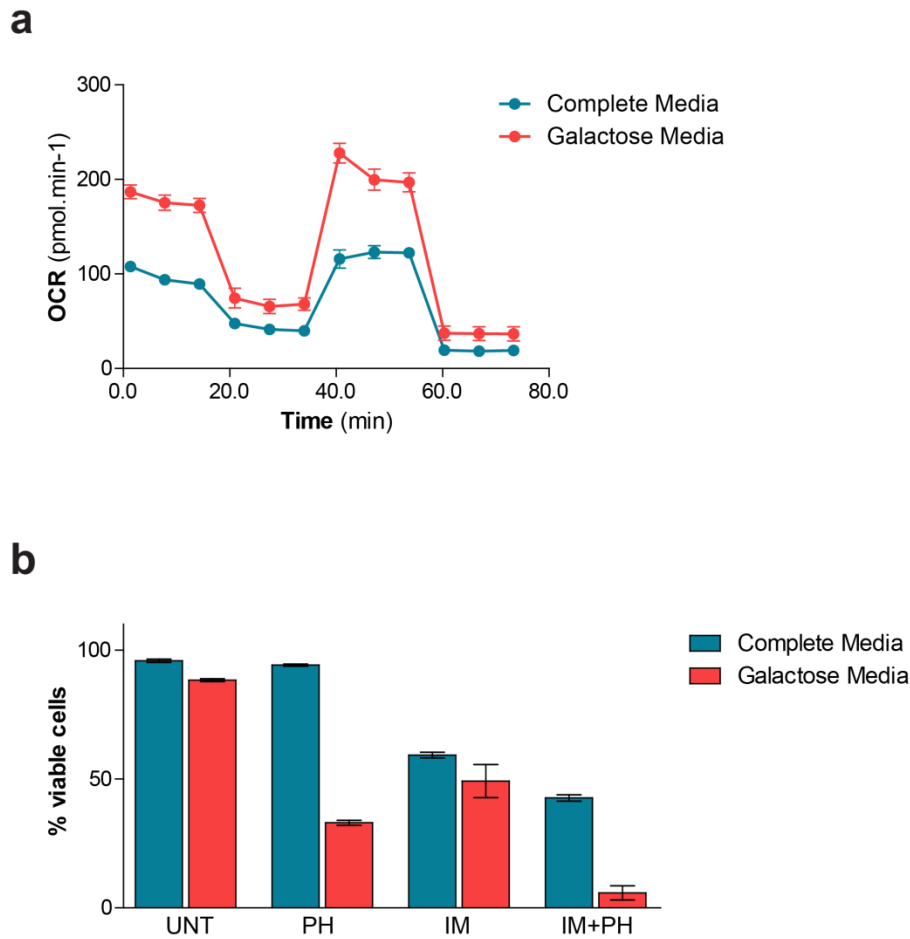


Figure 4. 4 Phenformin targets K562 cells by inhibiting mitochondrial respiration.

(a) Respirometer output for K562 cells cultured for 24 h in complete media or no-glucose media supplemented with galactose (11mM). n =1 independent experiment. (b) Cell death in K562 cells and (c) KCL22 cells cultured in complete media or no-glucose media supplemented with galactose (11 mM) and treated for 6 days with imatinib (500 nM), phenformin (10 μ M) or combination. n=2 independent experiments. Data are presented as Mean \pm S.E.M. Unt, untreated; PH, Phenformin; IM, imatinib.

4.2.3 Phenformin preferentially targets BCR-ABL expressing cells

To determine whether the combination of phenformin and imatinib selectively targets CML cells, parental Ba/F3 cells; a BCR-ABL-negative pro-B murine cell line, and Ba/F3 cells stably expressing BCR-ABL^{p210} (refer to as Ba/F3 p210) were used. Using these two cell lines allows us to determine the selectivity of a drug treatment for BCR-ABL cells and its potential toxicity towards cells not expressing BCR-ABL (normal cells).

Both parental Ba/F3 and Ba/F3 p210 cells were treated for six days with phenformin (10 μ M), imatinib (500 nM), or combination, and cell viability assessed by PI-exclusion. This revealed that the combination treatment arm reduced the percentage of Ba/F3 p210 viable cells by nearly 20% in comparison to imatinib (**Fig. 4.5a**). These results were in line with previous experiments showing that the combination of phenformin and imatinib significantly impairs the survival of BCR-ABL-expressing K562 cells in comparison to imatinib alone (**Fig. 4.3d,e**). On the contrary, the viability of parental Ba/F3 cells did not vary from untreated condition and was maintained at approximately 100% upon treatment with either phenformin, imatinib or the combination (**Fig. 4.5b**). Indeed, the percentage of viability was 95% and 98% respectively in the untreated and the combination arm.

These results demonstrated that cells lacking BCR-ABL expression are less sensitive to the combination of imatinib and phenformin than BCR-ABL expressing cells, suggesting a potential therapeutic window for the use of phenformin in combination with imatinib to target CML cells.

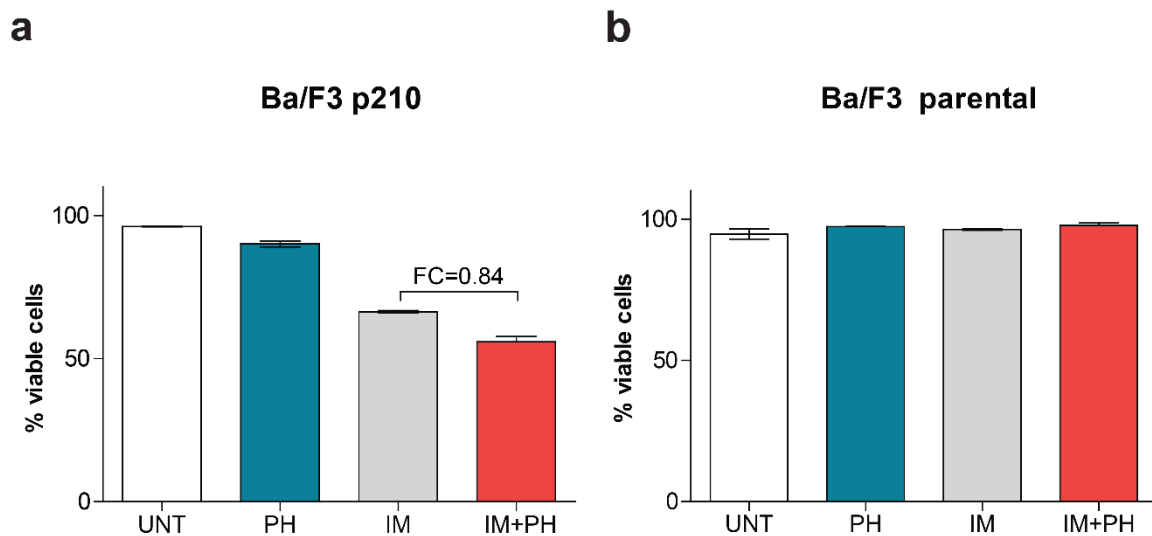


Figure 4. 5 Phenformin in combination with imatinib targets selectively BCR-ABL expressing cells.

(a) Cell death in Ba/F3 p210 and (b) parental Ba/F3 cells following 6-day *in vitro* treatment with imatinib (500 nM), phenformin (10 μ M) or the combination. Data are presented as Mean \pm S.E.M. n=2 independent experiments. FC, fold change relative to IM-treated cells. Unt, untreated; PH, phenformin; IM, imatinib.

4.2.4 Inhibition of aberrant oxidative metabolism with phenformin targets CML LSCs *in vitro*

We next performed experiments on stem cell-enriched CD34⁺ cells isolated from CML patients. To test the effect of phenformin on mitochondrial respiration in patient-derived cells, CD34⁺ CML cells were treated for 24 h with phenformin (10 μ M) and OCR were assessed by respirometry analysis. As previously observed in K562 cells, phenformin decreased ATP-linked and mitochondrial respiration in CD34⁺ cells isolated from two CML patients compared to vehicle treatment (**Fig. 4.6a,b**).

To assess whether phenformin was targeting CD34⁺ CML cells, CFC assays were next performed following 72 h of *in vitro* treatment with phenformin (20 μ M), imatinib (2 μ M) or the combination of phenformin and imatinib (20 μ M + 2 μ M). Imatinib decreased the number of progenitor-derived colonies by 62%, while the combination treatment resulted in 78% reduction on average (**Fig. 4.6c**). Of note, the effect of the combination was pronounced in only one out of the two CML samples tested.

As mentioned previously, CD34⁺ cells are composed of both progenitor and stem cells and are not a pure population of LSCs. To validate that phenformin can target CML LSCs in presence of imatinib, the functional capacity of LSCs was assessed by Long-Term Culture Initiating-Cell (LTC-IC) assays. As described in the Methods section (**2.2.8.2**), CD34⁺ CML cells were treated once with phenformin, imatinib or in combination and cultured for five weeks on a stromal cell layer before assessment of the remaining progenitor cells by CFC assay. Since progenitor cells present at the beginning of the five-week assay would have lost their colony forming potential over time, the measurement of the remaining viable progenitor cells after this time course ensures selective measurement of the functional capacity of LSCs. In line with previous published data, imatinib did not reduce the stem-cell potential of CML cells (**Fig. 4.6d**). However, phenformin, as a single agent, decreased the number of stem-cell derived colonies in three out of four CML patients and the combination of both drugs significantly reduced the number of colonies in all patient-derived samples by 71% on average.

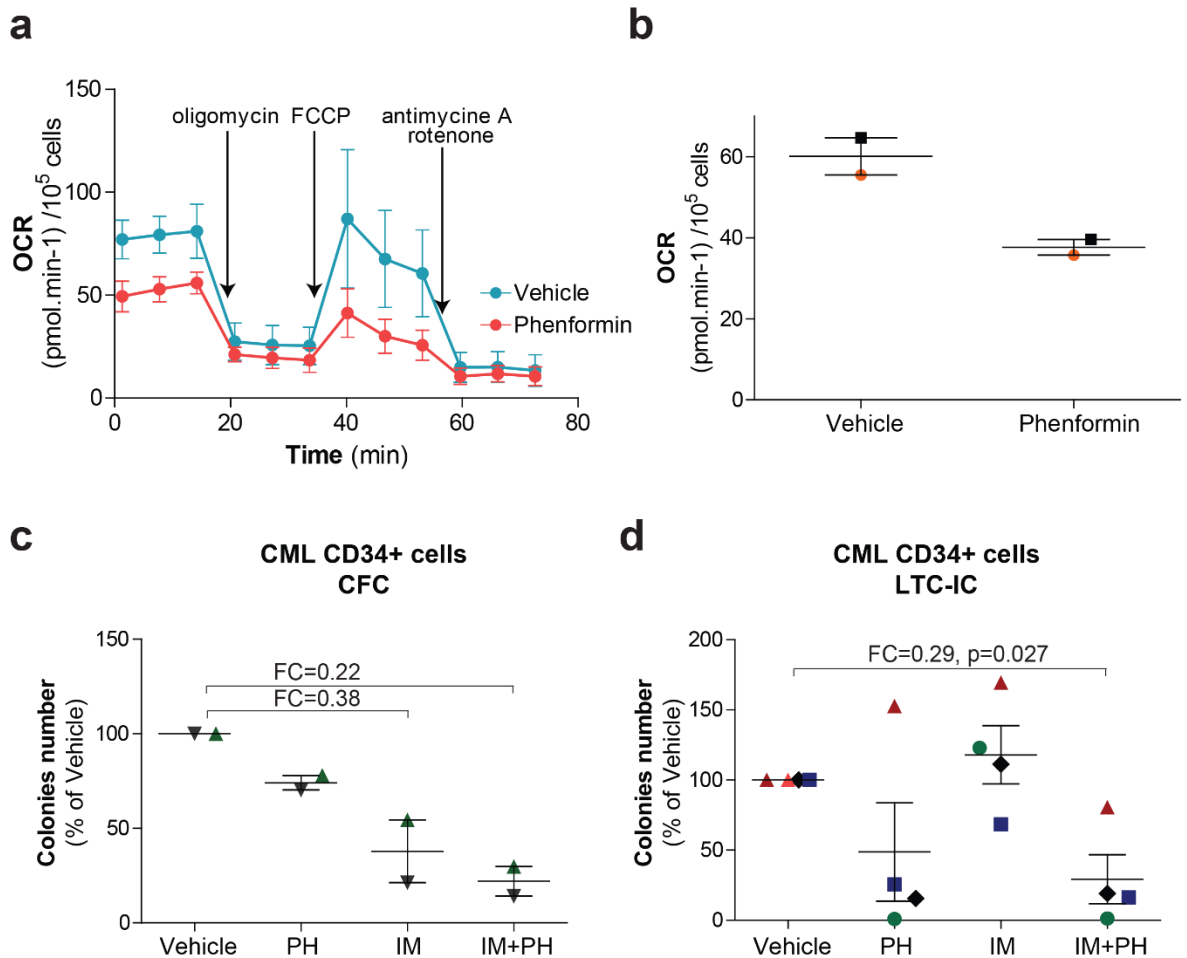


Figure 4. 6 Inhibition of aberrant oxidative metabolism with phenformin targets CML LSCs *in vitro*.

(a) Respirometer output in CD34⁺ CML cells exposed for 24 h to phenformin (10 μ M). n=1 patient sample. Data are presented as Mean \pm S.D. (b) Basal mitochondrial OCR in CD34⁺ CML cells exposed for 24 h to phenformin (10 μ M). Data are presented as Mean \pm S.E.M. n=2 patient samples. (c) Colony numbers following 3 days drug treatment of CD34⁺ CML cells with phenformin (20 μ M). Data are presented as Mean \pm S.E.M. n=2 patient samples. (d) Number of colonies measured by LTC-IC assay in CD34⁺ CML cells following single drug treatment with phenformin (20 μ M). Data are presented as Mean \pm S.E.M. n=4 patient samples. P values were calculated by paired Student's t-test. FC, fold change relative to vehicle-treated cells. PH, phenformin; IM, imatinib.

4.2.5 Modelling CML disease *in vivo* using a transgenic BCR-ABL mouse model

To determine whether phenformin could target LSCs *in vivo*, the DTG SCL-tTA-BCR-ABL mouse model was used. As mentioned earlier (1.3.4), the sole expression of BCR-ABL in mice is sufficient to induce leukaemogenesis that resembles human CML. In this mouse model, BCR-ABL expression is under the control of a tetracycline-responsive element (TRE), so that its expression is induced in the mice upon removal of tetracycline from the drinking water (Tet-OFF system). In the absence of tetracycline, the tetracycline transactivator protein (tTa) binds to TRE, which prevents the transcription of BCR-ABL. Moreover, the tTa has been placed under the control of a 3' region of the SCL gene that has been shown to have restricted expression in HSPCs and megakaryocytes. Expression of BCR-ABL is therefore induced primarily in the HSPC compartment upon tetracycline withdrawal.

The CD45 common antigen is expressed by all leucocytes and has two functionally identical alleles: CD45.1 and CD45.2. This is commonly used in research to differentiate hematopoietic cells from a donor and a recipient mouse. In our model, the leucocytes in the DTG mice possess the CD45.2 isotype (CD45.2 SCL-tTA-BCR-ABL mice) and the leucocytes of the wild type (WT) recipient mice express the CD45.1 allele (CD45.1 WT mice). Flow cytometric assessment of cell-surface expression of CD45.1 and CD45.2 can therefore determine the origin of haematopoietic cells following transplantation of CD45.2 BM cells from DTG mice into irradiated CD45.1 WT recipient mice.

BM cells were collected from two non-induced DTG mice, pooled, and transplanted into sub-lethally irradiated mice (n=20, 1 million cells per mouse). To ensure full recovery from irradiation toxicity and restoration of normal haematopoiesis before induction of leukaemia, the mice were kept on tetracycline for four weeks. Tetracycline was then removed from the drinking water to induce the expression of BCR-ABL and thus CML.

As weight loss is a clinical sign often observed upon the development of leukaemia in mice and humans, the mouse body weight was monitored upon tetracycline removal and used as an indication of leukaemogenesis. Following 18 days of

induction, the mice displayed an average weight loss of 13% compared to baseline (pre-induction weight), indicating the development of CML disease (**Fig. 4.7b**). Moreover, flow cytometry analysis of the blood collected from the tail vein indicated that the engraftment levels of CD45.2 donor cells was close to 100% in all mice transplanted (**Fig. 4.7c**). Treatment was therefore started at this time with vehicle (PBS, twice daily), phenformin (100 mg/kg, oral gavage, once daily), imatinib (100 mg/kg, oral gavage, twice daily) and combination (phenformin and imatinib) for four weeks. Importantly, we did not observe any clinical signs of toxicity during the drug treatments and following post-mortem analysis.

4.2.6 Phenformin and imatinib combination does not target LSCs *in vivo*

Following four weeks of *in vivo* treatment, mice were sacrificed for flow cytometry analysis of BM and spleen cells. As previously mentioned (**1.3.3**), CML is characterised by a splenomegaly due to the extra medullary infiltration of leukaemic cells which has been described as a valuable readout for the prognosis and the stage of CML disease. Spleen size was therefore used as an indication of the leukaemic burden in the different treatment conditions. As shown by the representative spleen pictures and weight, imatinib-treated mice displayed a significant decrease in their spleen weight compared to the vehicle treatment (**Fig. 4.8a,b**). However, phenformin as a single agent did not reduce the spleen weight compared to vehicle-treated mice, and adding phenformin to imatinib did not potentiate the effect of the TKI alone. Indeed, animals treated with imatinib or the combination had an average spleen weight of 144 mg and 157 mg respectively. In line with this, the percentage of donor CD45.2 granulocytes in the spleen was not further reduced by the addition of phenformin to the TKI (**Fig. 4.8c**). Similar results were obtained from the analysis of the percentage of BM CD45.2 granulocytes (**Fig. 4.8d**). The mean percentage of CD45.2 granulocytes was reduced significantly in the imatinib and the combination arm in comparison to vehicle-treated mice. However, with respective percentage of granulocytes in the BM of 36.9% and 36.8%, no significant difference were observed between imatinib-treated mice and the combination treatment.

Considering that a high leukaemic burden is frequently associated with anaemia, we next assessed the percentage of erythrocytes within the total BM cellular compartment. As expected, the percentage of erythrocytes was significantly increased in the BM of mice treated with imatinib compared to vehicle treatment (**Fig. 4.8e**). Although phenformin treatment resulted in a slight increase in the percentage of erythrocytes compared to vehicle-treated mice, the addition of phenformin to imatinib did not further increase the percentage of red blood cells in comparison to imatinib alone.

With similar percentage of granulocytes in the spleen and the BM between imatinib and the combination treatment arm, these results indicated that phenformin does not potentiate the effect of imatinib against differentiated leukaemic cells *in vivo*.

We next investigated whether the combination of phenformin and imatinib was able to target CML LSCs. To this end, we measured the percentage of CD45.2 LSCs present in the BM by flow cytometry. Multicolour flow cytometry analysis as described in **Figure 4.9a** allows distinguishing various haematopoietic cell subsets and assessment of their frequencies within a sample. To identify rare murine HSCs, differentiated cells are first gated out by labelling various differentiated cells using a cocktail of eight streptavidin-linked antibodies. Within the resulting lineage negative cells, primitive progenitor cells that contain most of the HSCs can be visualised. These cells are characterised by the Lin⁻Sca⁺ckit⁺ markers and are commonly referred to as LSK cells. Long-term HSC (LT-HSC) can finally be identified within these LSK cells and are defined as Lin⁻CD48⁺CD150⁻.

Flow cytometry analysis of the percentage of LSK cells within the BM of treated mice revealed that neither imatinib nor the combination of imatinib and phenformin decreased the frequencies of LSK cells compared to vehicle-treated mice (**Fig. 4.9b**). Noteworthy, imatinib and phenformin, when used as single agents, resulted in a decrease in LT-HSC in comparison to vehicle-treated mice, although this was not statistically significant (**Fig. 4.9c**). However, the combination treatment arm failed to decrease the percentage of LT-HSCs in comparison to vehicle-treated mice.

To further complement these experiments, equal volumes of BM cell suspension from all treatment arms were plated for CFC assay to analyse the relative number of viable and functional progenitors. As shown by the representative picture in **Figure 4.9d**, the number of colonies derived from both the vehicle and phenformin conditions were visibly reduced compared to imatinib and combination treatment arms. However, no difference in the number of colonies was observed between imatinib and the combination of imatinib and phenformin; an additional evidence of the lack of efficacy of the combination treatment to target leukaemic cells.

Altogether, these results demonstrated that imatinib significantly targets differentiated leukaemic cells, but, in accordance with previous studies, it failed to affect more primitive CML cells. Moreover, the combination of phenformin and imatinib did not potentiate the effect of imatinib in this *in vivo* setting. This was true for both stem and differentiated cells.

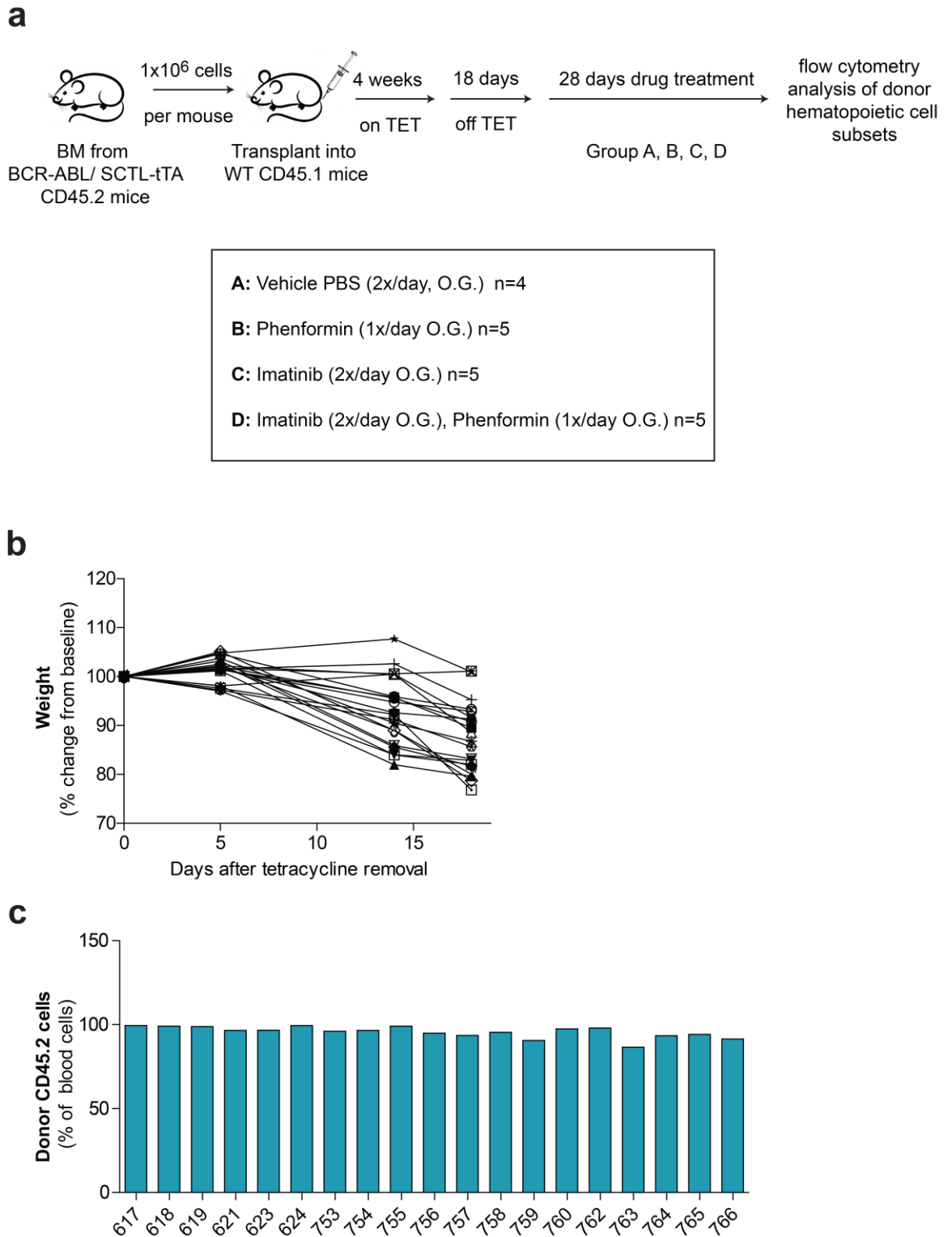


Figure 4. 7 Experimental outline using a DTG model to study *in vivo* drug/combination efficacy against CML cells.

(a) Outline of the experiment to study the *in vivo* effect of phenformin on LSCs. Total bone marrow cells were collected from 2 SCL-tTA-BCR-ABL mice (i.e. mice expressing BCR-ABL under the control of a tetracycline response element) and transplanted into sub-lethally irradiated CD45.1 WT mice (10⁶ cells per mouse, n=20 mice). The mice were kept on tetracycline for 4 weeks, followed by 18 days of tetracycline removal to induce expression of BCR-ABL. The mice were then treated with vehicle (PBS), phenformin, imatinib, and combination for 4 weeks. (b) Percentage of weight change from baseline (average weight before removal of tetracycline) upon removal of tetracycline. (c) Donor CD45.2 cell engraftment measured in the blood of WT recipient mice 10 days post tetracycline removal.

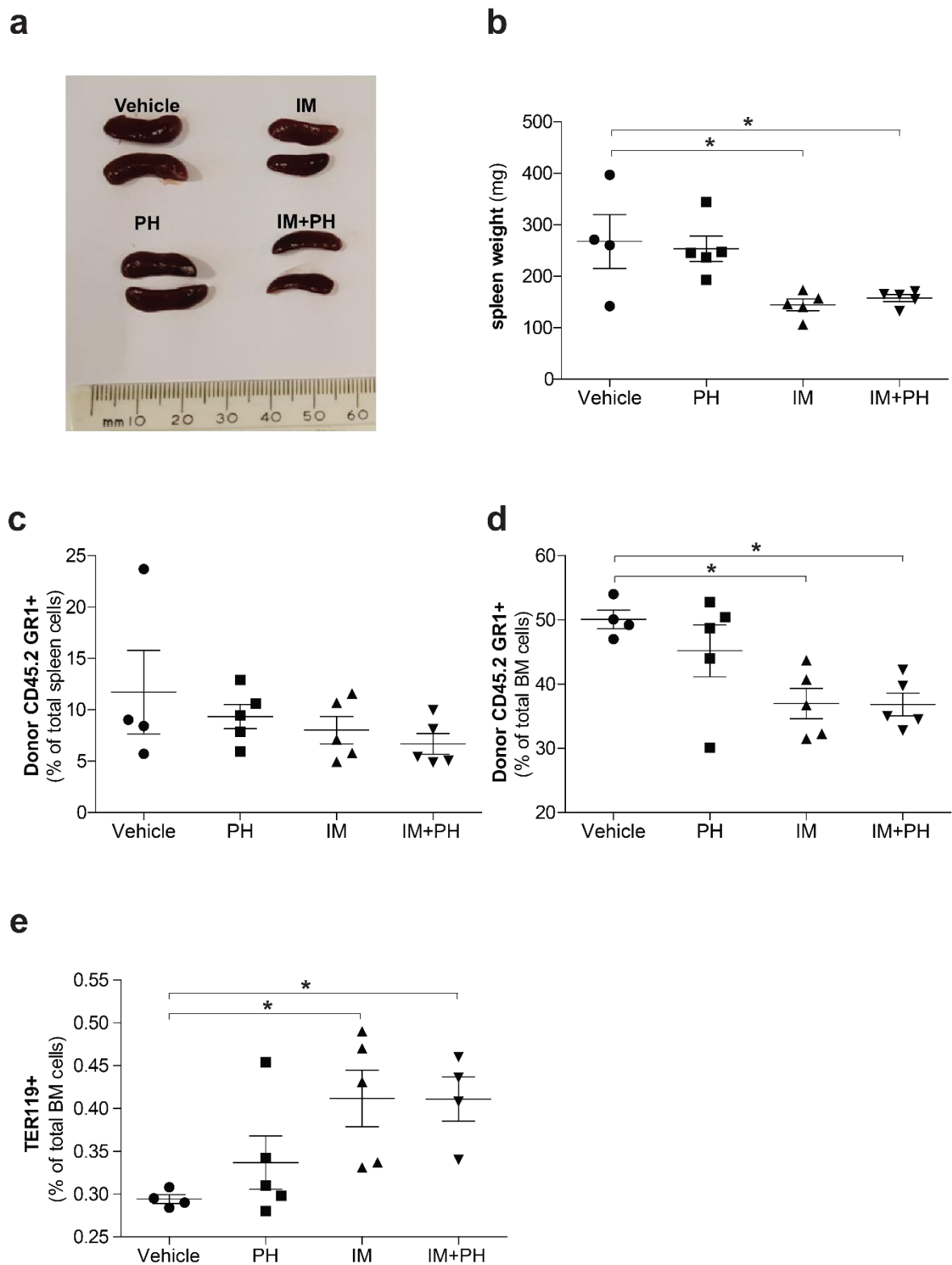


Figure 4. 8 The addition of phenformin does not potentiate the effect of imatinib against differentiated leukaemic cells.

(a) Representative spleen pictures and (b) spleen weight of WT mice transplanted with SCL-tTA-BCR-ABL BM cells and treated *in vivo* as described in Figure 7. (c-d) Percentage of donor CD45.2 granulocytes (Gr1⁺) in (c) the spleen and (d) BM. (e) Percentage of erythrocytes (TER 119⁺) in the BM. Data are presented as Mean \pm S.E.M. *P<0.05, evaluated by one-way ANOVA with post hoc Bonferroni analysis. PH, phenformin; IM, imatinib.

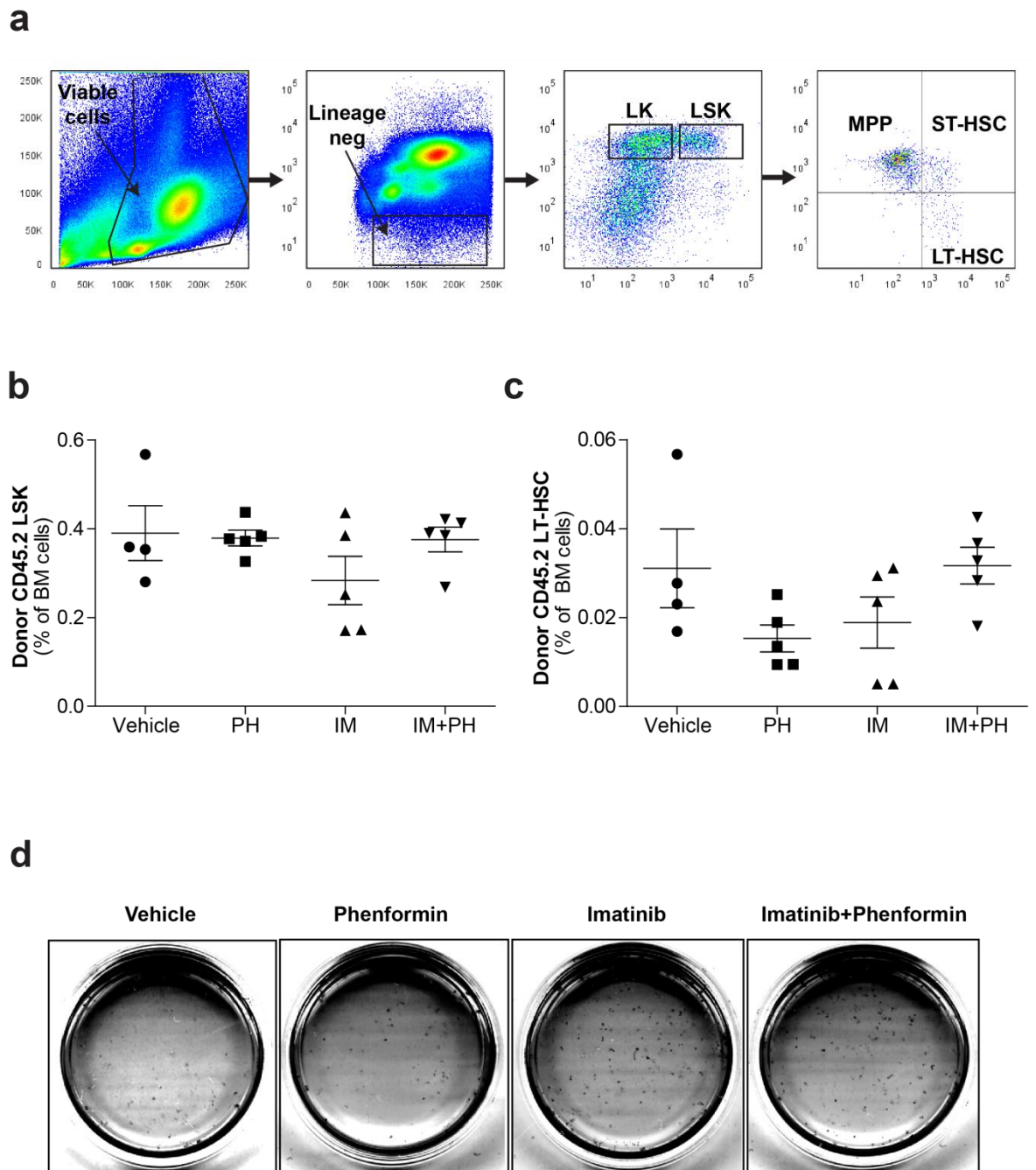


Figure 4. 9 Phenformin and imatinib combination does not target LSCs *in vivo*.

(a) Flow cytometry analysis and gating strategy for detection of murine HSCs. Debris and erythrocytes are first gated out from the FSC versus SSC plot. Lineage-negative cells are then selected, followed by the selection of Lin⁻Kit⁺Sca⁺ (LSK) cells. Murine HSCs are finally visualised from LSK cells as CD150⁺ cells. ST-HSC (Lin⁻Kit⁺Sca⁺CD150⁺CD48⁺) can be separated from LT-HSC (Lin⁻Kit⁺Sca⁺CD150⁺CD48⁻) based on the presence or absence of the CD48 marker. (b) Percentage of donor CD45.2 LSK and (c) LT-HSC in the BM of recipient mice. (d) Representative pictures of BM cell-derived colonies from recipient mice following CFC assay. In graphs, each dot represents one mouse. Data are presented as Mean ± S.E.M. PH, phenformin; IM, imatinib.

4.3 Discussion

In this chapter, we first demonstrated that phenformin is a 100 times more potent than metformin in inhibiting mitochondrial respiration. However, as mentioned previously (4.1), phenformin is more toxic than metformin and has been withdrawn from the market due to an increased risk of lactic acidosis. Nevertheless, a drug-induced toxicity might be more acceptable for cancer treatment than for diabetes, as evidenced by the use of antineoplastic chemotherapy that have significant adverse-effects. This might however not be the case for CML, as patients have at their disposition a targeted TKI therapy that improves survival rates and has manageable side effects in most cases. Nonetheless, the course of treatment is relatively short in some types of cancer compared to diabetes, which might prevent significant side effects. In line with this, one clinical trial is currently recruiting patients to investigate the efficacy of phenformin for the treatment BRAF-mutated melanoma in combination with MEK and BRAF inhibitors (249). Despite concerns relating to its clinical applicability, the greater potency of phenformin to inhibit mitochondrial metabolism was a strong argument for its use as a tool compound in the rest of our experiments.

We next demonstrated that phenformin synergises with imatinib to inhibit K562 CML cells proliferation. Moreover, the percentage of viable cells was significantly reduced upon addition of phenformin to imatinib in comparison to imatinib alone. Additionally, the percentage of viable cells was further reduced when cells were forced to rely on oxidative metabolism in presence of galactose, indicating that the effect of phenformin is mediated by inhibition of mitochondrial metabolism. Accordingly, many studies have shown that phenformin can target cancer cells *in vitro* by inhibiting mitochondrial complex I.

We next demonstrated that phenformin, as a single agent or in combination with imatinib, does not induce cell death of normal murine cells, while the survival of BCR-ABL-expressing cells is significantly impaired by the drug treatment. This suggests a potential therapeutic index for phenformin and imatinib use in the clinic. However, more stringent assays should be performed to validate the lack of toxicity of the drug combination. Accordingly, further investigations should assess the effect of the drug combination on normal primary cells *in vitro* and *in vivo*.

We next investigated the effect of phenformin in combination with imatinib to target CML progenitors and stem cells. This revealed that the combination reduced the number of progenitor-derived colonies in one out of two CML patient samples. With this limited number of patient samples, additional work is required to conclude whether the addition of phenformin sensitises CD34⁺ CML cells to imatinib. We next tested whether phenformin could target primitive stem cells by performing an LTC-IC assay, the most stringent *in vitro* stem cell assay available. This revealed that the combination of phenformin and imatinib was able to significantly reduce the number of CML LSCs in comparison to vehicle and imatinib treatment.

Taken together, our results showed that the combination of imatinib and phenformin does not consistently decrease the number of progenitor-derived colonies, while the LTC-IC assay indicated that the drug combination could target CML LSCs. This could suggest that phenformin, when combined with imatinib, preferentially targets primitive cells and has only a minor effect on more differentiated progenitor cells. Another explanation for this discrepancy between the two assays could lie in the time course of the treatment performed. When performing CFC assays, cells are pre-treated for three days before being placed in methylcellulose, whereas in the LTC-IC assay, cells are treated once and further kept for five weeks in culture. The fact that cells are being treated for an extended period of time in the LTC-IC assay could partially explain the increased efficacy of phenformin and imatinib combination.

Finally, we performed an *in vivo* experiment where BM cells from CD45.2 SCL-tTA-BCR-ABL (DTG) mice were transplanted into CD45.1 WT mice and expression of BCR-ABL induced by tetracycline withdrawal. A more straightforward approach would have been to directly use DTG mice and induce them for CML disease by tetracycline removal. However, the poor breeding performance of these DTG mice prevented us to perform an *in vivo* experiment requiring a total of twenty mice. To circumvent this issue, and avoid the extensive cost involved in generating DTG mice, the transplantation model was selected for this *in vivo* experiment as it allows the transplantation of BM cells originating from few donors into many recipient mice. Indeed, only one million of BM cells are necessary for the transplantation into WT mice and the commonly used harvesting isolation methods

collect on average a hundred million of BM cells per mouse. Moreover, transplantation of a pool of cells originating from the same donors results in a more homogeneous disease in the recipient mice.

Following appearance of CML disease, mice were treated with vehicle, phenformin, imatinib or combination following appearance of CML disease. This revealed that the combination of phenformin to imatinib had no beneficial effect on targeting either differentiated or stem cells compared to imatinib as a single agent. Several factors could have contributed the lack of efficacy of the combination treatment. First, it is very likely that the concentration of phenformin used in our *in vitro* studies is not achieved *in vivo*. Indeed, the concentration of phenformin measured in humans is 0.19 μM after a single 50 mg oral dose (250). Further studies are therefore required to test whether phenformin is able to hit its target *in vivo* and effectively inhibit complex I. As such, it would be interesting to treat mice with phenformin and assess the activity of complex I in snap frozen sections of the BM and the spleen. The lack of effect of phenformin *in vivo* could lie as well in the use of murine cells. Despite expressing BCR-ABL, these murine cells might be less sensitive than human CML cells to the drug treatment. Experiments assessing the sensitivity of murine myeloid cells from DTG donors to phenformin/imatinib treatment *in vitro* could clarify whether their response to drug treatment differs in comparison to human CML cells.

Due to a restricted number of mice available, we did not include non-induced control mice (i.e. on tetracycline; TET-ON) in our experiment. These TET-ON mice would have undergone the same experimental procedures (i.e. transplantation of DTG BM cells and sub-lethal irradiation) but never induced for CML disease and kept on tetracycline. The comparison of the percentage of granulocytes between TET-ON and imatinib-treated mice could have helped determine whether imatinib reduced the percentage of granulocytes to the levels of non-induced mice. If imatinib induced such a profound reduction in the leukaemic burden, it would not have been possible to further see a decrease in leukaemic cells in the combination treatment. Despite this, imatinib and other TKIs cannot fully eradicate CML disease and fail to target LSCs. Therefore, even if we consider that imatinib eliminated all differentiated cells in these mice, LSCs should not have been affected (or only marginally) by TKI treatment and the effect of the combination

could be seen at the stem cell level. Unexpectedly, imatinib decreased the percentage of LSK cells, and this effect was even more pronounced in LT-HSCs cells. This is highly unexpected, as previous experiments performed in this model have shown that imatinib and other TKIs do not have a significant effect on LT-HSCs. Interestingly, the colony-forming assay, performed on BM cells isolated from mice treated *in vivo*, revealed that the number of progenitors were increased in both the imatinib and the combination treatment arm in comparison to vehicle and phenformin conditions. This difference was not observed in flow cytometry analysis and highlights the importance of complementing flow cytometry analysis with functional assays. In any case, both flow cytometry and CFC experiment revealed that the combination treatment arm does not decrease the number of neither differentiated cells nor stem cells in comparison to imatinib.

4.4 In summary

In this chapter, we first investigated the potency of the two biguanides phenformin and metformin to inhibit mitochondrial respiration and selected the more potent inhibitor, phenformin, for further investigation in combination with imatinib. Interestingly, our results indicated the presence of a synergistic effect between phenformin and imatinib to inhibit the proliferation of CML cells. Moreover, this effect was not limited to reduction in cellular proliferation, as the combination of phenformin and imatinib significantly reduced the percentage of viable CML cells in comparison to imatinib alone. Using media containing solely galactose as a carbon source, which forces cells to rely on oxidative metabolism for energy production, we demonstrated that the effect of phenformin mediates its effect on cellular viability by inhibiting mitochondrial oxidative metabolism.

We next tested the effect of phenformin on primary patient-derived CML CD34⁺ cells. The addition of phenformin to imatinib significantly reduced the potential of CML LSCs to form colonies, while imatinib as a single agent did not. Given these encouraging *in vitro* results, we next tested the capacity of phenformin in combination with imatinib to target CML LSCs in a mouse model of CML disease. Unfortunately, the combination of phenformin and imatinib had no demonstrable effect against differentiated leukaemic cells or LT-HSCs in comparison to imatinib treatment.

This study provides an initial characterisation of the importance of mitochondrial oxidative metabolism for CML LSCs survival *in vitro*. While we did not validate this finding in a mouse model of CML, future investigation should test whether the combination of phenformin and combination with imatinib can target primary CML LSCs in a humanised mouse model of CML.

Chapter 5 Using tigecycline to target CML LSCs

5.1 Introduction

Thus far, our results have demonstrated that CD34⁺ CML cells have an increased oxidative metabolism in comparison to differentiated patient-matched CD34⁻ cells and to normal counterparts. Moreover, the complex I inhibitor phenformin in combination with imatinib significantly reduced CML LSCs potential in an *in vitro* setting, suggesting that inhibition of oxidative metabolism might be detrimental for CML LSCs survival. However, phenformin, as single agent or combined to imatinib, did not target BCR-ABL stem/progenitors expressing cells in the SCLtTA/BCR-ABL transgenic mouse model. The possible reasons behind the lack of efficacy of phenformin *in vivo* have been discussed in the previous chapter (4.3.3). Nonetheless, the poor outcome of phenformin treatment *in vivo* led us to test a second and more clinically relevant inhibitor of oxidative metabolism.

It is widely accepted nowadays that mitochondria originated from bacteria following endosymbiosis (251). In support to this endosymbiotic theory, several classes of antibiotics have been shown to target both bacterial and mitochondrial ribosomes, due to their similarity in structure. The mitochondrial genome encodes for 13 proteins that are components of the OXPHOS machinery. As a result, the use of certain antibiotics such as drugs from the tetracycline and glycyclcyline family can target the expression of subunits of OXPHOS complexes, and hence impair oxidative metabolism. For instance, tigecycline, an FDA approved glycyclcyline antibiotic, has been shown to impair the expression of mitochondrial-encoded proteins in tandem to inhibiting bacterial protein synthesis. Moreover, Skrtić *et al.* in a 2011 study demonstrated that tigecycline targets AML cells *in vitro* and *in vivo* and this effect was mediated by inhibition of oxidative metabolism (187). We therefore aimed to test the efficacy of this clinically approved inhibitor of oxidative metabolism against CML LSCs.

Similar to Chapter 3, the majority of data provided in this chapter were accepted for publication in August in Nature Medicine.

5.2 Results

5.2.1 Tigecycline mediated inhibition of mitochondrial oxidative metabolism targets CML cell lines

To confirm that tigecycline inhibits the expression of mitochondrial proteins in our model, K562 and KCL22 CML cell lines were treated with tigecycline at a concentration of 5 μM and the expression of subunits of complexes from the OXPHOS machinery was analysed following three days of drug treatment. More precisely, the expression of proteins encoded by the mitochondrial genome, namely cytochrome c oxidase subunit 1 (MT-CO1) and subunit 2 (MT-CO2), was compared to the expression of ubiquinol-cytochrome c reductase core protein II (UQCRC2) and ATP synthase subunit alpha (ATP5A), both nuclear-encoded proteins. In the two CML cell lines, tigecycline treatment reduced selectively the expression of mitochondrial encoded proteins while not affecting nuclear-encoded ones (Fig 5.1a,b).

To confirm that the decrease in mitochondrial protein expression translates to a reduction in oxidative metabolism, mitochondrial respiration was assessed in K562 and KCL22 cell lines following 24 and 48 h treatment with tigecycline (5 μM). Subsequent injections of oligomycin, FCCP, antimycin A and rotenone were performed to further test the metabolic profile of the mitochondria. This revealed that tigecycline treatment decreased mitochondrial respiration in both K562 cells and KCL22 cells following 24 h of treatment (Fig 5.1c-e). This effect was more pronounced after 48 h of tigecycline treatment, as shown by a 32% and 31% average inhibition of mitochondrial respiration in K562 and KCL22 cells respectively (Fig 5.1f,g).

Importantly, tigecycline impaired the proliferation of leukaemic cells at concentrations that can be achieved *in vivo*, with respective IC₅₀ values of 3.44 μM and 7.8 μM for K562 and KCL22 cell lines (Fig 5.2a,b). To test whether this was associated with a decrease in cell survival, K562 and KCL22 cells were plated for 72 h in presence of three different concentrations of imatinib (250, 500 and 1000 nM) in the presence or absence of tigecycline (5 μM). The addition of tigecycline to imatinib increased the percentage of cell death in comparison to imatinib as a single agent across all three doses of TKI tested in K562 cells (Fig 5.2c). Indeed,

at a concentration of 250 nM, imatinib induced cell death in 14% of the cells while 40% of the cells were targeted by the combination treatment. Similarly, the addition of tigecycline to imatinib significantly increased the percentage of dead cells in comparison to imatinib alone in a second CML cell line (**Fig 5.2d**). Noteworthy, this was observed across all three concentrations of imatinib in both CML cells lines.

Here, we demonstrated that tigecycline, by affecting the expression of mitochondrial encoded protein, reduces mitochondrial respiration in two CML cell lines. Moreover, inhibition of mitochondrial respiration with tigecycline in combination with imatinib significantly impairs the proliferation and survival of CML cells.

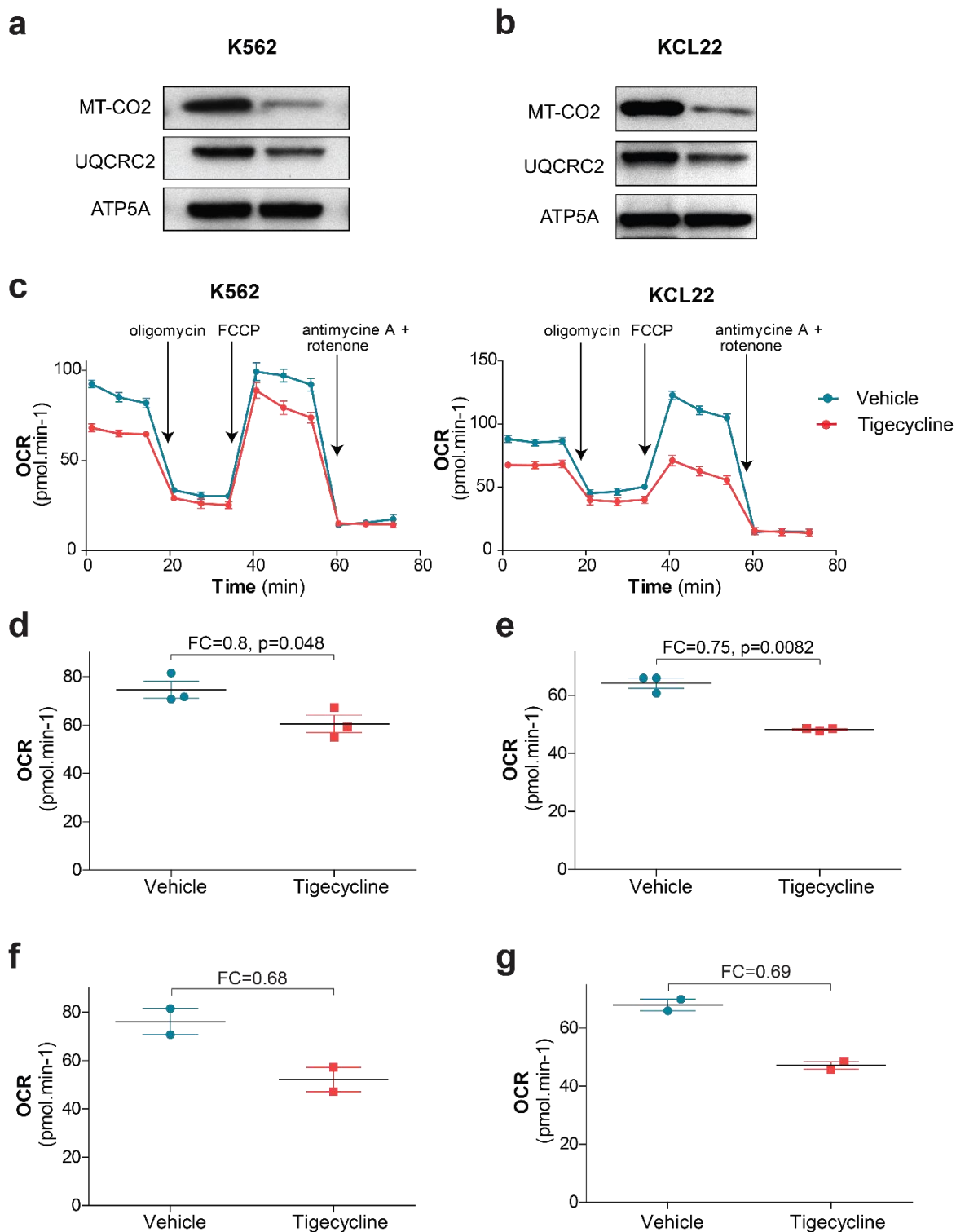


Figure 5. 1 Tigecycline inhibits mitochondrial respiration in CML cell lines.

(a-b) Protein expression of MT-CO2, UQCRC2 and ATP5A in (a) K562 and (b) KCL22 cells following 72 h *in vitro* treatment with tigecycline (5 μ M). 1 out of 2 independent experiments. (c) Representative respirometer output in K562 and KCL22 cells in the presence or absence of tigecycline (5 μ M) after 24 h of treatment. (d-e) Mitochondrial respiration following 24 h *in vitro* treatment with tigecycline or vehicle control in (d) K562 cells and (e) KCL22 cells. n=3 independent experiments. (f-g) Mitochondrial respiration following 48 h *in vitro* treatment with tigecycline or vehicle control in (f) K562 cells and (g) KCL22 cells. n=2 independent experiments. Data are presented as Mean \pm S.E.M. FC, fold change relative to vehicle-treated cells. P values were calculated by unpaired Student's t-test.

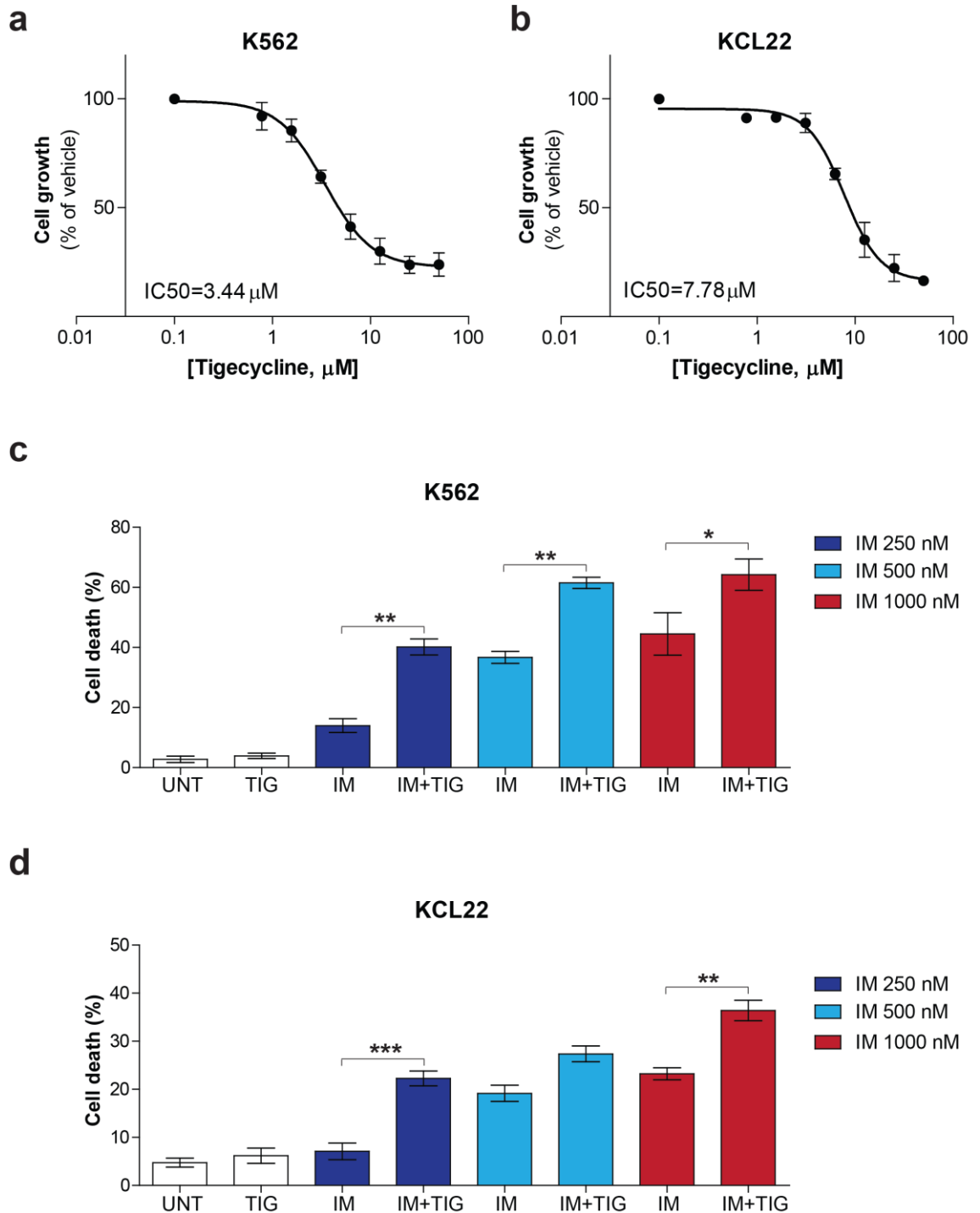


Figure 5. 2 Tigecycline in combination with imatinib targets CML cell lines *in vitro*.

(a-b) Proliferation of (a) K562 cells and (b) KCL22 cells upon exposure to various concentrations of tigecycline. n=3 independent experiments. (c-d) Cell death upon 72 h tigecycline treatment (5 μM) in combination with various concentration of imatinib (250 nM, 500 nM, 1000 nM) in (c) K562 cells and (d) KCL22 cells. n=3 independent experiments. Data are presented as Mean ± S.E.M. *P<0.05; **P<0.01; ***P<0.001, evaluated by one-way ANOVA with post hoc Bonferroni analysis. TIG, tigecycline; IM, imatinib.

5.2.2 Tigecycline preferentially inhibits cell proliferation of BCR-ABL expressing cells.

To test whether the effect of tigecycline was selective to CML cell lines, parental Ba/F3 cells and Ba/F3 p210 cells (4.2.3) were treated with increasing concentration of tigecycline. Following 72 h of treatment, the remaining number of cells were assessed by XTT assay. The half-maximal inhibitory concentration (IC₅₀) of tigecycline was more than five times higher in parental Ba/F3 compared to Ba/F3 p210 cells (Fig. 5.3). Indeed, the IC₅₀ of tigecycline in parental Ba/F3 and in Ba/F3 p210 cells was determined to be 57.4 μ M and 7.5 μ M respectively across three independent experiments, suggesting that tigecycline preferentially inhibits cellular proliferation of BCR-ABL expressing cells, and thus, potentially of CML cells. Noteworthy, the doubling time of parental Ba/F3 cells is similar to Ba/F3 p210 cells, which indicated that the therapeutic window observed for tigecycline treatment in CML cells is not dependent on the proliferative capacity but rather on the expression of BCR-ABL.

All together, these results indicated that tigecycline has a strong potential to target CML cells in a selective manner as the IC₅₀ of tigecycline was lower in BA/F3 p210 cells than in parental cells.

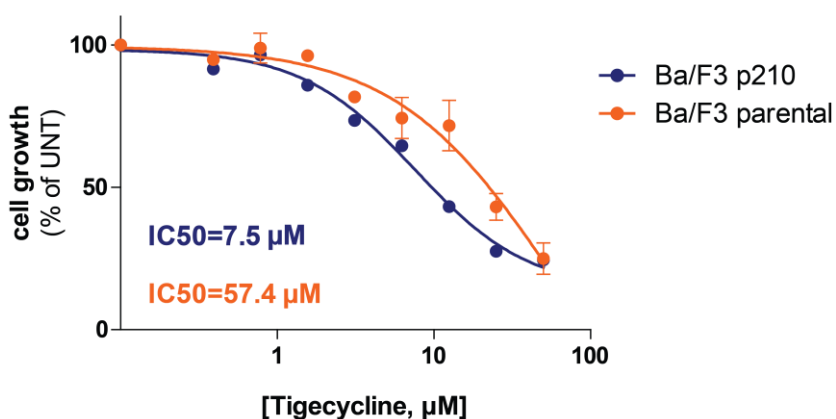


Figure 5. 3 Tigecycline preferentially targets BCR-ABL-expressing cells.

Cell proliferation normalised to vehicle treatment following 72 h tigecycline *in vitro* treatment in Ba/F3 p210 and parental Ba/F3 cells. n=3 independent experiments. Data are presented as Mean \pm S.E.M.

5.2.3 Tigecycline inhibits oxidative metabolism in primary CD34⁺ CML cells

To confirm the effect of tigecycline on mitochondrial protein expression in primary cells, CD34⁺ cells from two CML patients were treated for three days in the presence of 2.5 μM of tigecycline, a concentration that was shown to be achievable in human plasma. In line with the results obtained in CML cell lines, tigecycline decreased the expression of MT-CO1 and MT-CO2, both encoded by the mitochondrial genome (**Fig. 5.4a**). Importantly, tigecycline treatment did not affect, or to a minor extent, the expression of the nuclear-encoded proteins UQCRC2 and ATP5A. This demonstrated that tigecycline treatment, at a concentration achievable *in vivo*, is able to decrease the expression of mitochondrial-encoded proteins. This decrease in protein expression was accompanied with an increase in mRNA levels encoding for MT-CO2 and MT-CO1 (**Fig. 5.4b**).

We next tested whether the inhibition of mitochondrial protein expression observed with tigecycline treatment in CD34⁺ CML cells was linked to a decrease in oxidative metabolism. CD34⁺ cells derived from four CML patient samples were treated with tigecycline (2.5 μM) for 48 h and the mitochondrial respiration assessed. This confirmed that tigecycline is able to significantly inhibit mitochondrial respiration of CD34⁺ CML cells by 37% on average (**Fig. 5.4c**).

To gain a deeper understanding of the intracellular metabolic changes that occur upon tigecycline treatment, CD34⁺ CML cells were pre-treated for 24 h with tigecycline (2.5 μM) and, the following day, plated in presence of ¹³C₆-labelled glucose, in the presence or absence of tigecycline (2.5 μM). Following 24 h incubation with ¹³C₆-glucose, intracellular metabolites were extracted and subjected to LC-MS analysis. Analysis of the ¹³C isotopic enrichment revealed that the contribution of glucose derived carbons for citrate, glutamate and aspartate was significantly decreased in tigecycline-treated CML CD34⁺ cells (**Fig. 5.4d-f**). For instance, the isotopologues of citrate containing two or more ¹³C atoms were reduced by more than 70% in tigecycline-treated CML CD34⁺ cells in comparison to vehicle-treated cells. This decrease in glucose oxidation was linked to a reduction in the relative activity of PDH and PC (**Fig. 5.4g,h**).

Glutamine, the most abundant non-essential amino acid in the blood, is an anaplerotic precursor used by normal and cancer cells to replenish TCA cycle metabolites. Moreover, glutamine is a major mitochondrial substrate and plays an important role in maintaining mitochondrial potential and integrity. Given the effect of tigecycline on mitochondrial metabolism, we questioned whether glutamine metabolism was as well affected by the drug treatment. To this end, CD34⁺ CML cells were pre-treated for 24 h with tigecycline (2.5 μ M) and plated the next day in media containing ¹³C₅-labelled glutamine in presence or absence of tigecycline (2.5 μ M). After 24 h incubation, intracellular extracts were subjected to LC-MS analysis. Tigecycline treatment in CD34⁺ CML cells resulted in a significant reduction in the contribution of glutamine-derived ¹³C atoms into the TCA cycle metabolite citrate as well as the derived amino acids glutamate and aspartate (**Fig. 5.5a-c**).

We previously showed that FAO is significantly elevated in CD34⁺ CML cells in comparison to CD34⁺ normal cells. Similar to our experiment with labelled glucose and labelled glutamine, CD34⁺ CML cells were plated in presence of ¹³C₁₆ labelled palmitate, in the presence or absence of tigecycline (2.5 μ M) to understand the effect of tigecycline on fatty acid metabolism. A significant reduction in isotopologues containing ¹³C atoms for citrate, glutamate and aspartate was noted in tigecycline-treated CD34⁺ cells in comparison to vehicle condition, indicating that tigecycline mediates a decrease in palmitate oxidation (**Fig. 5.5d-e**).

These results demonstrated that tigecycline treatment in CD34⁺ CML targets the expression of proteins encoded by the mitochondrial genome. This leads to an overall decrease of mitochondrial oxidative metabolism as indicated by the reduction in glucose, glutamine and fatty acid oxidation following tigecycline treatment.

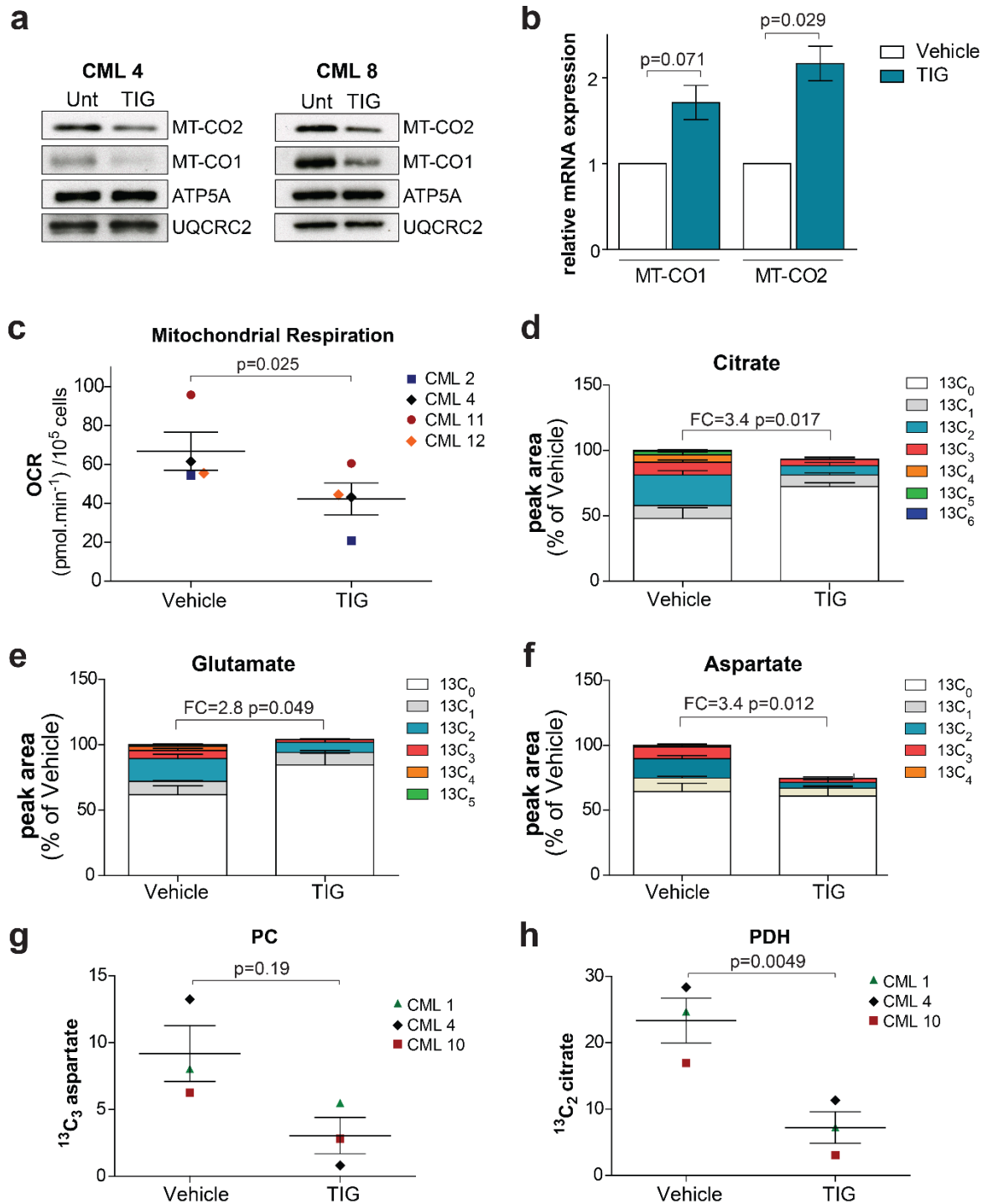


Figure 5. 4 Tigecycline inhibits oxidative metabolism in CD34⁺ CML cells through inhibition of mitochondrial protein expression.

(a) Protein expression in CD34⁺ CML cells following 72 h *in vitro* treatment with tigecycline (2.5 μ M). n=2 patient samples. (b) mRNA levels in CD34⁺ CML cells following 72 h *in vitro* treatment with tigecycline (2.5 μ M). n=3 patient samples. (c) Basal mitochondrial OCR in CD34⁺ CML cells following tigecycline treatment (2.5 μ M). n=4 patient samples. (d-f) Relative isotopologue distribution of (d) citrate, (e) glutamate and (f) aspartate in CD34⁺ CML cells measured by LC-MS following 24 h incubation with ¹³C₆-labelled glucose in presence or absence of tigecycline (2.5 μ M). Mean \pm S.E.M. n=3 patient samples. (g) Abundance of ¹³C₃ aspartate and (h) ¹³C₂ citrate in presence or absence of tigecycline (2.5 μ M) measured by LC-MS following 24 h incubation with ¹³C₆-labelled glucose. Mean \pm S.E.M. n=3 patient samples. P values were calculated by paired Student's t-test. TIG, tigecycline.

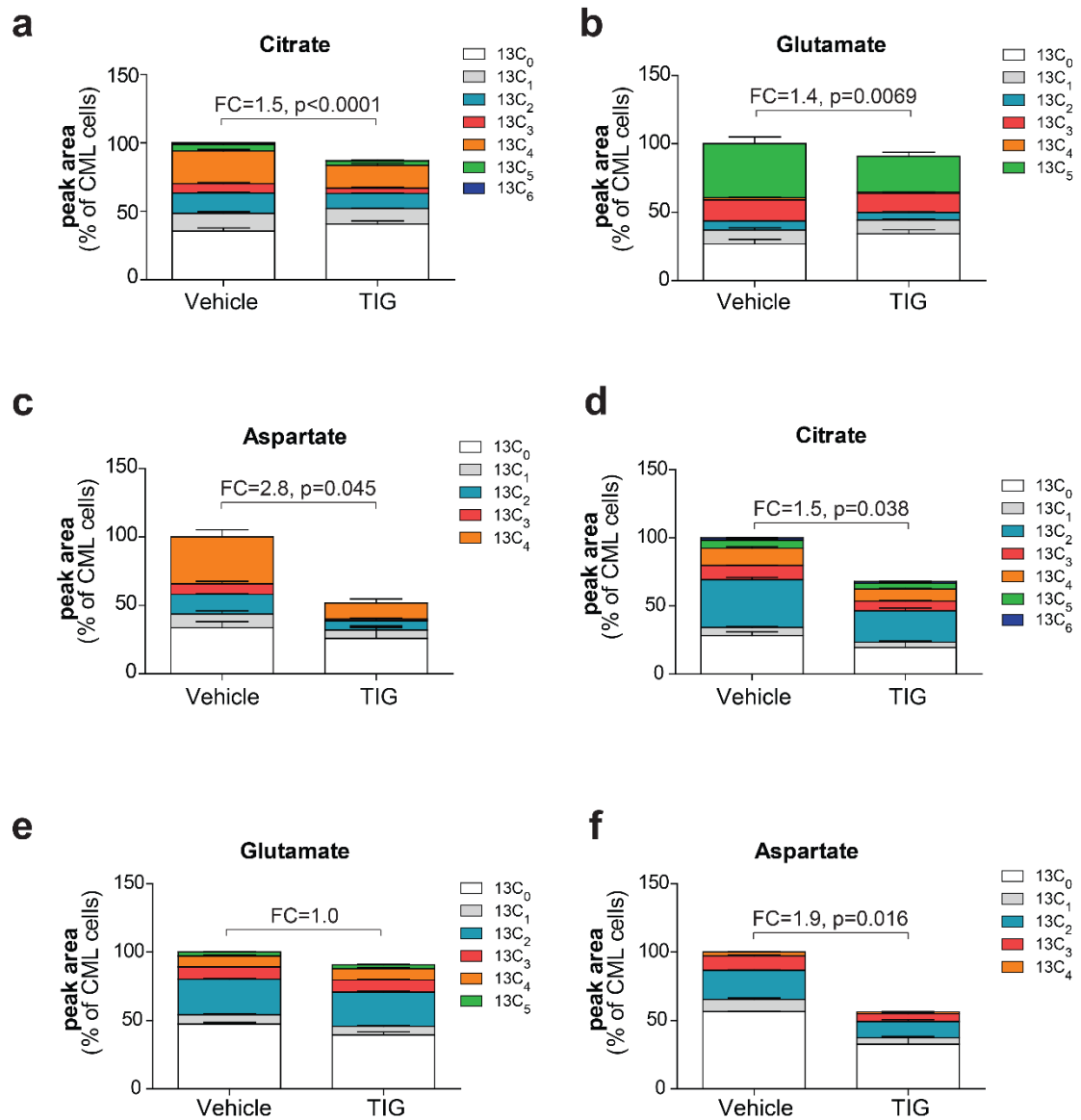


Figure 5. 5 Tigecycline inhibits glutamine oxidation and FAO in CD34⁺ CML cells.

(a-c) Relative isotopologue distribution of (a) citrate, (b) glutamate and (c) aspartate in CD34⁺ CML cells measured by LC-MS following 24 h incubation with ¹³C₅-labelled glutamine in the presence or absence of tigecycline (2.5 μM). Mean ± S.E.M. n=3 patient samples. (d-f) Relative isotopologue distribution of (d) citrate, (e) glutamate and (f) aspartate in CD34⁺ CML measured by LC-MS following 24 h incubation with ¹³C₁₆-labelled palmitate in the presence or absence of tigecycline (2.5 μM). Mean ± S.E.M. n=3 patient samples. P values were calculated by paired Student's t-test. TIG, tigecycline.

5.2.4 Tigecycline in combination with imatinib targets CD34⁺ CML cells *in vitro*

OXPHOS and anaplerosis are essential for growth and proliferation. To test the effect of tigecycline on the proliferation in CD34⁺ CML cells, we traced cellular division with a fluorescent dye (Cell Trace Violet). Following three days of incubation with indicated drugs, the number of cellular divisions that the cells have undergone were measured. This revealed that tigecycline alone or in combination with imatinib, strongly impaired proliferation of primary CD34⁺ CML cells, whereas imatinib alone had only a moderate effect, in line with its preferential effect on differentiated CD34⁻ cells (**Fig. 5.6a**). The assessment of the percentage of cells that went through one or more division revealed that almost all vehicle-treated cells divided over the 72 h *in vitro* culture (**Fig. 5.6b**). However, the percentage of cells divided decreased by more than 50% upon exposure to tigecycline in comparison to vehicle treatment. The effect observed with tigecycline alone was similar to the one seen upon imatinib treatment, with respective percentage of cells divided of 43% and 38%. The combination of imatinib and tigecycline showed the strongest effect, inhibiting cellular division by more than 80% in comparison to vehicle. Moreover, the combination induced a significant 50% decrease in the percentage of cells divided in comparison to imatinib alone. These results showed that combining imatinib to tigecycline potentiates the anti-proliferative effect of imatinib against CD34⁺ CML cells.

To understand the fate of CD34⁺ cells upon drug treatment beyond the effect on proliferation, we tested whether the combination of tigecycline and imatinib induced cell death. To this end, CD34⁺ CML cells were plated for 72 h in presence of vehicle, tigecycline, imatinib or their combination, and the percentage of Annexin V positive cells was assessed by flow cytometry. This revealed that combining tigecycline to imatinib significantly increased the percentage of Annexin V positive cells in comparison to imatinib alone. Moreover, tigecycline potentiated the effect of imatinib in all seven patients analysed, reflecting the robustness of this result (**Fig 5.7a**). The effect of the combination on the functional properties of CD34⁺ CML cells was next assessed by performing CFC assays. Treatment with either imatinib or tigecycline alone decreased the number of CFCs by 40% on average, which revealed that tigecycline is able to target CD34⁺

CML cells to the same extent as imatinib. Importantly, their combined application effectively reduced colony formation, with less than 15% of colonies remaining on average compared to vehicle treatment (**Fig. 5.7b,c**). To verify the selectivity of tigecycline against CML cells, as suggested previously by experiments in parental Ba/F3 and p210 cells (**Fig. 5.3**), CFC assays were performed on normal, non-leukaemic CD34⁺ cells. Importantly, neither drug, alone nor in combination, resulted in a significant decrease in the number of normal CFC, affirming a potential therapeutic window for tigecycline use in CML treatment (**Fig. 5.7d**).

Taken together, these results revealed that tigecycline in combination with imatinib selectively targets CD34⁺ CML cells *in vitro* by inducing cell death and cell growth arrest.

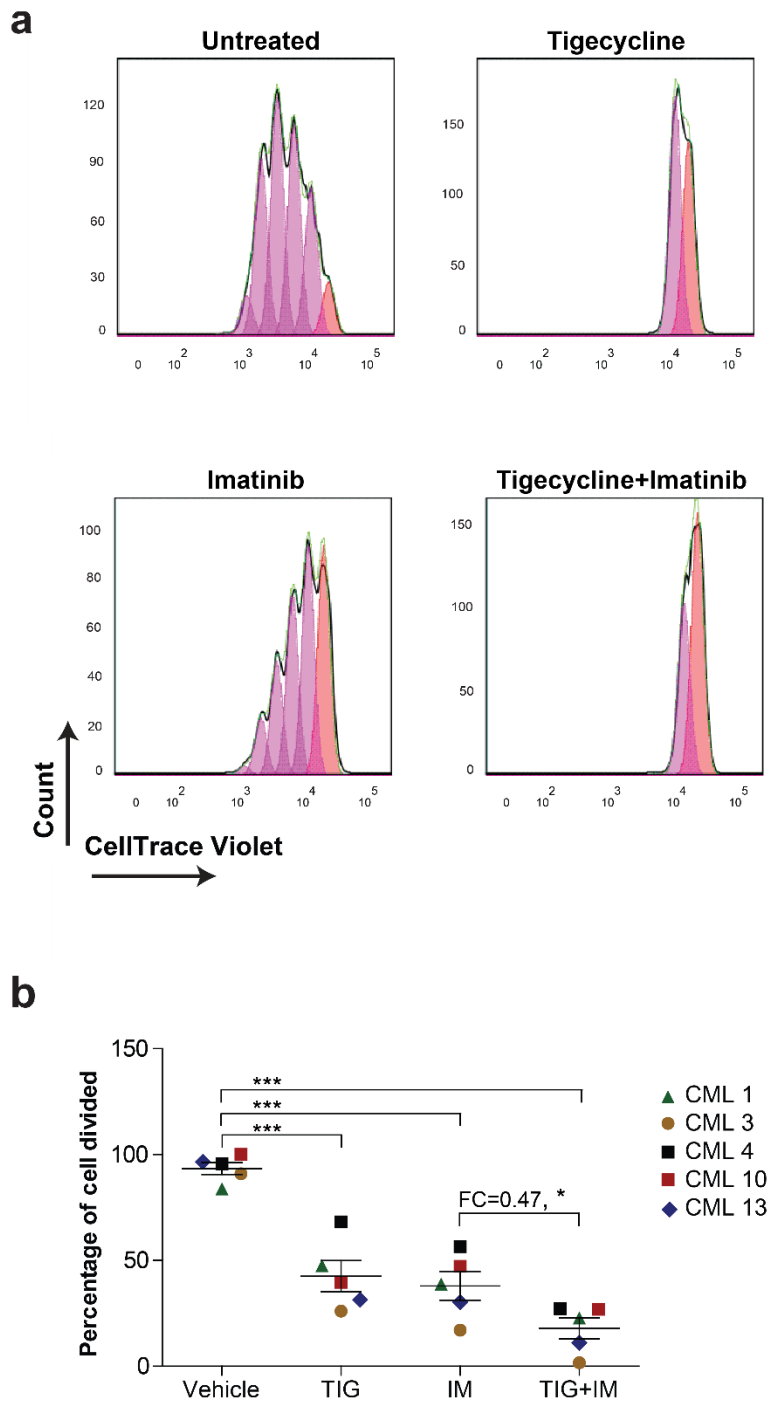


Figure 5. 6 Tigecycline is a potent inhibitor of CD34⁺ CML cells proliferation.

(a) Representative flow cytometry histograms obtained from cellular division tracking of CellTrace Violet-stained CD34⁺ CML cells following 72 h of treatment. n=1 patient sample. (b) Percentage of CML CD34⁺ cells divided following 72 h of drug treatment. n=5 patients samples. Data are presented as Mean \pm S.E.M. *P<0.05; ***P<0.001, evaluated by one-way ANOVA with post hoc Bonferroni analysis. FC, Fold change relative to IM-treated cells. Tigecycline (TIG) and imatinib (IM) were used at a concentration of 2.5 μ M and 2 μ M respectively.

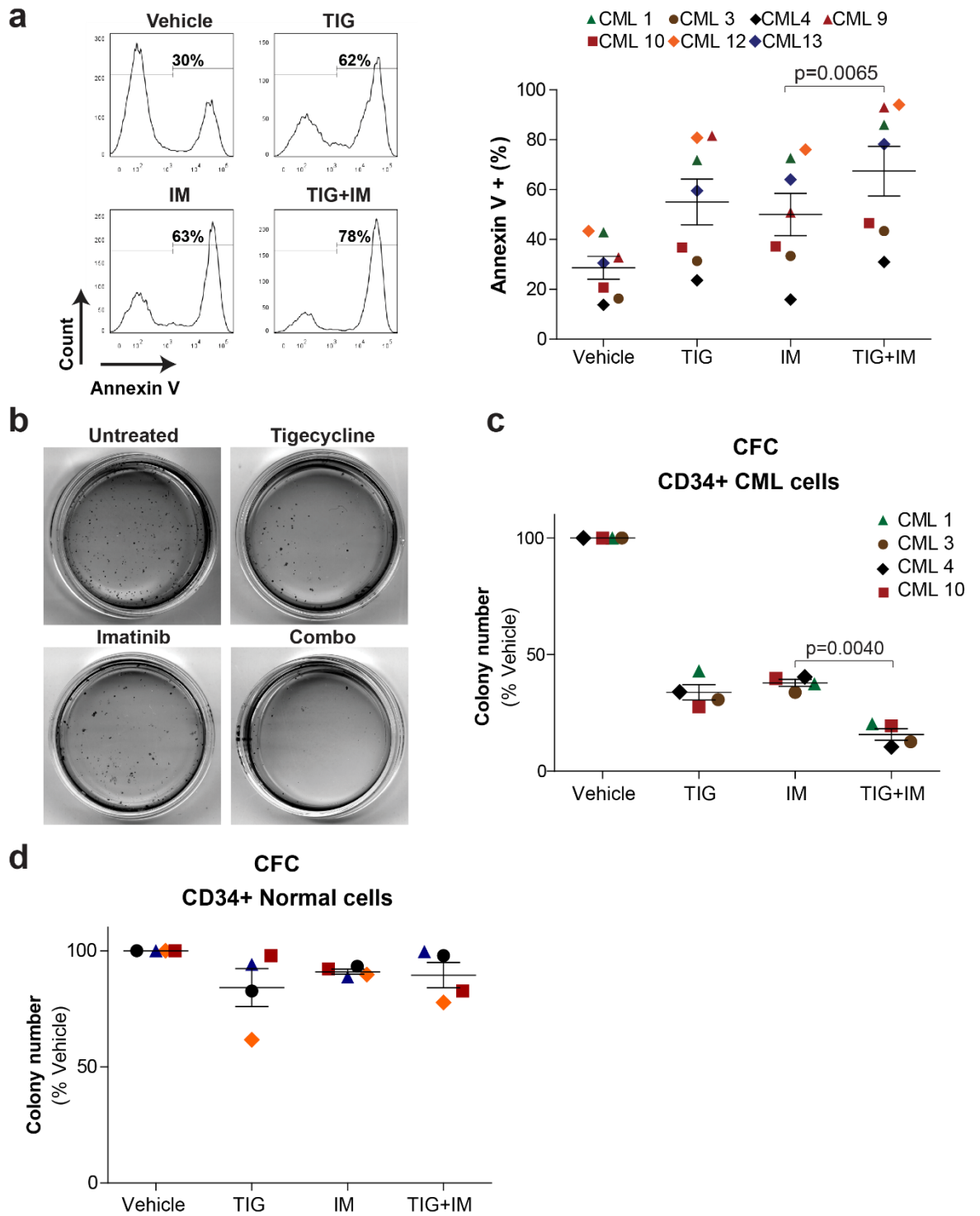


Figure 5. 7 Tigecycline combined to imatinib selectively targets CD34⁺ CML cells *in vitro*.

(a) Representative flow cytometry histograms obtained from Annexin V staining in CD34⁺ CML cells following 72 h *in vitro* drug treatment. (b) Percentage of Annexin V positive cells following 72 h of drug treatment in CD34⁺ CML cells. n=7 patients samples (c) Representative images of colonies and (d) relative colony numbers following 3 days drug treatment of CD34⁺ CML cells. n=4 patient samples. (e) Colony number following 72 h drug treatment of CD34⁺ normal cells. n=4 normal samples. All data are presented as Mean \pm S.E.M. P values were calculated by paired Student's t-test. Tigecycline (TIG) and imatinib (IM) were used at a concentration of 2.5 μ M and 2 μ M respectively.

5.2.5 Tigecycline in combination with imatinib targets CML LSCs *in vitro*

The combined effect of tigecycline and imatinib on CFCs suggested that the drugs affected two distinct populations; with imatinib targeting mature progenitors and tigecycline targeting the more oxidative, long-term LSCs. To test this hypothesis, experiments analysing the effect of tigecycline on LSCs were next performed.

Cultured human haematopoietic cells that express the CD133 marker have been shown to be enriched for HSCs (252). To verify that expression of CD133 following *in vitro* culture was associated with characteristics of LSCs in our experimental conditions, Cell Trace Violet-stained CD34⁺ CML cells were cultured for 72 h to track cellular proliferation, and then stained with anti-human CD133 and anti-human CD34 antibodies for phenotypic analysis by flow cytometry. As indicated in **Fig. 5.8a**, primary human CML cells expressing high levels of CD133 were also positive for the CD34 surface marker. Moreover, cells co-expressing high levels of CD133 and CD34 (CD133⁺/CD34⁺ cells) retained the highest levels of the CFSE dye (referred to as “CFSE Max”) despite 72 h of *in vitro* culture in the presence of physiological growth factors. In other words, CD133⁺/CD34⁺ cells were shown to reside within the quiescent population of CD34⁺ CML progenitor cells, known to be resistant to therapy. Of note, the low expression of CD133 seen in some cells was not due to cellular differentiation and a loss of the dye upon the 72 h *in vitro* culture as the percentage of CD133⁺ cells did not change significantly from day 0 to day 3.

We next analysed the percentage of viable CD133⁺/CD34⁺ cells remaining following 72 h of drug treatment with tigecycline, imatinib and combination. This revealed that the percentage of CD133⁺/CD34⁺ cells was significantly reduced in the combination treatment arm in comparison to vehicle and imatinib alone (**Fig 5.8b**). Noteworthy, imatinib did not significantly reduce the percentage of CD133⁺/CD34⁺ cells, in line with its lack of efficacy against primitive CML cells. We next tested whether the combination treatment was able to induce cell death in the quiescent fraction of CD34⁺ CML cells. To this end, CD34⁺ CML cells were stained at day 0 with the cell division tracker CFSE dye, and the percentage of Annexin V positive cells was analysed within the quiescent fraction (CFSE Max) following 72 h drug treatment. While imatinib did not significantly increase cell

death in the resistant quiescent fraction of CML CD34⁺ cells, the combination treatment resulted in a significant increase in the percentage of Annexin V positive CFSE^{Max} cells (**Fig. 5.8c**).

These results indicated that the combination of tigecycline and imatinib can significantly target CML LSCs *in vitro*. Given that these experiments were based on the phenotypical analysis of CML cells, we next performed functional assays to assess the stem cell potential following *in vitro* drug treatment.

As mentioned before (**3.2.4**), cells identified as CD34⁺CD38⁻ prior to *in vitro* culture are enriched for HSCs and represent about 5~10% of the total CD34⁺ cells. We therefore performed short-term CFC assays on FACS-sorted CD34⁺CD38⁻ from one CML patient following 72 h *in vitro* drug treatment. While imatinib and tigecycline as single agents decreased the number of colonies by about 30%, their combined application further reduced the number of CD34⁺CD38⁻-derived colonies (**Fig. 5.8d**). To complement this result, we next assessed the effect of vehicle, tigecycline, imatinib and the combination treatment in CML LSCs by LTC-IC assay. While imatinib did not significantly reduce LSCs potential, tigecycline, alone and when combined to imatinib, significantly reduced the number of LSCs (**Fig. 5.8e**).

Taken together, our data demonstrated that the combination of tigecycline to imatinib significantly targets CML LSCs *in vitro*, while imatinib alone was unable to impair their survival.

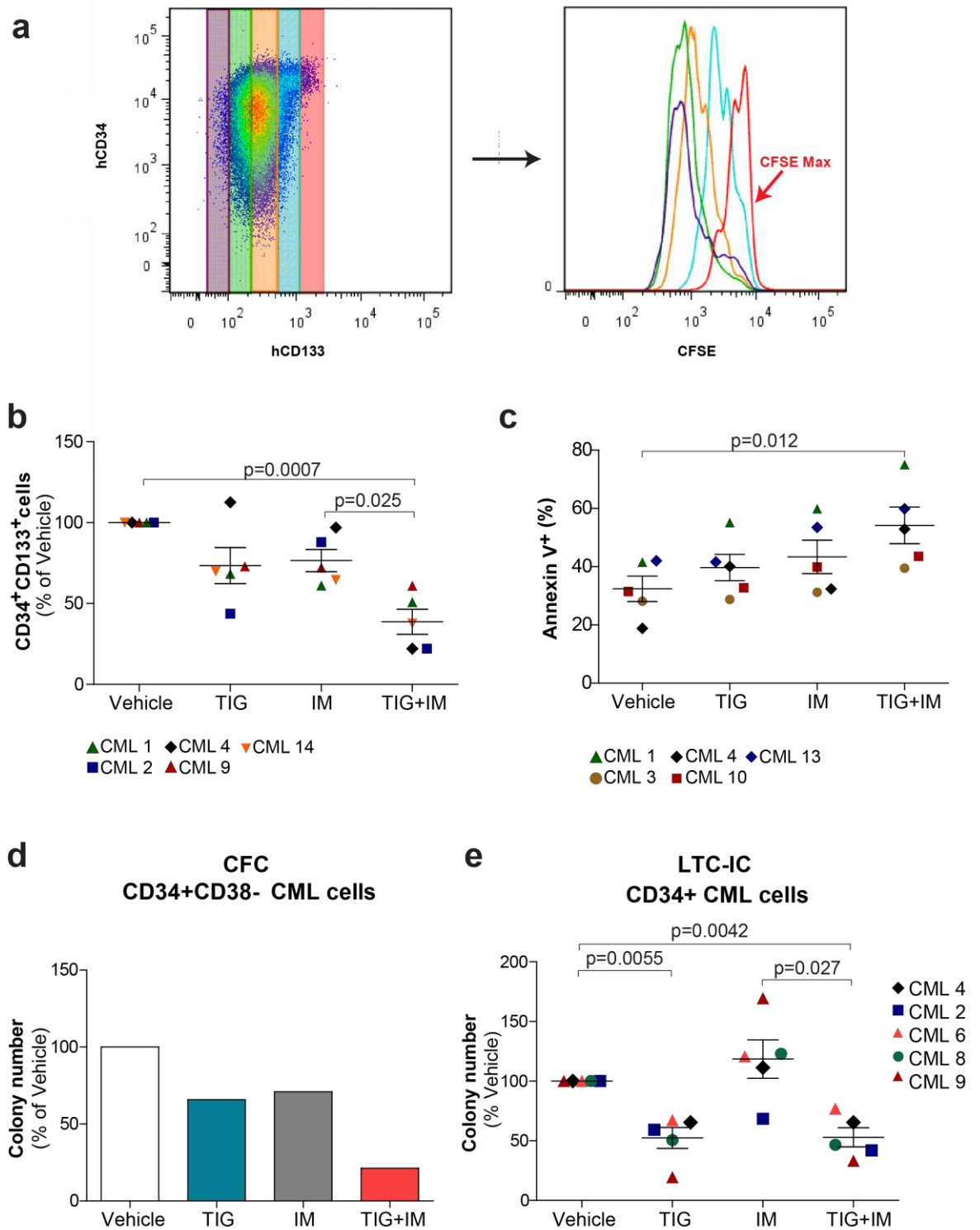


Figure 5. 8 Tigecycline in combination with imatinib targets LSCs *in vitro*.

(a) Representative expression levels of human CD34 and human CD133 following 72 h *in vitro* culture of CD34⁺ CML cells (left panel). Representative histograms reflecting the retention of the CFSE dye in cell subsets expressing different levels of CD133 (right panel). (b) Percentage of CD34⁺CD133⁺ remaining after 72 h *in vitro* treatment. n=4 patient samples. (c) Percentage of Annexin V positive cells in CFSE^{max} CD34⁺ CML cells following 72 h *in vitro* treatment. (d) Relative number of colonies measured by CFC assay following 72 h drug treatment of CD34⁺CD38⁻ CML cells. n=1 patient sample. (e) Relative number of colonies measured by LTC-IC assay in CD34⁺ CML cells. n=5 patient samples. All data are presented as Mean ± S.E.M. P values were calculated by paired Student's t-test. Tigecycline (TIG) and imatinib (IM) were used at a concentration of 2.5 μM and 2 μM respectively.

5.2.6 Tigecycline-mediated inhibition of oxidative metabolism targets LSCs *in vivo* when used in combination with imatinib

Our promising *in vitro* results suggested that combining tigecycline to imatinib could target LSCs. We next aimed to validate these findings *in vivo* using a transgenic mouse model of CML. As mentioned before, the DTG mouse model for CML disease consists of a TET-OFF system that prevents BCR-ABL expression in the presence of tetracycline. Tigecycline is a derivative of tetracycline and, as shown in Fig. 5.9a, both drugs share a similar structure. Therefore, we were concerned that tigecycline could bind to the tTa in the DTG mouse model, which would prevent the expression of BCR-ABL in HSCs. In that case, tigecycline treatment could revert CML disease by interfering with the expression of BCR-ABL, making it difficult to interpret the real effect of tigecycline against CML cells. To test whether tigecycline could interfere with the TET OFF expression system, we isolated haematopoietic progenitor cells (cKit⁺) from DTG mice and analysed BCR-ABL mRNA levels following a 48 h *in vitro* culture in the absence or presence of tetracycline, doxycycline and tigecycline. This revealed that all three antibiotics reduced BCR-ABL mRNA levels by more than 90% in comparison to untreated condition. Noteworthy, this was not due to a toxic effect of tigecycline against BCR-ABL-expressing cells, as no significant difference in cell death and cell number were noted between all conditions. This suggested that tigecycline, at a concentration used in all our *in vitro* assays (2.5 µM), was as potent as tetracycline and doxycycline to reduce BCR-ABL mRNA levels in cells isolated from the DTG model, confirming its ability to interfere with the TET OFF expression system. Therefore, the DTG mouse model was not suitable for testing the effect of tigecycline against CML LSCs *in vivo*.

To confirm that the combination of tigecycline with imatinib targets LSCs in an *in vivo* setting, we next used a robust humanised model of CML. CD34⁺ CML cells derived from one CML patient known to engraft 100 % of Ph-positive cells were transplanted into sub-lethally irradiated immuno-deficient NOD.Cg-Prkdc^{scid}Il2rg^{tm1Wjl}/SzJ (NSG) female mice. Six weeks post-transplantation, human cell engraftment was confirmed by analysing the presence of human leucocyte common antigen (hCD45⁺) in the blood of the mice. After ensuring equivalent human cell engraftment levels, the mice were split into four groups (A, B, C, D)

and treated for four weeks with vehicle only, tigecycline (escalating doses of 25-100 mg.kg⁻¹: see Methods), imatinib (100 mg.kg⁻¹) or both drugs combined (**Fig. 5.10a,b**).

Importantly, the mice did not show any clinical signs of toxicity during the drug treatments. Moreover, no significant changes in body and spleen weight, nor differences in BM cellularity were noted after the four-week treatment course, indicating that tigecycline or the combination is safe for use (**Fig 5.10c-e**). At end point, total BM cells from femurs and tibias were isolated and analysed for the expression of the following cell humans antigen by flow cytometry: CD45, present on leukocytes, CD34, present on progenitors and stem cells and CD38 to discriminate progenitors (CD34⁺CD38⁺) from LSCs (CD34⁺CD38⁻). Transplantation of CML patients samples into immunocompromised mice have been shown to result in low engraftment levels in the host. Similarly, in this experiment, the majority of BM cells isolated were non-leukaemic murine cells (human CD45⁻) and were not affected by any of the treatment regimen (**Fig. 5.10e and 5.11a**). However, the total number of CML-derived leukocytes (hCD45⁺) was decreased significantly in mice treated with imatinib and, importantly, the CML burden was further decreased in the combination arm (**Fig. 5.11b**). This effect was even more pronounced in more primitive CD45⁺CD34⁺ CML cells where the combination treatment decrease significantly the number of CD45⁺CD34⁺ CML cells in comparison to both vehicle and imatinib treated mice (**Fig. 5.11a,c**). The most striking effect though was seen within the more primitive human LSCs population. Whereas imatinib alone only marginally (and insignificantly) decreased the number of CD45⁺CD34⁺CD38⁻ CML cells, the combination treatment eliminated 95% of these cells (**Fig. 5.11d**).

Finally, to demonstrate that the effect of tigecycline is mediated by reduction in mitochondrial oxidative metabolism, a second *in vivo* experiment using the xenotransplantation model was performed with CD34⁺ cells derived from a second CML patient. Following six weeks of engraftment, mice were split into two groups and treated with either vehicle or tigecycline (escalating doses of 25-100 mg.kg⁻¹) for four weeks (**Fig. 5.12a**). At end point, total BM cells were sorted for human CD45⁺CD34⁺ cells and the expression of mitochondrial-encoded protein assessed. The assay could only be performed in four out of six vehicle and tigecycline-

treated mice due to an insufficient cell number isolated from the other animals. CD45⁺CD34⁺ CML cells isolated from tigecycline-treated mice displayed decreased level of MT-CO2 and MT-CO1 but not ATP5A in comparison to vehicle-treatment, which indicated that tigecycline reduces the expression of mitochondrial-encoded proteins in primary CD34⁺ cells *in vivo* (Fig. 5.12b)

Altogether, our results demonstrated that primitive stem/progenitor CML cells are sensitive to the inhibition of OXPHOS. Importantly, the combination of tigecycline with imatinib, the standard first-line therapy for CML, impaired the survival of both CD34⁺ and more primitive CML LSCs at clinically administrable doses in a selective manner.

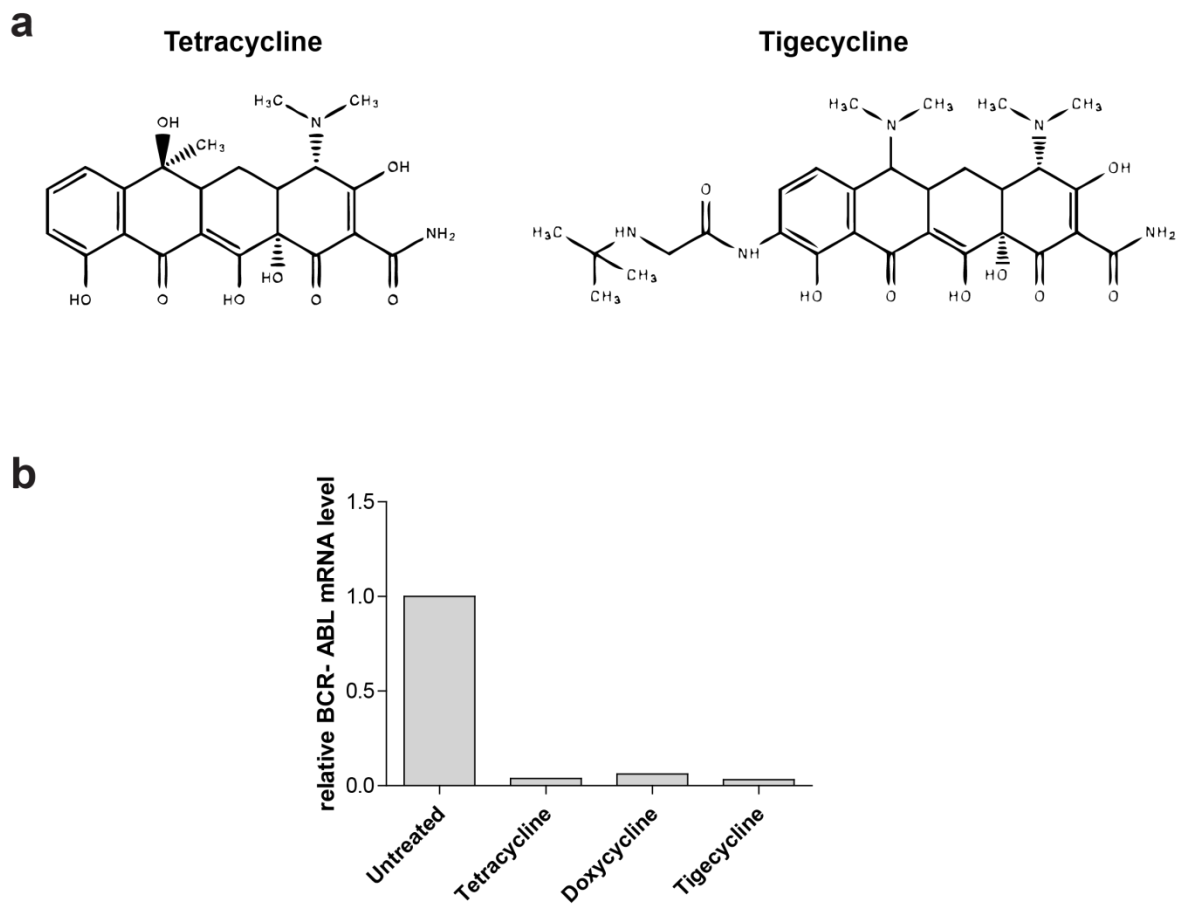


Figure 5. 9 Tigecycline affects the TET-OFF gene expression system.

(a) Structural formula of tetracycline and tigecycline. (b) BCR-ABL mRNA levels in cKit⁺ cells isolated from DTG mice following 48 h *in vitro* culture with indicated drugs. n=1 independent experiment. Tetracycline and doxycycline were both used at a concentration of 1 $\mu\text{g/ml}$. Tigecycline was used at a concentration of 2.5 μM .

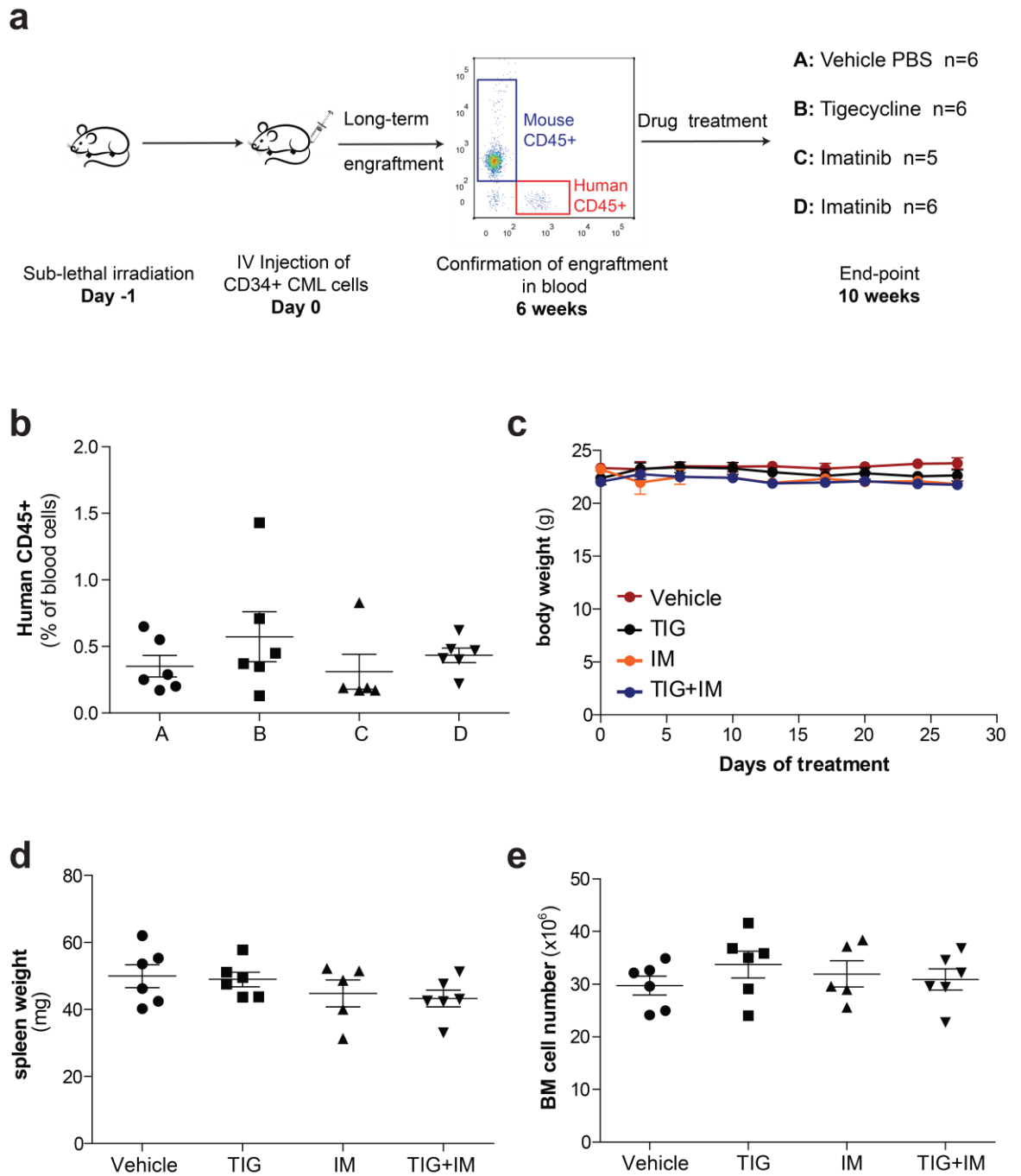


Figure 5. 10 Tigecycline alone or when combined to imatinib is not toxic towards normal cells.

(a) Mice were transplanted with CD34⁺ CML cells and analysis of human cell engraftment was performed following 4 weeks of *in vivo* drug treatment. (b) Percentage of human CD34⁺ cells in blood 6 weeks post-transplantation, before the start of treatment. (c) Mouse body weight during treatment course. (d) Spleen weight at endpoint. (e) BM cellularity measured in tibiae and femurs. All data are presented as Mean \pm S.E.M. TIG, tigecycline; IM, imatinib.

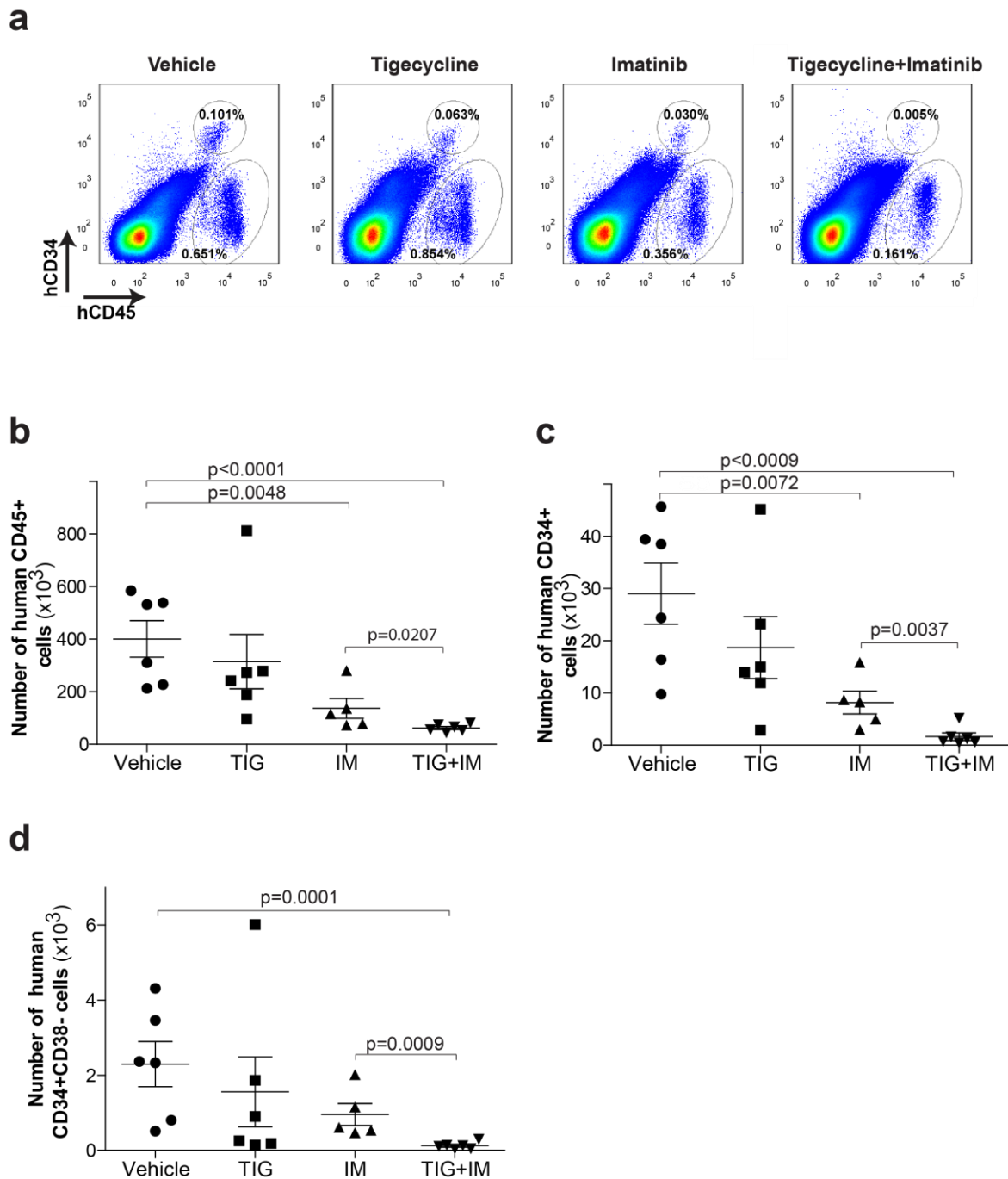


Figure 5. 11 Tigecycline in combination with imatinib targets human LSCs *in vivo*.

(a) Representative percentage of human CD45⁺ and human CD34⁺ cells from total BM cells. Number of (b) human CD45⁺ cells (c) human CD34⁺ cells and (d) human CD34⁺CD38⁻ cells engrafted in the BM of immunocompromised mice. All data are presented as Mean \pm S.E.M. P values were calculated by unpaired Student's t-test on logarithmic transformed variables to meet the assumption of normality. TIG, tigecycline; IM, imatinib.

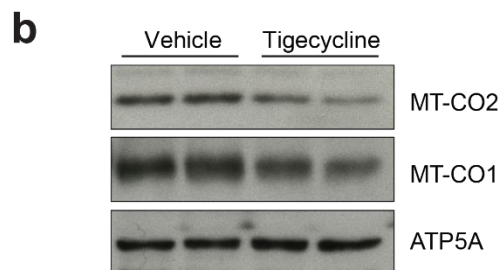
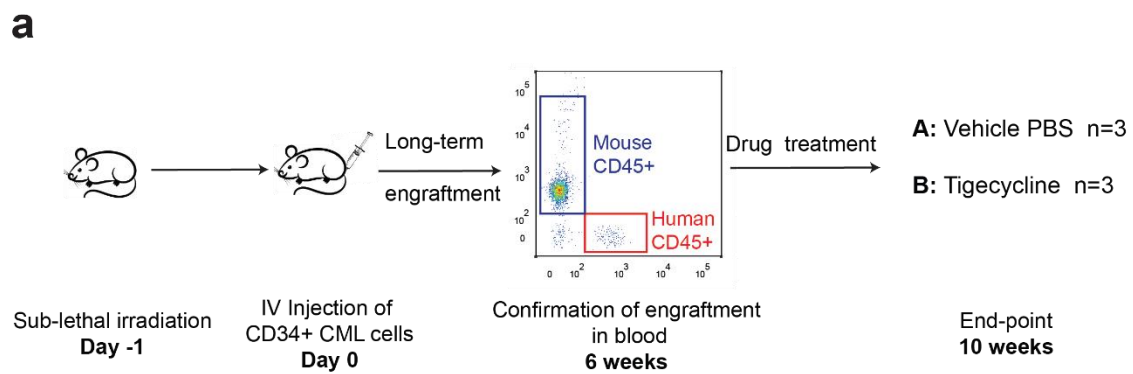


Figure 5. 12 Tigecycline inhibits the expression of mitochondrial-encoded proteins of CD34⁺ CML cells *in vivo*.

(a) Mice were transplanted with CD34⁺ CML cells and treated with tigecycline or PBS *in vivo* for 4 weeks. (b) Protein expression of MT-CO2, MT-CO1 and ATP5A in FACS-sorted CD34⁺ CML cells following 4 weeks *in vivo* treatment

5.2.7 The combination of tigecycline and imatinib marginally affects normal HSCs *in vivo*

We next performed a comparative analysis on normal HSCs to assess the selectivity and the therapeutic advantage for tigecycline treatment. Precisely, CD34⁺ cord blood cells were transplanted in immunocompromised mice and, similar to the experiment described in **Figure 5.10a** with CD34⁺ CML cells, treatment was started with PBS, tigecycline (escalating doses from 25-100 mg.kg⁻¹), imatinib (100 mg.kg⁻¹) and combination, after confirmation of equivalent engraftment levels in mice (**Fig. 5.13 a,b**). After four weeks of *in vivo* treatment, BM cells were isolated and expression of the human surface markers CD34 and CD38 were analysed by flow cytometry. The number of human CD34⁺ cells was decreased, although not significantly, in all treatment arms in comparison to vehicle treatment (**Fig 5.13c**). Importantly, the combination treatment did only decrease the number of human CD34⁺ normal cells marginally and insignificantly, in contrast the 95% elimination of human CD34⁺ CML observed previously (**Fig. 5.11c**). Moreover, this effect was even less pronounced in the primitive human HSC population. Imatinib induced a slight (and insignificant) decrease in the number of normal HSCs in comparison to vehicle condition (**Fig. 5.13d**). Importantly, the addition of tigecycline to imatinib did not further decrease the number of human CD34⁺CD38⁻ cells, as demonstrated by the equivalent number of normal HSCs measured in imatinib and the combination arm.

The percentage of human CD34⁺CD38⁻ cells within the total human CD34⁺ population can reflect the preferential toxicity of a drug against primitive HSCs or progenitor cells. As such, a decrease in the percentage CD34⁺CD38⁻ cells within the total CD34⁺ cells suggests that the drug preferentially targets primitive cells. In this experiment, both tigecycline alone and the combination treatment increased the percentage of CD34⁺CD38⁻ normal cells compared to vehicle, indicating that tigecycline, combined to imatinib or alone, might target normal cells to some extent; however, this effect is mainly directed against progenitor cells and not normal HSCs (**Fig. 5.13e**).

Altogether, these results demonstrated that tige cycline combined to imatinib does not significantly target normal HSCs, reinforcing the idea of a therapeutic index to target selectively CML LSCs.

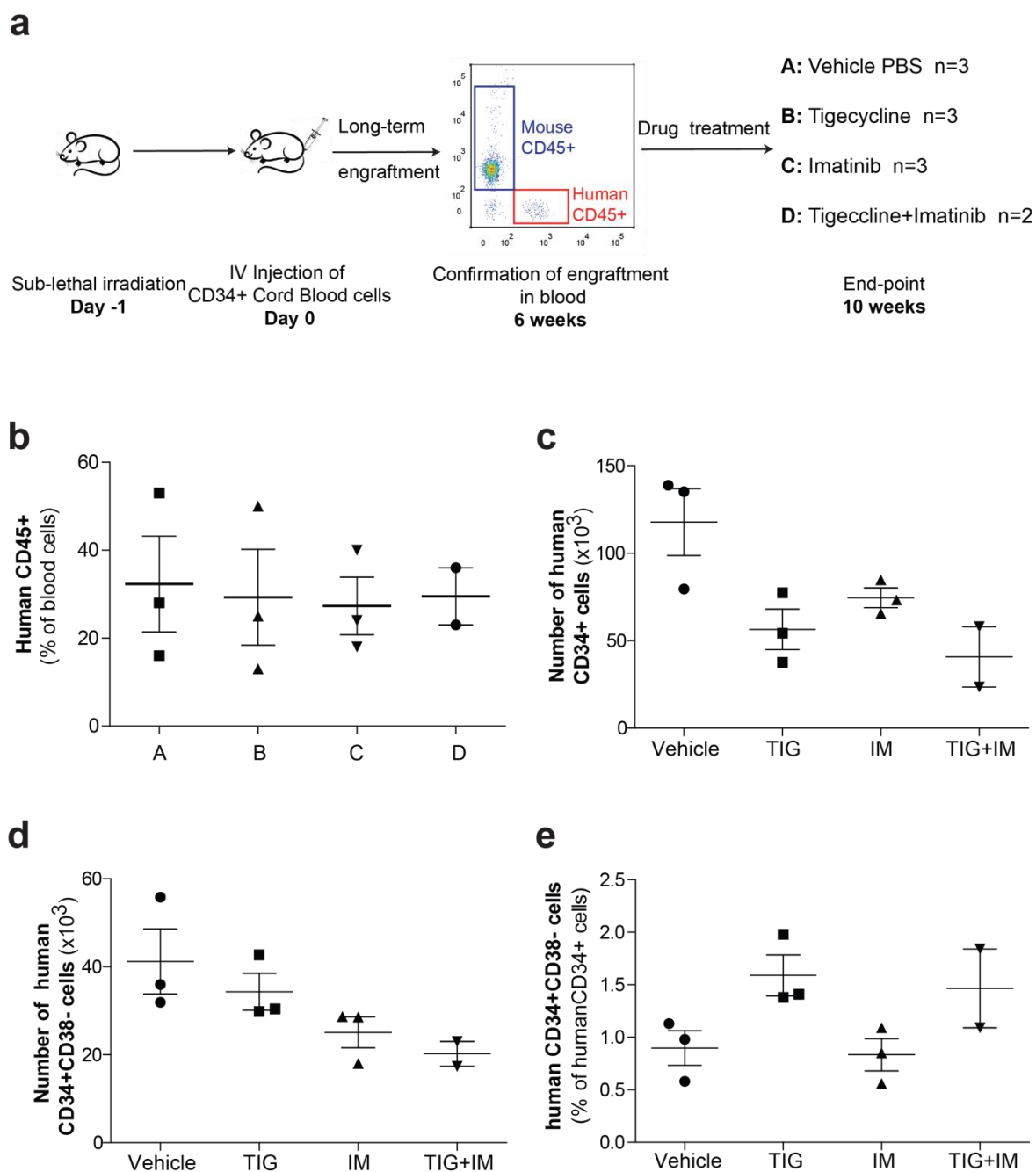


Figure 5. 13 The combination of imatinib and tige cycline marginally affects normal HSCs *in vivo*.

(a) CD34⁺ cord blood cells were transplanted into immunocompromised mice and left for 6 weeks to allow engraftment. The mice were then treated for 4 weeks before analysis of human cell engraftment. (b) Pre-treatment levels of human CD45⁺ cells engraftment. (c-d) Number of (c) human CD34⁺ cells and (d) human CD34⁺CD38⁻ cells engrafted in the bone marrow of immunocompromised mice. (e) Percentage of human CD34⁺CD38⁻ cells within the human CD34⁺ cell subset. All data are presented as Mean ± S.E.M. TIG, tige cycline; IM, imatinib.

5.2.8 The combination of tigecycline and imatinib prevents CML relapse

Finally, we assessed whether the combination of tigecycline and imatinib could prevent relapse following drug discontinuation in mice. CD34⁺ CML cells derived from a CML patient were transplanted into sub-lethally irradiated immunodeficient NSG female mice. Seven-eight weeks post-transplant, mice were treated with PBS, tigecycline (escalating doses from 25-100 mg.kg⁻¹), imatinib (100 mg.kg⁻¹) and combination for four weeks. The treatment was then discontinued for two weeks before assessment of the remaining LSCs in the BM of mice (Experiment 1, **Fig 5.14a**). To substantiate these results, we performed a second *in vivo* experiment in which mice were first treated for three weeks and then left untreated for a period of three weeks (Experiment 2, **Fig 5.14b**). Following imatinib discontinuation, the total number of human CML-derived CD34⁺ and CD34⁺38⁻ cells was not reduced in comparison to the vehicle treatment, indicating that imatinib-treated mice are unable to sustain low levels of CML LSCs (**Fig 5.14c,d**). On the contrary, mice that were treated with the combination of imatinib and tigecycline maintained significant low numbers of CML-derived CD34⁺ and CD34⁺38⁻ cells. Of note, only one mouse out of nine showed signs of relapse or failed to initially respond to the combination treatment.

Taken together, we have demonstrated that CML LSCs are highly susceptible to inhibition of mitochondrial oxidative metabolism. Indeed, combining the mitochondrial oxidative inhibitor tigecycline with imatinib selectively reduced the number of CML LSCs. This effect was seen even after three weeks drug discontinuation, indicating that the combination prevents, or at least significantly delays, CML relapse.

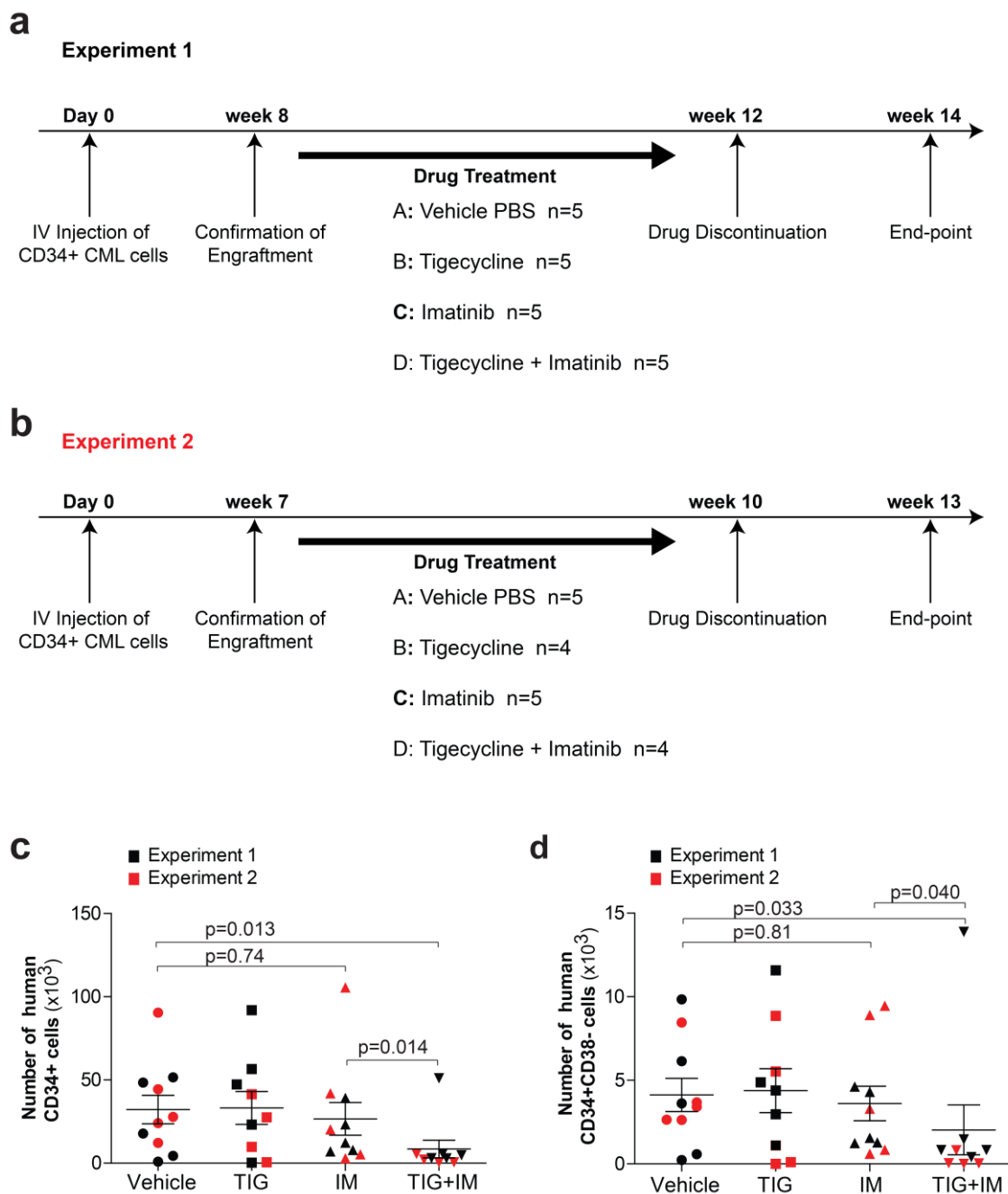


Figure 5. 14 Tigecycline in combination with imatinib prevents CML relapse.

(a-b) Mice were transplanted with CD34⁺ CML cells and left to engraft for 6-7 weeks. Mice were then treated *in vivo* for (a) 4 weeks and kept for an additional 2 weeks following drug discontinuation or (b) treated for 3 weeks and kept for an additional 3 weeks following drug discontinuation. (c-d) Number of (c) human CD34⁺ cells and (d) human CD34⁺CD38⁻ cells engrafted in the BM of immuno-compromised mice. All data are presented as Mean ± S.E.M. P values were calculated by unpaired Student's t-test on logarithmic transformed variables to meet the assumption of normality. TIG, tigecycline; IM, imatinib.

5.3 Discussion

In this section, we first demonstrated that tigecycline inhibits mitochondrial oxidative metabolism in two CML cell lines through inhibition of mitochondrial protein expression. Moreover, combination of tigecycline with imatinib significantly enhanced the effect of imatinib to target leukaemic cells in the two CML cell lines across three different concentrations of imatinib. CML cell lines represent an inexhaustible *in vitro* model useful for performing preliminary studies and optimising techniques, a necessary step before limited primary material is used. They can as well provide insights in the efficacy of a drug; our experiments suggested for instance that tigecycline can affect CML cells survival in combination with imatinib. However, these cell lines cannot be used as a genuine model for CML stem cells. As such, we tested the effect of tigecycline in primary stem-cell enriched CD34⁺ cells in the following sections.

Our investigation of tigecycline selectivity towards leukaemic cells revealed that the IC₅₀ value of tigecycline was about 7.7 fold higher in normal pro-B murine mouse cells compared to BCR-ABL expressing counterparts. This suggests a therapeutic window for tigecycline use to target leukaemic cells. Interestingly, while primary stem cell-enriched cells from normal donors (normal CD34⁺ cells) do not proliferate, parental Ba/F3 and Ba/F3 p210 cells, with a reported doubling time of 20 hours, have a similar proliferative capacity. This is a primordial aspect when testing the sensitivity of two different cell lines to a drug, as slow cycling cells might appear less sensitive. However, both parental Ba/F3 and Ba/F3 p210 cells are cell lines of mouse origin and care should be taken extrapolating these results to human cells. Moreover, the XTT assay performed here primarily assesses the effect of tigecycline against the proliferation of the cells. We therefore aimed to test whether tigecycline could affect the viability of normal progenitor cells in subsequent sections.

Similar to our findings in CML cell lines, tigecycline decreased mitochondrial oxidative metabolism by targeting the expression of mitochondrial-encoded proteins in CD34⁺ CML cells. Precisely, our comprehensive metabolomic analysis revealed that oxidation of glucose and glutamine as well as FAO were reduced upon tigecycline treatment in primary stem cell-enriched CML cells. Interestingly,

while the ^{13}C fraction of TCA cycle metabolites was significantly reduced upon tigecycline treatment, a clear increase in their unlabelled fraction was observed in comparison to vehicle condition. This elevated unlabelled fraction of TCA cycle metabolites could indicate that tigecycline-treated cells shift from glucose to another carbon source. We did however observe a significant reduction in the oxidation of the three substrates glucose, glutamine and palmitate. Therefore, a more plausible explanation could lie in the potential decrease in the catabolism of these metabolites that is associated with the growth arrest phenotype and the general metabolic slowdown due to tigecycline treatment (**Fig. 5.6**). In other words, an increase in the unlabelled fraction of TCA cycle metabolites following tigecycline treatment is not necessarily linked to an increase in the production of these metabolites from alternative sources, but rather a decrease in their catabolic rate. Of note, tigecycline seemed to partially impair glycolysis, as reflected by decreased ECAR in CD34^+ CML cells treated with tigecycline (**Fig. 5.15**). The reasons for this decrease are not known but indicate that tigecycline has a broad effect on cellular metabolism. This decrease in glycolysis could be the consequence of a general inhibition of cellular proliferation.

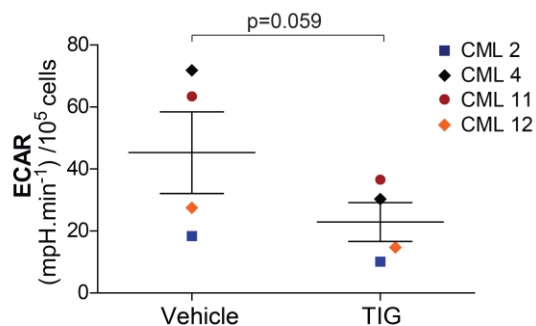


Figure 5. 15 Tigecycline impairs glycolysis in CD34^+ CML cells *in vitro*.

Basal ECAR in CD34^+ CML cells following treatment with tigecycline ($2.5 \mu\text{M}$). $n=4$ patient samples. P value was calculated by paired Student's t-test. Data are presented as Mean \pm S.E.M.

Our investigation of tigecycline effect against primary CD34⁺ CML cells revealed that tigecycline treatment in combination with imatinib strikingly reduced the proliferation and the colony-forming potential of CD34⁺ CML cells compared to imatinib alone. Moreover, this effect was shown to be selective to CML cells, as CD34⁺ normal cells were only marginally affected by the combination treatment. This was in line with our previous experiment in Ba/F3 cells that indicated that tigecycline targets preferentially BCR-ABL expressing cells (Fig. 5.3). Moreover, imatinib significantly impaired the ability of progenitors to form colonies in comparison to vehicle treatment; in agreement with other studies demonstrating that CML CD34⁺ progenitor cells are sensitive to imatinib, while more primitive cell populations are not affected by BCR-ABL inhibition. Although it is of clinically interest to target progenitor cells, these *in vitro* studies do not inform on the sensitivity of CML LSCs to the drug combination. We therefore tested the effect of tigecycline and imatinib in more rigorously defined CML LSCs.

By using various techniques, including the analysis of stem cell surface markers and the gold-standard *in vitro* LTC-IC assay, we next demonstrated that the addition of tigecycline to imatinib significantly impairs CML LSCs survival in comparison to imatinib as a single agent or vehicle treatment. Noteworthy, imatinib treatment had only a marginal (and not significant) effect in all experiments performed, confirming that these assays primarily focus on primitive TKI resistant CML cells. It would have been interesting to carry out similar experiments on normal counterparts in order to gain a deeper understanding of the selectivity of tigecycline and imatinib for leukaemic cells. However, we performed an *in vivo* experiment with cord blood cells in a subsequent study, which in our opinion was a sufficient and stronger argument of the therapeutic index for the proposed combination treatment.

Using a xenotransplantation model in which CD34⁺ CML cells were transplanted into immuno-deficient mice, we demonstrated that the combined action of imatinib and tigecycline eliminates the vast majority (95%) of CML LSCs following four weeks of *in vivo* treatment. Interestingly, the effect of the drug combination was more profound in primitive CD34⁺CD38⁻ cells than in the bulk of differentiated CD45⁺ cells, which could indicate that the treatment targets preferentially CML LSCs. Imatinib treatment induced a significant reduction in progenitor cells in

comparison to untreated condition, and this effect was lost when more primitive CD34⁺CD38⁻ cells were analysed. This is in accordance with previous published studies and reinforces the idea that analysing the effect of a drug treatment on CD34⁺CD38⁻ cells is a reliable method to see whether primitive stem cells, known to be insensitive to imatinib, are targeted. Contrary to our *in vitro* LTC-IC experiments in which tigecycline alone significantly reduced the number of CML LSCs, tigecycline had only a marginal (and non-significant) effect *in vivo* and only the combination treatment was able to significantly decrease primitive CD34⁺CD38⁻ cell number. The discordant results between the *in vitro* and *in vivo* assays could be due to many factors, including the complexity of living organism including the effect of the BM microenvironment.

We next transplanted normal CD34⁺ cord blood cells into mice and treated them with either vehicle, imatinib, tigecycline or the combination of both drugs. While the drug treatments (particularly imatinib) had some effect on the number of human CD34⁺CD38⁻ normal cells *in vivo*, there was no additive or synergistic effect following the combined treatment. Importantly, the effects were less dramatic compared with the response observed with leukaemic stem cells (albeit the number of available cord blood cells limited the number of animals used in this experiment). In combination with the lack of observed toxicity to normal spleen and BM cells of the host mice (**Fig. 5.10**) we concluded that there is an obvious therapeutic index for tigecycline' use in combination with imatinib. Moreover, we have previously demonstrated through metabolomic studies that CD34⁺CD38⁻ normal cells have low levels of mitochondrial oxidative metabolism. In addition, the ratio of oxidative to glycolytic metabolism was higher in more differentiated progenitor CD34⁺CD38⁺ normal cells compared to more primitive counterparts, suggesting that primitive HSCs are more glycolytic than normal progenitors/differentiated cells (**Fig 3.9**). Considering this metabolic phenotype, it is not surprising to see that *in vivo*, tigecycline (alone or combined to imatinib) affected preferentially CD34⁺ normal cells and had only a marginal effect on CD34⁺CD38⁻ normal cells.

One of the gold-standard method to functionally assess the efficacy of a drug treatment to target LSCs is to perform secondary-transplant and measure the number of leukaemic cells in secondary recipients. However, the number of CD34⁺

CML cells that can be collected from primary recipients are not sufficient to perform secondary transplantation. Therefore we performed experiments, using two separate mouse cohorts, in which mice were treated *in vivo* for three or four weeks and the remaining CML LSCs analysed following two-three weeks drug withdrawal. The two independent experiments demonstrated that the combination of imatinib and tigecycline induces sustainable low numbers of CML LSCs even upon three weeks treatment discontinuation. Interestingly, the mice treated with imatinib as a single agent relapsed following drug removal, as evidenced by similar number of CD34⁺ and CD34⁺CD38⁻ CML cells in both the imatinib and vehicle conditions. However, one out of the nine mice treated with the drug combination did show significant increased levels of CD34⁺ and CD34⁺CD38⁻ CML cells following two weeks of treatment discontinuation. BM aspiration at the end of the *in vivo* drug treatment would have helped to determine whether this mouse did not initially respond to the treatment or relapsed during drug withdrawal. Given the risk of losing mice when performing BM aspiration combined with the limiting number of mice in each treatment arms, we decided not to perform the procedure in our experiments.

5.4 In summary

In this chapter, we first validated the mechanism of action of tigecycline as an inhibitor of mitochondrial protein expression. Indeed, tigecycline treatment reduced the expression of mitochondrial proteins in two CML cell lines, which resulted in the inhibition of mitochondrial metabolism. Moreover, combining tigecycline to imatinib significantly increased the percentage of CML cell death in comparison to imatinib alone. We provided as well some evidence of the selectivity of tigecycline against CML cells, as non-expressing BCR-ABL murine cells were less affected by tigecycline treatment.

We next performed similar assays in more clinically relevant patient-derived CD34⁺ cells. Similar to our results in CML cell lines, tigecycline treatment decreased mitochondrial respiration by affecting the expression of mitochondrial proteins in CML CD34⁺ cells. We complemented these results by performing an in depth analysis of the metabolic perturbations induced by tigecycline. Indeed, we demonstrated that tigecycline reduced oxidation of glucose, glutamine and fatty

acids and this was linked to reduction in PDH and PC relative activity in CML CD34⁺ cells.

We next tested whether the inhibition of mitochondrial oxidative metabolism induced by tigecycline affects the survival of stem cell-enriched CML cells. Tigecycline impaired the proliferation of the CD34⁺ CML cells and targeted them for cell death. Moreover, the colony forming potential of CML progenitors was significantly reduced by the combination of imatinib and tigecycline in comparison to imatinib alone, while having minor effect on CD34⁺ normal cells. In addition, through functional and flow cytometric assays, we demonstrated that the combination of imatinib and tigecycline targets primitive leukaemic cells and reduces the stem cell potential of CML cells.

Finally, we used a humanised model of CML to test the efficacy of the drug combination to target CML LSCs *in vivo*. The combination of tigecycline and imatinib resulted in a near-to-complete elimination of primitive CD34⁺CD38⁻ CML cells, with 95% of CML LSCs targeted following four weeks of *in vivo* drug treatment, while normal counterparts were only marginally affected. We next performed two complementary *in vivo* experiments in which we evaluated the remaining CML LSCs following *in vivo* treatment discontinuation. Mice treated with the drug combination sustained low number CML LSCs, while imatinib-treated mice relapsed.

Altogether, our results demonstrated that inhibition of mitochondrial metabolism with tigecycline targets CML LSCs. Importantly, this effect was sustained following drug withdrawal, suggesting that the drug combination could potentially prevent relapse and might be an effective therapeutic strategy to eradicate TKI-resistant CML LSCs.

Chapter 6 Conclusion and future directions

In this thesis, we present the first in-depth investigation of the metabolism of CML LSCs and identification of mitochondrial oxidative metabolism as a metabolic vulnerability in CML LSCs. In the next paragraphs, we will discuss our findings in relation with the current literature in addition to discussing potential implications and future directions of this work.

6.1 Oxidative metabolism in LSCs

Thus far, most of the research has focused on the metabolic regulation of normal haematopoietic cells or stem cells derived from other leukaemias, such as AML. Indeed, to our knowledge, no study had investigated in depth the metabolism of primary stem cells from CML patients. We will therefore discuss how our findings associate with previous metabolic studies performed in AML cells and with recent transcriptomic data obtained from CML LSCs.

Studies performed in patient-derived AML cells demonstrated that mitochondrial metabolism is primordial for the survival of primitive and differentiated AML cells. Indeed, one study suggested that AML LSCs are less glycolytic than normal progenitor cells and might rely more on oxidative metabolism for energy production (188). The authors further demonstrated that BCL-2 inhibition targets AML LSCs by impairing their mitochondrial functions. Noteworthy, this study did not analyse the metabolism of similar subsets of cells and instead compared normal progenitor cells to primitive ROS-low AML cells. In another robust study, Škrtić *et al.* demonstrated that inhibition of mitochondrial translation with tigecycline treatment significantly impaired the survival of primary AML cells *in vitro* and *in vivo* (1.5.4) (187). These studies provided a first evidence of the mitochondrial metabolic requirements of primitive AML cells and are in agreement with our findings for a different type of myeloid leukaemia.

More recently, Giustacchini *et al.* performed single-cell transcriptomic analysis of LSCs and HSCs from CML patients and normal cells donors. This study revealed that BCR-ABL expressing CML stem cells displayed a significant enrichment for genes associated with OXPHOS and fatty acid metabolism in comparison to normal HSCs.

Moreover, several significant differences in the gene expression were noted between normal HSCs and BCR-ABL negative “bystander” cells from CML patients, indicating that non-expressing BCR-ABL stem cells from CML patients differ from normal HSCs. Interestingly, they found that OXPHOS-associated genes were significantly increased in normal HSCs in comparison to BCR-ABL negative cells isolated from CML patients. This could indicate that, within a CML patient, LSCs potentially modulate the metabolism of normal counterparts. While the mechanisms behind this possible regulation are unknown, CML LSCs might alter the metabolism of BCR-ABL negative cells through modification of the BM microenvironment, known to be disrupted in mouse models of CML. Our study did not touch on the role of the leukaemic BM microenvironment on the metabolism of CML cells, but it is likely that such regulations exist. In physiological conditions, normal HSCs are localised in two regions of the BM: the hypoxic endosteal region and a more vascularised compartment. The high levels of hypoxia-inducible factor 1-alpha (HIF-1 α) found in hypoxic regions of the BM activate pyruvate dehydrogenase kinase, isozyme 1 which in turns decreases PDH activity and reduces mitochondrial metabolism (253, 254). Accordingly, studies have shown that HSCs rely primarily on glycolysis for their energy requirements and have low levels of mitochondrial metabolism; a metabolic characteristic that is believed to be crucial for maintaining low oxidative stress and sustain their quiescence (1.4.3). Given these considerations, targeting mitochondrial metabolism in CML LSCs residing in hypoxic regions may prove ineffective. In contrast to the aforementioned points, a recent review argued that the high vascularity of the BM is not compatible with a severe hypoxic environment. Accordingly, Kiel & Morrison have reported that HSCs localise with haematopoietic progenitor cells in the BM and do not reside in anatomically distinct compartments (255). Moreover, recent advances in imaging techniques have shown that HSCs in the endosteum closely interact with microvessels of the BM (142).

In CML, studies have shown that LSCs hijack the BM microenvironment and prevent normal HSCs to function properly. This produces a ‘microenvironment-induced oncogenesis’ and a ‘malignancy-induced microenvironment’ that promotes the survival and proliferation of leukaemic cells (256). While many BM factors have been implicated in promoting and sustaining leukaemia, further work still remains to determine the contribution of the leukaemic BM microenvironment to the

aberrant metabolism of LSCs. Interestingly, recent studies have indicated that the close interaction between BM stromal cells and leukaemic cells can be used to transfer mitochondria between the two cell types (257). Moschoi *et al.* described that upon co-culture of AML cells with BM-derived cells, leukaemic cells uptake the mitochondria by endocytosis from the stromal cells. This resulted in an increase in their mitochondrial mass and LTC-IC potential, which led to a higher resistance to chemotherapy (257). Whether this mitochondrial exchange occurs in CML patients remains an avenue for further investigations. Nonetheless, a better understanding of the leukaemic microenvironment and its relationship with CML LSCs will undoubtedly provide more insights into the metabolism of CML LSCs *in situ*.

Most of the metabolic analyses performed in this thesis were done in CD34⁺ cells and, at the more primitive level, in CD34⁺CD38⁻ cells. As mentioned previously (3.3), more-defined LSCs have been identified, such as cells harbouring the CD34⁺CD38⁻CD90⁺CD45RA⁻ phenotypical markers. However, the number of CD34⁺CD38⁻CD90⁺CD45RA⁻ cells that can be isolated from patients and donors would be too limited to perform reproducible metabolic experiments. Future advances in the field of metabolomics at a single-cell level might prove useful to face the limitation in primary material and dissect the metabolism of primitive LSCs or rare cells in general. Nonetheless, this technique is still at its infancy and further improvements, notably in the sensitivity of detection, are necessary to detect less prevalent metabolites and get a better understanding of CML LSCs metabolism.

6.2 Metabolism of CML LSCs following TKI treatment

The vast majority of CML patients are treated with TKI in the clinics. While this was not the focus of our study, it would have been clinically relevant to assess the metabolic changes that occur following TKI treatment in more detail.

It is possible that part of the oxidative phenotype we observed in LSCs is driven by BCR-ABL, and hence its inhibition with imatinib would reduce partially the oxidative phenotype of LSCs. Accordingly, normal HSCs transduced with BCR-ABL display an increased oxidative metabolism in comparison to normal counterparts

(258). In contrast, one study has described that imatinib treatment induced a reduction in glycolysis and a compensatory increase in oxidative metabolism in CML cells (259). Of note, this study was performed in CML cell lines and further investigation is required to determine whether this switch occurs in primary stem cells following TKI treatment. Related to the above point, another study described that the increased expression of genes associated with OXPHOS in CML LSCs compared to normal counterparts is not reverted following imatinib treatment (260). However, this conclusion was only based on transcriptomics data and imatinib treatment of primary cells was performed *in vitro*. The direct comparison of untreated cells isolated from patients and cells cultured *in vitro* might therefore not be adequate. To address the metabolism of primary stem cells following imatinib treatment, further investigations could compare the metabolic difference between CML cells remaining after long-term TKI treatment and the bulk of CML cells present at baseline. A more robust approach would be to treat DTG mice *in vivo* with imatinib and assess the metabolic differences between stem cells isolated from TKI-treated and untreated mice.

In addition to the aforementioned considerations, CML LSCs possess increased levels of BCR-ABL and reside within a niche that renders them resistant to therapy (261, 262). Moreover, CML LSCs express lower levels of the transporter that actively uptakes of imatinib (organic cation transporter) and in contrast increased levels of the multidrug efflux transporter MDR1 (263). While we are not arguing that inhibition of BCR-ABL is not sufficient to target primitive leukaemic cells, BCR-ABL signalling might not be completely inhibited in CML LSCs from patients treated with TKI. Thus, the residual BCR-ABL signalling could drive oxidative metabolism in these primitive cells.

The metabolic consequences of imatinib treatment in CML LSCs remain an avenue of research for further investigation. Nonetheless, our results clearly showed that tigecycline-mediated inhibition of oxidative metabolism in combination with imatinib significantly impaired CML LSCs in mice, while either drug alone had only a marginal effect. In other words, this demonstrated that imatinib-treated CML LSCs require additional inhibition of mitochondrial metabolism for successful eradication.

6.3 Inhibiting oxidative metabolism targets CML cells in combination with TKI

Our investigation revealed that combining imatinib with inhibition of mitochondrial oxidative metabolism reduces LTC-IC potential and targets CML LSCs in a humanised mouse model. While the use of tigecycline to target CML LSCs is a new finding, some studies have described that combining mitochondrial inhibitors to TKI treatment can be of therapeutic value.

The pyruvate dehydrogenase (PDH) complex is essential for the conversion of pyruvate to acetyl CoA and its subsequent use into the TCA cycle. Interestingly, one enzyme of the PDH complex, dihydrolipoamide S-acetyltransferase (DLAT), was found to be crucial for the survival of imatinib-treated K562 CML cells (264). Indeed, short hairpin-RNA knockdown of DLAT remarkably sensitised CML cells to BCR-ABL inhibition. Accordingly, Alvarez-Calderon *et al.* demonstrated that the combination of dasatinib with the complex V inhibitor oligomycin significantly reduced the leukaemic burden in a mouse model of Ph⁺ B-Acute lymphoblastic leukaemia compared to TKI alone (264).

While all these studies indicate that TKI-treated CML cells can be effectively eliminated with inhibitors of mitochondrial metabolism they do not inform on the efficacy of these treatments in primary CML cells, let alone in CML LSCs, further emphasising the importance of our findings from a clinical perspective.

6.4 Tigecycline efficacy against TKI resistant cells

Overcoming drug resistance continues to be a major clinical challenge in many medical fields, including in CML. Often, resistance to current molecular targeted therapy in CML occurs by mutational changes in the BCR-ABL kinase domain in patients, such as the T315I mutation. While some of these patients can be treated with ponatinib (which inhibits the T315I mutant), others are resistant to all currently available TKIs and have no alternative treatment option. Indeed, some patients do not harbour any BCR-ABL kinase mutation that could explain their TKIs resistance and are believed to have acquired BCR-ABL independent mechanism of resistance. As such, targeting pathways independent of BCR-ABL kinase activity should be explored to overcome TKI resistance. Interestingly, our findings

revealed that tigecycline markedly reduced cell growth in primary stem cell-enriched CD34⁺ cells from CML patients. In addition, tigecycline reduced the ability of progenitors to form colonies to the same extent as imatinib. This suggests that the sole inhibition of mitochondrial function might have a significant effect against patient-derived CML cells. Therefore, we hypothesised that tigecycline, with a mechanism of action independent of BCR-ABL kinase activity, could be used as an alternative approach for targeting TKI-resistant CML cells.

To assess the effect of tigecycline on TKI-resistant cells, we used a human derived cell line that acquired resistance to all licensed TKIs following *in vitro* culturing in increasing concentration of ponatinib (KCL22^{PonRes}). The experiments presented in the next paragraph represents the “next step” and were performed by an undergraduate student, Lisa Malosse, under my laboratory supervision.

We first analysed the effect of imatinib, ponatinib and tigecycline on the proliferative capacity of TKI-resistant KCL22^{PonRes} and TKI-sensitive KCL22 cells. This revealed that EC50 values for imatinib and ponatinib were markedly increased in KCL22^{PonRes} compared to KCL22 WT cells, validating the resistance of KCL22^{PonRes} to currently available TKIs (**Fig. 6.1a-d**). On the contrary, tigecycline, with an IC50 value of 3.16 μ M, was able to inhibit KCL22^{PonRes} cell growth, indicating that tigecycline is able to impair proliferation of ponatinib-resistant cells at a concentration achievable *in vivo*. Interestingly, IC50 value for tigecycline was lower in KCL22^{PonRes} compared to KCL22 WT cells (**Fig. 6.1e,f**). Moreover, ponatinib as a single agent induced 40% of cell death in KCL22^{PonRes} cells, while it had only a modest effect in KCL22 WT cells (**Fig 6.2a,b**). The reasons behind the potential increased sensitivity of KCL22^{PonRes} to tigecycline are not yet fully understood. Nonetheless, these preliminary data suggest that inhibition of oxidative metabolism with tigecycline might a promising therapeutic strategy to target TKI-resistant cells. Further experiments should address this hypothesis in primary leukaemic cells isolated from CML patients not responding to TKI therapy and without detectable mutation in BCR-ABL kinase domain.

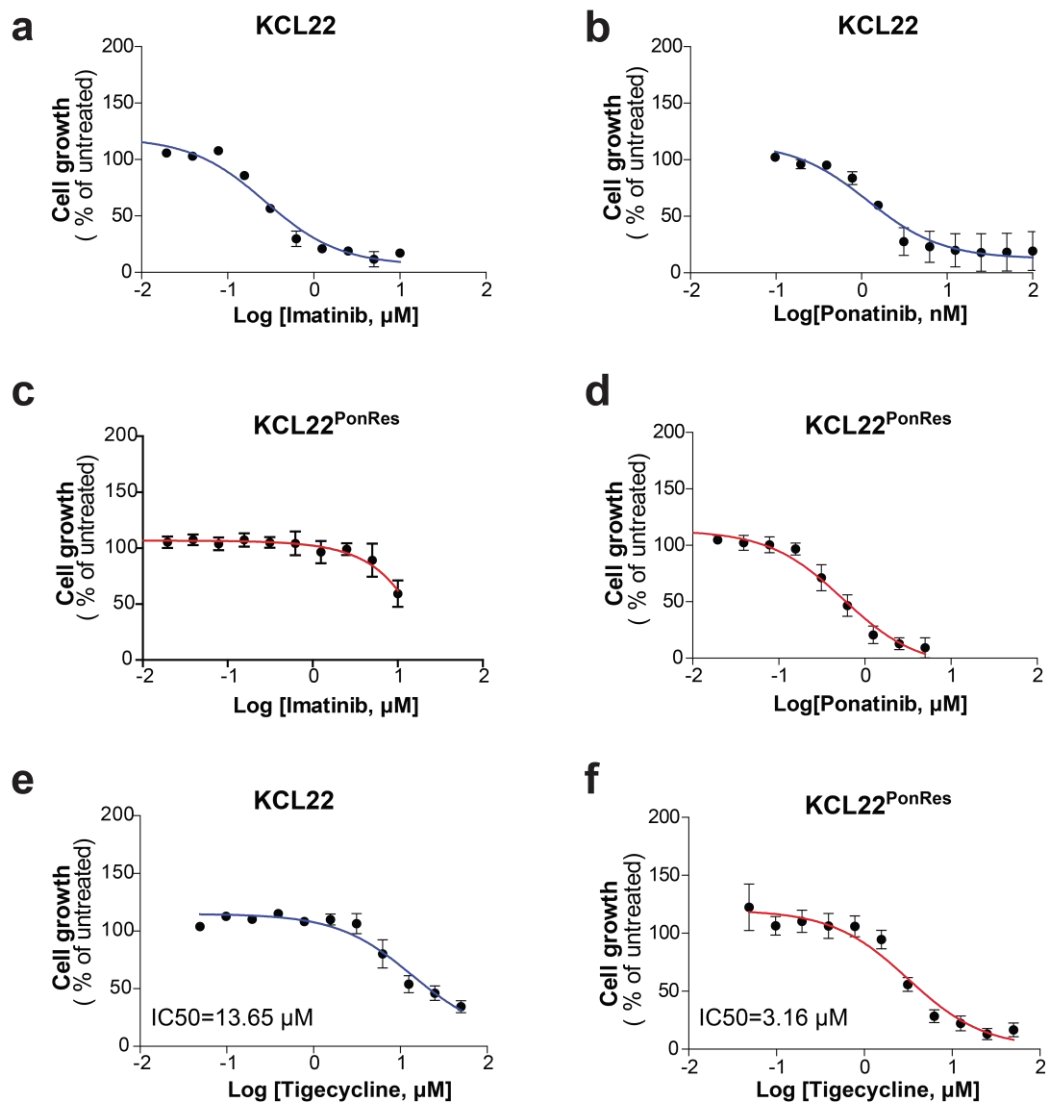


Figure 6. 1 Tigecycline impairs the proliferation of KCL22^{PonRes} cells.

(a-b) Proliferation of KCL22 cells upon exposure to various concentrations of (a) imatinib and (b) ponatinib for 72h. n=3 independent experiments. (c-d) Proliferation of KCL22^{PonRes} cells upon exposure to various concentrations of (c) imatinib and (d) ponatinib for 72h. n=3 independent experiments. (e-f) Proliferation of (e) KCL22 and (f) KCL22^{PonRes} cells upon exposure to various concentrations of tigecycline for 72 h. Data are presented as Mean \pm S.E.M.

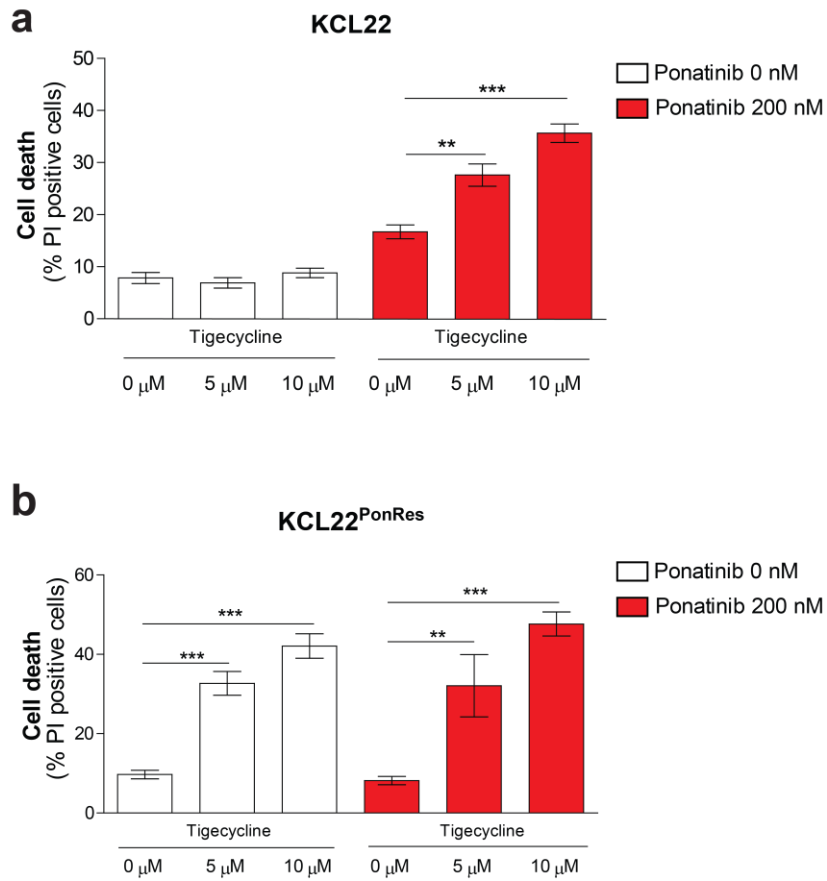


Figure 6. 2 Tigecycline targets KCL22^{PonRes} cells *in vitro*.

(a-b) Cell death in **(a)** KCL22 and **(b)** KCL22^{PonRes} cells following exposure with ponatinib (200 nM) and tigecycline (5 and 10 μM) for 72h. n=3 independent experiments. . **P<0.01; ***P<0.001, evaluated by one-way ANOVA with post hoc Bonferroni analysis.

6.5 Clinical applicability for tigecycline use

Tigecycline is already approved in the clinic for the treatment of complicated infections. Our study, demonstrating that tigecycline in combination with imatinib can target CML LSCs, might open new avenues for further investigation for the use of tigecycline in combination with imatinib in CML patients.

As mentioned previously, Škrtić *et al.* identified tigecycline from a chemical screening as a novel anticancer drug against AML cells (187). Motivated by positive pre-clinical results, Reed *et al.* next conducted a phase 1 study to determine the dose and safety profile of tigecycline use in AML patients (265). Tigecycline was administered five days per week intravenously for two weeks in 27 AML patients with relapsed or refractory disease. However, no significant clinical response was observed in any of the patients at end-point. Interestingly, this study reported a maximal plasma concentration of 12 μM at the 300 mg/day tigecycline dose in AML patients. However, at this concentration, the protein binding of tigecycline can exceed 87%. Moreover, tigecycline steady-state levels were approximately 1 μM at this dose, which did not show any efficacy against leukaemic cells in previous *in vitro* experiments (187). Accordingly, tigecycline treatment did not affect the expression of mitochondrial-encoded proteins in 24 out of 27 patients, indicating that the concentration achieved in AML patients was not sufficient to be effective and hit its target. Despite the negative outcome, future investigations should be conducted with the more stable tigecycline formulation, which could potentially result in a greater biological and clinical efficacy as an effective plasma concentration of tigecycline would be sustained for longer times. Moreover, the use of tigecycline as a single agent might not be adequate in the population of patients selected (i.e. heavily treated refractory and relapsed AML patients, with potential acquired drug resistance mechanism(s)). Combining tigecycline treatment with a second anticancer agent in a population of patients with stable disease might lead to a greater efficacy and clinical outcome, as the effective concentration of each single agent could be potentially lower when applied in combination. As such, more positive results might be obtained in studies testing the efficacy of the combination imatinib and tigecycline in CP-CML patients. Nevertheless, the intravenous mode of administration of tigecycline, together with its short half-life, might be too demanding for CP-CML patients responding to

TKI therapy (and could limit patient recruitment into a clinical trial) suggesting that combining tigecycline with TKI in patient who don't respond optimally to TKI treatment would be a better option. Of note, tigecycline has already been included in the following clinical trial grant: '*Defining leukaemic cell clonal architecture to inform and monitor drug responses in the Targeting Stem cell Resistance (TASTER) CML Phase II Clinical Trial*'. In this proposed study, the efficacy of novel agents, including tigecycline, in combination with TKI, will be evaluated in CML patients and against patient-derived CML stem cells using xenograft models.

6.6 Others inhibitors of oxidative metabolism

The direct clinical applicability of tigecycline and its reported effect as an inhibitor of mitochondrial metabolism *in vivo* made strong arguments for concentrating our research on this drug. Besides tigecycline and biguanides, other inhibitors of oxidative metabolism with antitumorigenic activity have been identified in recent studies. In this paragraph, we shall describe alternative inhibitors of oxidative metabolism that could potentially be tested against CML LSCs.

VLX600

To find novel agents against colon cancer, Zhang *et al.* performed a compound screen of 10,000 drugs and identified VLX600 with strong cytotoxic activity against quiescent colon cancer cells. The authors further demonstrated that VLX600 markedly impairs mitochondrial function by inhibiting the activity of complexes in the electron transport chain (266).

Gamitrinib

The chaperones heat shock protein-90 (HSP90) and tumour necrosis factor receptor-associated protein-1 (TRAP-1) play an important role in chaperoning the correct folding of ETC proteins. Inhibition of the HSP90 and TRAP-1 activity with gamitrinib, a small-molecule that accumulates in the mitochondria, induced a decrease in mitochondrial ATP production and in cancer cell growth across multiple experimental models (267-269).

CPT1a inhibitor

Finally, our metabolic profiling at steady-state in CD34⁻ CML, CD34⁺ CML and CD34⁺ normal cells revealed that FAO was significantly and selectively upregulated in primitive CD34⁺ CML cells. Therefore, inhibitors of FAO might show some clinical efficacy against CML LSCs and assessing the consequences of FAO inhibition could be an interesting topic of future investigation. Accordingly, inhibition of carnitine palmitoyl transferase 1a (CPT1a), a protein that catalyses the rate-limiting step for transfer of fatty acids into the mitochondria, induced cytostatic and cytotoxic effect in leukaemia cell lines and primary cells from AML patients (226, 270).

Accumulating evidence suggests that inhibiting mitochondrial metabolism can be a valuable therapeutic strategy in multiple experimental models of cancer. While further studies still need to assess the safety profile of these compounds in humans, their ability to inhibit oxidative metabolism may prove useful in targeting CML LSCs.

Given that many agents, including the ones cited above, might be too toxic for human use, repurposing drugs, such as tigecycline, has been seen as an attractive approach for cancer therapy. Indeed, only 8% of drugs that enter clinical investigation in humans manage to pass phase I clinical trials (271). Potentially, this number can be increased by using repurposed drugs, as they have already been tested and accepted for human use. In addition, the time between bench work and translation to the clinic is significantly reduced when using repurposed drugs in comparison to new agents. Interestingly, tigecycline efficacy in leukaemia was initially discovered by an FDA-approved drug screening in AML cells (187). This study, together with the work done in this thesis, where we have used the best pre-clinical CML model available, illustrates the potential of drug repurposing for anticancer therapy. It is hoped that this might prompt future investigation to test the effect of licensed drugs in stem cell-driven cancers or different malignancies and diseases in general.

6.7 Additional remarks

This study would not have been feasible without the access to primary patient-derived samples and as such without the collaboration with the NHS biorepository

department and access to the Paul O' Gorman research centre bio-bank. However, collection and isolation of primary cells comes with major challenges, including administrative tasks (ethics, written consent), and is often time-consuming. Nonetheless, primary material provides an invaluable pre-clinical resource to get insight into the biology of a given disease, which often compensates for the numerous challenges encountered. Indeed, this thesis demonstrates the value of combining the use of bio-banked samples together with advanced *in vitro* methodology and robust pre-clinical models to address a clinical question in a hypothesis-driven research project. Interestingly, the UK National Biobank has now collected biological specimens from over 500,000 people, which will enable the study of multi-factorial disease, such as cancer, and facilitate the discovery of new therapeutic targets and agents in the future (272).

Bibliography

1. Julien E, El Omar R, Tavian M. Origin of the hematopoietic system in the human embryo. *FEBS letters*. 2016;590(22):3987-4001.
2. Ciriza J, Thompson H, Petrosian R, Manilay JO, Garcia-Ojeda ME. The migration of hematopoietic progenitors from the fetal liver to the fetal bone marrow: lessons learned and possible clinical applications. *Experimental hematology*. 2013;41(5):411-23.
3. Becker AJ, McCulloch, Till JE. Cytological demonstration of the clonal nature of spleen colonies derived from transplanted mouse marrow cells. *Nature*. 1963;197:452-4.
4. Siminovitch L, McCulloch EA, Till JE. The Distribution of Colony-Forming Cells among Spleen Colonies. *Journal of cellular and comparative physiology*. 1963;62:327-36.
5. Till JE, McCulloch. A direct measurement of the radiation sensitivity of normal mouse bone marrow cells. *Radiation research*. 1961;14:213-22.
6. Morrison SJ, Uchida N, Weissman IL. The biology of hematopoietic stem cells. *Annual review of cell and developmental biology*. 1995;11:35-71.
7. Bryder D, Rossi DJ, Weissman IL. Hematopoietic stem cells: the paradigmatic tissue-specific stem cell. *The American journal of pathology*. 2006;169(2):338-46.
8. Morrison SJ, Kimble J. Asymmetric and symmetric stem-cell divisions in development and cancer. *Nature*. 2006;441(7097):1068-74.
9. Passegue E, Jamieson CH, Ailles LE, Weissman IL. Normal and leukemic hematopoiesis: are leukemias a stem cell disorder or a reacquisition of stem cell characteristics? *Proceedings of the National Academy of Sciences of the United States of America*. 2003;100 Suppl 1:11842-9.
10. Ito K, Suda T. Metabolic requirements for the maintenance of self-renewing stem cells. *Nature reviews Molecular cell biology*. 2014;15(4):243-56.
11. Anthony BA, Link DC. Regulation of hematopoietic stem cells by bone marrow stromal cells. *Trends in immunology*. 2014;35(1):32-7.
12. Adams GB, Scadden DT. The hematopoietic stem cell in its place. *Nature immunology*. 2006;7(4):333-7.
13. Silberstein LE, Lin CP. A new image of the hematopoietic stem cell vascular niche. *Cell stem cell*. 2013;13(5):514-6.
14. Spangrude GJ, Heimfeld S, Weissman IL. Purification and characterization of mouse hematopoietic stem cells. *Science*. 1988;241(4861):58-62.
15. Osawa M, Hanada K, Hamada H, Nakauchi H. Long-term lymphohematopoietic reconstitution by a single CD34-low/negative hematopoietic stem cell. *Science*. 1996;273(5272):242-5.
16. DiGiusto D, Chen S, Combs J, Webb S, Namikawa R, Tsukamoto A, et al. Human fetal bone marrow early progenitors for T, B, and myeloid cells are found exclusively in the population expressing high levels of CD34. *Blood*. 1994;84(2):421-32.
17. Baum CM, Weissman IL, Tsukamoto AS, Buckle AM, Peault B. Isolation of a candidate human hematopoietic stem-cell population. *Proceedings of the National Academy of Sciences of the United States of America*. 1992;89(7):2804-8.
18. Huang S, Terstappen LW. Lymphoid and myeloid differentiation of single human CD34+, HLA-DR+, CD38- hematopoietic stem cells. *Blood*. 1994;83(6):1515-26.
19. Hao QL, Thiemann FT, Petersen D, Smogorzewska EM, Crooks GM. Extended long-term culture reveals a highly quiescent and primitive human hematopoietic progenitor population. *Blood*. 1996;88(9):3306-13.
20. Wisniewski D, Affer M, Willshire J, Clarkson B. Further phenotypic characterization of the primitive lineage- CD34+CD38-CD90+CD45RA- hematopoietic stem cell/progenitor cell sub-population isolated from cord blood, mobilized peripheral blood and patients with chronic myelogenous leukemia. *Blood cancer journal*. 2011;1(9):e36.

21. Lapidot T, Sirard C, Vormoor J, Murdoch B, Hoang T, Caceres-Cortes J, et al. A cell initiating human acute myeloid leukaemia after transplantation into SCID mice. *Nature*. 1994;367(6464):645-8.
22. Bonnet D, Dick JE. Human acute myeloid leukemia is organized as a hierarchy that originates from a primitive hematopoietic cell. *Nature medicine*. 1997;3(7):730-7.
23. Al-Hajj M, Wicha MS, Benito-Hernandez A, Morrison SJ, Clarke MF. Prospective identification of tumorigenic breast cancer cells. *Proceedings of the National Academy of Sciences of the United States of America*. 2003;100(7):3983-8.
24. Gao MQ, Choi YP, Kang S, Youn JH, Cho NH. CD24+ cells from hierarchically organized ovarian cancer are enriched in cancer stem cells. *Oncogene*. 2010;29(18):2672-80.
25. Vincent Z, Urakami K, Maruyama K, Yamaguchi K, Kusuhara M. CD133-positive cancer stem cells from Colo205 human colon adenocarcinoma cell line show resistance to chemotherapy and display a specific metabolomic profile. *Genes & cancer*. 2014;5(7-8):250-60.
26. Ishikawa F, Yoshida S, Saito Y, Hijikata A, Kitamura H, Tanaka S, et al. Chemotherapy-resistant human AML stem cells home to and engraft within the bone-marrow endosteal region. *Nature biotechnology*. 2007;25(11):1315-21.
27. Saito Y, Kitamura H, Hijikata A, Tomizawa-Murasawa M, Tanaka S, Takagi S, et al. Identification of therapeutic targets for quiescent, chemotherapy-resistant human leukemia stem cells. *Science translational medicine*. 2010;2(17):17ra9.
28. Holyoake T, Jiang X, Eaves C, Eaves A. Isolation of a highly quiescent subpopulation of primitive leukemic cells in chronic myeloid leukemia. *Blood*. 1999;94(6):2056-64.
29. Holtz MS, Forman SJ, Bhatia R. Nonproliferating CML CD34+ progenitors are resistant to apoptosis induced by a wide range of proapoptotic stimuli. *Leukemia*. 2005;19(6):1034-41.
30. Visvader JE. Cells of origin in cancer. *Nature*. 2011;469(7330):314-22.
31. Takahashi K, Tanabe K, Ohnuki M, Narita M, Ichisaka T, Tomoda K, et al. Induction of pluripotent stem cells from adult human fibroblasts by defined factors. *Cell*. 2007;131(5):861-72.
32. Takahashi K, Yamanaka S. Induction of pluripotent stem cells from mouse embryonic and adult fibroblast cultures by defined factors. *Cell*. 2006;126(4):663-76.
33. Jamieson CH, Ailles LE, Dylla SJ, Muijtjens M, Jones C, Zehnder JL, et al. Granulocyte-macrophage progenitors as candidate leukemic stem cells in blast-crisis CML. *The New England journal of medicine*. 2004;351(7):657-67.
34. Miyamoto T, Weissman IL, Akashi K. AML1/ETO-expressing nonleukemic stem cells in acute myelogenous leukemia with 8;21 chromosomal translocation. *Proceedings of the National Academy of Sciences of the United States of America*. 2000;97(13):7521-6.
35. Valent P, Bonnet D, De Maria R, Lapidot T, Copland M, Melo JV, et al. Cancer stem cell definitions and terminology: the devil is in the details. *Nature reviews Cancer*. 2012;12(11):767-75.
36. Krivtsov AV, Twomey D, Feng Z, Stubbs MC, Wang Y, Faber J, et al. Transformation from committed progenitor to leukaemia stem cell initiated by MLL-AF9. *Nature*. 2006;442(7104):818-22.
37. Taussig DC, Miraki-Moud F, Anjos-Afonso F, Pearce DJ, Allen K, Ridler C, et al. Anti-CD38 antibody-mediated clearance of human repopulating cells masks the heterogeneity of leukemia-initiating cells. *Blood*. 2008;112(3):568-75.
38. Kennedy JA, Barabe F, Poepl AG, Wang JC, Dick JE. Comment on "Tumor growth need not be driven by rare cancer stem cells". *Science*. 2007;318(5857):1722; author reply
39. Schatton T, Murphy GF, Frank NY, Yamaura K, Waaga-Gasser AM, Gasser M, et al. Identification of cells initiating human melanomas. *Nature*. 2008;451(7176):345-9.
40. Quintana E, Shackleton M, Sabel MS, Fullen DR, Johnson TM, Morrison SJ. Efficient tumour formation by single human melanoma cells. *Nature*. 2008;456(7222):593-8.
41. Rohrbacher M, Hasford J. Epidemiology of chronic myeloid leukaemia (CML). *Best practice & research Clinical haematology*. 2009;22(3):295-302.
42. Harrison SJ, Johnson PR, Holyoake TL. The Scotland Leukaemia Registry audit of incidence, diagnosis and clinical management of new patients with chronic myeloid leukaemia in 1999 and 2000. *Scottish medical journal*. 2004;49(3):87-90.

43. Huang X, Cortes J, Kantarjian H. Estimations of the increasing prevalence and plateau prevalence of chronic myeloid leukemia in the era of tyrosine kinase inhibitor therapy. *Cancer*. 2012;118(12):3123-7.
44. Preston DL, Kusumi S, Tomonaga M, Izumi S, Ron E, Kuramoto A, et al. Cancer incidence in atomic bomb survivors. Part III. Leukemia, lymphoma and multiple myeloma, 1950-1987. *Radiation research*. 1994;137(2 Suppl):S68-97.
45. Vlaanderen J, Lan Q, Kromhout H, Rothman N, Vermeulen R. Occupational benzene exposure and the risk of chronic myeloid leukemia: a meta-analysis of cohort studies incorporating study quality dimensions. *American journal of industrial medicine*. 2012;55(9):779-85.
46. Kantarjian HM, Dixon D, Keating MJ, Talpaz M, Walters RS, McCredie KB, et al. Characteristics of accelerated disease in chronic myelogenous leukemia. *Cancer*. 1988;61(7):1441-6.
47. Jabbour E, Kantarjian H. Chronic myeloid leukemia: 2016 update on diagnosis, therapy, and monitoring. *American journal of hematology*. 2016;91(2):252-65.
48. Furtado VF, Santos GR, de Carvalho DS, Staziaki PV, Pasquini R, Funke VA. Accelerated phase chronic myeloid leukemia: evaluation of clinical criteria as predictors of survival, major cytogenetic response and progression to blast phase. *Revista brasileira de hematologia e hemoterapia*. 2015;37(5):341-7.
49. Hehlmann R, Saussele S. Treatment of chronic myeloid leukemia in blast crisis. *Haematologica*. 2008;93(12):1765-9.
50. Nowell PCH. D. A. A minute chromosome in human chronic granulocytic leukemia. *Science*. 1960

51. Nowell PC, Hungerford DA. Chromosome studies in human leukemia. II. Chronic granulocytic leukemia. *Journal of the National Cancer Institute*. 1961;27:1013-35.
52. Tough IM, Court Brown WM, Baikie AG, Buckton KE, Harnden DG, Jacobs PA, et al. Cytogenetic studies in chronic myeloid leukaemia and acute leukaemia associated with monogolism. *Lancet*. 1961;1(7174):411-7.
53. Rowley JD. Letter: A new consistent chromosomal abnormality in chronic myelogenous leukaemia identified by quinacrine fluorescence and Giemsa staining. *Nature*. 1973;243(5405):290-3.
54. de Klein A, van Kessel AG, Grosveld G, Bartram CR, Hagemeijer A, Bootsma D, et al. A cellular oncogene is translocated to the Philadelphia chromosome in chronic myelocytic leukaemia. *Nature*. 1982;300(5894):765-7.
55. Stam K, Heisterkamp N, Grosveld G, de Klein A, Verma RS, Coleman M, et al. Evidence of a new chimeric bcr/c-abl mRNA in patients with chronic myelocytic leukemia and the Philadelphia chromosome. *The New England journal of medicine*. 1985;313(23):1429-33.
56. Melo JV. The diversity of BCR-ABL fusion proteins and their relationship to leukemia phenotype. *Blood*. 1996;88(7):2375-84.
57. Daley GQ, Van Etten RA, Baltimore D. Induction of chronic myelogenous leukemia in mice by the P210bcr/abl gene of the Philadelphia chromosome. *Science*. 1990;247(4944):824-30.
58. Kelliher MA, McLaughlin J, Witte ON, Rosenberg N. Induction of a chronic myelogenous leukemia-like syndrome in mice with v-abl and BCR/ABL. *Proceedings of the National Academy of Sciences of the United States of America*. 1990;87(17):6649-53.
59. Gishizky ML, Johnson-White J, Witte ON. Evaluating the effect of P210 BCR/ABL on growth of hematopoietic progenitor cells and its role in the pathogenesis of human chronic myelogenous leukemia. *Seminars in hematology*. 1993;30(3 Suppl 3):6-8.
60. Fialkow PJ, Gartler SM, Yoshida A. Clonal origin of chronic myelocytic leukemia in man. *Proceedings of the National Academy of Sciences of the United States of America*. 1967;58(4):1468-71.

61. Fialkow PJ, Denman AM, Jacobson RJ, Lowenthal MN. Chronic myelocytic leukemia. Origin of some lymphocytes from leukemic stem cells. *The Journal of clinical investigation*. 1978;62(4):815-23.
62. Martin PJ, Najfeld V, Hansen JA, Penfold GK, Jacobson RJ, Fialkow PJ. Involvement of the B-lymphoid system in chronic myelogenous leukaemia. *Nature*. 1980;287(5777):49-50.
63. Abe A, Minami Y, Hayakawa F, Kitamura K, Nomura Y, Murata M, et al. Retention but significant reduction of BCR-ABL transcript in hematopoietic stem cells in chronic myelogenous leukemia after imatinib therapy. *International journal of hematology*. 2008;88(5):471-5.
64. Hughes T, Deininger M, Hochhaus A, Branford S, Radich J, Kaeda J, et al. Monitoring CML patients responding to treatment with tyrosine kinase inhibitors: review and recommendations for harmonizing current methodology for detecting BCR-ABL transcripts and kinase domain mutations and for expressing results. *Blood*. 2006;108(1):28-37.
65. Taagepera S, McDonald D, Loeb JE, Whitaker LL, McElroy AK, Wang JY, et al. Nuclear-cytoplasmic shuttling of C-ABL tyrosine kinase. *Proceedings of the National Academy of Sciences of the United States of America*. 1998;95(13):7457-62.
66. Melo JV, Deininger MW. Biology of chronic myelogenous leukemia--signaling pathways of initiation and transformation. *Hematology/oncology clinics of North America*. 2004;18(3):545-68, vii-viii.
67. Skorski T, Bellacosa A, Nieborowska-Skorska M, Majewski M, Martinez R, Choi JK, et al. Transformation of hematopoietic cells by BCR/ABL requires activation of a PI-3k/Akt-dependent pathway. *The EMBO journal*. 1997;16(20):6151-61.
68. Sillaber C, Gesbert F, Frank DA, Sattler M, Griffin JD. STAT5 activation contributes to growth and viability in Bcr/Abl-transformed cells. *Blood*. 2000;95(6):2118-25.
69. Pendergast AM, Quilliam LA, Cripe LD, Bassing CH, Dai Z, Li N, et al. BCR-ABL-induced oncogenesis is mediated by direct interaction with the SH2 domain of the GRB-2 adaptor protein. *Cell*. 1993;75(1):175-85.
70. Gale NW, Kaplan S, Lowenstein EJ, Schlessinger J, Bar-Sagi D. Grb2 mediates the EGF-dependent activation of guanine nucleotide exchange on Ras. *Nature*. 1993;363(6424):88-92.
71. Harvey Lodish AB, Lawrence Zipursky, Paul Matsudaira, David Baltimore, and James Darnell. *Molecular Cell Biology*. 4th edition. 2000.
72. Ilaria RL, Jr., Van Etten RA. P210 and P190(BCR/ABL) induce the tyrosine phosphorylation and DNA binding activity of multiple specific STAT family members. *The Journal of biological chemistry*. 1996;271(49):31704-10.
73. Sawyers CL, Callahan W, Witte ON. Dominant negative MYC blocks transformation by ABL oncogenes. *Cell*. 1992;70(6):901-10.
74. Rushing D, Goldman A, Gibbs G, Howe R, Kennedy BJ. Hydroxyurea versus busulfan in the treatment of chronic myelogenous leukemia. *American journal of clinical oncology*. 1982;5(3):307-13.
75. Hehlmann R, Heimpel H, Hasford J, Kolb HJ, Pralle H, Hossfeld DK, et al. Randomized comparison of busulfan and hydroxyurea in chronic myelogenous leukemia: prolongation of survival by hydroxyurea. The German CML Study Group. *Blood*. 1993;82(2):398-407.
76. Clift RA, Appelbaum FR, Thomas ED. Treatment of chronic myeloid leukemia by marrow transplantation. *Blood*. 1993;82(7):1954-6.
77. Jain N, van Besien K. Chronic myelogenous leukemia: role of stem cell transplant in the imatinib era. *Hematology/oncology clinics of North America*. 2011;25(5):1025-48, vi.
78. Verma DS, Spitzer G, Gutterman JU, Zander AR, McCredie KB, Dicke KA. Human leukocyte interferon preparation blocks granulopoietic differentiation. *Blood*. 1979;54(6):1423-7.
79. Italian Cooperative Study Group on Chronic Myeloid L, Tura S, Baccarani M, Zuffa E, Russo D, Fanin R, et al. Interferon alfa-2a as compared with conventional chemotherapy for the treatment of chronic myeloid leukemia. *The New England journal of medicine*. 1994;330(12):820-5.
80. Hehlmann R, Heimpel H, Hasford J, Kolb HJ, Pralle H, Hossfeld DK, et al. Randomized comparison of interferon-alpha with busulfan and hydroxyurea in chronic myelogenous leukemia. The German CML Study Group. *Blood*. 1994;84(12):4064-77.

81. Ohnishi K, Ohno R, Tomonaga M, Kamada N, Onozawa K, Kuramoto A, et al. A randomized trial comparing interferon-alpha with busulfan for newly diagnosed chronic myelogenous leukemia in chronic phase. *Blood*. 1995;86(3):906-16.
82. Randomized study on hydroxyurea alone versus hydroxyurea combined with low-dose interferon-alpha 2b for chronic myeloid leukemia. The Benelux CML Study Group. *Blood*. 1998;91(8):2713-21.
83. Broustet A, Reiffers J, Marit G, Fiere D, Jaubert J, Reynaud J, et al. Hydroxyurea versus interferon alfa-2b in chronic myelogenous leukaemia: preliminary results of an open French multicentre randomized study. *European journal of cancer*. 1991;27 Suppl 4:S18-21.
84. Kantarjian HM, O'Brien S, Cortes JE, Shan J, Giles FJ, Rios MB, et al. Complete cytogenetic and molecular responses to interferon-alpha-based therapy for chronic myelogenous leukemia are associated with excellent long-term prognosis. *Cancer*. 2003;97(4):1033-41.
85. Baccarani M, Rosti G, de Vivo A, Bonifazi F, Russo D, Martinelli G, et al. A randomized study of interferon-alpha versus interferon-alpha and low-dose arabinosyl cytosine in chronic myeloid leukemia. *Blood*. 2002;99(5):1527-35.
86. Tothova E, Fricova M, Kafkova A, Stecova N, Guman T, Raffac S, et al. Hematological and cytogenetic response of interferon alpha 2b alone and combined interferon alpha plus cytarabine as a first-line treatment in chronic myeloid leukemia. *Neoplasma*. 2000;47(2):125-8.
87. Dowding C, Gordon M, Guo AP, Maison D, Osterholz J, Siczkowski M, et al. Potential mechanisms of action of interferon-alpha in CML. *Leukemia & lymphoma*. 1993;11 Suppl 1:185-91.
88. Weng K, Xie X, Qiu G, Gu W. Clinical reagents of GM-CSF and IFN-alpha induce the generation of functional chronic myeloid leukemia dendritic cells in vitro. *Cytotechnology*. 2012;64(1):75-81.
89. Bhatia R, Verfaillie CM. The effect of interferon-alpha on beta-1 integrin mediated adhesion and growth regulation in chronic myelogenous leukemia. *Leukemia & lymphoma*. 1998;28(3-4):241-54.
90. Druker BJ, Tamura S, Buchdunger E, Ohno S, Segal GM, Fanning S, et al. Effects of a selective inhibitor of the Abl tyrosine kinase on the growth of Bcr-Abl positive cells. *Nature medicine*. 1996;2(5):561-6.
91. Druker BJ, Talpaz M, Resta DJ, Peng B, Buchdunger E, Ford JM, et al. Efficacy and safety of a specific inhibitor of the BCR-ABL tyrosine kinase in chronic myeloid leukemia. *The New England journal of medicine*. 2001;344(14):1031-7.
92. O'Brien SG, Guilhot F, Larson RA, Gathmann I, Baccarani M, Cervantes F, et al. Imatinib compared with interferon and low-dose cytarabine for newly diagnosed chronic-phase chronic myeloid leukemia. *The New England journal of medicine*. 2003;348(11):994-1004.
93. Hochhaus A, O'Brien SG, Guilhot F, Druker BJ, Branford S, Foroni L, et al. Six-year follow-up of patients receiving imatinib for the first-line treatment of chronic myeloid leukemia. *Leukemia*. 2009;23(6):1054-61.
94. Baccarani M, Deininger MW, Rosti G, Hochhaus A, Soverini S, Apperley JF, et al. European LeukemiaNet recommendations for the management of chronic myeloid leukemia: 2013. *Blood*. 2013;122(6):872-84.
95. Yang K, Fu LW. Mechanisms of resistance to BCR-ABL TKIs and the therapeutic strategies: A review. *Critical reviews in oncology/hematology*. 2015;93(3):277-92.
96. Branford S, Rudzki Z, Walsh S, Grigg A, Arthur C, Taylor K, et al. High frequency of point mutations clustered within the adenosine triphosphate-binding region of BCR/ABL in patients with chronic myeloid leukemia or Ph-positive acute lymphoblastic leukemia who develop imatinib (STI571) resistance. *Blood*. 2002;99(9):3472-5.
97. Cowan-Jacob SW, Guez V, Fendrich G, Griffin JD, Fabbro D, Furet P, et al. Imatinib (STI571) resistance in chronic myelogenous leukemia: molecular basis of the underlying mechanisms and potential strategies for treatment. *Mini reviews in medicinal chemistry*. 2004;4(3):285-99.
98. Shah NP, Nicoll JM, Nagar B, Gorre ME, Paquette RL, Kuriyan J, et al. Multiple BCR-ABL kinase domain mutations confer polyclonal resistance to the tyrosine kinase inhibitor imatinib (STI571) in chronic phase and blast crisis chronic myeloid leukemia. *Cancer cell*. 2002;2(2):117-25.

99. Gorre ME, Mohammed M, Ellwood K, Hsu N, Paquette R, Rao PN, et al. Clinical resistance to STI-571 cancer therapy caused by BCR-ABL gene mutation or amplification. *Science*. 2001;293(5531):876-80.
100. Quintas-Cardama A, Kantarjian HM, Cortes JE. Mechanisms of primary and secondary resistance to imatinib in chronic myeloid leukemia. *Cancer control : journal of the Moffitt Cancer Center*. 2009;16(2):122-31.
101. Barnes DJ, Palaiologou D, Panousopoulou E, Schultheis B, Yong AS, Wong A, et al. Bcr-Abl expression levels determine the rate of development of resistance to imatinib mesylate in chronic myeloid leukemia. *Cancer research*. 2005;65(19):8912-9.
102. Hochhaus A, Kreil S, Corbin AS, La Rosee P, Muller MC, Lahaye T, et al. Molecular and chromosomal mechanisms of resistance to imatinib (STI571) therapy. *Leukemia*. 2002;16(11):2190-6.
103. Larson RA, Druker BJ, Guilhot F, O'Brien SG, Riviere GJ, Krahnke T, et al. Imatinib pharmacokinetics and its correlation with response and safety in chronic-phase chronic myeloid leukemia: a subanalysis of the IRIS study. *Blood*. 2008;111(8):4022-8.
104. Peng B, Hayes M, Resta D, Racine-Poon A, Druker BJ, Talpaz M, et al. Pharmacokinetics and pharmacodynamics of imatinib in a phase I trial with chronic myeloid leukemia patients. *Journal of clinical oncology : official journal of the American Society of Clinical Oncology*. 2004;22(5):935-42.
105. Marin D, Bazeos A, Mahon FX, Eliasson L, Milojkovic D, Bua M, et al. Adherence is the critical factor for achieving molecular responses in patients with chronic myeloid leukemia who achieve complete cytogenetic responses on imatinib. *Journal of clinical oncology : official journal of the American Society of Clinical Oncology*. 2010;28(14):2381-8.
106. Watkins DB, Hughes TP, White DL. OCT1 and imatinib transport in CML: is it clinically relevant? *Leukemia*. 2015;29(10):1960-9.
107. Cortes J, O'Dwyer ME. Clonal evolution in chronic myelogenous leukemia. *Hematology/oncology clinics of North America*. 2004;18(3):671-84, x.
108. Kantarjian HM, Hochhaus A, Saglio G, De Souza C, Flinn IW, Stenke L, et al. Nilotinib versus imatinib for the treatment of patients with newly diagnosed chronic phase, Philadelphia chromosome-positive, chronic myeloid leukaemia: 24-month minimum follow-up of the phase 3 randomised ENESTnd trial. *The Lancet Oncology*. 2011;12(9):841-51.
109. Hochhaus A, Saglio G, Hughes TP, Larson RA, Kim DW, Issaragrisil S, et al. Long-term benefits and risks of frontline nilotinib vs imatinib for chronic myeloid leukemia in chronic phase: 5-year update of the randomized ENESTnd trial. *Leukemia*. 2016;30(5):1044-54.
110. Wei G, Rafiyath S, Liu D. First-line treatment for chronic myeloid leukemia: dasatinib, nilotinib, or imatinib. *Journal of hematology & oncology*. 2010;3:47.
111. Kantarjian H, Shah NP, Hochhaus A, Cortes J, Shah S, Ayala M, et al. Dasatinib versus imatinib in newly diagnosed chronic-phase chronic myeloid leukemia. *The New England journal of medicine*. 2010;362(24):2260-70.
112. Fujisawa S, Nakamae H, Ogura M, Ishizawa K, Taniwaki M, Utsunomiya A, et al. Efficacy and safety of dasatinib versus imatinib in Japanese patients with newly diagnosed chronic-phase chronic myeloid leukemia (CML-CP): Subset analysis of the DASISION trial with 2-year follow-up. *International journal of hematology*. 2014;99(2):141-53.
113. Cortes JE, Kim DW, Kantarjian HM, Brummendorf TH, Dyagil I, Griskevicius L, et al. Bosutinib versus imatinib in newly diagnosed chronic-phase chronic myeloid leukemia: results from the BELA trial. *Journal of clinical oncology : official journal of the American Society of Clinical Oncology*. 2012;30(28):3486-92.
114. Tim H. Brümmendorf JEC, H. Jean Khoury, Hagop M. Kantarjian, Dong-Wook Kim, Philippe Schafhausen, Mirjana Zeremski, Mark Shapiro, Eric Leip, Carlo Gambacorti-Passerini and Jeffrey H. Lipton. Bosutinib As Second-Line Therapy in Patients (Pts) with Chronic Phase Chronic Myeloid Leukemia (CP CML) Resistant or Intolerant to Prior Imatinib: 60-Month Update of a Phase 1/2 Study. *Blood*. 2014;124.
115. Labs. P. Bosulif (bosutinib) package insert. <http://labelingpfizercom/ShowLabeling.aspx?id=884>. 2015.

116. O'Hare T, Shakespeare WC, Zhu X, Eide CA, Rivera VM, Wang F, et al. AP24534, a pan-BCR-ABL inhibitor for chronic myeloid leukemia, potently inhibits the T315I mutant and overcomes mutation-based resistance. *Cancer cell*. 2009;16(5):401-12.
117. Khoury HJ CJ, Kim DW. . Analysis of the cardiovascular risk profile of Ph⁺ leukemia patients treated with ponatinib
American journal of clinical oncology. 2013.
118. Prasad V, Mailankody S. The accelerated approval of oncologic drugs: lessons from ponatinib. *Jama*. 2014;311(4):353-4.
119. Ariad Ends Phase III Leukemia Drug Trial. *Genetic Engineering and Biotechnology News*. 2013.
120. Mahon FX, Rea D, Guilhot J, Guilhot F, Huguet F, Nicolini F, et al. Discontinuation of imatinib in patients with chronic myeloid leukaemia who have maintained complete molecular remission for at least 2 years: the prospective, multicentre Stop Imatinib (STIM) trial. *The Lancet Oncology*. 2010;11(11):1029-35.
121. Ross DM, Branford S, Seymour JF, Schwarzer AP, Arthur C, Yeung DT, et al. Safety and efficacy of imatinib cessation for CML patients with stable undetectable minimal residual disease: results from the TWISTER study. *Blood*. 2013;122(4):515-22.
122. Chomel JC, Bonnet ML, Sorel N, Sloma I, Bennaceur-Griscelli A, Rea D, et al. Leukemic stem cell persistence in chronic myeloid leukemia patients in deep molecular response induced by tyrosine kinase inhibitors and the impact of therapy discontinuation. *Oncotarget*. 2016;7(23):35293-301.
123. Corbin AS, Agarwal A, Loriaux M, Cortes J, Deininger MW, Druker BJ. Human chronic myeloid leukemia stem cells are insensitive to imatinib despite inhibition of BCR-ABL activity. *The Journal of clinical investigation*. 2011;121(1):396-409.
124. Copland M, Hamilton A, Elrick LJ, Baird JW, Allan EK, Jordanides N, et al. Dasatinib (BMS-354825) targets an earlier progenitor population than imatinib in primary CML but does not eliminate the quiescent fraction. *Blood*. 2006;107(11):4532-9.
125. Graham SM, Jorgensen HG, Allan E, Pearson C, Alcorn MJ, Richmond L, et al. Primitive, quiescent, Philadelphia-positive stem cells from patients with chronic myeloid leukemia are insensitive to STI571 in vitro. *Blood*. 2002;99(1):319-25.
126. Hamilton A, Helgason GV, Schemionek M, Zhang B, Myssina S, Allan EK, et al. Chronic myeloid leukemia stem cells are not dependent on Bcr-Abl kinase activity for their survival. *Blood*. 2012;119(6):1501-10.
127. Jorgensen HG, Allan EK, Jordanides NE, Mountford JC, Holyoake TL. Nilotinib exerts equipotent antiproliferative effects to imatinib and does not induce apoptosis in CD34⁺ CML cells. *Blood*. 2007;109(9):4016-9.
128. Zhang B, Strauss AC, Chu S, Li M, Ho Y, Shiang KD, et al. Effective targeting of quiescent chronic myelogenous leukemia stem cells by histone deacetylase inhibitors in combination with imatinib mesylate. *Cancer cell*. 2010;17(5):427-42.
129. Chen Y, Hu Y, Zhang H, Peng C, Li S. Loss of the Alox5 gene impairs leukemia stem cells and prevents chronic myeloid leukemia. *Nature genetics*. 2009;41(7):783-92.
130. Zhao C, Chen A, Jamieson CH, Fereshteh M, Abrahamsson A, Blum J, et al. Hedgehog signalling is essential for maintenance of cancer stem cells in myeloid leukaemia. *Nature*. 2009;458(7239):776-9.
131. Neil P. Shah JEC, Giovanni Martinelli, B. Douglas Smith, Emer Clarke, Mhairi Copland, Lewis Strauss and Moshe Talpaz. Dasatinib Plus Smoothed (SMO) Inhibitor BMS-833923 in Chronic Myeloid Leukemia (CML) with Resistance or Suboptimal Response to a Prior Tyrosine Kinase Inhibitor (TKI): Phase I Study CA180323. *Blood*. 2014;124:4539.
132. Prost S, Relouzat F, Spentchian M, Ouzegdouh Y, Saliba J, Massonnet G, et al. Erosion of the chronic myeloid leukaemia stem cell pool by PPAR γ agonists. *Nature*. 2015;525(7569):380-3.
133. Rousselot P, Prost S, Guilhot J, Roy L, Etienne G, Legros L, et al. Pioglitazone together with imatinib in chronic myeloid leukemia: A proof of concept study. *Cancer*. 2017;123(10):1791-9.

134. Abraham SA, Hopcroft LE, Carrick E, Drotar ME, Dunn K, Williamson AJ, et al. Dual targeting of p53 and c-MYC selectively eliminates leukaemic stem cells. *Nature*. 2016;534(7607):341-6.
135. Berg JM TJ, Stryer L. *Biochemistry*. 5th edition. 2002.
136. Nicholson JK, Lindon JC, Holmes E. 'Metabonomics': understanding the metabolic responses of living systems to pathophysiological stimuli via multivariate statistical analysis of biological NMR spectroscopic data. *Xenobiotica; the fate of foreign compounds in biological systems*. 1999;29(11):1181-9.
137. Winkler IG, Barbier V, Wadley R, Zannettino AC, Williams S, Levesque JP. Positioning of bone marrow hematopoietic and stromal cells relative to blood flow in vivo: serially reconstituting hematopoietic stem cells reside in distinct nonperfused niches. *Blood*. 2010;116(3):375-85.
138. Parmar K, Mauch P, Vergilio JA, Sackstein R, Down JD. Distribution of hematopoietic stem cells in the bone marrow according to regional hypoxia. *Proceedings of the National Academy of Sciences of the United States of America*. 2007;104(13):5431-6.
139. Suda T, Takubo K, Semenza GL. Metabolic regulation of hematopoietic stem cells in the hypoxic niche. *Cell stem cell*. 2011;9(4):298-310.
140. Simsek T, Kocabas F, Zheng JK, DeBerardinis RJ, Mahmoud AI, Olson EN, et al. The Distinct Metabolic Profile of Hematopoietic Stem Cells Reflects Their Location in a Hypoxic Niche. *Cell stem cell*. 2010;7(3):380-90.
141. Shima H, Takubo K, Iwasaki H, Yoshihara H, Gomei Y, Hosokawa K, et al. Reconstitution activity of hypoxic cultured human cord blood CD34-positive cells in NOG mice. *Biochemical and biophysical research communications*. 2009;378(3):467-72.
142. Nombela-Arrieta C, Pivarnik G, Winkel B, Canty KJ, Harley B, Mahoney JE, et al. Quantitative imaging of haematopoietic stem and progenitor cell localization and hypoxic status in the bone marrow microenvironment. *Nature cell biology*. 2013;15(5):533-43.
143. Takubo K, Goda N, Yamada W, Iriuchishima H, Ikeda E, Kubota Y, et al. Regulation of the HIF-1alpha level is essential for hematopoietic stem cells. *Cell stem cell*. 2010;7(3):391-402.
144. Kiel MJ, Yilmaz OH, Iwashita T, Yilmaz OH, Terhorst C, Morrison SJ. SLAM family receptors distinguish hematopoietic stem and progenitor cells and reveal endothelial niches for stem cells. *Cell*. 2005;121(7):1109-21.
145. Spencer JA, Ferraro F, Roussakis E, Klein A, Wu J, Runnels JM, et al. Direct measurement of local oxygen concentration in the bone marrow of live animals. *Nature*. 2014;508(7495):269-73.
146. Takubo K, Nagamatsu G, Kobayashi CI, Nakamura-Ishizu A, Kobayashi H, Ikeda E, et al. Regulation of glycolysis by Pdk functions as a metabolic checkpoint for cell cycle quiescence in hematopoietic stem cells. *Cell stem cell*. 2013;12(1):49-61.
147. Warr MR, Passegue E. Metabolic makeover for HSCs. *Cell stem cell*. 2013;12(1):1-3.
148. Yu WM, Liu X, Shen J, Jovanovic O, Pohl EE, Gerson SL, et al. Metabolic regulation by the mitochondrial phosphatase PTPMT1 is required for hematopoietic stem cell differentiation. *Cell stem cell*. 2013;12(1):62-74.
149. Katajisto P, Dohla J, Chaffer CL, Pentinmikko N, Marjanovic N, Iqbal S, et al. Stem cells. Asymmetric apportioning of aged mitochondria between daughter cells is required for stemness. *Science*. 2015;348(6232):340-3.
150. Ito K, Bernardi R, Morotti A, Matsuoka S, Saglio G, Ikeda Y, et al. PML targeting eradicates quiescent leukaemia-initiating cells. *Nature*. 2008;453(7198):1072-8.
151. Ito K, Carracedo A, Weiss D, Arai F, Ala U, Avigan DE, et al. A PML-PPAR-delta pathway for fatty acid oxidation regulates hematopoietic stem cell maintenance. *Nature medicine*. 2012;18(9):1350-8.
152. Frauwirth KA, Thompson CB. Regulation of T lymphocyte metabolism. *Journal of immunology*. 2004;172(8):4661-5.
153. Rathmell JC, Vander Heiden MG, Harris MH, Frauwirth KA, Thompson CB. In the absence of extrinsic signals, nutrient utilization by lymphocytes is insufficient to maintain either cell size or viability. *Molecular cell*. 2000;6(3):683-92.
154. Fox CJ, Hammerman PS, Thompson CB. Fuel feeds function: energy metabolism and the T-cell response. *Nature reviews Immunology*. 2005;5(11):844-52.

155. Dang CV. Links between metabolism and cancer. *Genes & development*. 2012;26(9):877-90.
156. Ward PS, Thompson CB. Metabolic reprogramming: a cancer hallmark even warburg did not anticipate. *Cancer cell*. 2012;21(3):297-308.
157. Pavlova NN, Thompson CB. The Emerging Hallmarks of Cancer Metabolism. *Cell metabolism*. 2016;23(1):27-47.
158. Wong KK, Engelman JA, Cantley LC. Targeting the PI3K signaling pathway in cancer. *Current opinion in genetics & development*. 2010;20(1):87-90.
159. Elstrom RL, Bauer DE, Buzzai M, Karnauskas R, Harris MH, Plas DR, et al. Akt stimulates aerobic glycolysis in cancer cells. *Cancer research*. 2004;64(11):3892-9.
160. Robey RB, Hay N. Is Akt the "Warburg kinase"?-Akt-energy metabolism interactions and oncogenesis. *Seminars in cancer biology*. 2009;19(1):25-31.
161. Dang CV, O'Donnell KA, Zeller KI, Nguyen T, Osthus RC, Li F. The c-Myc target gene network. *Seminars in cancer biology*. 2006;16(4):253-64.
162. Kim JW, Gao P, Liu YC, Semenza GL, Dang CV. Hypoxia-inducible factor 1 and dysregulated c-Myc cooperatively induce vascular endothelial growth factor and metabolic switches hexokinase 2 and pyruvate dehydrogenase kinase 1. *Molecular and cellular biology*. 2007;27(21):7381-93.
163. Gao P, Tchernyshyov I, Chang TC, Lee YS, Kita K, Ochi T, et al. c-Myc suppression of miR-23a/b enhances mitochondrial glutaminase expression and glutamine metabolism. *Nature*. 2009;458(7239):762-5.
164. Cantor JR, Sabatini DM. Cancer cell metabolism: one hallmark, many faces. *Cancer discovery*. 2012;2(10):881-98.
165. Warburg O. On the origin of cancer cells. *Science*. 1956;123(3191):309-14.
166. Wallace DC. Mitochondria and cancer. *Nature reviews Cancer*. 2012;12(10):685-98.
167. Warburg O. On respiratory impairment in cancer cells. *Science*. 1956;124(3215):269-70.
168. Gallamini A, Zwarthoed C, Borra A. Positron Emission Tomography (PET) in Oncology. *Cancers*. 2014;6(4):1821-89.
169. Firth JD, Ebert BL, Pugh CW, Ratcliffe PJ. Oxygen-regulated control elements in the phosphoglycerate kinase 1 and lactate dehydrogenase A genes: similarities with the erythropoietin 3' enhancer. *Proceedings of the National Academy of Sciences of the United States of America*. 1994;91(14):6496-500.
170. Semenza GL, Jiang BH, Leung SW, Passantino R, Concordet JP, Maire P, et al. Hypoxia response elements in the aldolase A, enolase 1, and lactate dehydrogenase A gene promoters contain essential binding sites for hypoxia-inducible factor 1. *The Journal of biological chemistry*. 1996;271(51):32529-37.
171. Obach M, Navarro-Sabate A, Caro J, Kong X, Duran J, Gomez M, et al. 6-Phosphofructo-2-kinase (pfkfb3) gene promoter contains hypoxia-inducible factor-1 binding sites necessary for transactivation in response to hypoxia. *The Journal of biological chemistry*. 2004;279(51):53562-70.
172. Marin-Hernandez A, Gallardo-Perez JC, Ralph SJ, Rodriguez-Enriquez S, Moreno-Sanchez R. HIF-1alpha modulates energy metabolism in cancer cells by inducing over-expression of specific glycolytic isoforms. *Mini reviews in medicinal chemistry*. 2009;9(9):1084-101.
173. Ros S, Schulze A. Balancing glycolytic flux: the role of 6-phosphofructo-2-kinase/fructose 2,6-bisphosphatases in cancer metabolism. *Cancer & metabolism*. 2013;1(1):8.
174. Yalcin A, Telang S, Clem B, Chesney J. Regulation of glucose metabolism by 6-phosphofructo-2-kinase/fructose-2,6-bisphosphatases in cancer. *Experimental and molecular pathology*. 2009;86(3):174-9.
175. Bensaad K, Tsuruta A, Selak MA, Vidal MN, Nakano K, Bartrons R, et al. TIGAR, a p53-inducible regulator of glycolysis and apoptosis. *Cell*. 2006;126(1):107-20.
176. Zhao YH, Zhou M, Liu H, Ding Y, Khong HT, Yu D, et al. Upregulation of lactate dehydrogenase A by ErbB2 through heat shock factor 1 promotes breast cancer cell glycolysis and growth. *Oncogene*. 2009;28(42):3689-701.

177. Shim H, Dolde C, Lewis BC, Wu CS, Dang G, Jungmann RA, et al. c-Myc transactivation of LDH-A: implications for tumor metabolism and growth. *Proceedings of the National Academy of Sciences of the United States of America*. 1997;94(13):6658-63.
178. Semenza GL, Roth PH, Fang HM, Wang GL. Transcriptional regulation of genes encoding glycolytic enzymes by hypoxia-inducible factor 1. *The Journal of biological chemistry*. 1994;269(38):23757-63.
179. Martinez-Reyes I, Diebold LP, Kong H, Schieber M, Huang H, Hensley CT, et al. TCA Cycle and Mitochondrial Membrane Potential Are Necessary for Diverse Biological Functions. *Molecular cell*. 2016;61(2):199-209.
180. DeBerardinis RJ, Chandel NS. Fundamentals of cancer metabolism. *Science advances*. 2016;2(5):e1600200.
181. Weinberg F, Hamanaka R, Wheaton WW, Weinberg S, Joseph J, Lopez M, et al. Mitochondrial metabolism and ROS generation are essential for Kras-mediated tumorigenicity. *Proceedings of the National Academy of Sciences of the United States of America*. 2010;107(19):8788-93.
182. Wise DR, DeBerardinis RJ, Mancuso A, Sayed N, Zhang XY, Pfeiffer HK, et al. Myc regulates a transcriptional program that stimulates mitochondrial glutaminolysis and leads to glutamine addiction. *Proceedings of the National Academy of Sciences of the United States of America*. 2008;105(48):18782-7.
183. Vazquez F, Lim JH, Chim H, Bhalla K, Girnun G, Pierce K, et al. PGC1alpha expression defines a subset of human melanoma tumors with increased mitochondrial capacity and resistance to oxidative stress. *Cancer cell*. 2013;23(3):287-301.
184. Zaugg K, Yao Y, Reilly PT, Kannan K, Kiarash R, Mason J, et al. Carnitine palmitoyltransferase 1C promotes cell survival and tumor growth under conditions of metabolic stress. *Genes & development*. 2011;25(10):1041-51.
185. Reilly PT, Mak TW. Molecular pathways: tumor cells Co-opt the brain-specific metabolism gene CPT1C to promote survival. *Clinical cancer research : an official journal of the American Association for Cancer Research*. 2012;18(21):5850-5.
186. Sancho P, Burgos-Ramos E, Tavera A, Bou Kheir T, Jagust P, Schoenhals M, et al. MYC/PGC-1alpha Balance Determines the Metabolic Phenotype and Plasticity of Pancreatic Cancer Stem Cells. *Cell metabolism*. 2015;22(4):590-605.
187. Skrtic M, Sriskanthadevan S, Jhas B, Gebbia M, Wang X, Wang Z, et al. Inhibition of mitochondrial translation as a therapeutic strategy for human acute myeloid leukemia. *Cancer cell*. 2011;20(5):674-88.
188. Lagadinou ED, Sach A, Callahan K, Rossi RM, Neering SJ, Minhajuddin M, et al. BCL-2 inhibition targets oxidative phosphorylation and selectively eradicates quiescent human leukemia stem cells. *Cell stem cell*. 2013;12(3):329-41.
189. Viale A, Pettazoni P, Lyssiotis CA, Ying H, Sanchez N, Marchesini M, et al. Oncogene ablation-resistant pancreatic cancer cells depend on mitochondrial function. *Nature*. 2014;514(7524):628-32.
190. Ippolito L, Marini A, Cavallini L, Morandi A, Pietrovito L, Pintus G, et al. Metabolic shift toward oxidative phosphorylation in docetaxel resistant prostate cancer cells. *Oncotarget*. 2016;7(38):61890-904.
191. Caro P, Kishan AU, Norberg E, Stanley IA, Chapuy B, Ficarro SB, et al. Metabolic signatures uncover distinct targets in molecular subsets of diffuse large B cell lymphoma. *Cancer cell*. 2012;22(4):547-60.
192. Norberg E, Lako A, Chen PH, Stanley IA, Zhou F, Ficarro SB, et al. Differential contribution of the mitochondrial translation pathway to the survival of diffuse large B-cell lymphoma subsets. *Cell death and differentiation*. 2017;24(2):251-62.
193. Gaude E, Frezza C. Defects in mitochondrial metabolism and cancer. *Cancer & metabolism*. 2014;2:10.
194. Niemann S, Muller U. Mutations in SDHC cause autosomal dominant paraganglioma, type 3. *Nature genetics*. 2000;26(3):268-70.

195. Astuti D, Latif F, Dallol A, Dahia PL, Douglas F, George E, et al. Gene mutations in the succinate dehydrogenase subunit SDHB cause susceptibility to familial pheochromocytoma and to familial paraganglioma. *American journal of human genetics*. 2001;69(1):49-54.
196. Frezza C, Pollard PJ, Gottlieb E. Inborn and acquired metabolic defects in cancer. *Journal of molecular medicine*. 2011;89(3):213-20.
197. Selak MA, Armour SM, MacKenzie ED, Boulahbel H, Watson DG, Mansfield KD, et al. Succinate links TCA cycle dysfunction to oncogenesis by inhibiting HIF- α prolyl hydroxylase. *Cancer cell*. 2005;7(1):77-85.
198. Xiao M, Yang H, Xu W, Ma S, Lin H, Zhu H, et al. Inhibition of α -KG-dependent histone and DNA demethylases by fumarate and succinate that are accumulated in mutations of FH and SDH tumor suppressors. *Genes & development*. 2012;26(12):1326-38.
199. Wentzel JF, Lewies A, Bronkhorst AJ, van Dyk E, du Plessis LH, Pretorius PJ. Exposure to high levels of fumarate and succinate leads to apoptotic cytotoxicity and altered global DNA methylation profiles in vitro. *Biochimie*. 2017;135:28-34.
200. Dang L, White DW, Gross S, Bennett BD, Bittinger MA, Driggers EM, et al. Cancer-associated IDH1 mutations produce 2-hydroxyglutarate. *Nature*. 2009;462(7274):739-44.
201. Stein EM, DiNardo CD, Pollyea DA, Fathi AT, Roboz GJ, Altman JK, et al. Enasidenib in mutant IDH2 relapsed or refractory acute myeloid leukemia. *Blood*. 2017;130(6):722-31.
202. Administration USFD. FDA granted regular approval to enasidenib for the treatment of relapsed or refractory AML. Online article. 2017.
203. Kidd JG. Regression of transplanted lymphomas induced in vivo by means of normal guinea pig serum. II. Studies on the nature of the active serum constituent: histological mechanism of the regression: tests for effects of guinea pig serum on lymphoma cells in vitro: discussion. *The Journal of experimental medicine*. 1953;98(6):583-606.
204. Avramis VI, Tiwari PN. Asparaginase (native ASNase or pegylated ASNase) in the treatment of acute lymphoblastic leukemia. *International journal of nanomedicine*. 2006;1(3):241-54.
205. Zhang XD, Deslandes E, Villedieu M, Poulain L, Duval M, Gauduchon P, et al. Effect of 2-deoxy-D-glucose on various malignant cell lines in vitro. *Anticancer research*. 2006;26(5A):3561-6.
206. Maschek G, Savaraj N, Priebe W, Braunschweiger P, Hamilton K, Tidmarsh GF, et al. 2-deoxy-D-glucose increases the efficacy of adriamycin and paclitaxel in human osteosarcoma and non-small cell lung cancers in vivo. *Cancer research*. 2004;64(1):31-4.
207. Fantin VR, St-Pierre J, Leder P. Attenuation of LDH-A expression uncovers a link between glycolysis, mitochondrial physiology, and tumor maintenance (vol 9, pg 425, 2006). *Cancer cell*. 2006;10(2):172-.
208. Le A, Cooper CR, Gouw AM, Dinavahi R, Maitra A, Deck LM, et al. Inhibition of lactate dehydrogenase A induces oxidative stress and inhibits tumor progression. *Proceedings of the National Academy of Sciences of the United States of America*. 2010;107(5):2037-42.
209. Xie H, Hanai J, Ren JG, Kats L, Burgess K, Bhargava P, et al. Targeting lactate dehydrogenase-*a* inhibits tumorigenesis and tumor progression in mouse models of lung cancer and impacts tumor-initiating cells. *Cell metabolism*. 2014;19(5):795-809.
210. Yao F, Zhao T, Zhong C, Zhu J, Zhao H. LDHA is necessary for the tumorigenicity of esophageal squamous cell carcinoma. *Tumour biology : the journal of the International Society for Oncodevelopmental Biology and Medicine*. 2013;34(1):25-31.
211. Wang ZY, Loo TY, Shen JG, Wang N, Wang DM, Yang DP, et al. LDH-A silencing suppresses breast cancer tumorigenicity through induction of oxidative stress mediated mitochondrial pathway apoptosis. *Breast cancer research and treatment*. 2012;131(3):791-800.
212. Hong CS, Graham NA, Gu W, Espindola Camacho C, Mah V, Maresh EL, et al. MCT1 Modulates Cancer Cell Pyruvate Export and Growth of Tumors that Co-express MCT1 and MCT4. *Cell reports*. 2016;14(7):1590-601.
213. Polanski R, Hodgkinson CL, Fusi A, Nonaka D, Priest L, Kelly P, et al. Activity of the monocarboxylate transporter 1 inhibitor AZD3965 in small cell lung cancer. *Clinical cancer research : an official journal of the American Association for Cancer Research*. 2014;20(4):926-37.

214. Udai Banerji ERP. A Phase I Trial of AZD3965 in Patients With Advanced Cancer (NCT01791595). *ClinicalTrials.gov*.
215. Quinn BJ, Kitagawa H, Memmott RM, Gills JJ, Dennis PA. Repositioning metformin for cancer prevention and treatment. *Trends in endocrinology and metabolism: TEM*. 2013;24(9):469-80.
216. Ko Y, Choi A, Lee M, Lee JA. Metformin displays in vitro and in vivo antitumor effect against osteosarcoma. *Korean journal of pediatrics*. 2016;59(9):374-80.
217. Andrzejewski S, Gravel SP, Pollak M, St-Pierre J. Metformin directly acts on mitochondria to alter cellular bioenergetics. *Cancer & metabolism*. 2014;2:12.
218. Whitaker-Menezes D, Martinez-Outschoorn UE, Flomenberg N, Birbe RC, Witkiewicz AK, Howell A, et al. Hyperactivation of oxidative mitochondrial metabolism in epithelial cancer cells in situ: visualizing the therapeutic effects of metformin in tumor tissue. *Cell cycle*. 2011;10(23):4047-64.
219. Pollak M. Overcoming Drug Development Bottlenecks With Repurposing: Repurposing biguanides to target energy metabolism for cancer treatment. *Nature medicine*. 2014;20(6):591-3.
220. Shackelford DB, Abt E, Gerken L, Vasquez DS, Seki A, Leblanc M, et al. LKB1 inactivation dictates therapeutic response of non-small cell lung cancer to the metabolism drug phenformin. *Cancer cell*. 2013;23(2):143-58.
221. Yuan P, Ito K, Perez-Lorenzo R, Del Guzzo C, Lee JH, Shen CH, et al. Phenformin enhances the therapeutic benefit of BRAF(V600E) inhibition in melanoma. *Proceedings of the National Academy of Sciences of the United States of America*. 2013;110(45):18226-31.
222. Yuneva M, Zamboni N, Oefner P, Sachidanandam R, Lazebnik Y. Deficiency in glutamine but not glucose induces MYC-dependent apoptosis in human cells. *The Journal of cell biology*. 2007;178(1):93-105.
223. Gaglio D, Soldati C, Vanoni M, Alberghina L, Chiaradonna F. Glutamine deprivation induces abortive s-phase rescued by deoxyribonucleotides in k-ras transformed fibroblasts. *PLoS one*. 2009;4(3):e4715.
224. Wang JB, Erickson JW, Fuji R, Ramachandran S, Gao P, Dinavahi R, et al. Targeting mitochondrial glutaminase activity inhibits oncogenic transformation. *Cancer cell*. 2010;18(3):207-19.
225. Camarda R, Zhou AY, Kohnz RA, Balakrishnan S, Mahieu C, Anderton B, et al. Inhibition of fatty acid oxidation as a therapy for MYC-overexpressing triple-negative breast cancer. *Nature medicine*. 2016;22(4):427-32.
226. Samudio I, Harmancey R, Fiegl M, Kantarjian H, Konopleva M, Korchin B, et al. Pharmacologic inhibition of fatty acid oxidation sensitizes human leukemia cells to apoptosis induction. *The Journal of clinical investigation*. 2010;120(1):142-56.
227. Hernlund E, Ihrlund LS, Khan O, Ates YO, Linder S, Panaretakis T, et al. Potentiation of chemotherapeutic drugs by energy metabolism inhibitors 2-deoxyglucose and etomoxir. *International journal of cancer*. 2008;123(2):476-83.
228. Holubarsch CJ, Rohrbach M, Karrasch M, Boehm E, Polonski L, Ponikowski P, et al. A double-blind randomized multicentre clinical trial to evaluate the efficacy and safety of two doses of etomoxir in comparison with placebo in patients with moderate congestive heart failure: the ERGO (etomoxir for the recovery of glucose oxidation) study. *Clinical science*. 2007;113(4):205-12.
229. Mackay GM, Zheng L, van den Broek NJ, Gottlieb E. Analysis of Cell Metabolism Using LC-MS and Isotope Tracers. *Methods in enzymology*. 2015;561:171-96.
230. Karvela M, Baquero P, Kuntz EM, Mukhopadhyay A, Mitchell R, Allan EK, et al. ATG7 regulates energy metabolism, differentiation and survival of Philadelphia-chromosome-positive cells. *Autophagy*. 2016;12(6):936-48.
231. Abraham SA. Biological Analysis of Human CML Stem Cells; Xenograft Model of Chronic Phase Human Chronic Myeloid Leukemia. *Methods in Molecular Biology* 2016;1465:175-85.
232. Sullivan LB, Gui DY, Hosios AM, Bush LN, Freinkman E, Vander Heiden MG. Supporting Aspartate Biosynthesis Is an Essential Function of Respiration in Proliferating Cells. *Cell*. 2015;162(3):552-63.

233. Birsoy K, Wang T, Chen WW, Freinkman E, Abu-Remaileh M, Sabatini DM. An Essential Role of the Mitochondrial Electron Transport Chain in Cell Proliferation Is to Enable Aspartate Synthesis. *Cell*. 2015;162(3):540-51.
234. Cardaci S, Zheng L, MacKay G, van den Broek NJ, MacKenzie ED, Nixon C, et al. Pyruvate carboxylation enables growth of SDH-deficient cells by supporting aspartate biosynthesis. *Nature cell biology*. 2015;17(10):1317-26.
235. Jitrapakdee S, St Maurice M, Rayment I, Cleland WW, Wallace JC, Attwood PV. Structure, mechanism and regulation of pyruvate carboxylase. *The Biochemical journal*. 2008;413(3):369-87.
236. Bhatia M, Wang JC, Kapp U, Bonnet D, Dick JE. Purification of primitive human hematopoietic cells capable of repopulating immune-deficient mice. *Proceedings of the National Academy of Sciences of the United States of America*. 1997;94(10):5320-5.
237. Jos Domen AWAALW. Bone Marrow (Hematopoietic) Stem Cells. *Regenerative Medicine*. 2006;Chapter 2.
238. Nasri H, Rafieian-Kopaei M. Metformin: Current knowledge. *Journal of research in medical sciences : the official journal of Isfahan University of Medical Sciences*. 2014;19(7):658-64.
239. Fitzgerald E, Mathieu S, Ball A. Metformin associated lactic acidosis. *Bmj*. 2009;339:b3660.
240. Owen MR, Doran E, Halestrap AP. Evidence that metformin exerts its anti-diabetic effects through inhibition of complex 1 of the mitochondrial respiratory chain. *The Biochemical journal*. 2000;348 Pt 3:607-14.
241. Piel S, Ehinger JK, Elmer E, Hansson MJ. Metformin induces lactate production in peripheral blood mononuclear cells and platelets through specific mitochondrial complex I inhibition. *Acta physiologica*. 2015;213(1):171-80.
242. El-Mir MY, Nogueira V, Fontaine E, Averet N, Rigoulet M, Leverve X. Dimethylbiguanide inhibits cell respiration via an indirect effect targeted on the respiratory chain complex I. *The Journal of biological chemistry*. 2000;275(1):223-8.
243. Luengo A, Sullivan LB, Heiden MG. Understanding the complex-ity of metformin action: limiting mitochondrial respiration to improve cancer therapy. *BMC biology*. 2014;12:82.
244. Natrass M, Alberti KG. Biguanides. *Diabetologia*. 1978;14(2):71-4.
245. Administration UFD. Metformin Hydrochloride Tablets. <https://wwwfdagov/ohrms/dockets/dailys/02/may02/053102/800471e6pdf>.
246. Chaube B, Bhat MK. AMPK, a key regulator of metabolic/energy homeostasis and mitochondrial biogenesis in cancer cells. *Cell death & disease*. 2016;7:e2044.
247. Viollet B, Guigas B, Sanz Garcia N, Leclerc J, Foretz M, Andreelli F. Cellular and molecular mechanisms of metformin: an overview. *Clinical science*. 2012;122(6):253-70.
248. Dykens JA, Jamieson J, Marroquin L, Nadanaciva S, Billis PA, Will Y. Biguanide-induced mitochondrial dysfunction yields increased lactate production and cytotoxicity of aerobically-poised HepG2 cells and human hepatocytes in vitro. *Toxicology and applied pharmacology*. 2008;233(2):203-10.
249. Memorial Sloan Kettering Cancer Center MGH, Weill Medical College of Cornell University. Clinical Trial of Phenformin in Combination With Dabrafenib and Trametinib for Patients With BRAF-mutated Melanoma. <https://clinicaltrials.gov/ct2/show/NCT03026517>. 2017.
250. Natrass M, Sizer K, Alberti KG. Correlation of plasma phenformin concentration with metabolic effects in normal subjects. *Clinical science*. 1980;58(2):153-5.
251. Mentel WFMM. The Origin of Mitochondria. *Nature Education*. 2010;3(9)58.
252. Takahashi M, Matsuoka Y, Sumide K, Nakatsuka R, Fujioka T, Kohno H, et al. CD133 is a positive marker for a distinct class of primitive human cord blood-derived CD34-negative hematopoietic stem cells. *Leukemia*. 2014;28(6):1308-15.
253. Meijer TW, Kaanders JH, Span PN, Bussink J. Targeting hypoxia, HIF-1, and tumor glucose metabolism to improve radiotherapy efficacy. *Clinical cancer research : an official journal of the American Association for Cancer Research*. 2012;18(20):5585-94.
254. Cairns RA, Harris IS, Mak TW. Regulation of cancer cell metabolism. *Nature reviews Cancer*. 2011;11(2):85-95.

255. Kiel MJ, Morrison SJ. Uncertainty in the niches that maintain haematopoietic stem cells. *Nature reviews Immunology*. 2008;8(4):290-301.
256. Tabe Y, Konopleva M. Advances in understanding the leukaemia microenvironment. *British journal of haematology*. 2014;164(6):767-78.
257. Moschoi R, Imbert V, Nebout M, Chiche J, Mary D, Prebet T, et al. Protective mitochondrial transfer from bone marrow stromal cells to acute myeloid leukemic cells during chemotherapy. *Blood*. 2016;128(2):253-64.
258. Capala ME, Pruis M, Vellenga E, Schuringa JJ. Depletion of SAM50 Specifically Targets BCR-ABL-Expressing Leukemic Stem and Progenitor Cells by Interfering with Mitochondrial Functions. *Stem cells and development*. 2016;25(5):427-37.
259. Klawitter J, Anderson N, Klawitter J, Christians U, Leibfritz D, Eckhardt SG, et al. Time-dependent effects of imatinib in human leukaemia cells: a kinetic NMR-profiling study. *British journal of cancer*. 2009;100(6):923-31.
260. Flis K, Irvine D, Copland M, Bhatia R, Skorski T. Chronic myeloid leukemia stem cells display alterations in expression of genes involved in oxidative phosphorylation. *Leukemia & lymphoma*. 2012;53(12):2474-8.
261. Lane SW, Scadden DT, Gilliland DG. The leukemic stem cell niche: current concepts and therapeutic opportunities. *Blood*. 2009;114(6):1150-7.
262. Schepers K, Campbell TB, Passegue E. Normal and leukemic stem cell niches: insights and therapeutic opportunities. *Cell stem cell*. 2015;16(3):254-67.
263. Jiang X, Zhao Y, Smith C, Gasparetto M, Turhan A, Eaves A, et al. Chronic myeloid leukemia stem cells possess multiple unique features of resistance to BCR-ABL targeted therapies. *Leukemia*. 2007;21(5):926-35.
264. Alvarez-Calderon F, Gregory MA, Pham-Danis C, DeRyckere D, Stevens BM, Zaberezhnyy V, et al. Tyrosine kinase inhibition in leukemia induces an altered metabolic state sensitive to mitochondrial perturbations. *Clinical cancer research : an official journal of the American Association for Cancer Research*. 2015;21(6):1360-72.
265. Reed GA, Schiller GJ, Kambhampati S, Tallman MS, Douer D, Minden MD, et al. A Phase 1 study of intravenous infusions of tigecycline in patients with acute myeloid leukemia. *Cancer medicine*. 2016;5(11):3031-40.
266. Zhang X, Fryknas M, Hernlund E, Fayad W, De Milito A, Olofsson MH, et al. Induction of mitochondrial dysfunction as a strategy for targeting tumour cells in metabolically compromised microenvironments. *Nature communications*. 2014;5:3295.
267. Kang BH, Tavecchio M, Goel HL, Hsieh CC, Garlick DS, Raskett CM, et al. Targeted inhibition of mitochondrial Hsp90 suppresses localised and metastatic prostate cancer growth in a genetic mouse model of disease. *British journal of cancer*. 2011;104(4):629-34.
268. Kang BH, Siegelin MD, Plescia J, Raskett CM, Garlick DS, Dohi T, et al. Preclinical characterization of mitochondria-targeted small molecule hsp90 inhibitors, gamitrinibs, in advanced prostate cancer. *Clinical cancer research : an official journal of the American Association for Cancer Research*. 2010;16(19):4779-88.
269. Siegelin MD, Dohi T, Raskett CM, Orlowski GM, Powers CM, Gilbert CA, et al. Exploiting the mitochondrial unfolded protein response for cancer therapy in mice and human cells. *The Journal of clinical investigation*. 2011;121(4):1349-60.
270. Estan MC, Calvino E, Calvo S, Guillen-Guio B, Boyano-Adanez Mdel C, de Blas E, et al. Apoptotic efficacy of etomoxir in human acute myeloid leukemia cells. Cooperation with arsenic trioxide and glycolytic inhibitors, and regulation by oxidative stress and protein kinase activities. *PLoS one*. 2014;9(12):e115250.
271. Services UFDADoHaH. Innovation or Stagnation: Challenge and Opportunity on the Critical Path to New Medical Products. 2004.
272. De Souza YG, Greenspan JS. Biobanking past, present and future: responsibilities and benefits. *Aids*. 2013;27(3):303-12.